Fakultät für Maschinenwesen

Heating characteristics of fixed focus laser assisted Thermoplastic-Automated Fiber Placement of 2D and 3D parts

Andreas Michael Kollmannsberger

Vollständiger Abdruck der von der Fakultät für Maschinenwesen der Technischen Universität München zur Erlangung des akademischen Grades eines

Doktor-Ingenieurs

genehmigten Dissertation.

Vorsitzender:

    Prof. Dr.-Ing. Christian Große

Prüfer der Dissertation:

1.   Prof. Dr.-Ing. Klaus Drechsler

2.   Prof. Paul Compston, Ph.D. (Australian National University)

Die Dissertation wurde am 09.01.2019 bei der Technischen Universität München eingereicht und durch die Fakultät für Maschinenwesen am 13.05.2019 angenommen.

Technische Universität München
Fakultät für Maschinenwesen
Lehrstuhl für Carbon Composites
Boltzmannstraße 15
D-85748 Garching bei München

Tel.:   +49 (0) 89 / 289 – 15092
Fax.:   +49 (0) 89 / 289 – 15097
Email: info@lcc.mw.tum.de
Web: www.lcc.mw.tum.de

ACKNOWLEDGMENT

ABSTRACT

Automated manufacturing techniques are a key factor for the wider use of lightweight carbon fiber reinforced polymers in various industries. Automation allows higher mechanical, economical and environmental efficiency with respect to the use of this high performance material class. Furthermore, it enables new processing routes for the sub-category of carbon fiber reinforced thermoplastics with their typically high processing temperatures. With its additive nature, Automated Fiber Placement (AFP) is a lean process to produce high performance laminates in a fully automated manner. The possibility of in situ consolidation of thermoplastic composites further reduces the amount of production steps, as the lay-up and consolidation are combined in one process step.

So far, the Thermoplastic-AFP process with in situ consolidation is limited to steady-state processes on simple geometries like flat laminates. The aim of this thesis is to evaluate the capabilities of the process to manufacture general three-dimensional (3D) structures. A high energy density is melting the composite tape's matrix in a very short time. An exact understanding of the heating characteristics is required, as complex laser beam-geometry interactions lead to an inhomogeneous heating on 3D geometries. This will result in local overheating and thermal polymer degradation, if no process parameter adjustments are made.

The process is transferred to 3D geometries, based on an analysis of the steady-state two-dimensional lay-up. Experimental lay-up trials accompany thermal simulations. Exact modelling of the laser beam boundary conditions, including its kinematics during lay-up, provides the basis for developing an adjusted processing strategy. The 3D lay-up geometry causes a change of the laser spot size, which leads to an unintended increase or decrease of energy density. Two adapted processing strategies are experimentally tested. A homogeneous bonding temperature is achieved by locally adjusting the laser power and the laser spot's bias between incoming tape and substrate laminate. Beside temperature log analyses, specimens of both strategies are mechanically tested. Compared to standard processing, derived from flat laminates, a homogeneous and significantly higher bond strength is demonstrated for both strategies.

The aim of manufacturing 3D parts with equal laminate quality compared to flat specimens is achieved. The process's capabilities for industrial application are shown by the manufacture of a demonstrator with strongly convex geometry.

KURZFASSUNG

Automatisierung in der Fertigung ist ein Schlüsselfaktor für die weitere Etablierung des Leichtbauwerkstoffs kohlenstofffaserverstärkter Kunststoffe. Durch Automatisierung kann dieser Hochleistungswerkstoff in mechanischer, wirtschaftlicher und ökologischer Hinsicht besser ausgenutzt werden. Zusätzlich wird dadurch die Verarbeitung der Unterkategorie der faserverstärkten Thermoplaste mit ihren hohen Prozesstemperaturen ermöglicht. Durch den additiven Ansatz ist das Automated Fiber Placement (AFP) ein effizientes Verfahren zur vollautomatisierten Herstellung von Hochleistungsbauteilen. Die Möglichkeit der in situ Konsolidierung thermoplastischer Composites reduziert nochmals die benötigte Anzahl von Fertigungsschritten. Der Laminatherstellungsprozess ist bereits mit der Ablage abgeschlossen.

Bisher ist der Thermoplast-AFP Prozess mit in situ Konsolidierung auf die stationäre Ablage einfacher Geometrien wie ebene Laminate begrenzt. Ziel dieser Arbeit ist es, die Eignung des Prozesses zur Herstellung von allgemeinen dreidimensionalen Bauteilen zu untersuchen. Die hohe Energiedichte um die thermoplastische Matrix des Composites in kurzer Zeit aufzuschmelzen erfordert ein genaues Verständnis des Aufheizverhaltens. Komplexe Laserstrahl-Geometrie Interaktionen führen bei der 3D Ablage zu ungleichmäßiger Erwärmung. Dies kann zu lokaler Überhitzung und Schädigung der thermoplastischen Matrix führen, wenn keine geeigneten Gegenmaßnahmen ergriffen werden.

Ausgehend von der Analyse der zweidimensionalen Ablage, wird der Prozess auf dreidimensionale Strukturen übertragen. Begleitend zu experimentellen Ablageversuchen wird der Prozess mittels thermischer Simulation betrachtet. Durch eine exakte Modellierung der Laserstrahlrandbedingungen, einschließlich ihrer räumlichen und zeitlichen Veränderung während der Ablage, werden die Grundlagen für eine angepasste Prozessführung erarbeitet. Die dreidimensionale Ablagegeometrie bewirkt eine Veränderung der Größe des Laserbrennflecks, was zu einer unerwünschten Erhöhung oder Verringerung der Energiedichte führt. Es werden zwei angepasste Prozessführungen experimentell untersucht. Durch die lokale Anpassung der Laserleistung und deren Verteilung zwischen abzulegendem Band und bereits abgelegtem Laminat, wird eine gleichbleibende Fügetemperatur erreicht. Neben der Analyse von Temperaturmessdaten werden Probekörper beider Strategien mechanisch getestet. Im Vergleich zur Ablage mit Standardparametern zeigt sich ein konstanter und signifikant höherer Verlauf der Fügefestigkeit für beide neuen Prozessführungen.

Das Ziel einer gleichbleibenden Laminatqualität dreidimensionaler Bauteile, im Vergleich zu flachen Laminaten, wird dadurch erreicht. Die industrielle Eignung wird anhand eines Demonstrators mit stark konvexer Geometrie nachgewiesen.

Table of contents

Nomenclature

Arabic symbols	Unit	Description
A	m²	Area
A	m²	Cross-section
c_p	J/kg·K	Specific heat
d	m	Distance or thickness
dt	s	Time step duration
dx_i	m	Element size in i direction
D_{ic}	-	Degree of intimate contact
f	m	Focal distance
F	-	Clamping factor
F_c	N	Compaction force
h	W/m²·K	Heat transfer coefficient
h_0	m	Laser beam height at optics' exit
h_f	m	Laser beam height at focal distance
h_m	m	Height of mold
i	-	Current time step
I	m⁴	Moment of inertia
L	m	Clamping length
l_c	m	Compaction length by the compaction roller
L_p	m	Length of the simulated laminate
m	kg	Mass
n	-	Refractive index

Arabic symbols	Unit	Description
n	-	Number of layers
P	W	Laser power
Q	J	Energy
$\dot{Q}$	W	Energy flux
$\dot{q}$	W/m²	Specific energy flux
$\dot{q}_d$	W/m²	Specific energy flux by direct laser illumination
$\dot{q}_r$	W/m²	Specific energy flux by reflected laser illumination
R_c	m²·K/W	Thermal contact resistance
r_{c1}	-	Cooling factor of compaction roller during one rotation
r_{roller}	m	Radius of compaction roller
s	m	Distance
S	-	Shearing factor
t	s	Time
$t_{1/2}$	s	Half-time
t_L	m	Composite tape layer thickness
t_{roller}	m	Thickness of silicone layer of compaction roller
T	°C or K	Temperature
T_0	°C or K	Start temperature of element
T_∞	°C or K	Ambient temperature
T_c	°C or K	Crystallization temperature
T_g	°C or K	Glass transition temperature

Arabic symbols	Unit	Description
T_m	°C or K	Melting temperature
v	m/s	velocity
V	m³	Volume
w_0	m	Laser beam width at optics' exit
w_f	m	Laser beam width at focal distance
x_i	m	Coordinate axis
x_{rb}	m	Position of right boundary condition of compaction roller
x_{lb}	m	Position of left boundary condition of compaction roller
$X1_L$	m	Virtual laser beam origin (x_1-component)
$X3_L$	m	Virtual laser beam origin (x_3-component)

Greek symbols	Unit	Description
α	-	Absorptivity
α	m²/s	Thermal diffusivity
α	°	Laser angle to lay-up tool
β	°	Angle of incoming tape - mold
γ	°	Placement head angle - mold
δ	°	Laser beam widening angle
θ	°	Laser angle of incidence
θ_1	°	Angle of incidence by direct laser illumination
θ_2	°	Angle of incidence by reflected laser illumination
λ	W/m·K	Thermal conductivity

Greek symbols	Unit	Description
ν	-	Poisson's ratio
ρ	-	Reflectivity
τ	-	Transmissivity
φ	-	Fiber volume fraction
ψ	-	Fiber mass fraction

Abbreviations

Abbreviation	Description
1D	One-dimensional
2D	Two-dimensional
3D	Three-dimensional
Accurat3	Project „Automatisierte Ablage von Carbon Bändern mit thermoplastischer Matrix für 3D Bauteile – Untersuchung der Prozessparameter durch Test und Simulation für den instationären 3D TP-AFP Prozess"
AFP	Automated Fiber Placement
AFPT	Advanced Fiber Placement Technology GmbH
AG	Aktiengesellschaft
AiF	Arbeitsgemeinschaft industrieller Forschungsvereinigungen "Otto von Guericke" e.V.
AMU	Anwenderzentrum Material- und Umweltforschung
ANU	Australian National University
APC-2	A type of carbon fiber / Polyether ether ketone composite
AS4	A type of high strength carbon fiber
ASTM	American Society for Testing and Materials
ATL	Automated Tape Laying
BASF	Badische Anilin- & Soda-Fabrik Societas Europaea
BC	Boundary condition
BMWI	Bundesministerium für Wirtschaft und Energie
CAD	Computer aided design
CBS	curved beam strength according to ASTM D6415

Abbreviation	Description
CCPP	Coordinate Controlled Process Parameter
CF	Carbon fiber
cf.	Confer; Latin for "compare"
CFRP	Carbon fiber reinforced plastic / polymer
CFRTP	Carbon fiber reinforced thermoplastic
CLC	Closed loop control
CO_2	Carbon dioxide
COPRAS	Project "Composite parts for rocket applications with integrated sensors"
DEfcodoor	Project "Development of an ecological friendly final consolidation step using Thermoplastic Fibre Placement for a helicopter door"
DIN	Deutsches Institut für Normung e. V.
DISACOP	Project "Disassembly of eco-designed helicopter demonstrators"
DLR	Deutsches Zentrum für Luft- und Raumfahrt e.V.
DMA	Dynamic Mechanical Analysis
DSC	Differential Scanning Calorimetry
EADS	European Aeronautic Defence and Space Company Societas Europaea
e.g.	exempli gratia; Latin for "for example"
EN	European Standard
FD	Finite difference
Fig.	Figure
FLIR	Forward looking infrared / FLIR Systems Inc.
FVF	Fiber volume fraction

Abbreviation	Description
GF	Geometry factor
G_{Ic}	Mode I interlaminar fracture toughness
GmbH	Gesellschaft mit beschränkter Haftung
GroFi	Großbauteile in Fiberplacementtechnologie
HAZ	Heat affected zone
HBM	Hottinger Baldwin Messtechnik GmbH
i.e.	Id est; Latin for "that is"
ILSS	Interlaminar shear strength
Inc.	Incorporated
INSCAPE	Project "In situ manufactured carbon-thermoplast curved stiffened panel"
IPT	Fraunhofer-Institut für Produktionstechnologie
IR	Infrared
IROM	Inverse rule of mixture
ISINTHER	Project "Industrialization setup of Thermoplastics in situ consolidation process"
ISO	International Organization for Standardization
KUKA AG	Keller und Knappich Augsburg Aktiengesellschaft
Laser	Light amplification by stimulated emission of radiation
LCC	Lehrstuhl für Carbon Composites / Chair of Carbon Composites
LFA	Laser flash analysis
NC	Numerical control
Nd-YAG	Neodymium-doped yttrium aluminum garnet
OHC	Open hole compression

Abbreviation	Description
OUTCOME	Project "OUT of autoclave COMpositE wing"
PA	Polyamide
PC	Personal computer
PC	Post consolidation
PCLC	Predictive Closed Loop Control
PEEK	Polyether ether ketone
PES	Polyethersulfone
PhD	Doctor of Philosophy
PI	Polyimide
PP	Polypropylene
PPS	Polyphenylene sulfide
Prepreg	Preimpregnated
REXUS	Rocket Experiments for University Students
ROM	Rule of mixture
SA	Société Anonyme
SAS	Société par actions simplifiée
SE	Societas Europaea
SI	Système international d'unités
SWMS	Systemtechnik Ingenieurgesellschaft mbH
Tab.	Table
TC	Thermocouple
TCP	Tool center point

Abbreviation	Description
TESOS	Project "In-flight temperature measurements with structurally integrated fibre optic sensors"
TGA	Thermogravimetric Analysis
TLH	Tape laying head
TMDSC	Temperature-Modulated Differential Scanning Calorimetry
TP	Thermoplastic
TP-AFP	Thermoplastic-Automated Fiber Placement
TUM	Technische Universität München / Technical University of Munich
TS	Thermoset
TS-AFP	Thermoset-Automated Fiber Placement
UD	Uni directional
VCSEL	Vertical cavity surface emitting lasers
ZIM	Zentrales Innovationsprogramm Mittelstand
ZLP	Zentrum für Leichtbauproduktionstechnologie

List of figures

List of tables

1 Introduction

Parts made out of carbon fiber reinforced polymers (CFRP) offer great benefits in comparison to traditionally produced metal structures. The reinforcing fibers are capable to bear high loads while the weight is kept low. Along with other benefits like excellent fatigue behavior, the share of CFRP part in aerospace grew steadily over the past decades. Today's mostly used polymer types in CFRP laminates are thermoset resins due to the following reasons: easier fiber impregnation due to their generally lower viscosity and numerous existing part-manufacturing processes suitable for manual and automated manufacture. Another matrix type for CFRP parts are thermoplastic (TP) polymers. They feature entangled or partially oriented polymer chains and can be softened by heat treatment. Without inseparable crosslinks in between these polymer chains, thermoplastics can be formed in subsequently production steps or even be welded together. This opens new manufacturing routes compared to traditionally used thermoset matrices. Another benefit of thermoplastic matrix systems is their inherently ductile failure, which is transformed to the composite laminate.

Research on efficient manufacturing techniques is in the focus of many companies and researchers. A key factor to compensate the high raw material costs is automation. Many parts of today's newest airliners like the Airbus A350 and Boeing 787 are produced by Automated Fiber Placement (AFP). Automated Fiber Placement of composites is a lean manufacturing process for high quality and high performance parts. A fiber placement head is depositing carbon fiber reinforced tapes along a programmed path over a mold. This principle is repeated until a predefined laminate is generated. The generative nature of the lay-up allows the automated production of complex lay-ups from simple tape material with minimized production steps following a fully digitalized design process. Other technical benefits are high accuracy of fiber orientation, high repeatability and material efficiency. With the use of suitable online process monitoring techniques integrated into the AFP machine, the effort for part quality checks after production can be reduced as well. Large structures with a reduced geometric complexity as aircraft fuselages or wings are especially suitable for AFP. Part size is virtually unlimited by AFP lay-up.

State-of-the-art aerospace AFP parts with thermoset resin systems are consolidated and cured in an autoclave after lay-up. This two-step approach of lay-up and consolidation is also used for thermoplastic composite material. However, these typically require even higher temperatures, more expensive vacuum bagging materials, autoclave hardware and more energy. In situ consolidation of thermoplastic composites during AFP

lay-up allows saving the second consolidation process step and takes full advantage of the thermoplastic nature of the material.

Despite the material's mechanical, thermal, environmental and processing benefits, the use of thermoplastic composite materials is rather low, compared to thermoset composites. New processes have to be developed to meet the material's demands. TP-AFP machines for example often use a laser system to heat the thermoplastic composite tape. The required laser safety measures and the high process temperatures for welding the thermoplastic polymer forbid manual processes and require the use of automated manufacturing. Until today, TP-AFP is still subject of research in universities and laboratories and not established in the industrial production. Most research is carried out on optimizing the laminate quality by using basic geometries as flat specimens and cylindrical pipes. The process of such geometries can be regarded as a steady-state-process, as the boundary conditions do not change during lay-up. By finding an optimized set of process parameters, excellent laminate quality can be reached for the whole part. Often temperature controlled closed loop control is used to achieve optimum bonding temperature throughout the lay-up. Complex machine and laser beam-laminate interactions lead to inhomogeneous composite heating during lay-up of 3D curved parts. This can even lead to thermal degradation of the polymer matrix. Therefore, continuously adapted, geometry depending process parameters are required during the lay-up of a single path. Current closed loop controls are not able to compensate the strong thermal response of the laminate due to the 3D geometry. In this thesis, these heating effects are analyzed and new approaches to manufacture 3D structures by TP-AFP with in situ consolidation are developed.

1.1 Research objective

The overall objective of this thesis is to investigate the potential of laser-assisted TP-AFP with in situ consolidation for 3D parts with strong curvatures. Lay-up geometries can feature convex corners that are much smaller than the size of the laser spot. The change of the lay-up geometry results in a non-homogeneous heating profile of the laminate around the curved sections. Overheating with matrix polymer degradation occurs, if no adapted process parameters are used. In order to achieve the overall goal the thesis is split into eight chapters answering the following objectives:

What thermal properties of carbon fiber thermoplastic tape material are relevant to model the process and how can they be measured or calculated?

The thermal analysis of the TP-AFP process requires temperature dependent thermal properties of the composite material due to the large temperature range during processing. In this task, the experimental measurements of thermal properties are accompanied by calculations via models from literature to evaluate the high experimental effort. In literature, the existence of an interply thermal contact resistance is controversially discussed. In this thesis it is investigated experimentally and by simulation.

Its value can be used as a quality criterion to evaluate the quality of in situ consolidation. For modelling of the heat introduction by the laser beam the optical behavior of the composite tape is characterized as well.

What are the main process parameters determining the thermal behavior of quasi-steady-state 2D TP-AFP?

Temperature history of the composite laminate is the most dominant process parameter for TP-AFP processing. Laser-assisted TP-AFP is using a laser as a heat source, resulting in high heat flux density. High process temperatures are required to bond the thermoplastic composite tape during lay-up. The high process temperatures result in high temperature gradients for heating as well as for cooling. TP-AFP lay-up of flat parts (2D) is a quasi-steady-state process as the process conditions do not change with respect to the placement head. The thermal process conditions of 2D TP-AFP are described and implemented in a finite-difference code for a detailed analysis.

What are the process changes during non-steady-state 3D lay-up?

The 3D lay-up through TP-AFP is following the same principle as for flat laminates. However, during 3D lay-up the main process parameters' boundary conditions are changing due to the change of the lay-up geometry. Special attention is required for the robot movement determining the relative position of the placement head and the laser optics to the lay-up tool and composite.

In this thesis, a laser TP-AFP system with fixed focus laser optics is used. Fixed focus laser optics are well established for the process and can be used with very high power lasers. The optics form a rectangular laser spot with a homogeneous beam density. The projection of the laser spot on the laminate is defining the heated zone before the nip-point. During 3D lay-up on a changing geometry the size of this heat affected zone (HAZ) changes. Furthermore, due to the movement of the tape laying head the heating time of the composite changes as well. In order to understand the 3D lay-up process behavior, these effects of the laser spot size and illumination time need to be described and quantified. The effect on the resulting process temperature and the bonding quality will be characterized by simulations and by experiments.

In addition, the change of compaction pressure and its distribution under the compaction roller along a 3D lay-up path will be content of research.

Is non steady-state 3D lay-up with fixed focus laser spot optics possible?

Currently highly advanced TP-AFP machines use a high power diode laser with optics forming a fixed laser spot to heat the composite. These machines were originally designed for Automated Tape Winding or for flat TP-AFP lay-up. The geometrical limits for 3D parts that can be produced by these machines is unknown. This thesis explores the feasibility of today's machines to produce 3D composite parts with strong curvature without affecting the bonding quality. 3D laminates are manufactured with adjusted process parameters along the lay-up path. The resulting process temperature is evaluated and mechanical tests are used to measure the bonding quality.

A thermal simulation for 3D lay-up is used to evaluate the process temperatures during 3D lay-up and the effects of different process parameters.

What process adaptions are required for 3D lay-ups?

The result of the thesis is a description of the process parameters and process boundary conditions that need to be addressed in order to optimize the lay-up of 3D composite parts by TP-AFP with in situ consolidation.

1.2 Outline

The thesis is structured in six main chapters:

Chapter 2 describes the basic principles of the TP-AFP process and current state-of-the-art machines. The TP-AFP system, used in this thesis, is described together with its existing closed loop control system.

In **Chapter 3**, the optical and thermal properties of two different thermoplastic composite tapes are investigated. To describe the process properly, the materials properties have to be investigated over the full temperature range of the process. Experimentally determined properties are compared to model predictions from literature, using the carbon fiber and matrix properties. Additionally, the in situ bond quality is evaluated by determining the thermal contact resistance between adjacent laminate plies.

Subsequently, the material properties are used in a thermal simulation of the process for flat laminates in **Chapter 4**. Experimental lay-up trials with temperature measurement are used to validate the thermal simulation. The heating characteristics of this steady-state process is analyzed and discussed through parameter variations.

In **Chapter 5**, lay-up trials in 3D test geometries are conducted. The process parameters are based on the process parameters for flat lay-ups and the influence of the geometry on the process and laminate quality is studied. Due to the 3D geometry, strong overheating occurs locally. The effect of processing temperature on polymer degradation and insufficient bonding is tested.

The previously developed thermal simulation is adapted for the analysis of 3D geometries in **Chapter 6**. A detailed analysis of the change of the laser heating boundary condition is presented and an optimized process is developed.

Based on the observations from the thermal simulation, two new strategies for laser assisted TP-AFP processing on 3D geometries are presented in **Chapter 7**. Both strategies are tested by manufacturing of v-shaped specimens for mechanical testing. Finally, the applicability for industrial production is shown by the manufacture of a demonstrator with challenging geometry and laminate lay-up.

Chapter 4 to 6 each start with a literature review on their according topic.

2 Overview of Thermoplastic-Automated Fiber Placement (TP-AFP) with in situ consolidation

This chapter gives an overview from literature about the Automated Fiber Placement of thermoplastic composite tapes with in situ consolidation. Automated Fiber Placement (AFP) and Automated Tape Laying (ATL) are two very similar processes that follow the same principle. While typically one wide tape is deposited in the ATL process, up to 32 narrow tapes can be simultaneously laid down in the AFP process [1]. A tape laying machine for one single tape is used in this thesis. It is considered and referred as AFP process, as the tape width of 12 mm and 25 mm more typical for AFP than for ATL. The main aspects can be transferred to ATL as well. In the following sections the AFP / ATL process, machine and heating principles are summarized. Additionally, the machine for Thermoplastic-AFP (TP-AFP) that was used for the experimental work is described. The aim of the thesis is to investigate the one step process of in situ consolidation on 3D geometries. Therefore, the idea of in situ consolidation and the preliminary work in literature are presented. TP-AFP produces laminates from prepreg tape material with thermoplastic matrix. Characteristics of the thermoplastic prepreg tape material that determine the final laminate quality are described in the last section of this chapter.

2.1 TP-AFP process

In the following section the AFP / ATL principle is described. The main functional units of a placement head are explained and examples from different machine manufacturers are presented. The main process parameter for TP-AFP is the heating of the tape material. A short description of different heating methods, investigated in literature, is given.

2.1.1 AFP principle

The Automated Fiber Placement (AFP) process of thermoplastic (TP) tape material follows the same basic principle as the state-of-the-art aerospace AFP process for thermoset (TS) prepreg material. Fully impregnated prepreg tapes of fibers and matrix are deposited on a mold or tooling by a placement head. The placement head moves relatively to the mold according to a computer programmed path (Fig. 2-1). As path after path and layer after layer are deposited according to the ply-book, the laminate is

generated in an additive manner. The paths can be oriented in different directions across the part and either straight or curved (steered) paths are possible.
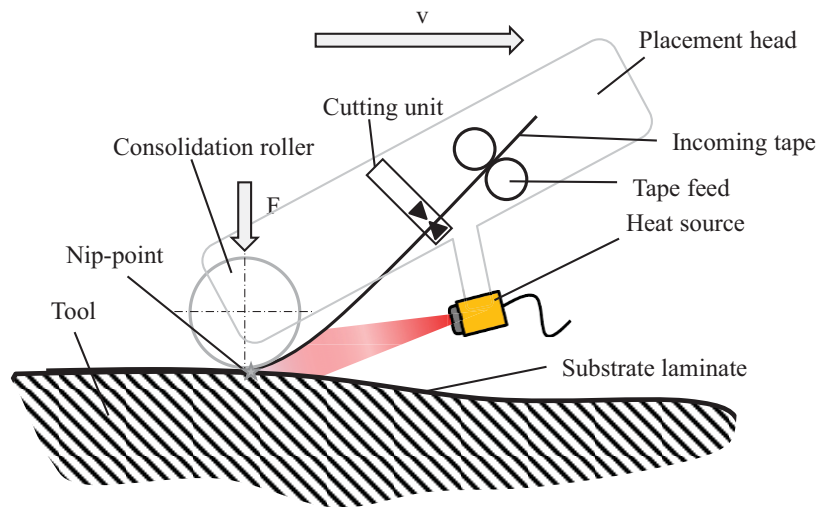
Fig. 2-1:   AFP principle and the main functional units in an AFP head

While the placement head moves along the lay-up path, the composite tape is heated by a heat source and pressed to the substrate laminate by a compaction roller. This way these two partners are bonded together.

At the end of a lay-up path the tape is cut inside the placement head. While the placement head moves to the next starting point, a tape feed unit feeds the feed tape towards the compaction roller for the next path. The tape material can either be stored at the placement head or in a cabinet nearby. In this case, the tape has to be guided to the placement head without damage. A placement head typically has four main functional units:

Compaction / consolidation unit

In order to form a bond between tape material and substrate laminate, heat and pressure are required for a certain duration. Different types of compaction units are used in AFP machines (Fig. 2-2). Rollers and in some applications shoes are the most common types. For both types, rigid and conformable units are used [2, 3]. In recent years, different machine manufacturers established conformable rollers as they reduce peak force, increase compaction time and are applicable for non-flat laminates [1]. Conformable rollers are either segmented or made out of soft materials like foam or silicone. Also multilayer compaction roller systems are used [4].

a)   b)   c)   d)
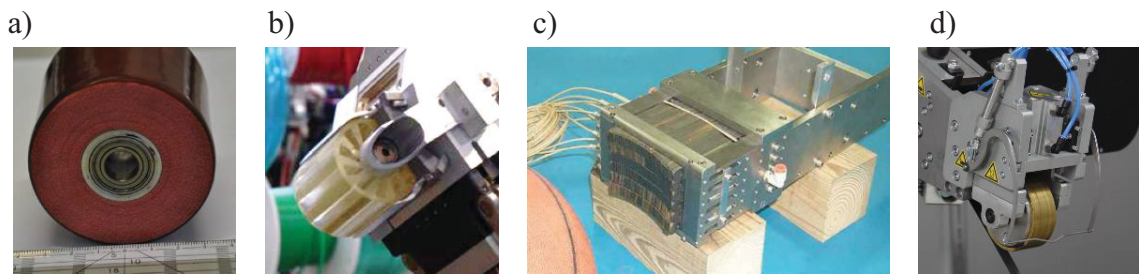
Fig. 2-2:   **Compaction rollers from different machine manufacturers**
            a) Coriolis Composites SAS: Multilayer foam compaction roller [5]
            b) Electroimpact Inc.: Conformable hollow compaction roller [6]
            c) Accudyne Systems Inc.: Conformable metal shoe [7]
            d) AFPT GmbH: Brass roller [8]

For TP-AFP the compaction roller has to withstand high process temperature because it is constantly in contact with hot tape in the heat affected zone (HAZ). In case of hot gas or flame heaters, unintentional heating of the roller has to be compensated. Therefore cooling of the roller is essential. Low absorption of laser radiation is also critical for laser assisted TP-AFP compaction rollers, as the laser typically irradiates the roller at the edges of the tape.

Cutting unit

Cutting carbon fiber tapes is a very abrasive process and can wear down the cutting unit quickly. Machine manufacturers use different cutting principles. Coriolis Composites SAS (Queven, France) for instance uses knifes that are hammered against an ambos with the tape in between. This way cutting happens very fast which reduces wear of the knifes. AFPT GmbH (Dörth, Germany) uses a scissor or guillotine principle to cut the tapes that are fed through the unit. TUM's machine has a hinged guillotine cutting unit that can move along with the tape inside the head during cutting for wear reduction (Fig. 2-3).
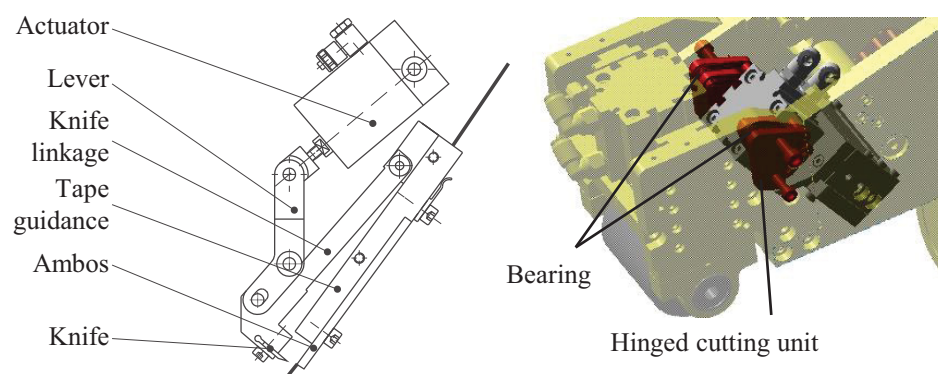
Fig. 2-3:   **Principle of knife-ambos cutting unit (left) according to [9] and hinged guillotine cutting unit by AFPT in TUM system [10] (right)**

Both systems are capable to cut-on-the-fly, so that the lay-up speed does not have to be reduced for cutting.

The distance between the cutting unit and nip-point is defining the minimum lay-up length. After cutting, the tape cannot be guided as before, as tension cannot be applied to the tape anymore, making steering impossible and the tape may drop down onto the laminate uncontrolled. Manufacturers aim to minimize the distance in order to be able to lay-up short paths as well.

Tape feed unit

The main task of the tape feed unit is to feed the feed tape to the nip-point in time after cutting and before the next lay-up starts. Tape feed has to be within a defined tolerance, as it determines the accuracy at the start of the laminate placement. Between tape feed unit and compaction roller the tape has a free length, so it can be heated before the nip-point. Typically, the cutting unit is in between tape feed unit und compaction roller to minimize the minimum lay-up length. In order to increase the tape feed accuracy, tape guiding systems restrict undesired lateral movement and out of plane buckling of the tape. Coriolis Composites SAS for example specifies a cutting and feeding tolerance of ± 2.5 mm [11]. TUM's TP-AFP machine by AFPT GmbH achieves a start tolerance within ± 1.5 mm (Fig. 2-4).
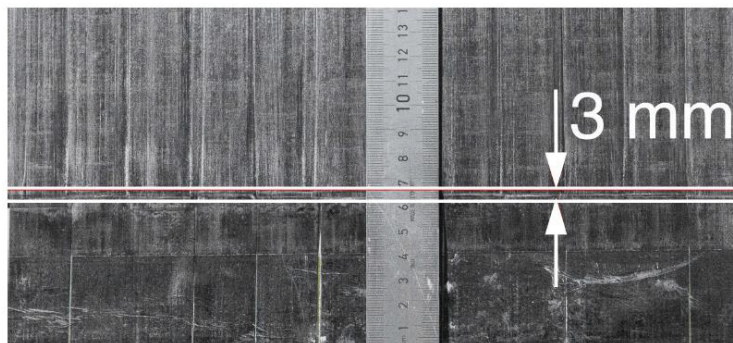
Fig. 2-4:   **Tolerance at start of a lay-up path at TUM's TP-AFP machine [12]**

In contrast to thermoset prepreg tapes, non-sticky thermoplastic tapes need no backing paper. This also means that feeding of the carbon tapes has to be done without the aid of backing paper. However, in contrast to thermoset prepreg tapes, thermoplastic carbon tapes are fully impregnated, solidified and thus stiffer. Typically the tape feed unit consists of a gripped motorized roller for each tape that is pressed against it.

During lay-up the tape feed unit can be used to apply a defined tape tension or to compensate undesired tape friction within the head.

Heat source

The heat source is mounted directly onto the placement head and moves along with it during lay-up. It heats the tape material and / or substrate laminate before it is compacted by the consolidation roller. Depending on the power of the heat source and temperature needed for polymer bonding, the heat source fully or partially melts the thermoplastic composite tape and substrate laminate. Different types of heat sources are used for heat transfer by convection, radiation, contact heating or heating by ultrasonic vibration. The most common types for TP-AFP are described in more detail in section 2.1.3. Depending on the machine manufacturer's concept the heating location and heating length of the composite vary.

2.1.2   AFP machines

Thermoplastic-AFP as well as Thermoset-AFP (TS-AFP) heads can be designed in accordance with multiple requirements e.g. lay-up rate, part complexity, lay-up accuracy or heating system. Many TP-AFP machines are variants derived from TS-AFP designs. Some placement heads are capable to process both types of material after minor modifications.

The four main characteristics of AFP machines are the following:

Multitow / singletow lay-up

Lay-up heads can process one or more tapes simultaneously. Tape width as well as number of simultaneously processed tapes are a key factor to influence the lay-up rate. Heads with narrow tapes or a small number of tapes can produce more complex parts, while the lay-up rate is reduced. AFP heads are available from one to 32 tapes to be placed along one lay-up path. Each tape has its own tape feed and cutting unit, while a single heating unit heats homogeneously over the width of all tapes. Also, the compaction unit is as wide as the overall lay-up width. Some AFP heads are additionally capable of bidirectional lay-up. This means the head can lay-up material in two directions, forward and backward. This reduces nonproductive time of the AFP head.

Kinematic system

The placement head moves along the lay-up path relative to the tooling with the help of a kinematic system. Depending on the size and geometric complexity of the parts to be manufactured, different kinematic systems are used.

The first AFP systems were based on NC-machines and used either gantry or column type layouts. Both types use up to six-degrees of freedom, while column type machines often use an additional rotating lay-up tool (Fig. 2-5). As it can be seen in the pictures below, these type of machines require a big workshop with a suitable fundament.
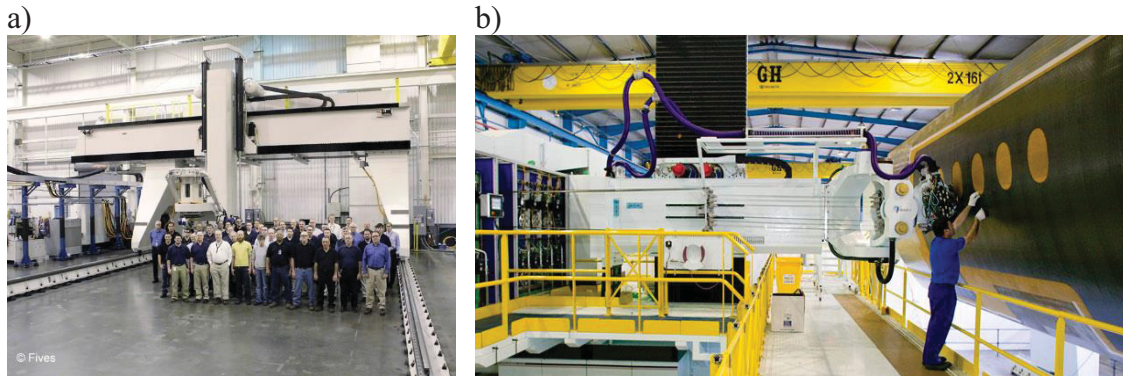
Fig. 2-5:   **Gantry and column type AFP machines**
a)   Fives Cincinnati Gemini: gantry type AFP machine [13]
b)   MTorres column type AFP machine [14]

With a wider use of industrial robots in various applications, their use for AFP machines increased as well. They are valued for their high flexibility and low investment costs. With the use of external linear and rotating axes, the size of robot based production cells can be as big as for gantry or column type machines (Fig. 2-6). On the other side, small robotic AFP machines became also affordable to research institutes, which boosted research opportunities in the field of AFP.
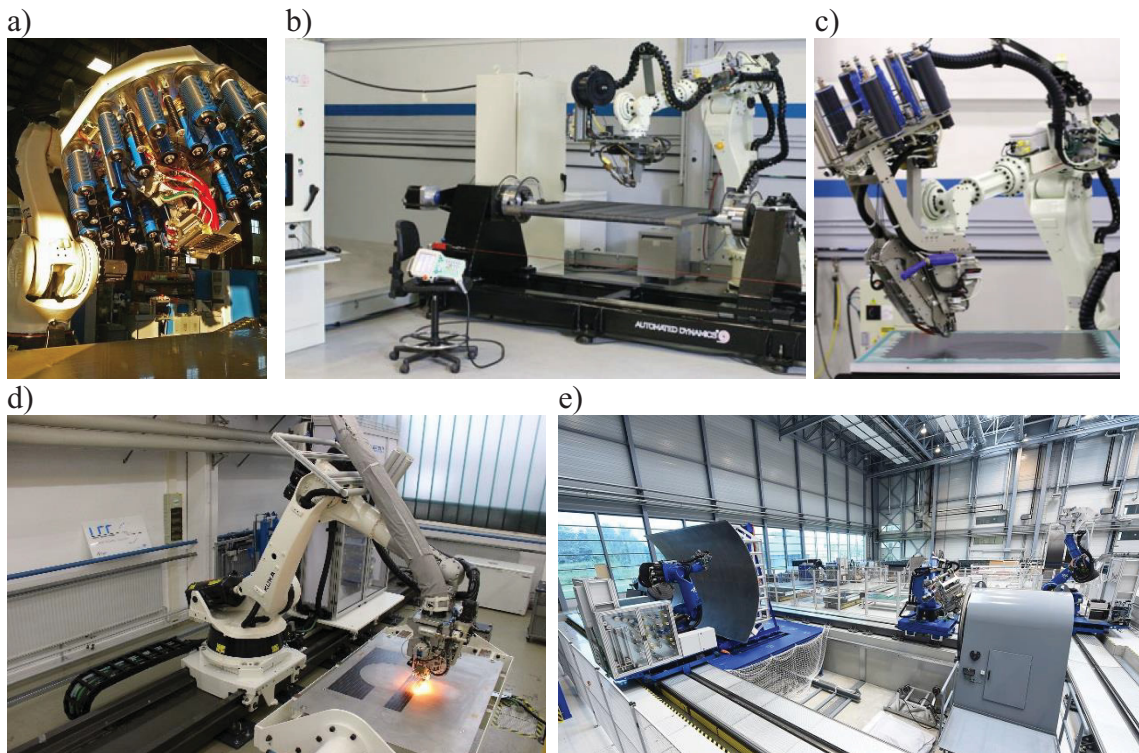
Fig. 2-6:   **Robot based AFP machines**
a)   Electroimpact AFP head on a robot [15]
b) & c)   Automated Dynamics placement cell and head detail [16]
d)   Robot based TS-AFP machine at TUM by Coriolis Composites SAS
e)   DLR ZLP: GroFi robot based AFP center [17]

Material storage at head / cabinet

As shown in Fig. 2-6 the composite tape material can be stored directly at the placement head (picture a, b and c) or in a nearby cabinet (d and e). Tape storage directly at the placement head leads to less complicated machine design and faster material spool exchange. In the second case, the tapes need to be guided to the nip-point from distance without damaging it. In advantage, the tape placement head can be designed smaller with less weight. This enables lay-up of more complex geometries. More material can be installed in the machine at a time. In case of thermoset material it can be cooled for longer shelf life while it is in the cabinet.

Programming

AFP machines can either be programmed using the hardware manufacturer's software or by third party software. Some machines can only be programmed with the software from the hardware manufacturer, some hardware manufacturers rely completely on third party software specialists (Tab. 2-1). Starting with the composite lay-up design, a digital ply book is generated on top of the tool surface and the kinematic movement of the whole system is calculated. A kinematic simulation of the lay-up can be performed to avoid machine collisions.

Tab. 2-1: AFP hardware manufacturers and programming software

AFP hardware manufacturers	Corresponding in-house programming software
Automated Dynamics	FPM – Fiber Placement Manager
AFPT GmbH	-
Coriolis Composites SAS	CADFiber, CATFiber
Electroimpact	-
Fives	ACES - Advanced Composites Environment Suite
Ingersoll Machine Tools, Inc.	iCPS, CPS2
Mikrosam A.D.	MikroPlace
M.Torres Diseños Industriales S.A.U	TORFIBER, TORRESFIBERLAYUP

AFP software manufacturer	Corresponding software
Autodesk Inc.	Truplan
Cevotec GmbH	Tape Artist, Motion Artist
CGTech Inc.	VERICUT Composite Programming / Simulation
SWMS GmbH	Tapestation
Seifert and Skinner & Associates Inc.	ComposiCAD
Siemens AG	Fibersim

2.1.3   Material heating for TP-AFP

A main process during AFP is the heat introduction into the composite prepreg tape during lay-up. In TS-AFP the thermoset prepreg tape is heated to increase the tack, so it will stay in place when deposited. State-of-the-art TS-AFP machines use infrared heating lamps. Typical process temperatures are around 50 °C to 70 °C [1, 18, 19]. Calawa and Nancarrow estimate a power density of 3.8 W/cm² sufficient for high speed (850 mm/s) lay-up, when neglecting conductive and convectional energy loss [20]. After lay-up, a cure and consolidation step in an autoclave or oven under vacuum is required.

In contrast to thermoset prepreg tape, thermoplastic tapes are non-tacky and need to be molten for fusion bonding to the laminate. Thus, processing temperatures, depending on the matrix system, are between 200 °C and 600 °C [21, 22]. Following Calawa's and Nancarrow's estimation [20], a mean power density of 111 W/cm² is necessary to heat up thermoplastic prepreg from room temperature to 400 °C for the same lay-up speed.

While few investigations used infrared heaters for thermoplastic lay-up [23, 24], most researchers used either hot gas, open flame or different types of lasers as a heat source. These systems provide higher heat flux compared to infrared (IR) heaters. Schledjewski compared IR, hot gas and flame heating systems by achievable wedge peel force of CF/PEEK laminates [25]. Detailed comparisons of heating systems can be found in [26, 27].

Hot gas (Fig. 2-7) and open flame systems were historically preferred over lasers due to their easy implementation, lower investment costs and wider spread heating area. In comparison to laser systems the heat input is less focused, which decreases the process sensitivity to heater orientation [26]. However, the heat input into the composite tape is limited by forced convection [28]. Heat transfer can be adjusted by either gas or flame temperature or convectional speed of the gas. Both aspects can interfere with the tape and lead to unintended heating of placement head components. As a consequence the limited heat transfer reduces the maximum placement speed of the whole TP-AFP machine [29]. Neitzel et al. [30] name a power density of 200 W/cm² to 300 W/cm² and an efficiency of 3 % to 5 % for hot gas systems and a power density of 300 W/cm² to 450 W/cm² with an efficiency of 4 % to 6 % for flame heating systems.
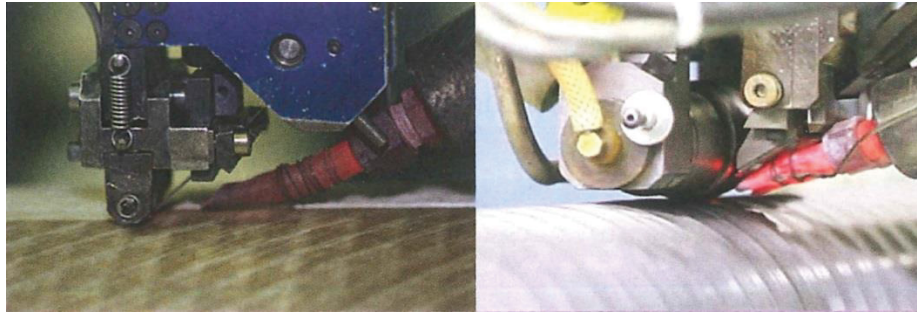
Fig. 2-7:   **Two generations of hot gas heating by Automated Dynamics [31]**

In 2009, Schledjewski and Miaris conducted a cost-efficiency analysis of different heating systems [32]. The most important criteria identified was the maximum available power of the heating system. Based on the comparison, the authors chose a CO_2 laser for specimen manufacturing on a TP-AFP test rig and varied laser power, laser spot distribution, laser angle of attack and laser spot size. Other researchers used CO_2 lasers as well, especially in the 1990s. Due to their big size, CO_2 lasers cannot be mounted directly to the placement head [27, 33]. The CO_2 laser's long wavelength of around 10.6 µm impedes the laser beam to be transferred by laser light cable to the placement head [29]. It has to be transferred to the nip-point by a system of mirrors.

CO_2, Nd-YAG and diode lasers provide the highest heating efficiency, as energy absorption of the carbon prepreg tapes is very high within their wavelength. CO_2 laser radiation is absorbed by the polymer matrix at the surface of the tape. The carbon fiber reinforcement within the tape absorbs the near infrared radiation of Nd-YAG and diode lasers [9]. Nd-YAG lasers have an electric-optical efficiency of 2 % - 3 %, while for CO_2 lasers the efficiency is between 10 % and 25 % [27]. The highest efficiency is reached by diode lasers with about 30 % to 50 % electric-optical efficiency [34, 35].

Diode lasers attracted interest, as they are scalable and became more cost efficient. Current systems are available up to 25 kW [35]. A big advantage of diode lasers is that the laser beam, with a wavelength of 900 nm – 1080 nm, can be transferred to the placement head by light cable. At the placement head, compact laser optics form the laser spot (Fig. 2-18). The size of the spot can be adjusted by choosing suitable optics according to the tape width. Different laser spot sizes are used in literature. The laser spot is typically wider than tape width, resulting in an overshoot of 5 % to 10 % [27]. The laser spot height varies from 8 mm to 57 mm in a plane perpendicular to the beam's axis at focal distance [22, 36]. The laser spot height determines the heating time of the tape material as it passed through the laser spot. A detailed overview of laser systems used in publications can be found in [37].

Besides the high energy intensity the biggest advantage of laser heating systems is the fast response time within milliseconds. Hot gas and open flame systems can react to process changes within 1 s to 15 s and infrared heaters within 1 s to 5 s [38, 39].

Combined with a temperature measurement system an online closed loop control of the process temperature can be implemented for laser heating systems. First described in 1991 by Zaffiro in a patent [40], Kölzer implemented such a system for a diode laser placement head in 2008 [27]. In addition to the laser power closed loop control, he added a closed loop control to adjust the laser spot distribution between incoming tape and substrate laminate (Fig. 2-8). He achieved to keep the temperature within ±5 % with respect to the set-point temperature.
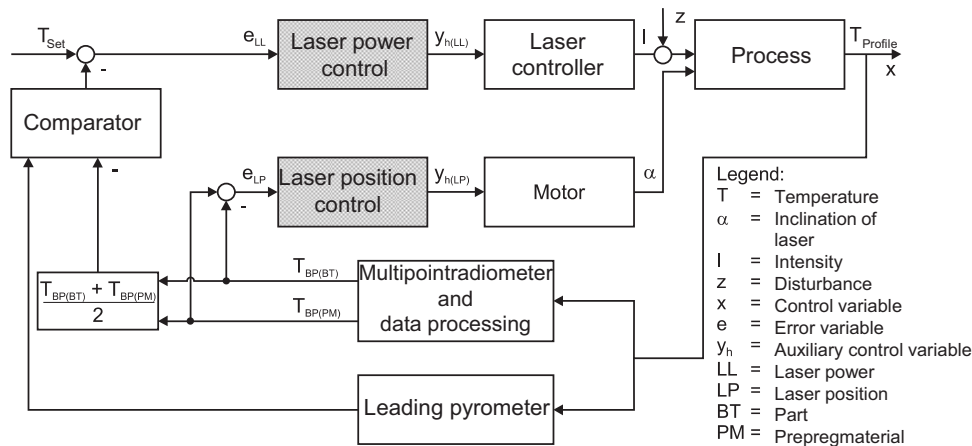
Fig. 2-8:   Closed loop control for laser power and distribution by Kölzer, according to [27]

AFPT GmbH uses such a closed loop control system for their machines. Grouve [21] and Stokes-Griffin [8] used a laser assisted machine from AFPT GmbH, similar to the one used in this thesis (section 2.4). Schaefer used the exact same machine at TUM [41].

Most TP-AFP machines, regardless of hot gas, flame or laser heating system, use a nip-point heating strategy. That means the heat source is aiming at the nip-point right before the material is compacted by the roller (Fig. 2-9). This way both joining partners are heated at the interface of the future bond. As heating takes place at the bonding surfaces, thick tapes can be processed as well. Some machine concepts use additional preheating of the tape and secondary heating at the nip-point to reach the final processing temperature [29, 42].

The most common heating type is nip-point heating, where the laser spot is projected into the wedge, formed between incoming tape and substrate laminate before the nip-point. The laser angle of attack, beam divergence and roller diameter determine the actual shape of the heat affected zone (HAZ), see Fig. 2-9.
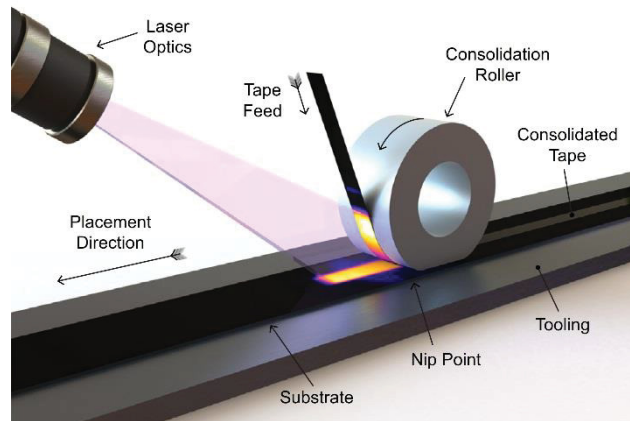
Fig. 2-9:   **Heat affected zone (HAZ) in the wedge between incoming tape and substrate laminate [43]**

EADS-France [44] developed another concept, using through thickness heating of the incoming tape and two compaction rollers (Fig. 2-10). The tape material is heated in between the two compaction rollers from the top. Thus, the heat has to be conducted through the incoming tape to reach the bonding surfaces.
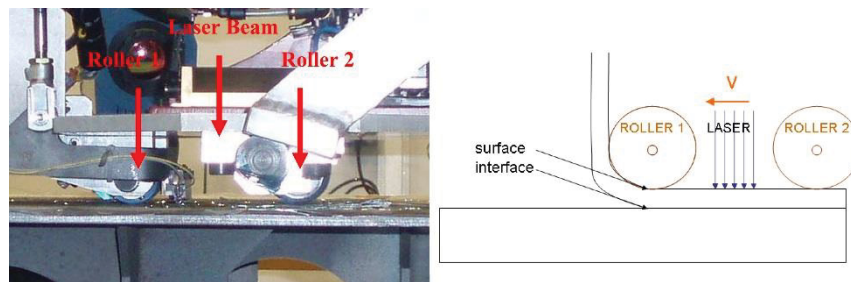
Fig. 2-10:   **Placement head and principle of EADS-France's through thickness laser heating [44]**

Fokker developed an AFP head with ultrasonic vibration activation for preliminary tacking of the tapes. After lay-up, the stack has to be consolidated in an autoclave to achieve full strength [45, 46].

Other heating systems have recently been developed and are in the early stages of implementation to research AFP systems. Heraeus Noblelight GmbH developed a pulsed light heat source with a prism-like light enclosure until right before the nip-point (Fig. 2-11, left). Heraeus claims the same fast controllability and similar energy intensity but lower investment costs compared to laser heating systems, especially regarding safety measures. [47, 48]

Philipps GmbH has developed vertical cavity surface emitting lasers (VCSEL), a semiconductor module consisting of a multitude, up to several thousands, of small radiation sources (Fig. 2-11, right). The VCSEL chips emit in a similar wavelength (808 nm) as diode lasers and achieve similar heating efficiency for carbon fiber tapes. Instead of using homogenizing optics, the VCSEL module can be mounted directly under the placement head. VCSEL technology promises a locally adjustable laser spot and heating profile, as the power of the miniaturized radiation cells in a module can be

adjusted independently. Thus, the heat distribution in the HAZ can be controlled electronically within milliseconds. No optics need to be moved mechanically, as each VCSEL cell has its own micro lens. [49–53]
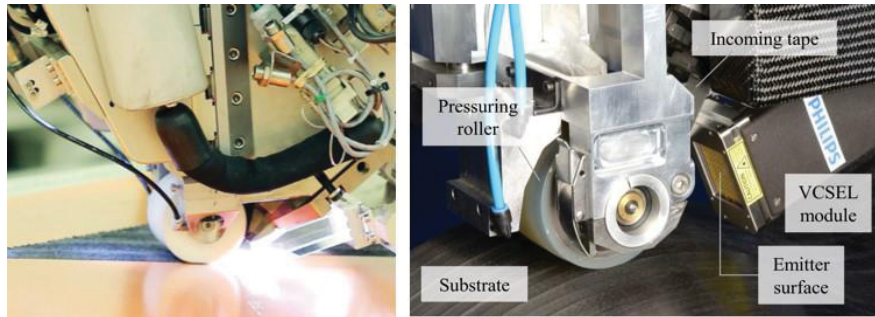
Fig. 2-11:   **Humm3 heating device by Heraeus Noblelight GmbH (left) [48], and VCSEL emitters by Philipps GmbH [49]**

2.2 In situ consolidation during TP-AFP lay-up

Two different process routes were developed for Thermoplastic-AFP. One follows the same route as already established for Thermoset-AFP. Composite lay-up and consolidation are separated into subsequent process steps. During lay-up the tapes are deposited and preliminary joined by the placement head. After lay-up the whole laminate stack gets prepared for hot-press, oven or mostly autoclave consolidation, where the full bonding is achieved. Same as for the initial lay-up this second post consolidation step requires higher process temperatures than for thermoset composites. Autoclaves with a maximum temperature of up to 420 °C [54] are used.

The second TP-AFP processing strategy is to reach full consolidation already during lay-up. This "in situ consolidation" requires no subsequent additional consolidation step. In situ processing can reduce processing time and costs, as well as investment costs for the autoclave and additional high temperature autoclave tooling. In addition, the effect of thermal expansion is minimized though still present. In contrast to autoclave consolidation, only a small part of the laminate heats up at a time. This reduces the overall thermal expansion of the laminate and tooling during processing [55].

On the other hand, processing is more challenging, because both the placement process and the bonding process of the thermoplastic polymer matrix need to be within their individual tolerance to achieve a competitive laminate quality. Lay-up faults, e.g. due to insufficient heating or overheating, lead to bad bonding and laminate quality that cannot be compensated afterwards. Another challenge is the limited heated time of the material, as it passes the placement head. As matrix flow is limited, it is not possible to eliminate voids within the tape during lay-up. Thermoplastic composite tape development for in situ consolidation is still under development [56–59] (see also section 2.3). The faster cooling results in a lower crystallinity content of the thermoplastic matrix within the tape [60, 61]. This inner structure of the matrix influences its chemical, thermal and structural behavior, as well as residual stress development.

Reaching excellent laminate quality by in situ consolidation attracted attention of many researchers. Both experimental as well as simulation work was carried out to determine the best process parameters. A detailed review of the TP-AFP simulation publications is given in section 4.1. This section concentrates on literature review of experimental studies. Process development started with flat laminates and tube-structures. For these simple part geometries, the process is a quasi-steady-state process with respect to material flow and the placement head. Thus, process conditions like heating, cooling and compaction, can be optimized more easily. Bad laminate quality at start and end can be trimmed after the lay-up is completed.

2.2.1 Experimental work

A mechanical comparison of hot gas produced specimens and autoclave reference specimens from CF/PEEK is presented by Qureshi et al. in [28]. Two different hot gas nozzles with varying nitrogen gas flow were examined. Additionally, samples produced by a laser heating system were also compared via interlaminar shear strength (ILSS). The hot gas samples reached 55 % and the laser produced samples reached 85 % of the autoclave samples during ILSS testing. The inconsistent and low heat flux of the hot gas torch is considered as the main reason for this difference. It is also identified as a limitation for higher process speed. From the pictures in [28] it is assumed that a metal roller with a diameter of 12 mm, similar to Fig. 2-7, left, was used. This roller was heated by the hot gas torch as well causing lay-up problems.

Lamontia presents a comparison of mechanical properties achieved by an Accudyne Inc. in situ TP-AFP capable lay-up head, and an autoclave consolidated laminate for CF/PEEK [58]. The Accudyne system has a multitude of gas torches for heating and segmented compactors for an adjustable heating and cooling profile (Fig. 2-12). The compression values of the in situ processed specimens are 3 % to 11 % lower than autoclave consolidated specimens.
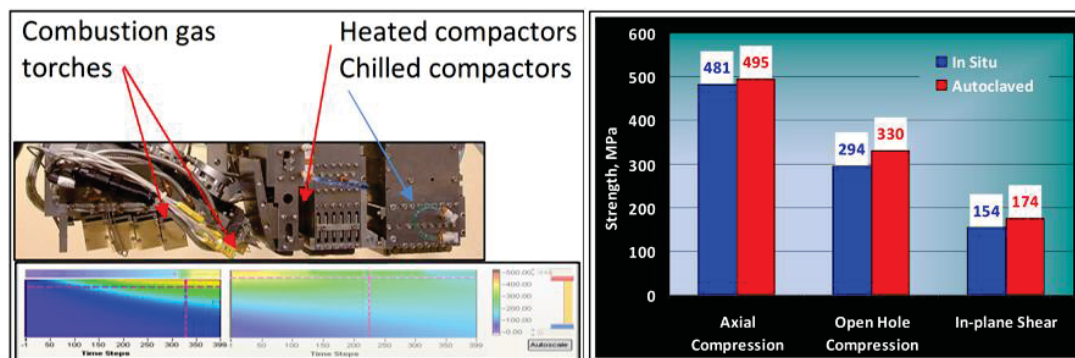
Fig. 2-12: **Accudyne Inc. placement head with heating and cooling zones (left) and comparison of compression and shear properties achieved by in situ and autoclave consolidation (right) [58]**

Brecher et al. compare CF/PEEK samples, manufactured by IR and laser heat source, via micrographs [62]. Samples manufactured by laser show a more homogeneous inner structure with less voids. Brecher et al. also compare CF/PEEK samples, manufactured by open flame heater and laser irradiation by the means of wedge peel test. The laser manufactured samples show more than double peel force compared to the open flame specimens. It has to be noted, that the laser processed specimens had 55 % fiber content, while the open flame specimens had 60 % fiber content. This can influence interply bonding and peel force.

Schledjewski and Miaris [32] investigated the influence of different process parameters for laser assisted TP-AFP. They state that a 60 % / 40 % laser spot distribution in favor to the incoming tape can result in 94 % three-point-bending strength compared to autoclave manufactured samples.

Similar results are reported by Henne et al. [10] for CF/PPS for a laser assisted TP-AFP machine using a closed loop temperature control by AFPT GmbH. Compression values are about 4 % less than reference hot press consolidated specimens. This is mainly due to the higher void content, which cannot be healed completely during the short time of the polymer in a melt state during TP-AFP lay-up. In situ processed specimens show a void content on par with the initial tape material, while the hot press can remove almost all voids during consolidation. It is concluded that an optimized in situ TP-AFP process does not introduce additional voids at the bond interface between the plies, but cannot heal intraply voids.

Comer et al. compare CF/PEEK laminates produced by laser assisted in situ TP-AFP and autoclave post consolidation by means of wedge peel test, interlaminar shear strength (ILSS), three-point-bending and open hole compression tests (OHC) [63]. The in situ TP-AFP samples are superior in interlaminar bonding (wedge peel test) but reach only 68 % to 78 % in the other tests. The authors conclude that the crystallinity of the in situ TP-AFP samples was below optimum and the void content was too high. Therefore, further process and machine optimization is necessary to reach autoclave similar laminate quality.

Comer et al. [60] and Henne et al. [10] compare the interlayer bonding quality by wedge peel tests for CF/PEEK and CF/PPS laminates produced by in situ TP-AFP and post consolidated laminated in an autoclave or oven. Radlmaier et al. [61] compare the Mode I interlaminar fracture toughness G_{Ic} of CF/PPS laminates in reference to laminate cooling rate during manufacturing. The consequent crystallinity is correlated to the fracture toughness. G_{Ic} fracture toughness, wedge peel strength and crystallinity ratio are investigated for TP-AFP in situ consolidated CF/PA6 in [41]. In all studies a correlation between cooling rate and thus crystallinity development and peel force or fracture toughness is discussed. TP-AFP laminates with in situ consolidation feature the fastest cooling rate and highest peel forces or G_{Ic} values as crystallinity is low.

Lay-up speed of up to 400 mm/s showed no significant decrease on short beam strength of in situ processed carbon fiber/PEEK samples or interply shear strength [21, 64]. For cylindrical winding Funck states a possible winding speed of up to 2666 mm/s [38]. However most investigations for in situ consolidation are conducted at lower processing speed, mainly between 30 mm/s [58] and 100 mm/s [28, 32, 60].

A major process improvement was achieved by implementing a closed loop control for the fast response laser heat source. This way the processing temperature is kept more constant despite placement changes (speed and acceleration), machine changes (tape width, change of optics or its position) and raw material quality variations (voids, fiber matrix distribution). Such a closed loop control was first described in [40] and later developed by Kölzer [27] and is now implemented in TP-AFP systems e.g. by AFPT GmbH, Fraunhofer IPT and Automated Dynamics Inc. [65, 66].

2.2.2 Application and demonstrators

In 2013 Automated Dynamics Inc. presented a 3D stiffened helicopter tail boom, manufactured by a hot gas TP-AFP machine with in situ consolidation [67]. Furthermore, the stiffeners were also bonded to the skin during placement. The 3D curvature of the part is rather moderate and shows soft transitions between the sections (Fig. 2-13). This demonstrator shows the potential for aerospace application. CF/PEEK material was used for the demonstrator.
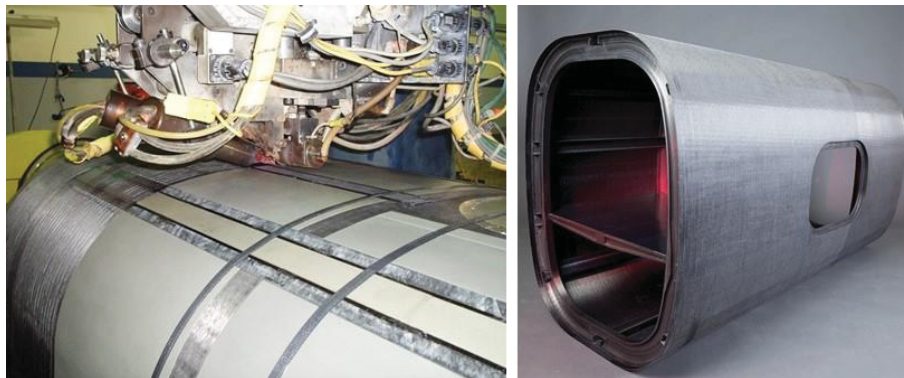
Fig. 2-13: **Automated Dynamics Inc. in situ placement head manufacturing a helicopter tail boom demonstrator [67]**

Another example of the technology's capabilities is presented in Henne et al. [10] for space applications. Two pressure vessels of up to 2.5 m length and 1.3 m diameter were manufactured by TP-AFP with in situ consolidation from CF/PPS (Fig. 2-14). In total more than 50.000 tapes were placed in more than 300 layers without any process malfunctions.
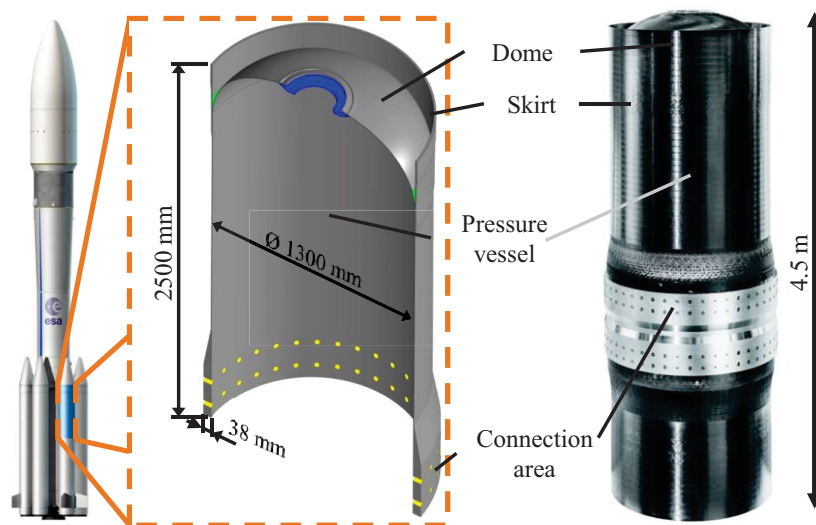
Fig. 2-14:   TUM Booster demonstrator manufactured by TP-AFP with in situ consolidation [10]

Thermoplastic composites and TP-AFP with in situ consolidation are not established in the industry, yet. However, it is in the focus of the aerospace industry, as the big number of demonstrators in the CleanSky1&2 and Horizon 2020 funding schemes of the European Union show. The projects DEfcodoor, DISACOP, ISINTHER, OUT-COME and INSCAPE, for instance, aim for primary aircraft structures from TP-AFP with in situ consolidation [68]. A first in situ consolidated full carbon structure is planned to be launched into space in 2019. A segment of a research rocket is developed by TUM in the COPRAS/TESOS project, funded by DLR within the REXUS programme.

2.3 Carbon fiber reinforced thermoplastic (CFRTP) tape material

Composite tapes for TP-AFP consist of thermoplastic matrix and reinforcing fibers. Typically, carbon fibers are aligned in production direction of the tape, resulting in unidirectional reinforced tapes. Tapes are provided by manufacturers with different matrix types and different fiber volume fractions, typically around 50 %. The tapes are produced in a steady-state impregnation process from polymer melt and powder or solvent, depending on the matrix polymer. After manufacturing, the tapes are cut into the desired width. These tapes are called "slit tapes". In contrast, "tow pregs" are manufactured in the final TP-AFP processing width, but may be less accurate with respect to tape with and fiber matrix distribution. An overview of the thermoplastic prepreg tape production techniques can be found in [26, 27, 69].

Tape properties, determining the capabilities for in situ processing during TP-AFP, are fiber-matrix content and distribution and void content. All three properties can be evaluated by micrographs (Fig. 2-15).
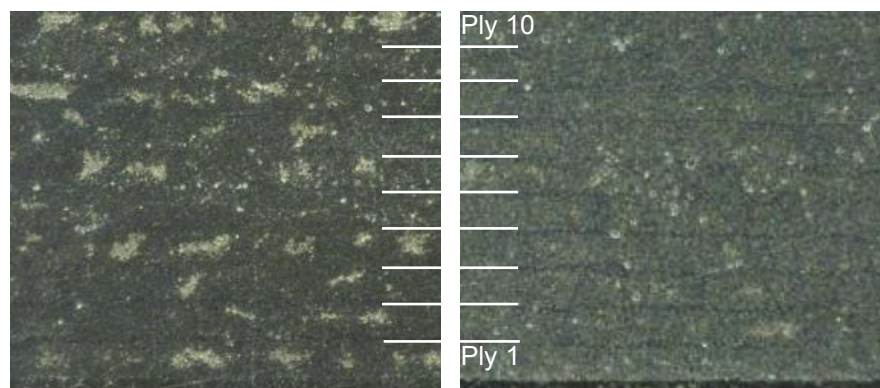
Fig. 2-15: **Micrographs of thermoplastic carbon fiber prepreg tapes of different quality [10]**
Left: high porosity within the tape material already before processing
Right: low raw material porosity, processed with the same parameters

During in situ consolidation, voids within the tape cannot be removed during lay-up, due to the short heating, compaction and cooling phases [59]. A homogeneous fiber matrix distribution in width is essential for uniform heating and good mechanical load distribution [26].

Resin rich surface of the tape is considered to help in situ bonding of good quality laminates during TP-AFP [28, 56, 57]. Gruber et al. [57] give detailed recommendations for an in situ capable thermoplastic prepreg tape, derived from experiments with an Accudyne Inc. TP-AFP machine (Tab. 2-2):

Tab. 2-2: **Thermoplastic carbon fiber tape recommendations for in situ consolidation, according to [57]**

Description:	Value:
Fiber areal weight:	145 g/m²
Resin weight fraction:	35 % ±1 %
Uniform fiber/resin distribution	-
Surface resin content thickness:	~ 7 μm (one carbon filament diameter)
Thickness variation:	< 6 %
Width variation:	+0.00 mm to -0.10 mm
Void content:	<1 %

Further criteria like uniform tape thickness and width, edge quality and surface roughness are described in [7, 26, 70].

Most researchers use CF/PEEK (e.g. APC2 from Cytec) as it has been available for a long time and is of big interest of the aerospace industry [8, 25, 27, 43, 58, 59, 62–64, 71–73]. But also carbon fiber tapes with PPS, PES, PEI, PA and PP are in the focus of research [41, 55, 61, 74].

In chapter 3, the CF/PES tapes from Suprem SA and CF/PA6 tapes from Celanese GmbH are described and analyzed in detail. Material characterizations of optical and thermal behavior are conducted in order to simulate the tapes' thermal history during TP-AFP processing. Micrographs of unprocessed tape and manufactured laminates are shown, too.

2.4 TP-AFP system used in this thesis

The experimental work in this thesis was conducted with a state-of-the-art TP-AFP system from AFPT GmbH (Dörth, Germany). The placement head is mounted on a standard industrial robot and uses a diode laser for heating. Fig. 2-16 shows the overall system and the placement head in detail.
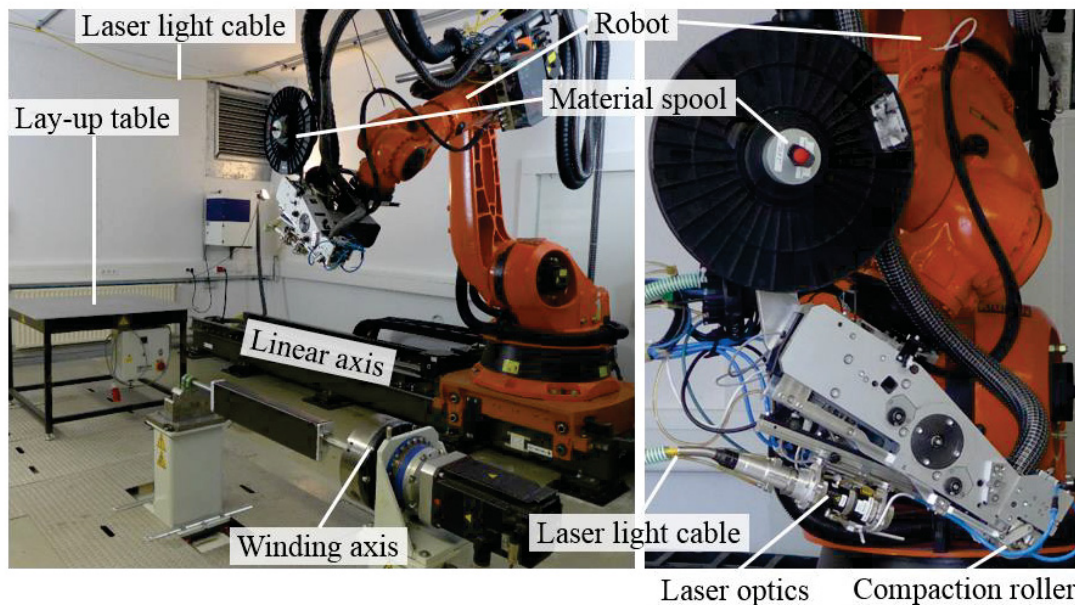
Fig. 2-16:   TUM TP-AFP system from AFPT GmbH and its main components

The TP-AFP system consists of several components that are described in the following sections. All components communicate with each other by an industrial control PC.

2.4.1 Tape laying head with closed loop control

The tape laying head was developed by AFPT GmbH and installed at TUM in 2012. It is a single tape laying head and can process tapes from 6 mm to 55 mm width. Different standard laser optics can be mounted to the placement head to form a rectangular laser spot with a homogenous laser output intensity. The laser optics are pivot-mounted underneath the placement head, so that the laser spot distribution between incoming tape and substrate laminate can be adjusted during processing. By hand, the optics can be moved towards or away from the nip-point on a track in order to adjust the laser spot height and width according to the tape width.

A specialty of AFPT's system is the integrated temperature control by a closed loop control (CLC) system (Fig. 2-17). It is based on Kölzer's PhD thesis [27] at Fraunhofer IPT Aachen. The closed loop control uses a calibrated infrared (IR) camera to measure the temperature distribution within the laser spot around the nip-point area. A control unit (industrial control PC) interprets the data and adjusts the laser power and the laser optics orientation. By this, the maximum temperature within the laser spot is kept at the user set temperature and the temperature difference between the incoming tape and the substrate laminate is minimized. The IR camera measures the black body (emissivity = 1.0) temperature and not the actual temperature of the composite. The actual temperature of the composite can be calculated during post processing with the material, temperature and view of angle dependent emissivity coefficient.
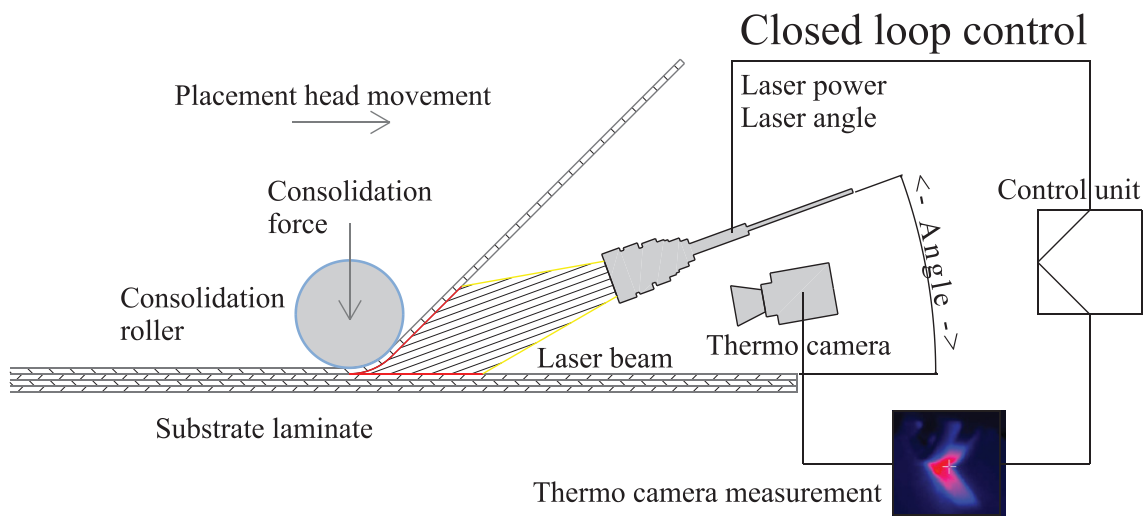
Fig. 2-17:   **Principle the closed loop control by AFPT GmbH**

Despite this closed loop control, the machine can also operate with fixed laser power and fixed laser optics orientation.

Laser power, optics orientation and infrared thermal camera data, as well as other sensor data of the tape laying head, are displayed live during lay-up in the graphical user interface of the control software and as value over time diagrams. This enables live interpretation of the process by the user. The data can be stored after lay-up for post processing and further interpretation.

TUM's TP-AFP system is capable of start to end consolidation. The placement head can perform track start and cutting at full typical lay-up velocity [12].

The machine uses a conformable silicone roller for compaction after nip-point. A silicone roller with a water-cooled aluminum core can be additionally cooled from the outside by pressurized air. This enables high endurance and constant process conditions even for long lay-up durations [10]. Consolidation force can be pneumatically adjusted with a limit of 750 N.

2.4.2   Kinematic system

The tape laying head is mounted on an industrial robot from KUKA AG (type: KR180-2 series 2000, running on KR C V5.6.10). The robot is mounted on a 3.5 m long linear track (type: KL1500-3). For winding or mixed winding - AFP processing an external rotating axis is installed (compare Fig. 2-16). All eight axes can move simultaneously. During lay-up, the tool center point (TCP) of the robot is set to the midpoint of the compaction roller's area that is in contact with the tool or laminate. The robot permanently sends the TCP's coordinates (x-y-z values) to the control PC.

2.4.3   Laser heating system

An LDF 4000-100 diode laser from Laserline GmbH (Mülheim, Germany) is used as a heat source. The laser consists of one diode stack with 1030 nm and two diode stacks with 1060 nm wavelength. The maximum output power of the laser is 4400 W.
The laser beam is guided from the laser to the placement head via laser light cable. Homogenizing optics transform the laser beam to a rectangular shape with almost homogeneous intensity (Fig. 2-18). This type of homogenizing optics is widely used in industry as they are robust and scalable in laser power and spot size. The efficiency is around 90 %. Due to their internal water-cooling, they are suitable for continuous use [75].
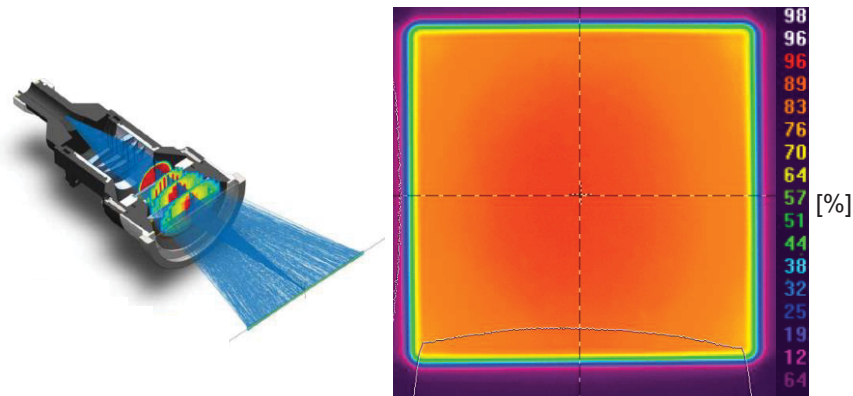
Fig. 2-18:   **Inner structure of laser homogenizing optics (left) [75] and measurement of laser spot intensity by Laserline before delivery to TUM (right)**

The laser beam shows a divergent behavior with a most sharp laser spot in focal distance of the optics.

3 CFRTP tape material characterization for thermal simulation[1].

For a deeper understanding of the process and to be able to model the TP-AFP process in a thermal simulation (chapter 4), the optical and thermal material properties are studied. Both, absorptivity and reflectivity of the tape material are dominant material properties that characterize the heat input from the laser. Subsequently, the heat spreads throughout the laminate. The material properties to describe this effect are specific heat and thermal conductivity within a ply and in between neighboring plies. In the next sections, experimental work is described which shows how to measure these properties directly from the composite tape. The experimental data are compared to models from literature, which calculate the composite's properties from its components.

Two types of unidirectional carbon fiber tapes are investigated in this thesis. Carbon fiber (CF) tapes with Polyethersulfone (PES) and Polyamide 6 (PA6) matrix are used for the experimental studies.

CF/PES tapes from Suprem SA (Yverdon-les-Bains, Switzerland) with the name "Suprem™ T 55% AS4 / PES-4100 0.14 x 25.4" are used. The tow preg tape has a fiber volume fraction (FVF) of 55 %. Four 12k rovings of unsized "AS4" carbon fibers are directly impregnated with "Sumikaexcel PES 4100 MP" to a 25.4 mm wide tape. The thickness is typically 0.14 mm. PES is a fully amorphous polymer.

The CF/PA6 tape is manufactured by Celanese Cooperation (Sulzbach, Germany) and is called "Celstran® CFR-TP PA6 CF60-01" [76]. This tape is manufactured in 275 mm width and is then slit into 12 mm width. Exact polymer and carbon fiber type are unknown. Mechanical properties indicate a high tenacity carbon fiber is used. The tape has a FVF of 48 % and a nominal thickness of 0.13 mm. PA6 is a semi-crystalline polymer that forms both, an amorphous and a crystalline phase.

---

[1] Parts of this chapter were published in:

Kollmannsberger A., Lichtinger R., Hohenester F., Ebel C., Drechsler K.:

Numerical analysis of the temperature profile during the laser assisted automated fiber placement of CFRP-tapes with thermoplastic matrix. Journal of Thermoplastic Composite Materials, 2017, http://journals.sagepub.com/doi/10.1177/0892705717738304

Schaefer, P.M.; Gierszewski, D.; Kollmannsberger, A.; Zaremba, S.; Drechsler, K.:

Analysis and improved process response prediction of laser-assisted automated tape placement with PA-6/carbon tapes using Design of Experiments and numerical simulations. Composites Part A: Applied Science and Manufacturing 96, 2017, 137-146, http://doi.org/10.1016/j.compositesa.2017.02.008

The properties investigated in this section are used in newly developed thermal model of the process. Section 4.3 describes the thermal properties of the consolidation roller and lay-up tool and the thermal boundary conditions of the process implemented in a thermal simulation.

3.1 Optical properties

During the investigated TP-AFP process, a laser heats the carbon tapes above melting temperature through radiation. TUM's TP-AFP machine uses a laser with three diode laser stacks: one stack generates a laser beam with 1060 nm and two diode stacks operate at 1060 nm. The absorption behavior of a material determines the heat input by laser radiation. This section measures the absorptivity of the two carbon fiber tapes (CF/PES and CF/PA6) experimentally and shows the applicability of Fresnel's law.

A detailed description of the carbon fiber tape's reflection, scattering and absorption behavior can be found in [8, 43, 74].

With the help of the acquired optical material properties, the heat input can be calculated for the thermal simulation in chapter 4.

3.1.1 Introduction

The energy of the laser beam is partly absorbed, reflected or transmitted when it hits a body (Fig. 3-1).
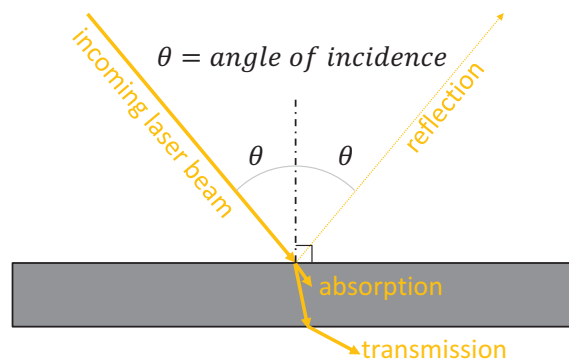
Fig. 3-1:   **Absorption, reflection and transmission of radiation**

According to Grouve [74] and Stokes-Griffin [8] the absorptivity of UD carbon fiber tapes results from the high absorption of carbon fibers and the reflectivity of the polymer matrix, covering the top surface of the tape (Fig. 3-2). Polymers have a very low absorptivity and high transmissivity in the wavelength spectrum of diode lasers.
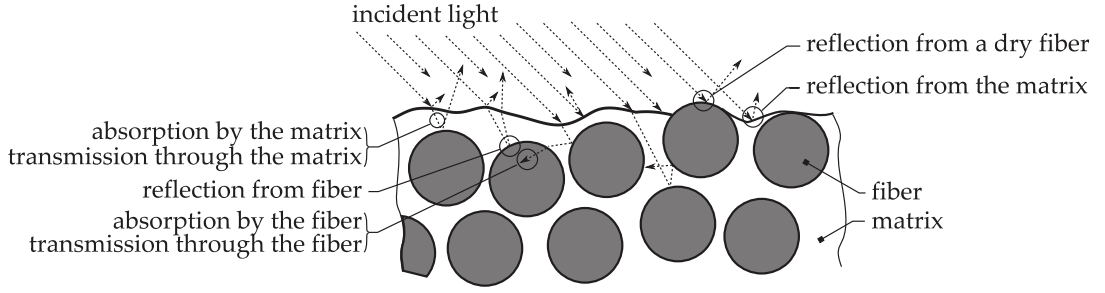
Fig. 3-2:   **Absorption, reflection and transmission of laser light on microscale for composite tapes [74]**

The law of energy conservation describes the three portions of the total laser energy hitting the composite tape:

$$\alpha + \rho + \tau = 1 \tag{3-1}$$

As described in [8, 43, 74], the transmissivity τ of opaque materials like carbon fiber tapes is zero. Thus, the absorptivity α can be described solely by the reflectivity ρ:

$$\alpha = 1 - \rho \tag{3-2}$$

Fresnel's law describes the reflection and transmission behavior of electromagnetic waves on flat surfaces. For non-conductive polymer surfaces exposed to unpolarized radiation, Fresnel's equation describes the reflectivity as a function of angle of incidence θ and refractive index n [77]:

$$\rho(\theta, n) = \frac{1}{2}\left[\left(\frac{n^2 \cdot cos\theta - \sqrt{n^2 - sin^2\theta}}{n^2 \cdot cos\theta + \sqrt{n^2 - sin^2\theta}}\right)^2 + \left(\frac{cos\theta - \sqrt{n^2 - sin^2\theta}}{cos\theta + \sqrt{n^2 - sin^2\theta}}\right)^2\right] \tag{3-3}$$

Besides the angle of incidence, the absorptivity can also depend on surface roughness, wavelength and polarization of radiation as well as material temperature.

Stokes-Griffin developed an optical model with an absorbing layer and micro half cylinder surface structure (diameter 10 μm ~ diameter of carbon fibers) to account for the scattering by rough tape surface and surface near carbon fibers. [8, 43]
Kölzer [27] investigated the temperature dependency of the absorptivity for CF/PEEK and CF/PA12 tapes. From his experimental data, he developed linear approximations:

$$\alpha_{CF/PEEK} = -0.4 \cdot 10^{-3} \cdot T\,[K] + 1.0365 \tag{3-4}$$

$$\alpha_{CF/PA12} = -0.2 \cdot 10^{-3} \cdot T\,[K] + 0.9943 \tag{3-5}$$

3.1.2   Measurement method

A Perkin Elmer LAMBDA 1050 UV/Vis/NIR spectrophotometer with an integrating sphere at Australian National University (ANU, Canberra, Australia) is used for measurements of CF/PES and CF/PA6 tapes. First, the transmissivity is tested for wavelengths from 900 nm to 1300 nm on two CF/PES samples. Second, the reflectivity is measured by using a rotatable sample mount in the center of the integrating sphere. The reflectivity is also measured from 900 nm to 1300 nm for five samples of CF/PES with an angle of incidence from 5° to 85°. Stokes-Griffin et al. measure the absorption of Celanese's CF/PA6 with the same experimental setup for 1060 nm in [78]. All measurements are conducted at room temperature with unprocessed tapes.

3.1.3   Results

Transmissivity of the tapes is measured at 0 %, as stated by Grouve [74] and Stokes-Griffin [8]. Furthermore, no significant variation is found for absorptivity in the measured wavelengths. Fig. 3-3 shows the spectrophotometer results of CF/PES and CF/PA6 for 1060 nm in comparison to the results calculated by Fresnel's equations. A refractive index of 1.65 is used for PES [79] and 1.53 is used for PA6 respectively [80]. The absorptivity is very high and constant for angles below 50°. For higher angles of incidence, the absorptivity decreases rapidly as reflectivity increases. Fresnel's equations are in line with the material behavior over angle of incidence. For both tape materials, Fresnel's equations overestimate the absorptivity for angles below 75° by about 4 % to 5.5 % and underestimate the absorptivity for higher angles.

The measured data values are summarized in Appendix a.
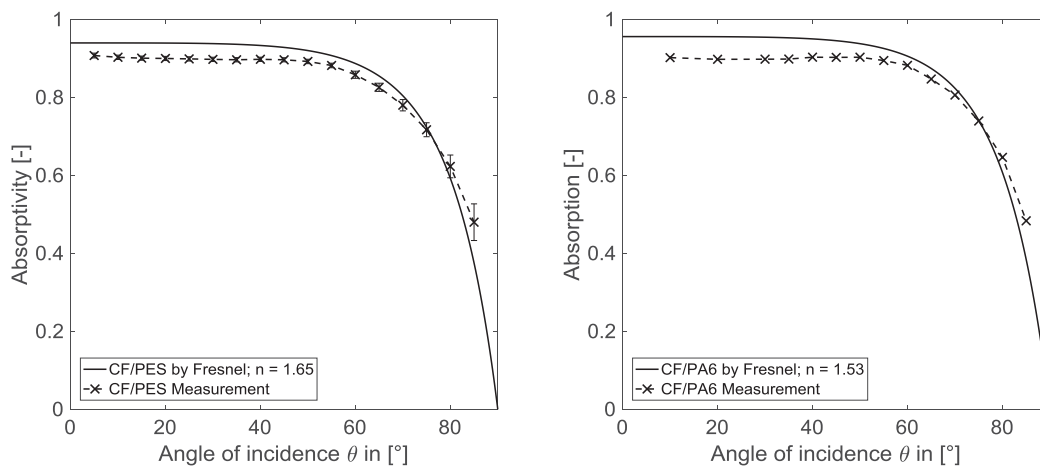
Fig. 3-3:   **Absorptivity of CF/PES tape and CF/PA6 tape from spectrophotometer measurements and by Fresnel's law**

3.1.4 Discussion

Measuring the absorptivity via spectrophotometer leads to overall high quality data of the tape's optical behavior. High accuracy is achieved for angles below 75°. The inaccuracy for high angles of incidence (see error bars in Fig. 3-3) is attributed to specimen positioning inaccuracy, as little change of the angle of incidence leads to a large change of absorptivity. The comparison of the measured absorptivity with data from Stokes-Griffin (CF/PEEK), Grouve (CF/PPS) and calculated by Fresnel's equation shows a good correlation. All absorptivity data follow the same curve over angle of incidence. The difference between Fresnel's equation and the measured values is below 5.5 %. The measurements confirm the observations of Grouve and Stokes-Griffin that the polymer matrix is determining the reflection behavior while the carbon fibers inside the tape are determining the absorption behavior.

Kölzer's linear relation for temperature dependent absorptivity of CF/PEEK, equation (3-4), is used for CF/PES and equation (3-5) is used for CF/PA6 in the thermal simulation (see chapter 4).

3.2 Specific heat

The following sections describe the importance of specific heat for the thermal simulation, followed by the measurement method via Differential Scanning Calorimetry (DSC). The measured values for specific heat of the used composite tapes are presented. Subsequently, they are compared to a model which follows the rule of mixture by using the properties of carbon fiber and of the polymer matrix.

3.2.1 Introduction

Specific heat is a material property quantifying the required energy to heat up a specific mass of a material. Alternatively, it describes the amount of energy that can be stored by a material with respect to its temperature change. Thus, sometimes it is also referred to as specific heat capacity. The SI unit of specific heat is J/kg·K. Specific heat under isobaric environmental conditions is defined as

$$c_p = \frac{\Delta Q}{m \cdot \Delta T}$$

(3-6)

ΔQ = energy difference; m = mass; ΔT = temperature difference

Specific heat of polymer composites changes with its temperature. Due to the big temperature range during TP-AFP processing from room temperature to above melting temperature, the specific heat needs to be characterized over the processing temperature range.

3.2.2 Measurement method

Differential Scanning Calorimetry is established in research and industry to measure specific heat or other thermal properties like glass transition temperature (T_g) of polymers [81, 82]. Different types of DSC measurements have been developed.

The specific heat capacity of CF/PES tapes is measured by Standl [83] via Temperature-Modulated Differential Scanning Calorimetry (TMDSC) with a Q1000 machine from TA Instruments. Three TP-AFP processed layers of CF/PES tapes from Suprem SA are analyzed. An average TMDSC heating rate of 3 K/min from 10 °C to 420 °C was used. It is modulated by a sine function with an amplitude of 1 K and a period of 100 s. Five samples are tested and the mean value is determined.

Schaefer measured the specific heat of CF/PA6 tapes from BASF with a FVF of 47 % by DSC, too but using a sapphire method to reference the measured values [41].

3.2.3 Results

The left graph in Fig. 3-4 shows the specific heat of the AS4 fiber, PES matrix and the CF/PES tape calculated by rule of mixture (ROM) and from the TMDSC measurements. It can be observed that the specific heat differs from model and measurement for lower temperatures and converges around the glass transition temperature (T_g).
The right side of Fig. 3-4 shows the comparison for CF/PA6 tapes. Values of AS4 carbon fiber, neat PA6 matrix, ROM results and the baseline from Schaefer's measurements of BASF CF/PA6 are shown [41].

For both materials the specific heat increases with increasing material temperature. Amorphous polymers like PES show a change in specific heat around T_g. Semi-crystalline polymers like PA6 typically show an endothermal peak for melting of the crystallites. After the material is molten, a linear increase can be observed. Stokes-Griffin notes that the heat flux of the heating unit during TP-AFP is much higher than the heat release due to crystallization and concludes that this peak can be neglected for thermal analysis [8]. Schaefer also neglected the peak for further analysis and derived a linear baseline, as shown in the figure.

According to Schürmann [82], specific heat of a UD layer of carbon fibers and polymer matrix can be calculated by rule of mixture with the help of the fiber mass fraction ψ:

$$c_{p\,UD\,tape} = c_{p\,Fiber} \cdot \psi + c_{p\,Matrix} \cdot (1 - \psi) \qquad (3\text{-}7)$$

Specific heat values for AS4 carbon fibers are taken from Hexcel's product data sheet [84] and are combined with the temperature dependency from Johnston [85]. For temperatures below 185 °C, Johnston's values are smaller than the ones provided by Hexcel. Therefore, Johnston's temperature dependent equation is used for temperatures above 185 °C, while the constant value from Hexcel is used for temperatures

below this. Temperature dependent values of specific heat of PES are described in [86] and of PA6 in [87–90]. The values in this thesis and in Fig. 3-4 are taken from Kaye et al. [90]. All data values of Fig. 3-4 can be found in Appendix a.
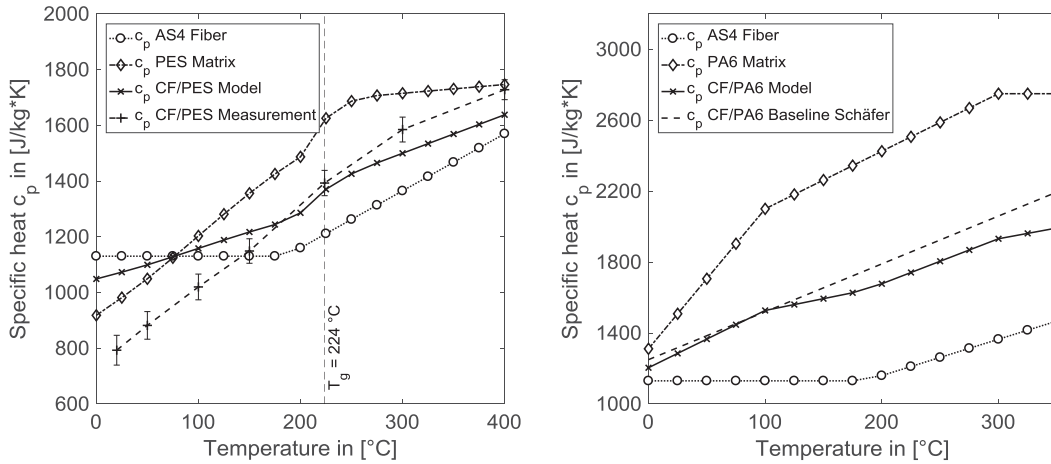
Fig. 3-4: **Specific heat of CF/PES tape [36] and CF/PA6 tape and their components**

3.2.4 Discussion

The measured and calculated values for CF/PES show good agreement from 180 °C and higher temperatures. For lower temperatures, the specific heat of model and measurement differ until they converge around 180 °C. Specific heat values of both approaches, experimental and by model will be used for further evaluation in the thermal simulation in chapter 4.

The specific heat values for CF/PA6 tape, obtained by the rule of mixture model are in good agreement with the baseline developed by Schaefer (see Fig. 3-4 right). The calculated values for the CF/PA6 are a little below the baseline. This can be explained by the higher FVF of the Celanese CF/PA6 tapes compared to the BASF CF/PA6 tape, used by Schaefer. As it can be seen in Fig. 3-4, the specific heat of carbon fibers is lower than for PA6 matrix.

3.3 Heat conductivity

Within a solid body heat is transferred by thermal conduction, driven by a temperature difference. Unidirectional carbon fiber composite tapes possess a transversal isotropic conductivity behavior. Thus, thermal conductivity has to be described in fiber direction and in transverse direction. In this section, heat conductivity measured via laser flash apparatus (LFA) and determined by models from literature is compared. The measurements were done for CF/PES for different temperatures and for CF/PA6 tapes at room temperature.

3.3.1 Introduction

Anisotropic heat transfer across a cross-section A of a solid body in steady-state systems follows Fourier's law:

$$\dot{Q} = \lambda \cdot A \cdot \frac{\Delta T}{d} \tag{3-8}$$

$\dot{Q}$ = Energy flux; λ = heat conductivity; A = cross-section; ΔT = temperature difference, d = thickness

Three-dimensional specific heat transfer for anisotropic materials can be described by:

$$\frac{\dot{Q}}{A} = \begin{bmatrix} \dot{q}_x \\ \dot{q}_y \\ \dot{q}_z \end{bmatrix} = \begin{bmatrix} \lambda_x & 0 & 0 \\ 0 & \lambda_y & 0 \\ 0 & 0 & \lambda_z \end{bmatrix} \cdot \begin{bmatrix} \partial T/\partial x \\ \partial T/\partial y \\ \partial T/\partial z \end{bmatrix} \tag{3-9}$$

For non-steady-state systems the heat energy equation, neglecting heat sinks or sources is:

$$\frac{\partial}{\partial x}\left(\lambda_x \frac{\partial T}{\partial x}\right) + \frac{\partial}{\partial y}\left(\lambda_y \frac{\partial T}{\partial y}\right) + \frac{\partial}{\partial z}\left(\lambda_z \frac{\partial T}{\partial z}\right) = \rho c_p \frac{\partial T}{\partial t} \tag{3-10}$$

ρ = material density

Besides temperature difference over distance and time and specific heat c_p (section 3.2), the main material property is heat conductivity λ.

3.3.2 Measurement method

Thermal conductivity can be measured by various methods. The measurement methods can be divided into steady-state or transient methods. Steady-state methods use the heat flux under equilibrium to calculate the thermal conductivity of the specimen according to Fourier's law, equation (3-8). Often one-dimensional heat flux experiments are used. DIN EN ISO 22007 describes different methods in detail [91]. For transient measurements, hot plate, hot wire or immersion heater methods and mostly laser flash analysis (LFA) are used [41, 92, 93].

Parker et al. presented the LFA method in 1960 [94]. The LFA method cannot measure heat conductivity directly. It determines the thermal diffusivity α of a specimen by heating it from one side with a short laser flash and measures the delayed temperature response at the specimen's backside. Thermal diffusivity is calculated with specimen thickness d and half-time of the backside's temperature rise $t_{1/2}$:

$$\alpha = 0.1388 \, \frac{d^2}{\pi^2 \cdot t_{1/2}} \tag{3-11}$$

The thermal conductivity of a specimen can then be calculated with the help of specific heat c_p and density ρ according to:

$$\lambda = \alpha \cdot \rho \cdot c_p \tag{3-12}$$

It is not important to know the exact amount of laser pulse energy that is heating the specimen at the front side for the analysis of the LFA measurements.

Fig. 3-5 shows the sample preparation procedure for in-fiber direction conductivity measurements of CF/PES samples. The sample size for in-fiber heat conductivity is 10 x 10 x 1 mm. UD stripes with 7-layers are laid down by TP-AFP with the machines closed loop control (Fig. 3-5 a). These stripes are cut, stacked and post consolidated in a hot plate under vacuum (Fig. 3-5 b and c). A compression mold is used on top of the seven-layer stripes to achieve a rectangular cross-section (Fig. 3-5 d). Post consolidation is done at 400 °C for approximately 20 minutes. In total 84 layers are stacked and post consolidated to one brick. Slices of 1 mm thickness are cut by a water-cooled diamond saw. These slices are then cut to 10 x 10 mm to fit the sample holder of the LFA machine (Fig. 3-5 e and f).
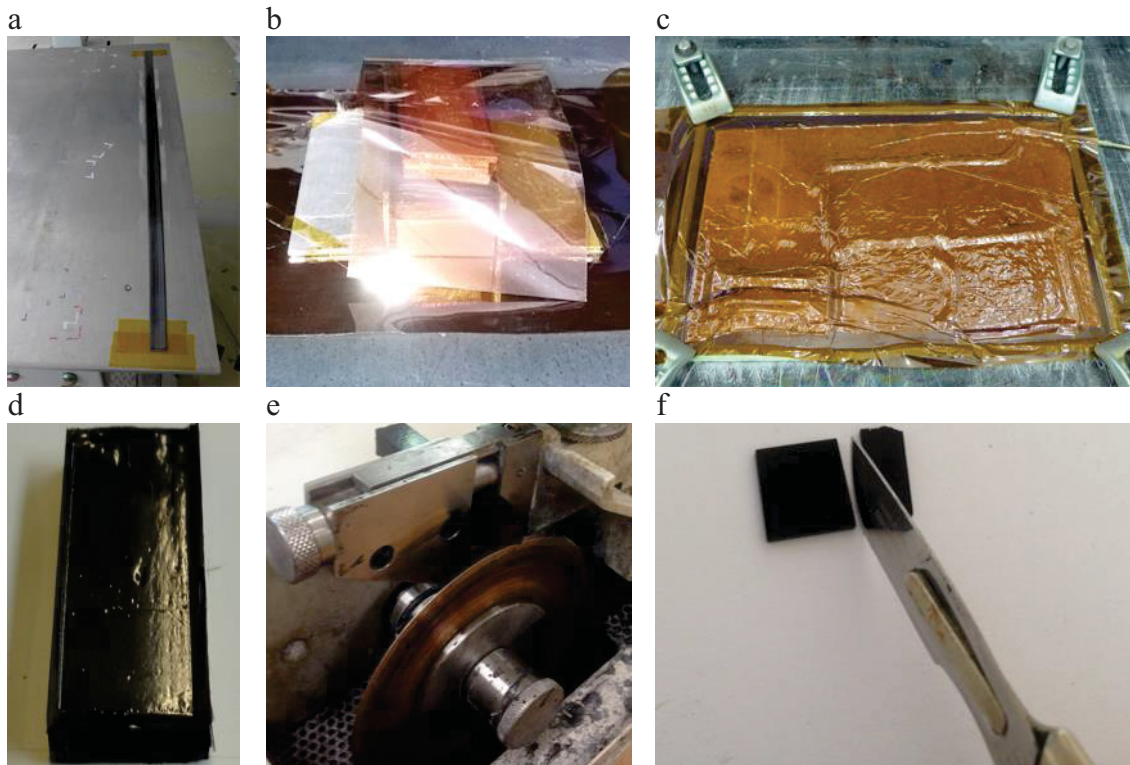
Fig. 3-5:   Sample preparation for in-fiber heat conductivity measurements of CF/PES

Circular (Ø 16 mm) one-layer samples of CF/PES tapes are used to measure the transverse thermal conductivity in thickness direction via LFA.

All LFA samples are coated with a thin layer of graphite for homogeneous laser absorption (Fig. 3-6). A detailed description of the sample preparation and LFA meas-

urements for CF/PES can be found in [S8]. All CF/PES measurements are done by a "LINSEIS LFA 1000" machine at ANU (Canberra, Australia). The measurement cell of the LFA system can be heated for measurements at elevated temperatures.
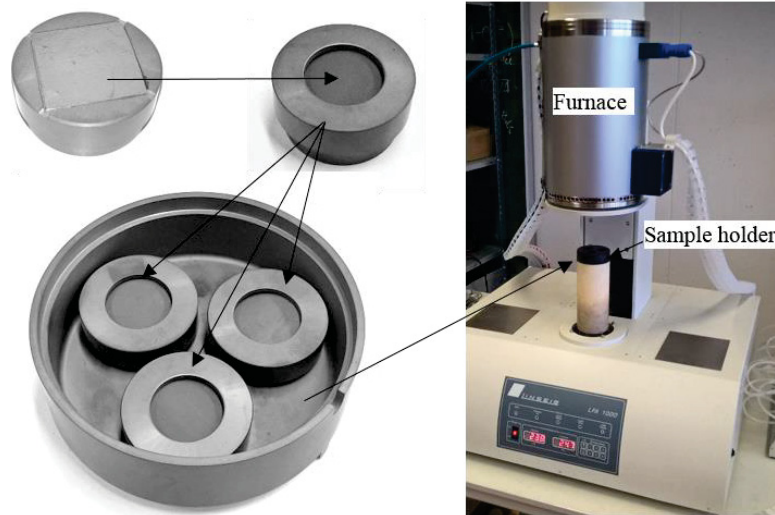
Fig. 3-6:   LFA specimen in sample holder with graphite coating and LINSEIS LFA 1000

3.3.3   Heat conductivity in fiber direction

The left graph of Fig. 3-7 shows the results for the longitudinal heat conductivity of CF/PES. Also, the conductivity of AS4 carbon fiber according to [85], PES matrix according to [95] and by ROM model is given. According to [82] heat conductivity in fiber direction of a UD layer can be calculated, analog to the specific heat by rule of mixture. However, the fiber volume fraction (FVF) has to be used instead of fiber mass fraction. The thermal diffusivity of CF/PES is measured at distinct temperatures from room temperature up to 450 °C. Five samples are measured five times at each temperature level. The conductivity is then calculated with the temperature dependent values for specific heat (see Fig. 3-4) and density. At around 350 °C the samples start to sag under their own weight due to softening. Thus, the surfaces of the samples are not perpendicular to the laser flash and detector anymore. This explains the change of the measured conductivity at high temperatures. A linear extrapolation is used for the simulation instead of these values. Besides this effect the measured values and calculated values by ROM are in very good agreement. Thus, experimental investigations for CF/PA6 are not conducted. The values by ROM and of the tape's components are given in Fig. 3-7, right. Temperature dependent thermal conductivity from [96] is used for the ROM model of CF/PA6. Although the thermal conductivity of PA6 matrix is a little higher than for PES, the CF/PA6 tape's lower fiber volume content leads to a lower in-fiber conductivity of the tape.

The data values of Fig. 3-7 can be found in Appendix a.
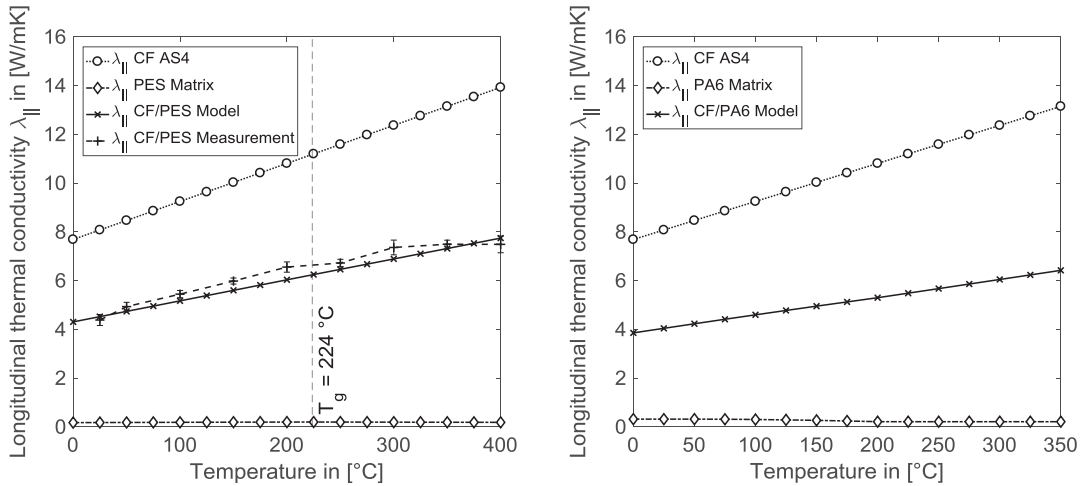
Fig. 3-7: **Longitudinal in-fiber heat conductivity of CF/PES tape, CF/PA6 tape and their components**

3.3.4 Heat conductivity transverse to fiber direction

The left side of Fig. 3-8 shows the transverse heat conductivity of CF/PES by LFA measurements and by a model from Springer and Tsai [97] and Twardowski et al. [98]. It can be seen that carbon fiber increases the heat conductivity by a factor of about two compared to neat polymer. Nevertheless, the polymer property dominates the tape's transverse conductivity. Model and measurement of CF/PES tape's transverse conductivity differ noticeably for temperatures below T_g and converge for higher temperatures. Other models from literature, e.g. inverse rule of mixture, self-consistent and a model by Rolfes and Hammerschmidt [99], were also used, but not regarded as good as Springer and Tsai / Twardowski over the whole temperature range.

On the right side of Fig. 3-8, the thermal conductivity of CF/PA6 is shown. Values for neat PA6 are taken from [96]. Together with the transverse conductivity of AS4 carbon fibers from [85] the model from Springer and Tsai / Twardowski was used to calculate the composite tape's transverse conductivity. Similar results from experimental LFA measurement are reported by Schaefer et al. for a different CF/PA6 tape [41, 100]. The data values of Fig. 3-8 can be found in Appendix a.
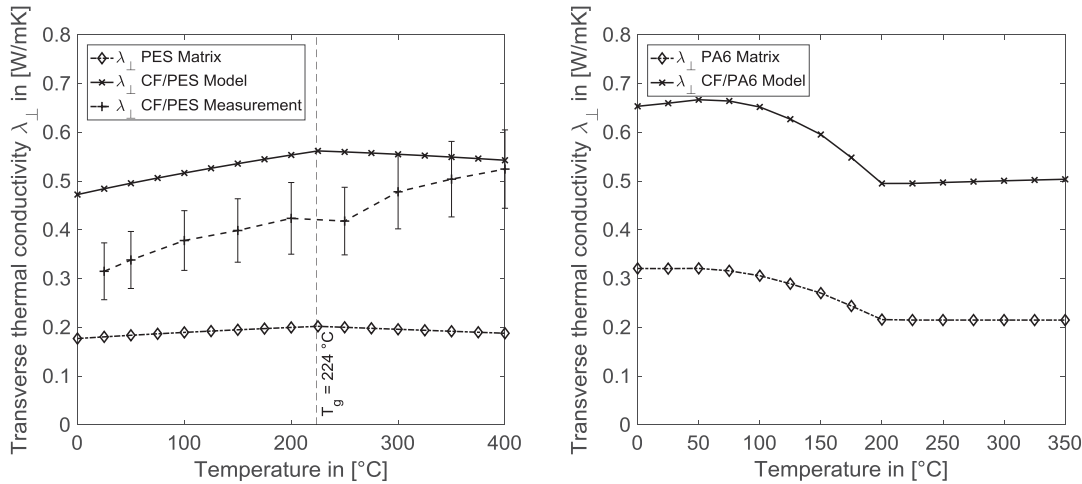
Fig. 3-8:   **Transverse heat conductivity of CF/PES tape, CF/PA6 tape and their matrix systems**

3.3.5   Discussion

The in-fiber direction thermal conductivity is investigated for both composite tape materials. Post consolidated 84 layer samples of CF/PES tape are analyzed experimentally by means of LFA. The measurements are compared to the rule of mixture model, as proposed by literature. Good agreement is found between the measurement and ROM model. As the tape components' data are available in literature, no further experimental work is necessary to determine the in-fiber heat conductivity of CF/PA6. The matrix's heat conductivity is less important. The carbon fiber and the fiber volume fraction dominate the resulting thermal conductivity in fiber direction of the composite tape.

Transverse heat conductivity of single layer CF/PES tape was also investigated through LFA measurements. Models from literature vary more in comparison to in-fiber heat conductivity. The model from Springer and Tsai / Twardowski was found in best agreement over the whole temperature range and was applied for CF/PA6 as well. The model's prediction is in good agreement with experimental measurements from literature.

3.4   Interlayer thermal contact resistance

Through thickness heat transfer between the plies may be limited by an interlayer thermal contact resistance. Most process models in literature neglect the presence of a thermal contact resistance and assume perfect thermal contact between the plies. Others emphasize the importance to consider an interply thermal contact resistance for correct process modelling [44, 101, 102]. The presence and influence of such a thermal contact resistance is investigated by experiments in this section. Two complementary approaches are followed. The first approach compares about 1 mm thick seven-layer samples' heat conductivity, TP-AFP processed with in situ consolidation and

with additional post consolidation. The measurements by LFA are compared to a model and experimental work from literature. The second approach measures the heat conductivity of one to seven layer thick samples by LFA and its evolution during lay-up of additional layers. Furthermore, the layer thickness evolution is measured by micrographs of one to seven layer thick samples.

3.4.1   Multilayer transverse heat conductivity

Studies from Barasinski et al. [44, 101] point out the presence and importance modelling a thermal resistance between the layers due to insufficient bonding. Barasinski et al. used the TP-AFP placement system from EADS-France, with top laser heating as shown in Fig. 2-10. Levy et al. [103] developed a model to describe the interply thermal contact by surface roughness and degree of bonding. A hot plate consolidation of cross-plies with low consolidation pressure over a long time was used by Levy et al. to validate the model. Later the same authors modified the model and applied it to EADS' TP-AFP process [102]. The presence of a significant thermal contact resistance can indicate insufficient consolidation during TP-AFP lay-up and thus improper in situ consolidation.

Investigations on thermal contact resistance are performed for CF/PES laminates and can be transferred to CF/PA6 laminates as shown in section 3.4.2.

3.4.1.1   Measurement method

Transverse thermal conductivity of seven-layer in situ TP-AFP processed laminates are compared to samples that are additionally post consolidated afterwards. Lay-up is performed with the closed loop control of the TP-AFP machine. Post consolidation is done following the same heating and cooling cycle as for the in-fiber direction specimens in section 3.3. A temperature of 400 °C is applied to the specimens for 20 minutes under vacuum pressure. Bonding of these post consolidated specimens is considered as perfect, while the non-post consolidated specimens (only in situ TP-AFP processed) are expected to have a more distinct interface between the layers (Fig. 3-9). For both types of seven-layer CF/PES specimens, the thermal conductivity is investigated by LFA between room temperature and 250 °C, in steps of 25 °C.
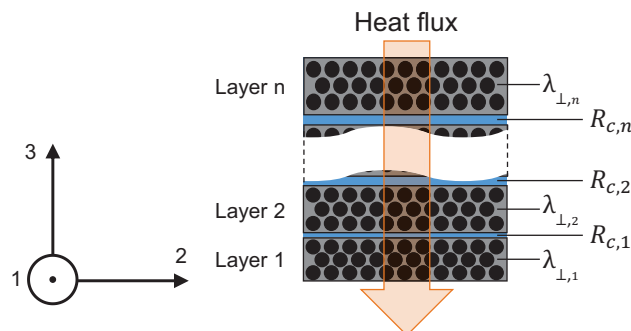
Fig. 3-9:   **Thermal contact resistance in between the layers**

The thermal contact resistance R_C between n layers with thickness t_L and $(n - 1)$ interfaces is calculated by:

$$R_C = \frac{n \cdot t_L}{n - 1} \left(\frac{1}{\lambda_{TP-AFP}} - \frac{1}{\lambda_{Post\ consolidation}} \right) \tag{3-13}$$

Five samples are tested for each type of specimen manufacturing. A detailed description of the specimen preparation and of the LFA measurements can be found in [S8].

3.4.1.2 Results

Fig. 3-10 shows on the left side the transverse thermal conductivity of in situ TP-AFP processed seven-layer samples and the samples that are additionally post consolidated. For comparison, the transverse thermal conductivity of one-layer samples from Fig. 3-8 is also plotted. The transverse thermal conductivity of the seven-layer in situ TP-AFP samples is constantly higher than for the one-layer samples. Further, the transverse thermal conductivity of the post consolidated samples is higher than for the in situ TP-AFP samples. By comparing the measured values of these two seven-layer specimens, the thermal contact resistance is calculated and is plotted in Fig. 3-10, right. The model from Levy et al. [102] is used for different degrees of intimate contact (D_{ic}). Levy et al. assumes a D_{ic} of 0.57 in [102] for TP-AFP. According to Levy et al. [103] a surface roughness of 21.1 µm is used.

The data values of Fig. 3-10 can be found in Appendix a.
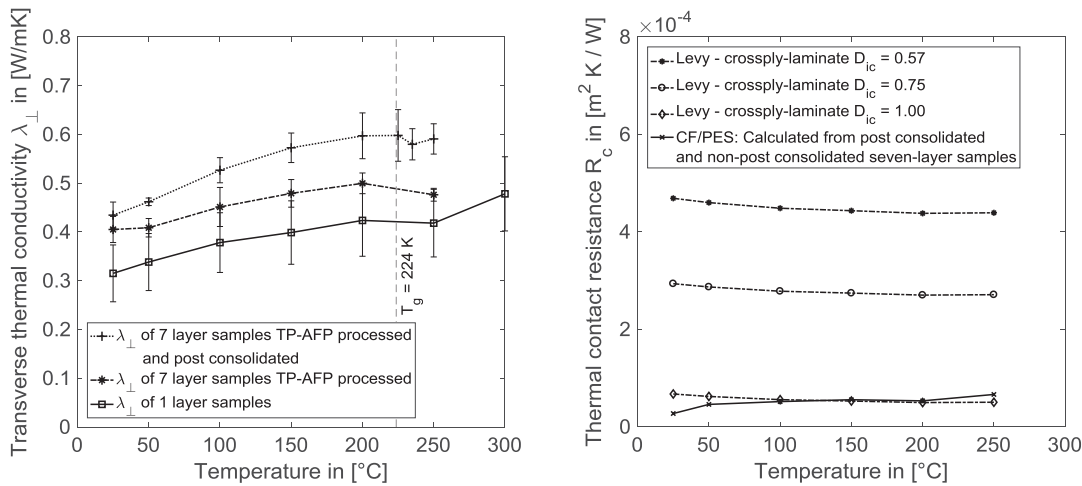
Fig. 3-10:   **Comparison of transverse heat conductivity of CF/PES seven-layer laminate in situ processed and post consolidated and one-layer samples (left) and comparison of corresponding thermal contact resistance (right) with the model from [103]**

3.4.1.3 Discussion

Different values for transverse thermal conductivity of CF/PES for different processing routes are measured. Unprocessed tape has the lowest conductivity, in situ TP-AFP processed laminate is in between unprocessed and additionally post consolidated laminate. This can be explained by the compaction while the material is molten, as this leads to matrix squeeze out, lateral spreading and decrease in layer thickness. These effects can be observed during TP-AFP lay-up and especially for post consolidated laminates. As a consequence the laminates exhibit a higher fiber volume fraction, which has a big influence on the transverse thermal conductivity of composites.

Fig. 3-10 shows the comparison of a model from literature for different degrees of intimate contact (D_{ic}) and the measured thermal contact resistance of the in situ TP-AFP processed CF/PES laminate. Levy et al. [103] first developed the model for APC2 CF/PEEK and a different consolidation process than TP-AFP. Thus, the predictions of the model cannot be directly applied on the fast heating, cooling and compacting TP-AFP process. Later is was adapted for the TP-AFP process [102]. The model still overestimates the thermal contact resistance between the plies. When assuming perfect bonding ($D_{ic} = 1.00$), the model predicts similar thermal contact resistance than measured indirectly by LFA. Schaefer measured the interply thermal contact development for CF/PA6 according to the experimental setup of Levy et al. [103]. Fully consolidated laminates by a hot press show very low thermal contact resistance between $0.25 \cdot 10^{-4}$ m²K/W and $0.98 \cdot 10^{-4}$ m²K/W [41]. These values are in very good agreement with the in situ TP-AFP processed seven-layer CF/PES laminates. This indicates a very good in situ consolidation during TP-AFP processing.

To examine the effect on temperature prediction, both approaches, model by Levy et al. and the measured thermal contact resistance, are implemented in the thermal model (chapter 4).

Further experimental investigations are conducted to measure the evolution of thermal contact resistance during processing of follow up layers (see next section 3.4.2).

3.4.2 Layer thickness evolution

As seen in Fig. 3-10 the transverse thermal conductivity depends on the processing history of a tape. It can be observed that the tape gets slightly wider after heating and compaction. Equally, the tape thickness is decreased due to this lateral material flow. Samples of CF/PES and CF/PA6 from one to seven layers are produced, LFA tested and examined via micrographs. The development of the overall transverse heat conductivity and layer thickness is studied. It is assumed that the overall thermal conductivity of the samples will decrease with an increasing number of layers respective interfaces in between.

3.4.2.1   Measurement method

Samples with one to seven layers are manufactured by the TP-AFP machine with the help of its closed loop control. The LFA measurements are conducted with a "LINSEIS LFA 1000" machine at AMU (Augsburg, Germany). All measurements are conducted at room temperature. Three samples are measured for each layer thickness and the mean value is calculated. Additionally, an unprocessed tape from the spool is measured.

An Olympus SZX10 microscope is used for the micrograph captions and layer thickness analysis. The individual layer thickness of each of the five samples for each set of layers is measured with the help of the microscope's software at multiple cross-sections and the mean values and standard deviations are calculated.

3.4.2.2   Results

The mean thickness of each layer and the corresponding standard deviation of the one-layer to seven-layer samples of CF/PES and CF/PA6 are shown in Fig. 3-11. E.g., the first set of bars shows the layer thickness of all first layers of all samples. No clear trend can be observed for increasing number of layers. The mean thickness of each layer stays within the measurement variation.
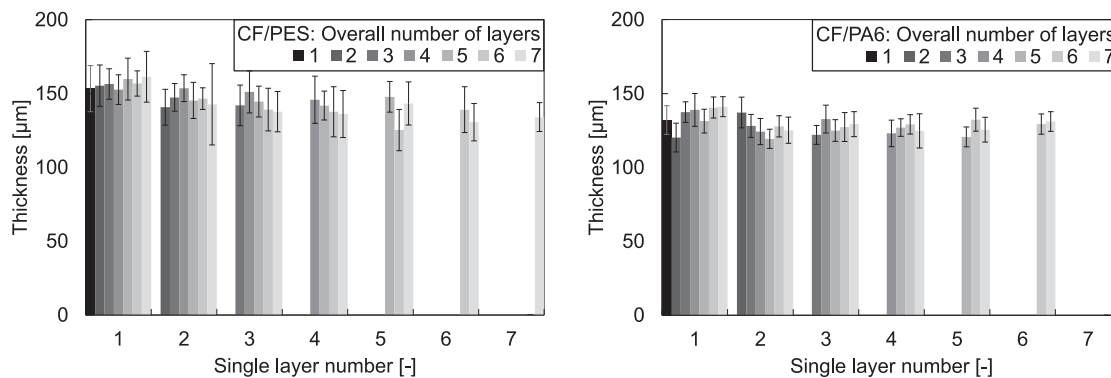
Fig. 3-11:   **Individual layer thickness evolution with increasing number of layers for CF/PES (left) and CF/PA6 (right)**

Fig. 3-12 shows the results of the LFA and mean overall layer thickness measurements for CF/PES and CF/PA6.
The mean layer thickness of the CF/PES laminates is slightly decreasing with increasing number of plies, although the mean layer thickness stays within the measured variation. No clear trend of increase or decrease can be found for the transverse thermal conductivity.

The mean layer thickness stays constant for CF/PA6, from one-layer tape to seven-layer laminates. The mean overall thermal conductivity increases slightly. However, the increase is within the measured variation.
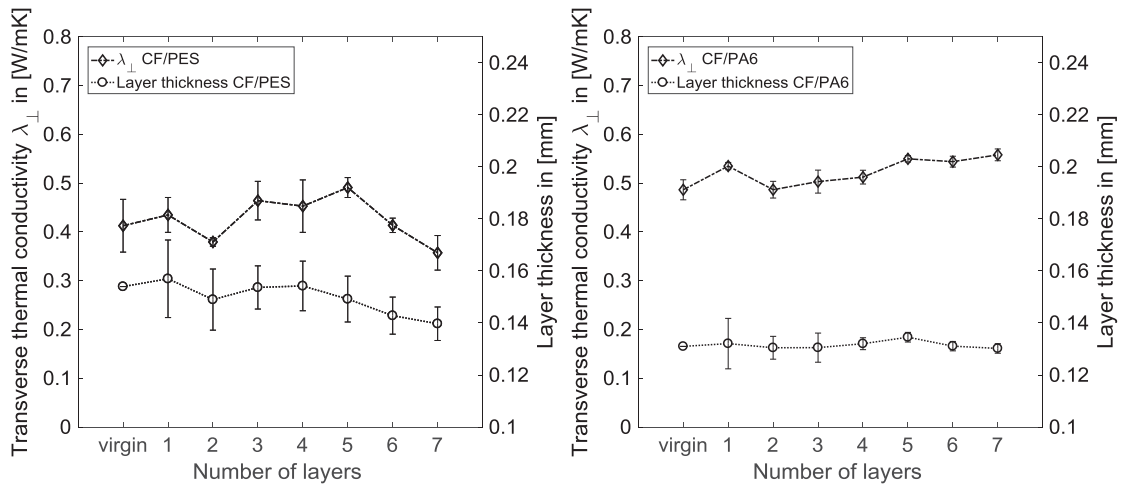
Fig. 3-12: **Mean layer thickness and transverse thermal conductivity evolution with increasing number of layers for CF/PES (left) and CF/PA6 (right)**

Fig. 3-13 shows micrographs of CF/PES (left) and CF/PA6 (right) before processing (top) and of a seven-layer laminate (bottom) by in situ TP-AFP.
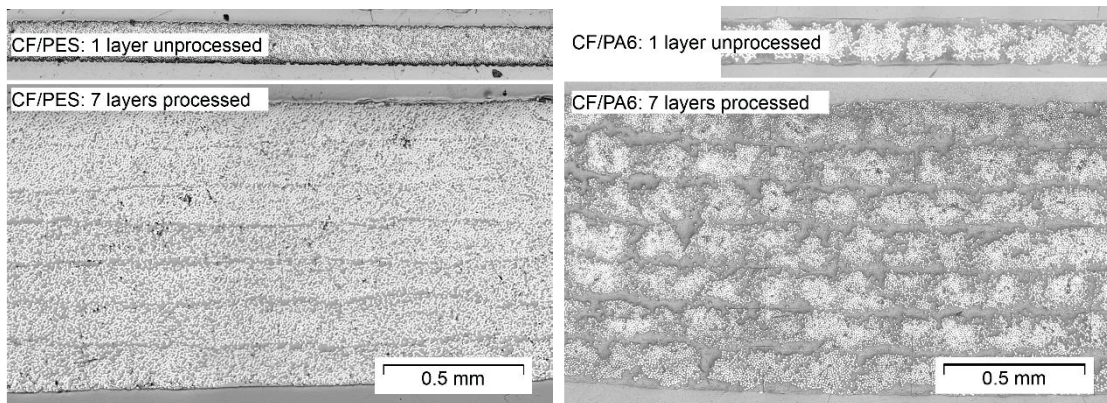
Fig. 3-13: **Micrographs of CF/PES (left) and CF/PA6 tape and seven-layer laminates**

3.4.2.3 Discussion

For both tapes of CF/PES and CF/PA6 it is concluded that only a minor change of transverse thermal conductivity and layer thickness occurs during lay-up of subsequent layers. No clear trend can be measured. The micrographs support the findings of measuring only a small interply thermal contact resistance from section 3.4. Sound in situ consolidation seems to be achieved for the samples.

The initial CF/PES tape is fully impregnated and shows a homogeneous fiber distribution with a matrix-rich surface and low void content. After processing, a thin matrix-rich area is visible between the layers but almost no voids are visible at this interface. Thus, excellent bonding can be expected. However, some voids inside the tape layer are visible. As discussed in section 2.2, it is observed that intraply voids cannot be removed during the short TP-AFP processing time.

The investigated CF/PA6 tapes are of lower fiber volume content than the CF/PES tapes. The fibers are not as equally distributed along the cross-section and are arranged in bundles. With more matrix available for bonding, excellent bonding is observed. No interply voids are seen, but the layers are still clearly visible. Some voids can be seen inside the tapes, located within bundles of carbon fibers. It is assumed they already exist in the unprocessed tape, due to difficult impregnation.

From literature (see section 2.3) and micrographs, it is concluded that tapes of high quality are necessary for excellent in situ laminate quality. Dominating factors for the tape quality are degree of impregnation, void content, fiber and matrix distribution, especially on the tape surface and surface roughness. When processing good quality tapes, excellent in situ consolidation by TP-AFP is possible. The thermal properties and layer thickness do not change significantly with additional layers.

3.5 Conclusion

Two approaches for material characterization are followed. A study to experientially determine the properties of the consolidated CF/PES tape is conducted. Additionally, the properties of the CF/PES tape are calculated by models from the literature according to properties of fiber and matrix. A comparison of the measured and modeled tape properties shows that the specific heat differs only for temperatures below T_g and converges for higher temperatures. Also, the longitudinal thermal conductivity $\lambda_\parallel$ of the measured and modeled CF/PES tape is in very good agreement. However, modeled and measured values of the transverse thermal conductivity $\lambda_\perp$ differ up to 35 % for lower temperatures.

It can be concluded that for the optimal description of the thermal properties the transverse thermal conductivity $\lambda_\perp$ should be determined or verified by measurements. Specific heat c_p, longitudinal thermal conductivity $\lambda_\parallel$ and the laser absorption behavior can be calculated by models to reduce the experimental time and effort. The CF/PA6 tape material description is based on this. Modeled thermal tape properties are compared to selected experimentally determined properties and properties from literature. A good correlation was found for the modeled tape properties of CF/PA6.

The presence and possible influence of a thermal contact resistance between layers, due to insufficient bonding, is investigated. A thermal contact resistance is derived from the difference of the overall thermal conductivity of post consolidated and solely TP-AFP processed seven-layer laminates. The measured thermal contact resistance of the TP-AFP processed samples is smaller than predicted by a model from literature. Additionally, a test campaign to determine the contact resistance from the overall transverse conductivity of one- to seven-layer samples is presented. There is no significant change in overall transverse conductivity with increasing number of layers detected by the LFA measurements. Micrographs of the samples support this hypothesis.

4 Development of a thermal simulation for flat TP-AFP parts[1]

Based on the thermal properties of the composite tapes from chapter 3, this chapter describes the 2D thermal simulation of flat TP-AFP lay-up. TP-AFP on a flat table is a steady-state process, when neglecting the start and stop of the lay-up path. Thus, implementation of a thermal simulation is rather easy and the process parameters can be studied in detail. A detailed literature review is the basis for the implementation of the thermal process simulation. The structure of the simulation and implementation in a 2D finite difference code of the processes' boundary conditions is described. The simulation is validated for both investigated materials: CF/PES and CF/PA6. The aim of the simulation is to give a better insight into the TP-AFP process. Thus, parameters are varied to investigate the influence of individual process parameters.

4.1 Literature review

For out of autoclave manufacturing / in situ consolidation of thermoplastic composites, the quality of the final part is solely dependent on the process parameters during TP-AFP lay-up. The main processes, that determine the quality of the final thermoplastic composite, are the heat up and cool down of the tape as well as compaction pressure. These determine bond formation, void growth, polymer degradation, residual stress and in the case of semi-crystalline matrices also crystallization [72, 73, 104–108]. Main quality parameters of TP-AFP laminates depend on the temperature history of the part. Therefore, many thermodynamic models of the tape laying process were developed.

Mantell and Springer [105] created a two-dimensional (2D) thermo-chemical model of a TP-AFP process in order to determine consolidation, interlaminar bonding and residual stress and strain. Although it is possible to consider heat flux or temperature distri-

bution on the top ply, the calculation of the actual distribution was not part of the study. The temperature dependencies of specific heat and thermal conductivity of CF/PEEK were only considered between the glass transition temperature and the melting temperature. While Mantell and Springer also considered filament winding and press forming, Sarrazin and Springer [109] focused on the thermo-chemical and mechanical aspects of tape laying. They assumed uniform heating of the composite and a linear temperature dependency of the specific heat capacity and the thermal conductivity.

Pitchumani et al. [73] analyzed the interfacial bonding and void dynamics during fiber placement. As in the previous papers [105, 109], the incoming tape is modeled as instantaneously laid down and heated from above. Their thermodynamic model considers the thermal dependency of specific heat capacity and thermal conductivity, but assumes uniform heat input and perfect heat transfer between the plies.

Sonmez and Hahn [107] used a nip-point heating tape placement head similar to the one used in this study. The interface between incoming tape and laminate is heated by a heat source and therefore the maximum temperature is achieved at the bonding interface. The compaction roller is modeled as a heat sink with constant temperature. A heat transfer coefficient between the incoming tape and the compaction roller is introduced. Based on the results, Sonmez and Hahn calculated the interlaminar bond strength, thermal degradation and crystallinity [104]. Later, Sonmez and Akbulut [106] used the relationships between process and quality parameters to optimize the process velocity.

Tierney and Gillespie [110] created a simplified 1D model in order to determine the void dynamics. They neglected the heat transfer in laying direction, arguing the heat transfer in laying direction is driven by the mass transport of the incoming material.

During placement, the highest temperatures occur at the irradiated areas of the laminate and the incoming tape. Therefore, it is necessary to know the exact temperature distribution especially at the irradiated areas. The aforementioned studies did not analyze the energy input distribution and therefore the calculated temperature distribution deviates from the real values in a critical area of the composite during AFP processing.

Agarwal et al. [111] showed in their study the importance of the exact modeling of the heat input and that not all energy from the laser source is absorbed by the tape and laminate. Grove [112] measured the reflectance of a laser beam at the tape surface and used the mean reflectance to calculate the heat distribution input. Grouve [74] analyzed the reflectance of the laser light at the surface of the tape and found that a part of the reflected beam is scattered and leaves the 2D plane. However, the majority of the radiation is reflected specular and it is reasonable to use the Fresnel equations. A downside of his optical model is that it neglects laser beam divergence, which reduces

the local heat flux. The results of the optical model serve as input for a thermal model, which is similar to the one from Tierney and Gillespie [110].

Stokes-Griffin and Compston [43] created a 3D ray tracing model to determine the heat input by the laser. In order to consider the scattering effect of the tape surface and fibers, the tape is modeled with a surface of half cylinders with a diameter of 10 µm and a fully absorbing layer underneath. Therefore, the reflected and scattered radiation impinges only partly on laminate and tape and the heat energy input is not as high as with a perfect specular surface. However, this effect is decreasing with decreasing distance to the nip-point, as close to the nip-point almost all of the scattered irradiation impinges on tape or laminate. The results from the 3D ray tracing model are used as boundary conditions for the heat input distribution in a former developed 2D thermal model [43, 113]. The model accounts for temperature-dependent material parameters. However, thermal contact resistance between the composite layers is neglected.

All of the aforementioned studies assume perfect thermal contact between the plies of the laminate. This can lead to a higher heat flux within the substrate and therefore leading to a lower maximum temperature. Recent studies indicate that thermal contact resistance has to be considered.
Barasinski et al. [44, 101] measured and simulated a TP-AFP process and determined a thermal contact resistance between the layers due to imperfect bonding. However, no nip-point heating laser TP-AFP machine was used. Levy et al. [103] created a function to connect the degree of intimate contact, surface roughness and transverse thermal conductivity. The experimental setup used a hot press and no TP-AFP setup. Longer compaction phases and lower compaction forces were used. On other studies Levy et al. [102, 114] refined the function to model the interlayer thermal contact resistance during a laser assisted fiber placement process with a through thickness heating principle, like the one used by Barasinski et al. [44, 101], see also Fig. 2-10.

A full 3D thermo-mechanical simulation was developed by Lichtinger [4] for Thermoset-AFP and is currently in development for Thermoplastic-AFP by ESI Group [115]. These 3D models provide a more detailed insight to process and material behavior but require much more calculation time, making virtual process parameter variations very time consuming.

Two modeling approaches are used in literature. The majority of thermal simulation models the process in an Eulerian approach. The coordinate system is fixed to the tape laying head and the material is convected through. This modeling strategy is often used to describe the process in steady-state. In the second method, the Lagrangian approach, the process is defined in a frame attached to the tooling. The tape laying head is moving along the modeling space, defined by a Cartesian coordinate system. A detailed overview of both strategies in literature can be found in [37].

Most thermal models don't focus on the heat input and omit its calculation, although they illustrate the importance of the temperature history [73, 105, 107, 109, 110, 113].

Other studies focus on the modeling of the heat input [43, 74, 112]. The accuracy of the modeled heat input is experimentally verified. Others concentrate on the thermal contact resistance between the layers, due to insufficient bond development [44, 101, 114]. The quality of the calculated temperature distribution not only depends on the heat input model, but also on the quality of the thermodynamic model. The most advanced heat input models are evaluated with thermodynamic models that omit certain aspects, mostly thermal contact resistance between the layers [43, 74, 112]. Therefore, it is neither possible to assign existing differences between simulation and experimental results to the heat input model nor to the thermodynamic model.

In order to investigate this, the presented simulation includes all of these phenomena. Calculation of non-uniform heat input by laser is combined with a thermodynamic model including temperature-dependent material properties and thermal contact resistance between the layers. The effects of the individual aspects in the model are investigated. Experimental lay-up trials validate the model.

4.2 2D Finite Difference (FD) model

Based on the TP-AFP machine used in this thesis (see section 2.4), a thermodynamic, two-dimensional model of the laser assisted AFP process with implicit transient heat transfer equations is developed. An Lagrangian modeling approach is used to describe the process. The vertical tool axis and the deposition path determine the plane of investigation of the 2D model. In addition to the tape, the tool and the compaction roller are part of the model. Fig. 4-1 shows the heat boundary conditions, implemented in the model. Heat conduction is considered within the mold, the tapes and the roller. Heat transfer is modeled between these parts by heat transfer coefficients. Heat transfer to the ambient air (T_0) is implemented by free convection or forced convection, depending on the boundary condition. Fig. 4-1 also shows the distinctive points for the laser boundary conditions (BC) on the incoming tape and laminate that are calculated by the model. The thermal contact between the incoming tape and laminate is only modeled after the nip-point. The area in front of the nip-point, both on the laminate and incoming tape, is exposed to laser heating and cooling due to the colder ambient air. The water-cooled compaction roller acts as a heatsink and is accounted in the area, where it is in contact with the incoming tape. After placing the whole length of the tape, the compaction roller returns to the starting position in order to place the next ply and the hot composite cools down.
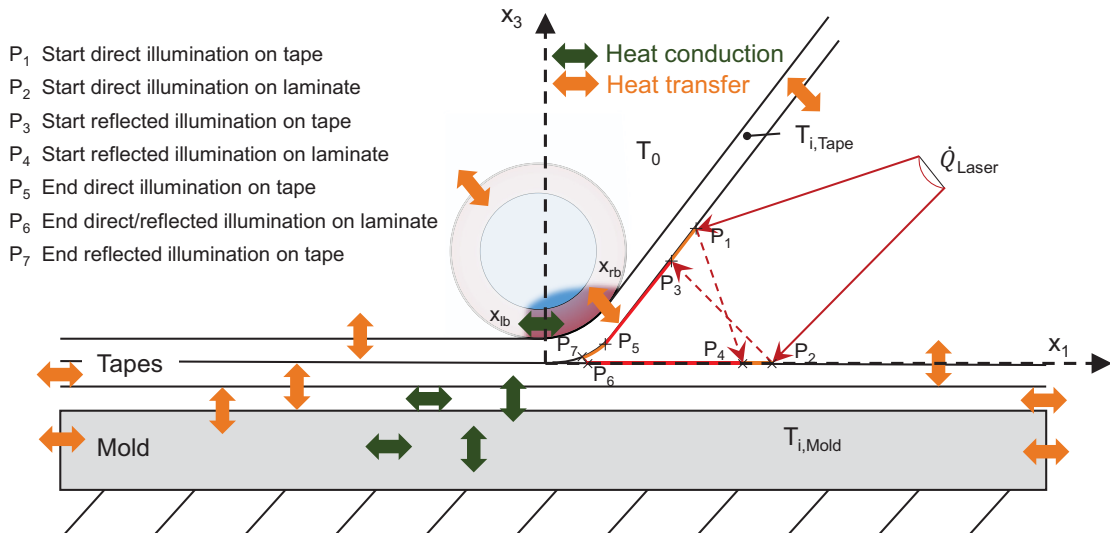
Fig. 4-1: **Two-dimensional thermal and optical model of the TP-AFP process**

To cover the temperature dependency of material parameters, implicit transient heat transfer equations are used. Taking the general law of energy conservation

$$\frac{\partial}{\partial t}\int_V \rho\, c_p\, dV = -\int_{\partial V} \dot{q}_i\, dA_i \tag{4-1}$$

and the definition of Fourier's Law

$$\vec{q} = -\lambda\, \nabla\, \mathrm{T}(\vec{x}) \tag{4-2}$$

ρ = density, c_p = specific heat capacity, V = equivalent volume, A = equivalent surface, λ = temperature and direction dependent heat conductance, T = temperature

an adequate transient thermal model can be derived.

The simulation sequence is based on a validated 2D model for Thermoset-AFP (TS-AFP) with an infrared heat lamp for tack activation [4]. The heat transfer equations are solved in the commercial software MATLAB by Finite Difference (FD) method. The simulation sequence can be seen in Fig. 4-2.
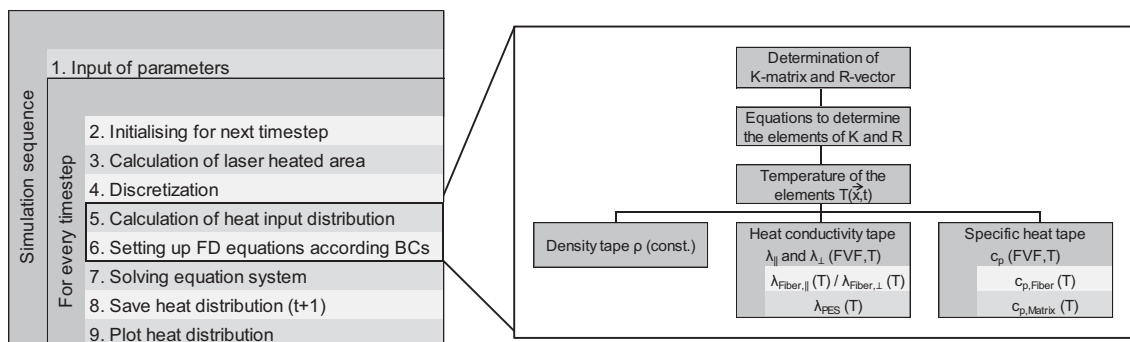
Fig. 4-2: **Sequence of the simulation program**

K-matrix = heat transfer matrix of FD system of equation;
R-vector = Residue vector of FD system of equation

Restrictions of the model

The model is a two-dimensional model. Thus, it neglects the heat flux in the third dimension (2-direction of UD laminate coordinate system). This assumption is rated tolerable as the heat input of the laser is constant over the tape width and the composite's heat flux is strongly driven by the much higher heat conductivity of the tape in fiber direction and the higher temperature difference in laminate thickness direction. The divergent behavior of the laser beam, as described below, is considered to calculate the boundary points of the laser heated area and its local intensity. The angle of the laser on the substrate is simplified to the mean angle α. Thus, the angle of incidence of the laser with respect to the substrate is assumed constant.

Fiber orientation of the substrate laminate has to be in lay-up direction. Additionally, the tool and laminate need to be flat due to the fact that the heat input is strongly dependent on the angle of incidence of the laser beam. To minimize the modeling effort, the element size in fiber direction (x_1) is the same for the tape, mold and roller. Element size alters in thickness direction (x_3) for the three components.

The model is designed for a constant lay-up speed. However, laser power, laser angle and tape laying head angle can be changed during simulation. Hence, the laser boundary condition will be calculated again, if the boundary conditions change.

4.3   Boundary conditions

Fig. 4-1 shows the heat flux at the composite's boundaries implemented into the thermal model. The next subchapters describe the mathematical implementation of these boundary conditions. The heat flux from the laser beam is heating the material during processing. Hot composite surfaces exchange heat with the ambience by natural and forced convection. Heat is also exchanged with the compaction roller and to the tooling below.

4.3.1   Laser input

The laser spot geometry on the laminate and incoming tape is calculated according to the lay-up head used for experimental validation (section 4.4). The laser optics form a rectangular laser spot with homogenous intensity in the plane perpendicular to its optical axis (see Fig. 2-18). The laser spot shows a divergent behavior and gets bigger with increasing distance to the optics. Thus, the laser intensity decreases respectively. In order to characterize this divergent behavior, experimental measurements of the laser spot size with the help of a FLIR A325sc thermal camera together with Schaefer [41], according to Stokes-Griffin [8], are conducted. Fig. 4-3 shows the laser spot size (height and width) of the two optics used in this thesis with respect to distance from the optics. The linear approximations are listed in Appendix b.
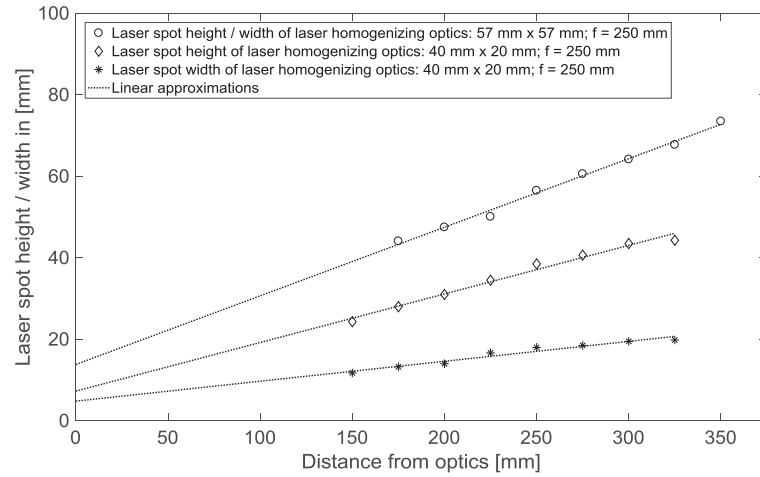
Fig. 4-3: **Divergent behavior of laser spot optics**

From the divergent behavior and origin of the laser spot, linear equations were developed to calculate the intersections of the laser beam with substrate laminate and incoming tape. A top-hat laser intensity distribution is assumed within the laser beam. The shadow directly in front of the nip-point is also calculated for both components.

The absorptivity of the laser energy by the composite tape is depending on the angle of incidence. The absorption and reflection behavior of both materials CF/PES and CF/PA6 are implemented as described in chapter 3.1. Kölzer [27] describes a linear temperature dependency of the absorption behavior for CF/PEEK and CF/PA12. Equation (3-4) is used for CF/PES and (3-5) for CF/PA6 respectively.

With this information, it is possible to determine the average heat input during the lay-up for each time step. The average heat flux density during one time step dt in a 2D element with a length dx_1 in fiber direction (x_1) is

$$\dot{q}_d = \frac{\dot{Q}}{dx_1 \cdot dt} \int_0^{dt} \int_x^{x + dx_1} \frac{\left(1 - \rho_r(\theta_1(X, t), n)\right) \cdot \cos(\theta_1(X, t))}{A(X, t)} \, dX \, dt \quad (4\text{-}3)$$

where $\dot{Q}$ is the laser power, ρ_r is the reflectivity, depending on the angle of incidence θ_1 and the refractive index n and A the size of the laser spot at point x. Due to the divergent laser beam, the laser spot area A is dependent on the distance between the laser optics and the investigated point x. The heat flux density depends on the angle of incidence with factor $\cos(\theta_1(x, t))$. Since the tape laying head is moving, the angle θ_1 and the laser spot size A at point x are dependent on time.

For irradiation of the laminate, the angle of incidence θ_1 is constant. For irradiation of the incoming tape, the integration variable is s instead of x and the angle of incidence depends on s as the incoming tape bends around the roller during movement (see Fig. 4-4).
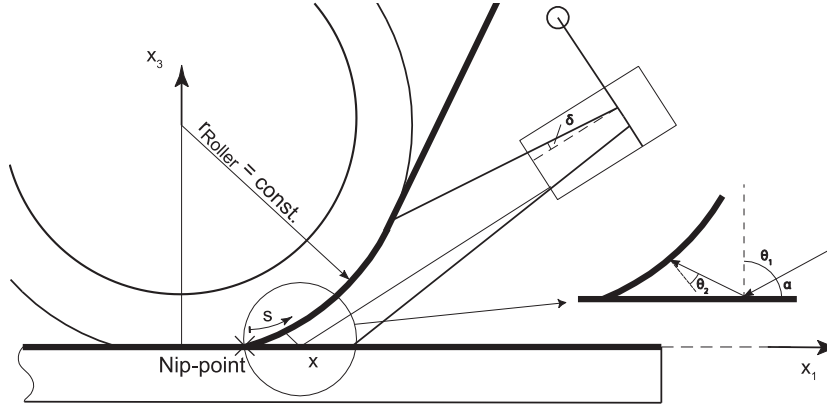
Fig. 4-4:   **Heat input by laser in the tape and laminate by direct and reflected radiation**

Additionally to the energy input by direct illumination, the model also calculates the energy input by the first reflection from the other side. The amount of energy of second and higher order of reflection are very small compared to the overall energy and therefore neglected in this model [74]. The average heat flux density originating from the reflected irradiation is

$$\dot{q}_r = \frac{\dot{Q}}{dx_1 dt} \int_0^{dt} \int_x^{x+dx_1} \frac{\rho_r(\theta_1(X,t),n) \cdot (1 - \rho_r(\theta_2(X,t),n)) \cdot \cos(\theta_2(X,t))}{A(X,t)} \, dX \, dt \quad (4\text{-}4)$$

where θ_2 is the angle of incidence of the laser after the first reflection with respect to the absorbing element. Compared to equation (10), the factor $\rho_r(\theta_1,n)$ is added to account for the percentage that is absorbed at the first reflectance. In this case, the distance the laser beam travels between the laser and the point of impact consists of the distance between the laser and the point of reflection and the distance between the point of reflection and the point of absorption. The heat flux density in the irradiated area is the sum of $\dot{q}_d$ and $\dot{q}_r$.

4.3.2   Boundary conditions to ambience

To fully describe and solve the numerical model, boundary conditions are applied according to the test setup. The following boundary conditions are implemented:

- The initial temperature T_0 at $t = 0$ s for the tool, the tapes and the compaction roller equals the constant ambient temperature.

- Thermal insulation at the bottom of the tool

$$\dot{q}_3 = \left. \lambda_3 \frac{dT}{dx_3} \right|_{x_3=0} = 0 \quad\quad\quad (4\text{-}5)$$

with λ_3 being the transverse heat conductance of the tool.

- Free convection at outer areas of the laminate, tool and incoming tape in contact to ambient air is

$$\dot{q}_{x_i} = h \, dA \, dT \tag{4-6}$$

where h is the heat transfer coefficient and A the area of heat exchange. The heat transfer coefficients are calculated during the simulation with respect to the material's temperature and geometry [88].

- According to Toso et al. [116] and Stokes-Griffin [8] the amount of energy dissipation from composite tape to ambience by heat radiation is rather low, compared to convection and laser heat flux. Additionally, in the hottest region, the laser heated zone before the nip-point, heat loss by radiation will be absorbed by the opposing surface. That means, heat from incoming tape's surface will be absorbed by the substrate laminate and vice versa. When the process is set up correctly the two joining partners, incoming tape and substrate laminate are at the same temperature level. Thus, only a minimal temperature difference exists that could act as a driver for heat exchange. Therefore, the thermal model neglects heat loss to ambience by radiation.

4.3.3   Interlayer thermal contact resistance

In order to investigate the influence of a potential thermal contact resistance between the layers (see section 3.4) two different boundary conditions are applied in between the composite tapes.

Heat exchange by thermal conductance at the contact surfaces between the tapes is calculated by:

$$\dot{q}_{x_3} = h_3(\mathrm{T}) \, dA \, dT \tag{4-7}$$

with $h_3(\mathrm{T})$ as the heat transfer coefficient in thickness direction of the tape.

- In the ideal case of no thermal contact resistance, $h_3(\mathrm{T})$ is determined by bulk material transverse thermal conductivity of the composite tapes:

$$h_3(\mathrm{T}) = \frac{\lambda_\perp(T)}{dx_3} \tag{4-8}$$

with $\lambda_\perp(T)$ being the temperature dependent transverse heat conductivity of the tape (see section 3.3) and dx_3 being the distance between the discretized tied volume elements of the laminate in thickness direction.

- In the case of a thermal contact resistance, the heat transfer coefficient $h_3(T)$ between composite tapes is

$$h_3(T) = \frac{1}{R_c(T)} \tag{4-9}$$

with $R_c(T)$ as thermal contact resistance from section 3.4.

4.3.4 Consolidation roller and lay-up tool

Heat exchange also occurs between the different components: compaction roller – composite tape and composite tape – lay-up tool:

- The thermal conductance at the contact surfaces between compaction roller and composite tape is

$$\dot{q}_{x_3} = h_{r,roller}\, dA\, dT \tag{4-10}$$

with $h_{r,roller}$ as the heat transfer coefficient between composite tape and compaction roller. The heat transfer coefficient between the incoming tape and the compaction roller $h_{r,roller}$ is assumed to be 500 W/m²K according to Stokes-Griffin et al. [113].

- Constant temperature T_R can be assumed at the inner diameter of the roller due to internal water cooling.

- Thermal insulation is considered at the left boundary surface x_{lb} (Fig. 4-1) of the compaction roller in the model due to the rotational symmetry of the compaction roller and low temperature difference

$$\dot{q}_1 = \lambda_{\text{roller}} \left. \frac{dT}{dx_1} \right|_{x_1 = x_{lb}} = 0 \tag{4-11}$$

- A reduced temperature at the right boundary surface x_{rb} of the compaction roller is considered in the model due to the cooling of the compaction roller while not in contact to the incoming tape during rotation

$$T(x_{rb})^i = T(x_{lb})^{i-1} - r_{c1}[T(x_{lb})^{i-1} - T_\infty] \tag{4-12}$$

where r_{c1} is the cooling factor, i the current time step and T_∞ the ambient temperature. The cooling factor r_{c1} was measured by a FLIR A325sc infrared camera during test lay-up and determined to 0.44 for CF/PES and 0.41 for CF/PA6.

- The conductive heat exchange between the first layer of composite tape and lay-up tool is

$$\dot{q}_{x_3} = h_{r,tool}(\mathrm{T}) \, dA \, dT \tag{4-13}$$

with $h_{r,tool}(\mathrm{T})$ as the heat transfer coefficient between composite tape and tooling. The heat transfer coefficient of the interface between the tool and the first tape layer $h_{r,tool}$ is estimated by the thickness and conductivity of the adhesive tape for first layer fixation at 1650 W/m²K.

Two types of lay-up tool material are investigated. An aluminum alloy with high thermal conductivity and a mild steel are used during the experiments. The thermal properties of the isotropic materials of compaction roller and tool are taken from literature and listed in Appendix c. No optical properties of the compaction roller's material or tooling material are needed for the simulation, since the lay-up of the first layer is not in the focus of this thesis and is not simulated. The composite tape prevents all direct and reflected laser radiation of the compaction roller in the simulated 2D plane. Stokes-Griffin et al. present absorptivity measurements of different aluminum surfaces in [78].

4.4 Validation of TP-AFP simulation of flat parts

The simulation model for flat lay–up is validated and compared to experimental data in the following paragraphs. First, the experimental setup is described that is used for the validation of both materials. The experiments were partly conducted together with Schaefer [41] and follow the principle of Stokes-Griffin and Compston [43]. The same setup was used for CF/PES and CF/PA6, but with different laser optics. Second, experimental and simulated data are compared and discussed for both materials.

4.4.1 Experimental setup

TUM's fiber placement machine from AFPT GmbH (Dörth, Germany) is used for placement trials (see section 2.4). A system from AFPT GmbH was also used by Stokes-Griffin et al. [43, 113] and Grouve [74]. Schaefer used TUM's TP-AFP machine from AFPT GmbH, too [41]. The placement head is mounted on a six axis robot. A conformable silicone consolidation roller with a diameter of 64 mm is used for compaction. A near infrared diode laser (wavelength 1030 nm – 1060 nm) heats the material during lay-up. The optics form a rectangular laser spot heating both, the incoming tape and the substrate laminate.

An unheated aluminum tool is used for the lay-up trials. Fully impregnated carbon fiber / Polyethersulphone (CF/PES) tapes with 55 % fiber volume fraction (FVF), 0.14 mm thickness and 25.4 mm width ("Suprem™ T 55% AS4 / PES-4100 0.14 x 25.4") from Suprem SA (Yverdon-les-Bains, Switzerland) are used for the validation

experiments for CF/PES. The nominal laser spot size is 57 mm x 57 mm in 250 mm focal distance.

CF/PA6 tapes from Celanese Cooperation (Sulzbach, Germany) ("Celstran® CFR-TP PA6 CF60-01") with 48 % FVF, 12 mm width and 0.13 mm thickness are used for CF/PA6 validation experiments. For these narrow tapes, a laser optics is used that forms a nominal laser spot of 40 mm x 20 mm in 250 mm focal distance.

Three stripes of 0.5 m length and 15 layers are manufactured with each material (Fig. 4-5). A thin polyimide tape and a double sided adhesive tape on top are used for first layer fixation. On layer ten thin thermocouples (type K: Omega CHAL-002 and IEC-TFAL-003-15M/ IEC-TFCY-003-15M) are welded onto the tape with a soldering iron. The thermocouple data are measured by an amplifier (MX840A from Hottinger Baldwin Messtechnik GmbH) at 150 Hz. The mean value of the thermocouple temperature of the stripes is used for validation of the simulation. After each layer, the lay-up process is halted until the thermocouple temperatures dropped under 30 °C.
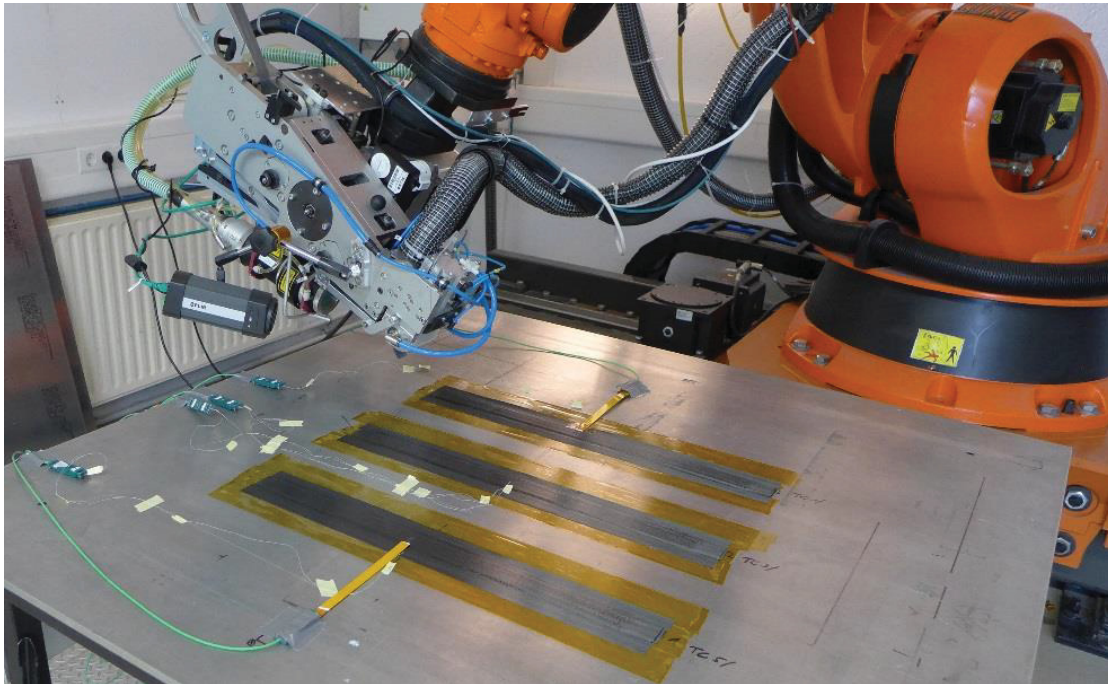
Fig. 4-5:　　**Experimental setup with thermocouples embedded in the laminate**

A FLIR A325sc infrared camera with high temperature calibration (up to 1200 "C) is used to monitor the surface temperatures of the tape and the substrate around the nip-point during lay-up. The cooling of the consolidation roller is also monitored by the infrared camera during the pause. For the validation experiments, fixed laser power and fixed laser optics angle are used. According to the laser and laser optics manufacturer Laserline GmbH an efficiency of 90 % is assumed for the laser optics [117].

Fig. 4-6 and Tab. 4-1 describe the geometry of the tape laying head and laser beam as used for the experimental validation of CF/PES and CF/PA6 lay-up.
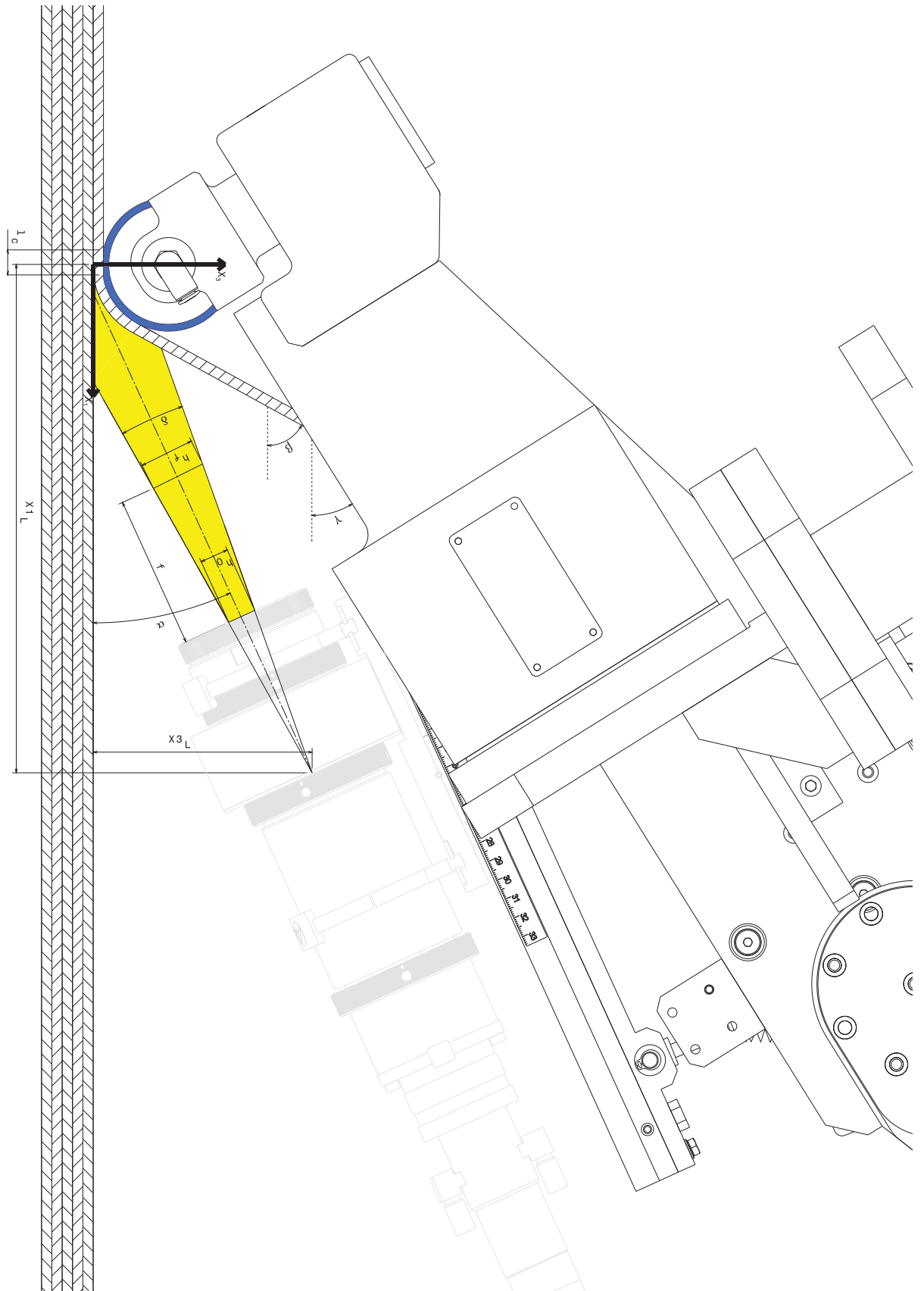
Fig. 4-6: **Schematic of tape laying head and laser spot for CF/PES and CF/PA6 lay-up βγα**

Tab. 4-1:   **Simulation and process parameters for CF/PES and CF/PA6 lay-up**

		CF/PES		CF/PA6	
Name:	**Description:**	**Value:**	**Unit:**	**Value:**	**Unit:**
$X1_L$	Virtual laser beam origin (x_1-component)	248.7	mm	311.1	mm
$X3_L$	Virtual laser beam origin (x_3-component)	82.8	mm	109.2	mm
f	Focal distance	250	mm	250	mm
h_0	Laser beam height at optics' exit	13.8	mm	7.3	mm
h_f	Laser beam height at focal distance	56.5	mm	37.1	mm
w_0	Laser beam width at optics' exit	13.8	mm	4.8	mm
w_f	Laser beam width at focal distance	56.5	mm	17.1	mm
α	Angle laser - lay-up tool	21.2	deg	21,4	deg
β	Angle of incoming tape - mold	57.3	deg	58.1	deg
γ	Angle placement head - mold	28	deg	28	deg
δ	Laser beam widening angle	4.9	deg	3.4	deg
v	Lay-up velocity	100	mm/s	75	mm/s
P	Laser power	1833	W	450	W
l_c	Length of compaction zone under compaction roller	14.0	mm	16.7	mm
F_C	Compaction force of the roller (no input parameter for the simulation)	245	N	245	N
w_C	Width of compaction roller during experiment (no input parameter for the simulation)	60	mm	30	mm
h_M	Height of mold	24	mm	24	mm
t_L	Composite tape layer thickness	0.14	mm	0.13	mm
r_{Roller}	Radius of compaction roller	32	mm	32	mm
t_{Roller}	Thickness of silicone layer of compaction roller	7	mm	7	mm
T_0	Start temperature of tape, compaction roller, mold and ambient air	26	°C	23	°C
L_P	Length of the simulated laminate	200	mm	200	mm

4.4.2 CF/PES

The simulation calculates the temperature distribution of the composite, roller and mold for each time step. Fig. 4-7 shows the temperature plot during lay-up of the 12th CF/PES layer. The plot simplifies the geometry of the incoming tape and roller. The height of the elements representing the composite is magnified compared to the mold and roller elements. A virtual thermocouple (TC) is put between layer 10 and 11 as in the experiments. Also the relevant laser points from Fig. 4-1 are highlighted in the plot.
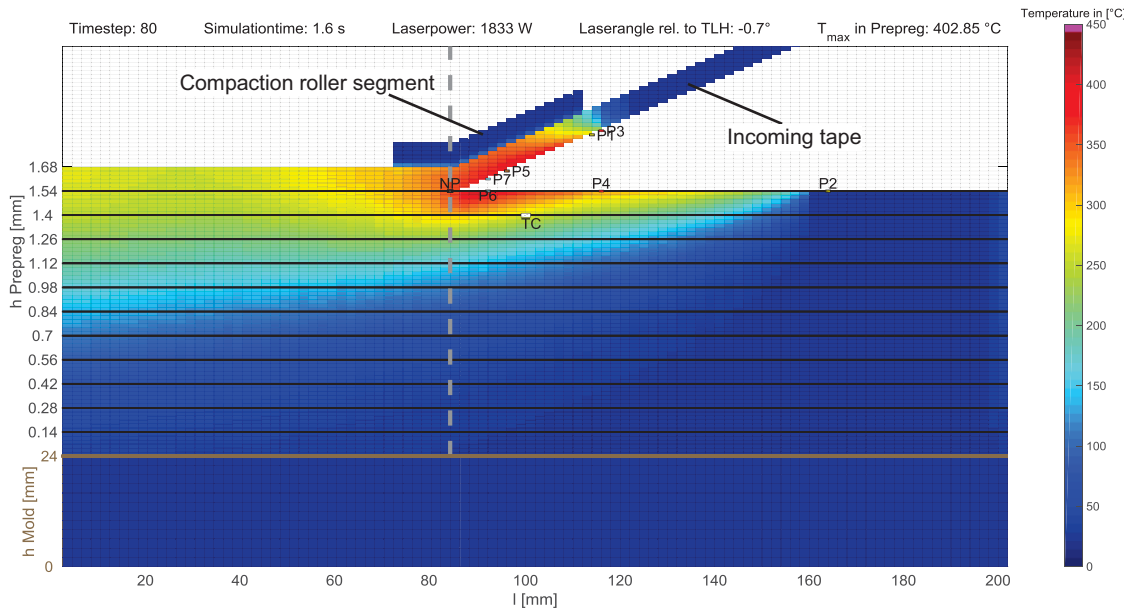
Fig. 4-7:   **Simulated temperature distribution of CF/PES lay-up**
          Simulation of the 12th layer, with compaction roller segment and laser points

A convergence study is carried out to investigate the influence of the size of the simulation time step (dt) and element size in fiber direction (dx_1) and in thickness direction (dz). Fig. 4-8 shows the maximum temperature of a virtual thermocouple on layer 10 during the lay-up of layer 12 for different time steps. Lay-up speed, element size in fiber direction and time step, and are linked by:

$$v = dx_1/dt \tag{4-14}$$

Time steps smaller than 0.02 s achieve consistent results.
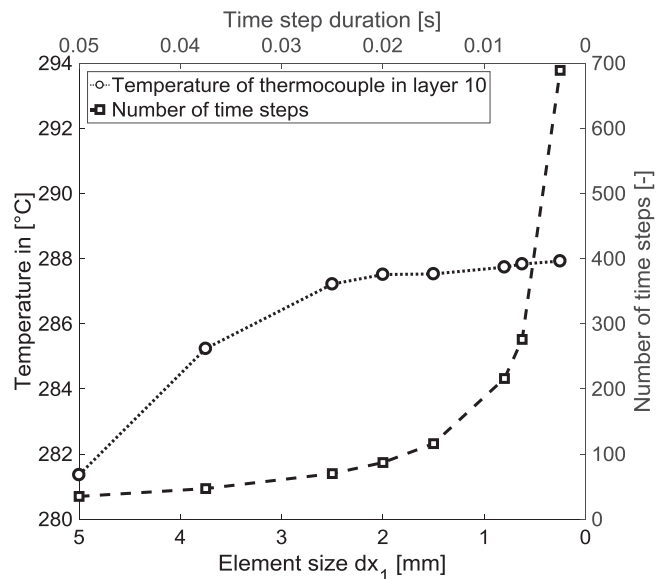
Fig. 4-8:   **Convergence study of virtual thermocouple temperature on layer 10 when laying down layer 12 with respect to element size and time step duration**

The energy flux distribution on the incoming tape and the substrate laminate is calculated during the simulation according to the geometric design of the lay-up head and the laser optics (Fig. 4-9). The graphs in the figure show the amount of energy input by direct illumination and first order reflection from the other side. The sum of both parts is the total energy input. The energy flux is shown for both modeling strategies. The calculated energy input by Fresnel's law is indicated by dots and the bars represent the energy input based on the measured absorption and reflection behavior of the tape (see section 3.1). The energy flux distribution of modeled and measured absorption behavior is very similar. The difference of the totally absorbed energy is less than 1 %. The heated length of the laser on the incoming layer is about half of the length as on the laminate substrate, but reaching a higher intensity level.

On the incoming tape the heated area by reflection is longer than by direct laser illumination. As the compaction roller causes a shadow, there is no direct illumination on the incoming tape right before the nip-point. The reflected laser radiation reaches up to the first element at the nip-point. As the laser angle θ_1 is constant for the substrate laminate the reflected energy from the substrate to the incoming layer is only depending on the local energy density. The energy density on the substrate by direct illumination depends on the elements proximity to the laser optics, as the laser beam has a divergent behavior. The reflection from the incoming tape to the substrate laminate starts at 35 % of the direct laser illuminated area and the reflected energy increases towards the nip-point due to the increase of the angle of attack θ_1 of the laser on the incoming tape towards the nip-point. The reflected energy decreases just before the nip-point due to the shadowing effect of the roller. Around 22 % of the absorbed laser energy on tape and substrate laminate has previously been reflected from the other side.

Fig. 4-9 also shows that the heat input of the laser is determined by the incoming tape's and substrate's geometry. Non-uniform heat input has to be considered, especially for the incoming tape.
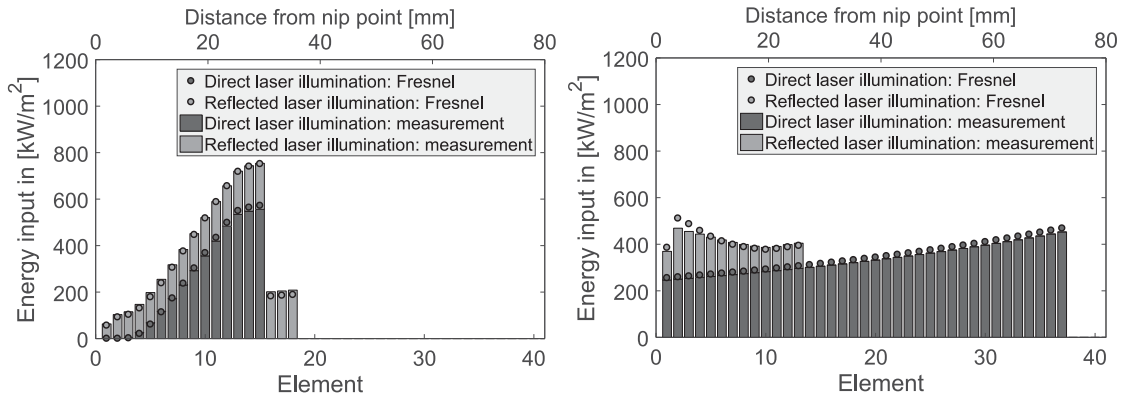
Fig. 4-9: **Energy input of laser into incoming layer (left) and substrate (right) by laser for CF/PES lay-up**
Direct illumination, first reflection from the other side and total energy input for Fresnel's absorption/reflection (points) and measured absorption/reflection (bars).

A comparison between the mean value of the thermocouple measurements and the simulation's virtual thermocouple is shown in Fig. 4-10. Simulations are conducted with the modeled optical and thermal material properties as well as with the measured optical and thermal material properties of CF/PES. Thermal contact resistance according to Levy et al. [102], with $D_{ic} = 0.75$, is used for the modeled CF/PES tape, while results from the LFA measurements are used for the measured CF/PES tape. Additionally, a simulation without the reflected energy input is done.

The temperature increase at the beginning is softer in the experiments and steeper in the simulation. This can be attributed to a softer runout of the laser intensity at the boundaries of the laser spot in reality (see Fig. 2-18). The laser beam is modeled as a top hat profile with divergent distribution. Stokes-Griffin and Compston [43] already showed that an emittance function improves the laser spot intensity representation. Simulation results show a drop in temperature rise before the maximum temperature is reached. The following additional temperature rise is attributed to the reflected energy. Heat input by direct illumination decreases towards the nip-point until the heat input increases due to additional reflected laser illumination before the nip-point. In contrast to the experimental setup, the modeled laser with a top hat intensity profile has a more distinct change in intensity at the transition to the reflected area (see transition from element 13 to 14 in Fig. 4-9, right). The simulation with only direct illumination confirms this. At the beginning, the temperature curve of the virtual thermocouple is congruent to the simulation with reflection, but lacks the second temperature rise. This results in a lower maximum temperature of 252 °C instead of 294 °C.

At the beginning, the temperature rise is stronger with the measured CF/PES properties compared to the simulation with modeled material properties. This changes before the maximum temperature is reached. It is assumed that this is due to the presence of a significant thermal contact resistance in the laminate by the model from Levy et al. A higher maximum temperature is reached in the simulation with modeled CF/PES mate-

rial properties (+ 21 °C). Despite these deviations the simulation predicts the overall temperature rise, the maximum temperature and the temperature drop very well.
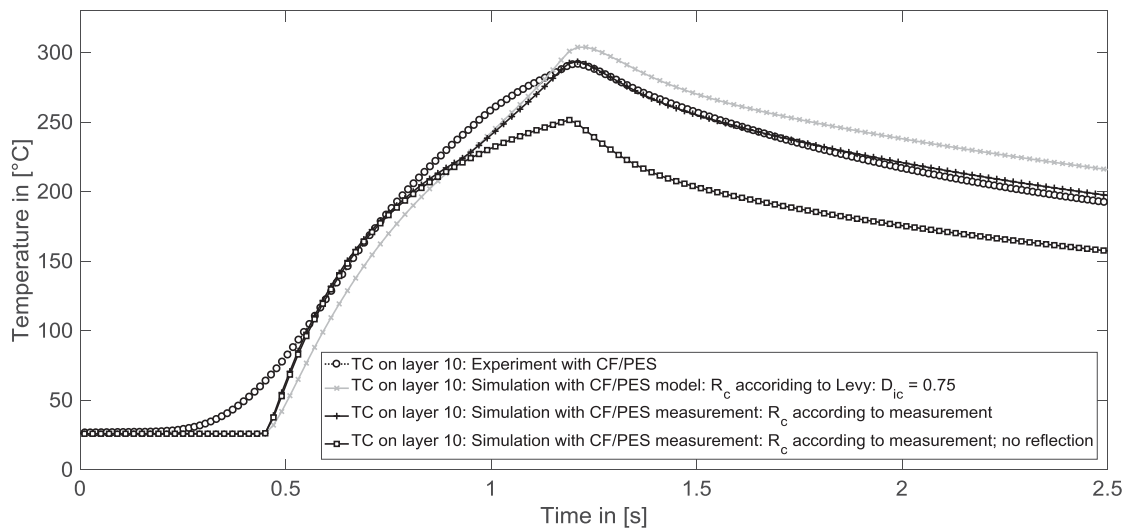
Fig. 4-10: **Comparison of experimental thermocouple and virtual thermocouple on layer 10 while lay-up on layer 12 for different simulation strategies**

To examine the effect of the modeled thermal contact resistance between the CF/PES layers, both the measured thermal contact resistance and the resistance according to the model of Levy et al. (with $D_{ic} = 0.75$) are simulated. Additionally no thermal contact resistance (R_c) but the tape's transverse heat conductivity ($\lambda_\perp$) as it is modeled inside the layers is simulated between the CF/PES layers. Fig. 4-11 shows the vertical temperature profile from the bottom (mold) to the top (roller) under the nip-point (NP) for these simulations (see also dashed vertical line in Fig. 4-7). A significant drop in temperature at each layer interface can be observed for the thermal resistance according to the model by Levy et al. Almost no temperature steps can be observed for the experimentally determined thermal contact resistance. There is only a very small difference to the simulation without thermal contact resistance, but $\lambda_\perp$ between the layers. This indicates that the thermal conductivity at the interface between the layers is equivalent to the conductivity inside the CF/PES tape. The vertical temperature profile is almost identical for both simulations with modeled and measured CF/PES properties with no thermal contact resistance between the layers. Barasinski et al.'s conclusion in [101] is that the thermal contact resistance influences the in depth temperature distribution can be confirmed. However, the results show that modeling the thermal contact resistance for the investigated nip-point laser heating process seems not critical. This heating strategy produces laminates with low thermal contact resistance.

The simulation results suggest together with the $\lambda_\perp$ measurements of the one- to seven-layer samples in the LFA (compare section 3.4) that a fully consolidated laminate can

be produced with the presented combination of CF/PES tape, process conditions and TP-AFP machine. Sound in situ consolidation is reached.
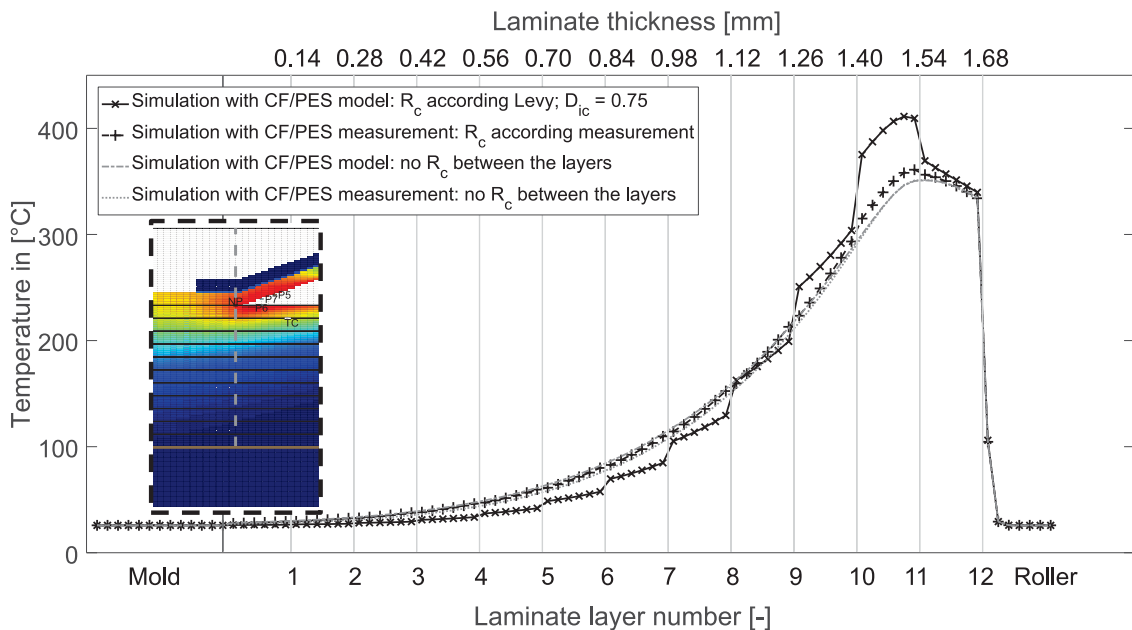
Fig. 4-11: **Influence of thermal contact resistance**
Vertical temperature profile from simulations with modeled, measured and with no thermal contact resistance between the CF/PES layers

4.4.3 CF/PA6

The simulation is also experimentally validated for a flat lay-up of CF/PA6. The experimental and simulation parameters are listed in Tab. 4-1 as well. The CF/PA6 tapes are half as wide as the CF/PES tapes. Therefore, different laser homogenizing optics with a rectangular instead of a quadratic laser spot are used (see section 4.3.1). Also, a narrower consolidation roller with half of the width, 30 mm, is used. The rest of the experimental setup is kept constant. A set-point temperature of about 270 °C is aimed for during lay-up at the nip-point. Due to the different polymer, tape thickness and width a constant laser power of 450 W is programmed during lay-up.

Fig. 4-12 shows the temperature distribution during lay-up of the 12th layer. The relevant laser points for start and end of directly irradiated area and by reflection on the incoming tape and substrate laminate are highlighted as well. Same as for CF/PES, the heat does not penetrate through the laminate to the interface between laminate and tooling.
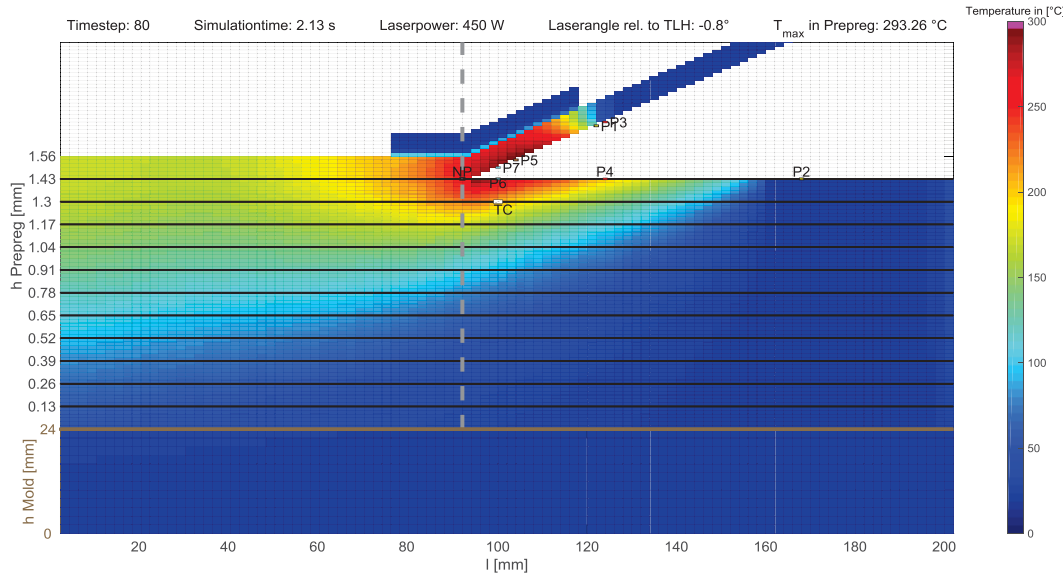
Fig. 4-12:   **Simulated temperature distribution of CF/PA6 lay-up**
Simulation of the 12th layer, with compaction roller segment and laser points

The first step of the simulation is to calculate the energy input boundary condition. The heat input to the incoming tape and substrate laminate by direct illumination and first order reflection is shown in Fig. 4-13. The optical property of the CF/PA6 tape is described by Fresnel's equations (refractive index = 1.53, section 3.1.3) and are shown as dots. Spectrophotometer measurements are shown as bars. Same as for CF/PES, both strategies result in a very similar calculation for the heat input. While the total amount of energy is lower compared to CF/PES, the distribution of the energy input is analog. At the incoming tape, the length heated by reflected laser light is longer than by direct illumination. Also, the heated length of the substrate laminate is about twice as long as for the incoming tape. The laminate length, heated additionally by reflection from the incoming tape is about 36 % of the total heated length. This is very similar to CF/PES lay-up.
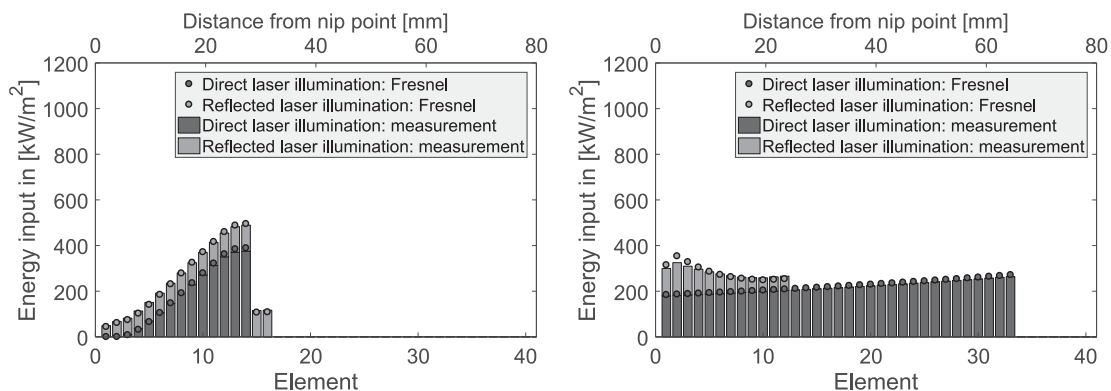
Fig. 4-13:   **Energy input of laser into incoming layer (left) and substrate (right) by laser during CF/PA6 lay-up**
Direct illumination, first reflection from the other side and total energy input for Fresnel's absorption/reflection (points) and measured absorption/reflection (bars).

To validate the thermal simulation of CF/PA6, also experimental measurements with high sensitive thermocouples are conducted. The same thermocouple setup as for CF/PES is used. Fig. 4-14 shows the experimental and simulated temperature curve of a thermocouple on top of layer 10 during lay-up of layer 12 (see "TC" in Fig. 4-12). The simulation overestimates the maximum temperature of the thermocouple by 18 °C. Measurements for R_c from section 3.4 are used for CF/PA6 in the simulation. When simulating without thermal contact resistance between the layers the simulation over-estimates the maximum temperature by 16 °C. However, the simulation describes the overall slope of heat up and cool down very well.
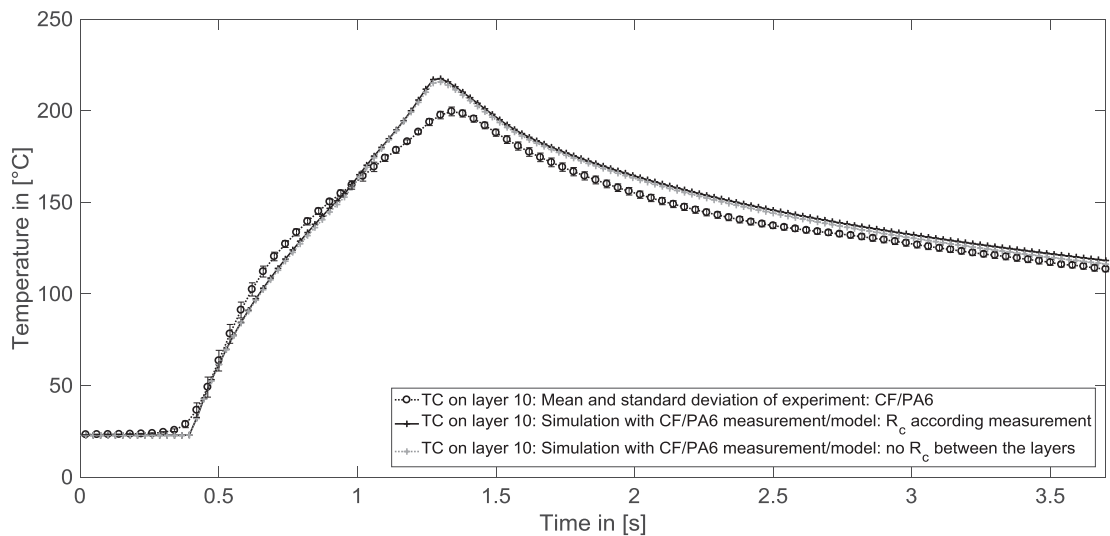
Fig. 4-14: **Comparison of experimental thermocouple and virtual thermocouple on layer 10 while lay-up on layer 12 for different simulation strategies of CF/PA6**

Fig. 4-15 shows the vertical temperature profile of the simulations with measured and without thermal contact resistance between the layers for CF/PA6. Same as for CF/PES the temperature declines within a few layers. The mold's temperature is not affected due to the lay-up.
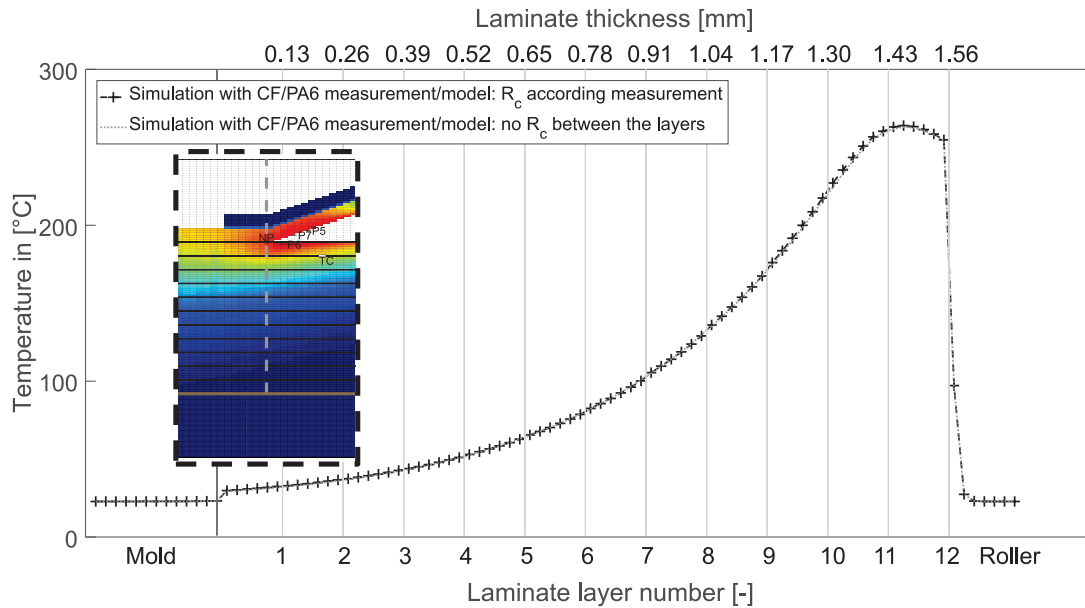
Fig. 4-15:   Vertical temperature profile from simulations with measured and with no thermal contact resistance between the CF/PA6 layers

4.5 TP-AFP parameter study

In the previous sections, the thermal simulation is validated for two different materials. As a next step, parameters of the TP-AFP process are varied to study their effects. The presented parameter study is using CF/PA6, as this material will be used in the following studies of this thesis.

A process parameter attracting much interest in research is the placement speed. It directly influences the process' productivity but also affects many thermal aspects as the required heating power, heating ramp, heat soak, compaction time, cooling ramp and resulting crystallinity of the composite. Stokes-Griffin and Compston [21] show that CF/PEEK can be in situ processed with up to 400 mm/s without affecting the samples' short beam strength. With increasing lay-up speed they also increased the process temperature and adjusted the laser distribution between incoming tape and substrate laminate. Although Stokes-Griffin and Compston show that lay-up speed can be increased significantly for in situ consolidation, future studies are needed to determine the limit. Recent studies on the effect of placement speed from Stokes-Griffin can be found in [8] and from Weiler et. al. in [118]. Effects of the lay-up speed are also discussed by Schaefer et. al [100] and by Schaefer [41] using the same thermal simulation as introduced in this chapter.

Due to the already published research on placement speed, this parameter study is putting its focus on three other aspects of the process. First, the effects of the tape laying head angle γ on the surface temperature within the laser spot is investigated. Second, the effect of a heated lay-up tool is discussed. The last section investigates the

effect of the transverse conductivity of the composite tape on heat soak of the substrate laminate.

4.5.1   Effect of tape laying head angle

The first parameter to be investigated is the tape laying head angle γ with respect to the substrate laminate or lay-up table. When the tape laying head angle is altered, the laser angle alters, too, as the laser optics is mounted to the placement head. The laser bias between incoming tape and substrate laminate changes as well and has to be adjusted to achieve similar temperature distributions. Obviously, the absorption of the laser energy in the substrate laminate is affected as described in section 3.1. The tape laying head angle and the corresponding laser angle have a major impact on the laser heating boundary on both, incoming tape and substrate laminate.

Fig. 4-16 shows on the left side the predicted surface temperature of the incoming tape and substrate laminate for varied tape laying head angles. Laser power and laser angle α are adjusted to achieve similar temperatures in the nip-point and the area next to it. All other parameters were kept constant from the validation simulation of section 4.4.3. With an increasing tape laying head angle, the laser angle α has to be increased as well to compensate the higher absorption of the substrate laminate. This requires a reduction of the laser power as well, to avoid overheating of the incoming tape. As a result, the direct laser heating length on the substrate laminate is reduced and the heating length on the incoming tape is increased. Fig. 4-16 shows on the right side the adjustments of the laser power and laser angle α to the corresponding tape laying head angle. Both parameters show a linear dependency of the tape laying head angle, when a similar nip-point surface temperature is aimed for.
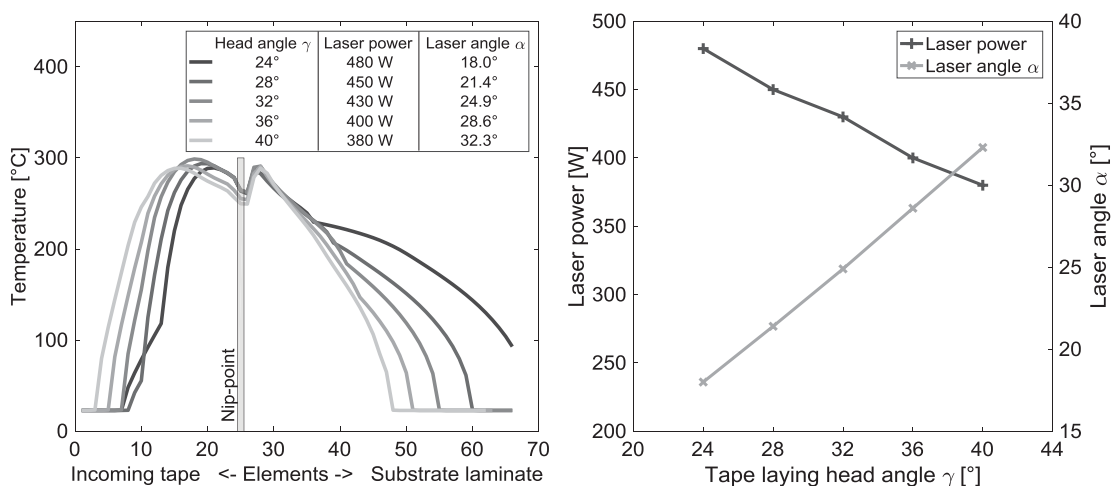
Fig. 4-16:   **Parameter study: Tape laying head angle I**
          Left: Surface temperature in the heated regions of incoming tape and substrate laminate
          Right: Linear correlation of laser power and angle to reach the same nip-point temperature

Fig. 4-17 shows the temperature profiles of a virtual thermocouple between layer ten and eleven for these simulations. Despite the same surface temperature in the

nip-point area, the maximum temperature of the virtual thermocouple is decreasing with increasing tape laying head angle. The heating ramps are steeper for increasing tape laying head angles, while the cooling rates are very similar.

The shorter heating lengths on the substrate laminate for higher tape laying head angles result in a shorter heating time and higher heating ramps. Less heat soak in the substrate laminate is achieved, as indicated by the lower maximum temperature of the thermocouple.

Head angle	Laser power	Laser angle α
24°	480 W	18.0°
28°	450 W	21.4°
32°	430 W	24.9°
36°	400 W	28.6°
40°	380 W	32.3°
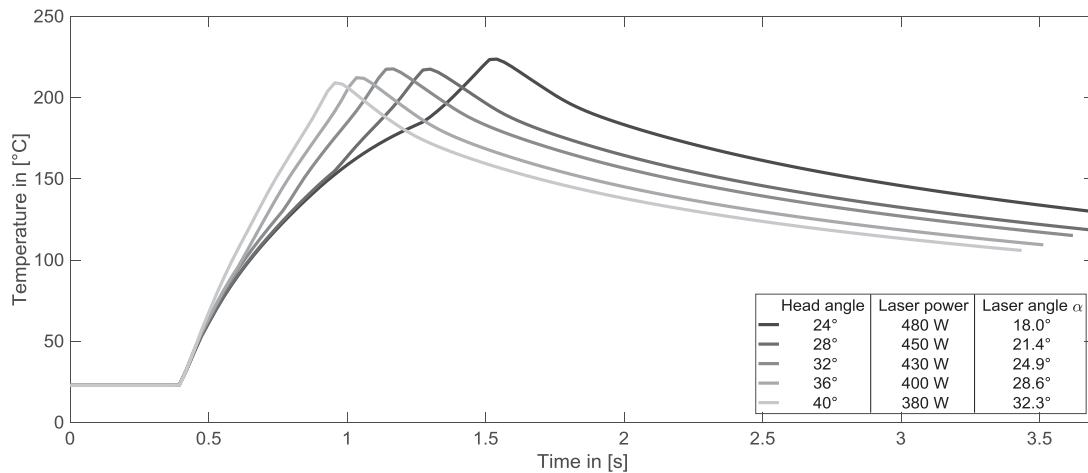
Fig. 4-17:   Parameter study: Tape laying head angle II
Comparison of virtual thermocouple predictions on layer 10 while lay-up on layer 12 for different tooling temperatures for CF/PA6

4.5.2   Effect of heated lay-up tool

The second parameter to be investigated is the lay-up tool temperature. Its effect on required heating power and on the cooling rate of the material is of special interest. A heated lay-up tool reduces the required laser power to heat up the substrate laminate and reduces the cooling rate of tape and substrate laminate after lay-up. This can lead to a higher crystallinity of the polymer and can increase the bond strength [60].

Four simulations with increasing lay-up tool temperature are compared. In order to achieve similar surface temperature in the nip-point area, the laser power and laser angle α need to be adjusted. All other parameters were kept constant from the validation simulation from section 4.4.3.

Fig. 4-18 shows on the left side the surface temperature distribution in the nip-point area from incoming tape to the substrate laminate. The change of the laser angle α results in a longer heating length on the incoming tape, while the heated tool results in a higher constant temperature of the substrate laminate before laser heating. Fig. 4-18 shows on the right side the correlation of laser power and laser angle α with respect to the lay-up tool temperature. Both parameters show a linear dependency of the lay-up tool temperature, when a similar nip-point surface temperature is aimed for.
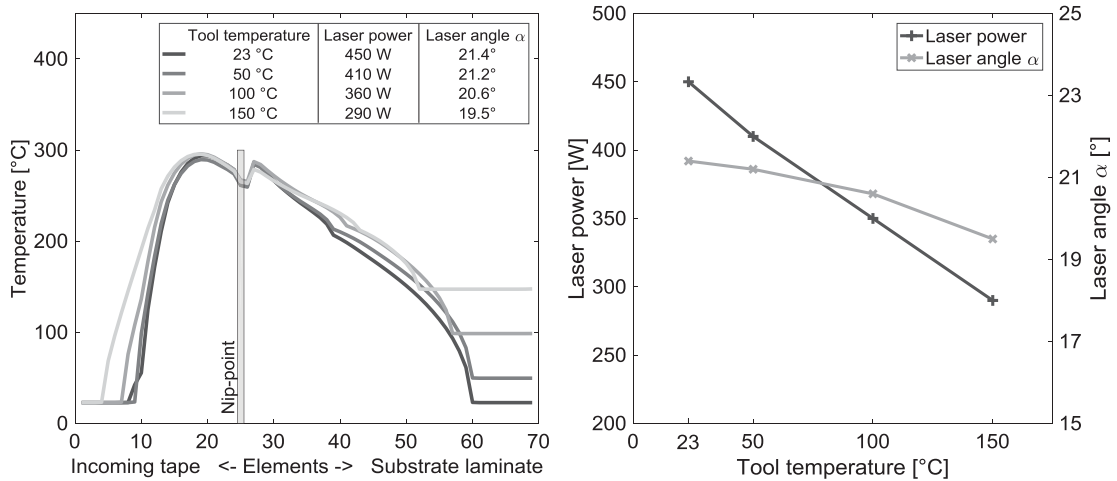
Fig. 4-18: **Parameter study: Lay-up tool temperature I**
Left: Surface temperature in the heated regions of incoming tape and substrate laminate
Right: Linear correlation of laser power and angle to reach the same nip-point temperature

Fig. 4-19 shows the temperature profile of a virtual thermocouple between layer ten and eleven during the lay-up of layer twelve for these four simulations. With increasing lay-up tool temperature, a higher maximum temperature in layer ten is predicted. The heating gradients are lower for higher tool temperatures. But the most dominant effect is predicted for the cooling rates. Obviously, high lay-up tool temperatures result in lower cooling rates. This can have a decisive effect on the crystallinity of semi-crystalline polymers like polyamides. The crystallinity and its effects on the composite need to be investigated in detail and are not in the focus of this thesis.
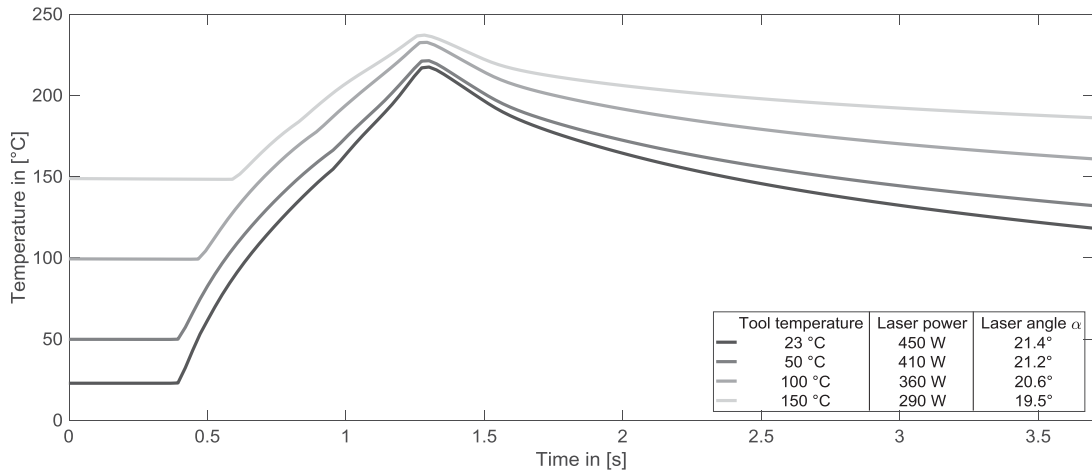
Fig. 4-19: **Parameter study: Lay-up tool temperature II**
Comparison of virtual thermocouple predictions on layer 10 while lay-up on layer 12 for different tooling temperatures for CF/PA6

4.5.3   Effect of transverse heat conductivity

The third parameter to be investigated is the transverse heat conductivity of the composite. This material parameter has a direct effect on the heat soak and cooling behavior of the laminate. A comparison of experimental and modeled transverse heat conductivity is provided in section 3.3.4 for CF/PES and CF/PA6. It is depending on the fiber volume content and reinforcement fiber type. In the future, additional fillers like carbon nano tubes or graphene particles can influence it intentionally.

Four simulations with varied transverse heat conductivity of the CF/PA6 tapes are compared. All other process and material parameters are kept constant, as described in section 4.4. The thermal contact resistance between the layers is also kept constant. Fig. 4-20 shows the vertical temperature profile under the nip-point for these four simulations. As expected, the surface temperature decreases and the heat soak increases with increasing transverse heat conductivity of the composite. For composite laminates with increased transverse heat conductivity, the interlayer thermal contact resistance becomes more and more dominant. This can be seen in Fig. 4-20 by the distinct temperature differences at the layer interfaces.
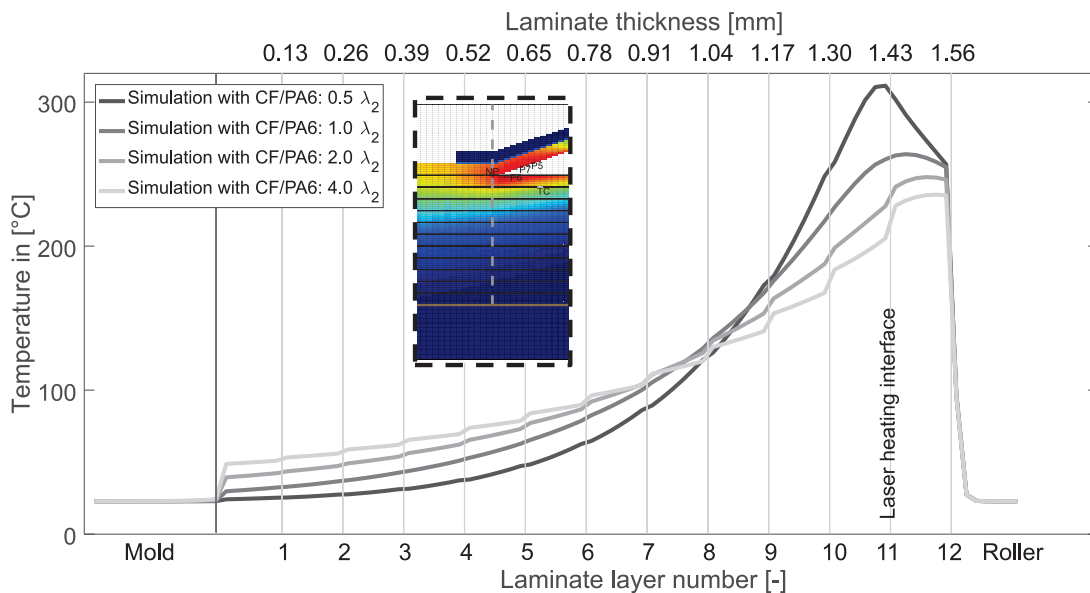
Fig. 4-20:   **Parameter study: Transverse heat conductivity**
Vertical temperature profiles under the nip-point from simulations with varied transverse heat conductivity of CF/PA6 layers

It is concluded that with higher transverse conductivity the impact of an interlayer thermal contact resistance on the vertical temperature profile increases. Thus, achieving sound in situ consolidation becomes even more important.

4.6 Conclusion

A 2D simulation for the analysis of the temperature distribution during flat TP-AFP lay-up with an integrated energy input calculation is presented. A realistic, non-uniform heat input profile is calculated by the simulation with only limited numerical cost. The simulation shows that the first order reflection has to be taken into account, as 22 % of the energy would otherwise be neglected. This would result in a significant lower temperature prediction within the laminate. A comparison of the absorption behavior of the CF/PES and CF/PA6 tapes according to Fresnel's law and measurements in a spectrophotometer shows only minor difference in the resulting laser energy input (less than 1 %).

Simulations with both approaches for the CF/PES tape material properties and thermal contact resistances (see chapter 3) are compared with experimental thermocouple measurements during lay-up trials. Best results are found with the measured tape properties. The simulation predicts the temperature rise and cooling of the laminate very well. The model by Levy et al. [102] overestimates the thermal contact resistance between the layers for the TP-AFP process. The simulation results confirm the experimental investigations on thermal contact resistance from section 3.4. It seems that there is no significant thermal contact resistance present in the laminate. The machine used in this study from AFPT GmbH has a laser heating system with a relatively large laser spot heating both joining partners directly before the nip-point and is capable for in situ processing the investigated material.

The thermal simulation is also validated with similar experimental data for CF/PA6 composite material. A different laser optics is used, as the tape width is only 12 mm. Same as for CF/PES, the thermal contact resistance is identified to be negligible.

Parameter studies to investigate the influence of the tape laying head angle and lay-up tool temperature are presented. The aim is to compare the inner temperature distribution of the composite when processing with equal surface temperature under different conditions. Therefore, laser power and laser angle need to be adjusted with the altered main parameter tape laying head angle or lay-up tool temperature. Linear dependencies are identified between the parameters.

Additionally, a parameter study on the influence of the transverse heat conductivity of the composite material is described. This material parameter influences the heat soak of the substrate laminate. With increasing transverse heat conductivity, the interlayer thermal contact resistance becomes more dominant. Processing with sound in situ consolidation becomes more necessary.

5 Challenges of Thermoplastic-AFP of 3D parts[1]

In the previous chapter, the TP-AFP process of flat laminates is analyzed. Based on the findings, the following sections investigate the laser assisted lay-up on 3D geometries. Real life parts often exhibit a 3D curvature. Moreover, the 3D curvature can be a very small corner radius. The angle between the surfaces connected by such a corner radius is often up to 90°. Beadings or stiffening ribs can be included within rather flat surfaces to increase protection against buckling or to provide connection to the neighboring part. Other stiffening parts like C-shaped ribs inhibit such corners by nature. Today, such parts are manufactured by TS-AFP but cannot be produced by laser assisted TP-AFP and especially not with in situ consolidation, yet. In this chapter, general investigations for the laser assisted TP-AFP process are performed to describe its the specialties of laying up 3D parts.

First, a brief literature review is presented. This is followed by the definition of the geometry's characteristics of interest in this work. Manufacturing trials with standard TP-AFP process setup were performed. During specimen manufacturing, local overheating occurs around the 3D corner. This overheating exceeds the degradation temperature of the CF/PA6 tape material. To find the reasons for this overheating the robot kinematics, resulting compaction pressure distribution and laser spot characteristics are described when the tape laying head is moving around the 3D corner. Additionally, specimens are manufactured and tested to identify the optimum and maximum process temperature which the tape is allowed to be exposed to during 3D lay-up.

5.1 Literature review

TP-AFP on 3D geometries is hardly described in literature. Most TP-AFP research presented in literature is dealing with basic laminate lay-up of test stripes or test plates to optimize the bond quality or lay-up efficiency. Historically, the thermoplastic tape winding process was developed from wet filament winding process before TP-AFP [1]. This is also a steady-state process, with the mandrel moving continuously under-

---

[1] Parts of this chapter were published in:

Kollmannsberger, A.; Ladstätter, E.; Drechsler, K.; "Challenges for Thermoplastic-Automated Fiber Placement (TP-AFP) with in situ consolidation on 3D parts". in Proceedings of the 17th European Conference on Composite Materials, June 2016, Munich, Germany, ISBN: 978-3-00-053387-7

neath the lay-up head. For both processes, the tape laying head does not change its orientation with respect to the tooling during processing. Therefore, the process can be optimized and the parameters can be kept constant during lay-up. A closed loop control helps to find the optimum process parameters. It keeps the temperature distribution constant and can compensate tape variabilities. A similar process, but with changing geometry during lay-up is winding of pressure vessels. Vessels consist of a cylinder section and two domes on each end. To achieve good structural integrity, the lay-up head deposits fibers in all three sections, including the transition zones. The radius of the cylindrical section determines the domes' curvature, as smooth transition is desirable (Fig. 2-14).

Beresheim introduces a parametric geometric model to describe the geometrical part complexity in order to determine its manufacturability and effects on manufacturing time [70]. He considers the paths the tape laying head has to follow at convex and concave corners. He considers constant lay-up speed at all sections and calculates the minimum radius and angle of the part's geometry according to machine and lay-up parameters. When considering the benefits of in situ consolidation, he estimates a lay-up speed of 6 to 7 m/min for the TP-AFP process competitive to TS-AFP. No thermal aspects are taken into account by his model.

Kermer-Meyer investigates the laser assisted TP-AFP process to manufacture complex shaped 3D structures [69]. The focus is to increase steering capabilities and to minimize process induced deformations. The investigated geometries are of rather small curvature and the heating aspects due to the geometry are not in the focus of the investigation.

Zenker et al. [71] investigate the thickness variations at lay-up section boundaries. In [119] Zenker and Schwab experimentally investigate the steering behavior of a multi-tow lay-up of CF/PA6 (see also [S18]). Both aspects occur during lay-up on double-curved 3D surfaces. However, the investigations were only done by flat lay-up generation.

Lichtinger investigates the heat distribution during lay-up on ramps of sandwich panels with chamfered edges [4]. Experimental investigations and 3D thermal simulations are presented. An overheating of the laminate is observed, due to the movement of the robot and change of the heating unit's alignment. However, the investigations are carried out for TS-AFP with an IR heater.

While hot gas or open flame heating units spread the heat in a wider area [26], the heat input of lasers is highly concentrated. It is obvious that the laser input boundary conditions at the cylindrical and dome sections of a pressure vessel vary. A closed loop control system can adjust to this change of heat input, when the transition is rather smooth and slow (Fig. 5-1).
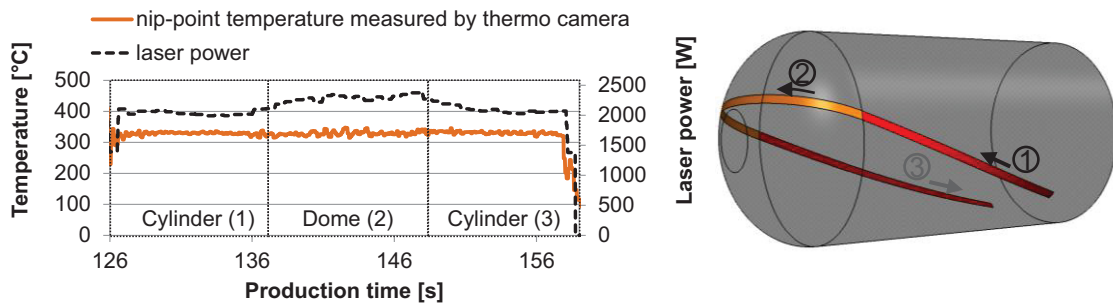
Fig. 5-1: **Process temperature during pressure vessel manufacturing**
The closed loop control keeps the process temperature constant by adjusting the laser power in the dome section (②); [10]-presentation

Same as for pressure vessels, the published 3D demonstrators of Automated Dynamics Inc. show big corner radii with smooth transitions (e.g. Fig. 2-13). Metal rollers (Fig. 2-7) or segmented compaction units, as shown in Fig. 2-12, would prohibit sound compaction pressure application on strong 3D geometries.

The literature for 3D laser assisted TP-AFP processing is very limited. As the process is not yet widely used in the industry, research seems to slowly evolve from flat test laminates to 3D parts. This is especially true for in situ consolidation of 3D laminates.

5.2 Definition of 3D part geometry

The curvature of a 3D part can either be of concave or convex nature. The minimum concave radius to be manufactured by AFP is often limited by the AFP head and the kinematic system. This is especially valid for laser assisted TP-AFP, as the laser homogenization optics need more space underneath the placement head than IR heaters for TS-AFP (Fig. 5-2). Often concave geometries can be transferred to a convex shape by laying up from the other side on a male tool.
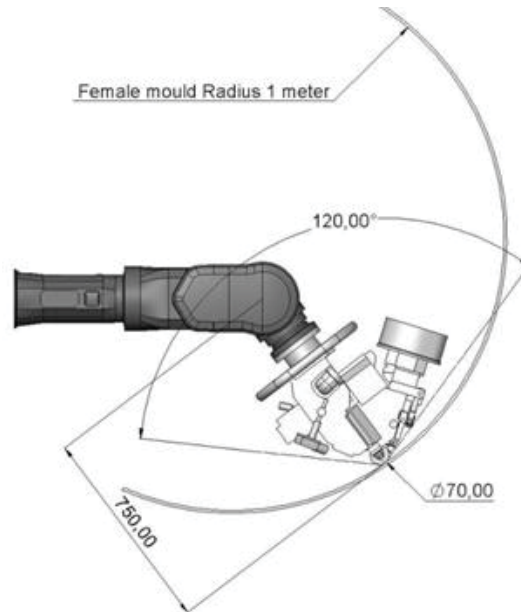
Fig. 5-2:   **The tape laying head limits the lay-up geometry on female molds / concave geome-tries [120]**

Therefore, the focus of this investigation is the placement on flat geometries connected by convex corners with a small radius. The change of curvature and respectively corner radius is meant to be smaller than the laser spot in the substrate laminate. Typical laser spot length for sound in situ consolidation is between 60 mm to 70 mm (cf. Fig. 4-9 - right and Fig. 4-13 - right). This means that the substrate geometry and the resulting laser absorption changes within the laser spot for the substrate laminate when approaching the corner. A complex heating boundary condition results from that. Especially the transition to and away from the corner adds complexity.

Parts with such a geometry are C-spars in aeronautics or other structural applications. In composite intensive airplanes like the Airbus A400M, Boeing 787 or Airbus A350XWB C-spars are used in the fuselage and wing. C-spars typically have a cross-section of three rather flat surfaces each perpendicular to each other that are connected by corners of almost 90°. State-of-the-art composite C-spar manufacturing can be done by TS-AFP (Fig. 5-3).
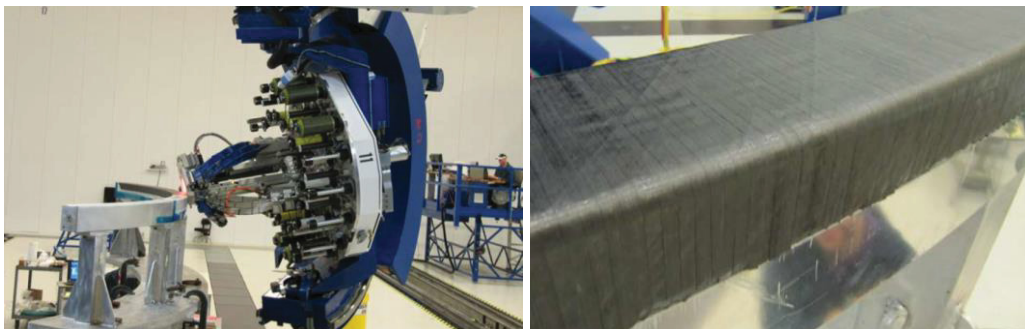
Fig. 5-3:   **State-of-the-art C-shaped spar manufacturing by TS-AFP [6]**
                  The C-spar has a width of 100 mm and corner radii of about 6 mm

In order to investigate the manufacture of such C-spar like structures by means of laser assisted TP-AFP with in situ consolidation, a specimen geometry with a corner radius of 6.5 mm is used. In compliance with the four-point-bending test of ASTM D6415 a leg angle of 90° is used. To investigate the influence of the leg angle, specimens with a leg angle of 105° and 120° are used as well. Fig. 5-4 shows the three specimen geometries used for process development and the lay-up with the laser assisted TP-AFP machine. When comparing the scale of the specimen to the TP-AFP head it can clearly be seen, that the corner radius is much smaller than the heat affected zone on the laminate.
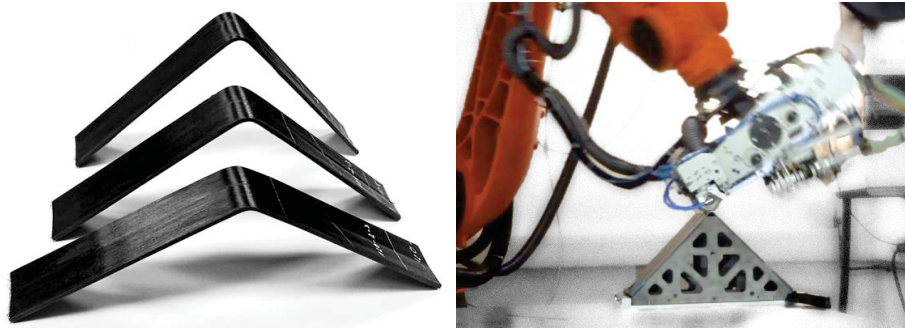
Fig. 5-4: **Corner specimen with 90°, 105° and 120° leg angle (left) and manufacturing of specimen with TP-AFP machine (right)**

5.3 Result of standard TP-AFP processes on 3D parts

Based on the process parameters for flat TP-AFP lay-up, first placement trials on the v-shaped geometries from Fig. 5-4 are conducted. Besides lay-up with closed loop control, also the resulting process temperature with constant laser power is examined. The aim of these lay-up trials is to examine the suitability of a state-of-the-art laser heating TP-AFP machine for 3D lay-up with convex corners. The process is monitored and evaluated by the machines log data. Based on the findings, improvements of the process for 3D lay-up can be developed. During the lay-up trials overheating of the composite is observed. Reasons for this are evaluated and tests to measure the degradation threshold temperature are conducted.

Mechanical tests of the specimen by wedge peel test and four-point-bending test according to ASTM D6415 are demonstrated, together with specimens manufactured by an improved 3D TP-AFP process, in section 7.2.

5.3.1 Lay-up with closed loop control

Similar process parameters as for the flat lay-up in section 4.4.3 of CF/PA6 were chosen. After the first layer, the closed loop control for the laser optics angle is turned on. Tab. 5-1 summarizes the process parameters.

Tab. 5-1:   **Process parameters for 3D lay-up trials with CF/PA6**

Name:	Description:	Value:	Unit:
α	Range of angle laser - lay-up tool (by CLC)	24.5 to 25.0	deg
γ	Angle placement head - mold	32	deg
v	Lay-up velocity	75	mm/s
T_{set}	Temperature set-point for CLC	300	°C
l_c	Length of compaction zone under compaction roller	13.1	mm
F_C	Compaction force of the roller	130	N
w_C	Width of compaction roller during experiment	30	mm
h_M	Thickness of unheated mold	2	mm
r_{Roller}	Radius of compaction roller	32	mm
t_{Roller}	Thickness of silicone layer of compaction roller	7	mm
T_0	Start temperature of tape, compaction roller, mold and ambient air	23	°C

The lay-up tools are manufactured from bent sheet metal steel with 2 mm thickness and are bonded to three rips. They are not heated prior or during lay-up. UD laminates of about 2 mm thickness (18 plies) are manufactured for testing according to ASTM D6415 (see section 7.2.4). Sufficient leg lengths are chosen to achieve a stable lay-up process by the closed loop control before reaching the corner. Excessive material is trimmed before testing. Fig. 5-5 shows the lay-up sequence of the manufacturing of a set of 90° specimens. Each set consists of 13 adjacent tracks in every layer. Four specimens are cut from one manufacturing set. Fig. 5-6 shows the corresponding thermal camera images of the nip-point region. The thermal camera is mounted to the placement head, pointing to the nip-point area. In the thermal images, the heating of the incoming tape and of the substrate laminate can be observed. Parts of the compaction roller can be seen as well. The composite layers of the substrate laminate are captured in a light blue color, as a bit of heat of the previously laminated layers dwells on. The first and last picture show the lay-up on the flat legs of the geometry. A red to orange color, like in picture 1, indicated nominal processing temperature. Lay-up here is not different from flat lay-up as described in chapter 4. Within picture 2 to 5 the lay-up head reorients around the corner. The projection of the laser spot can be observed indirectly by the heated regions.
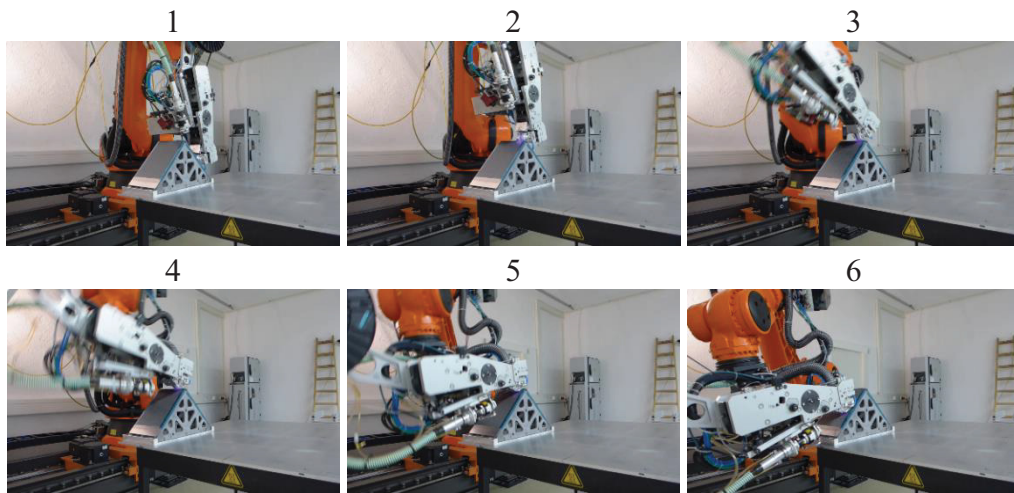
Fig. 5-5: Lay-up sequence for 90° specimen
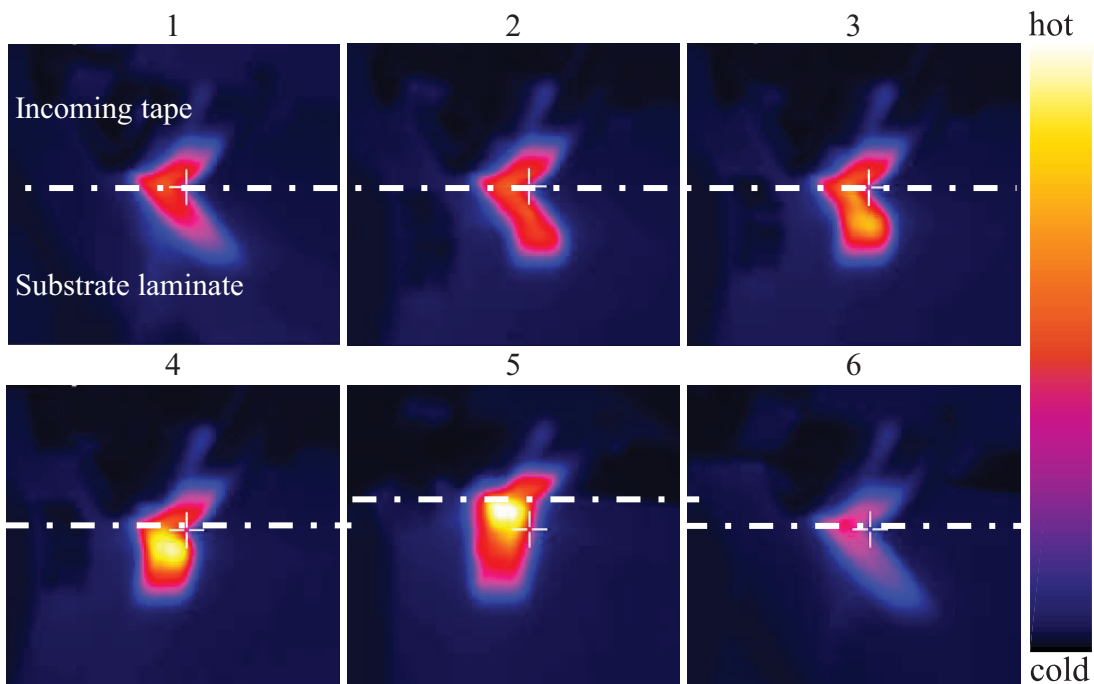
Fig. 5-6: Thermal camera images of the nip-point region during lay-up around the corner of a 90° specimen with closed loop control (dashed lines mark the nip-point)

Three things can be observed in the pictures:

First, the corner area are overheated (picture 3 to 5). Comparing with picture 1, where a stable 2D process is established, the yellow and white color indicate a hotter temperature.

Second, the nip-point (marked with white dashed lines) is shifted upwards with respect to the laser spot. The robot deviates from its programmed path around the corner, forcing the compaction roller upwards (picture 5). This means, the tape's peeling velocity within the placement head is reduced during this short time. As a result, the

time it remains in the laser spot increases.

Third, after the corner (picture 6), the purple color of the laser spot indicates that the process temperature is reduced.

With the help of the machine's log data, these observations can be examined in more detail. Fig. 5-7 shows the process data of an exemplary track in the middle of the 18-layer laminate (track 6 in layer 12). The maximum process temperature, laser power, tape speed and compaction roller's stroke deflection are plotted with respect to the position on the lay-up tool geometry (black dashed line). It has to be noted, that all temperature values from the machine's infrared camera are to be seen as black body temperature values. Although the composite tape has a lower emissivity for heat, a constant value of 1.0 is used within the machine's control unit. Emissivity may vary by polymer type, tape temperature, angle of attack of the infrared camera or carbon fiber orientation.
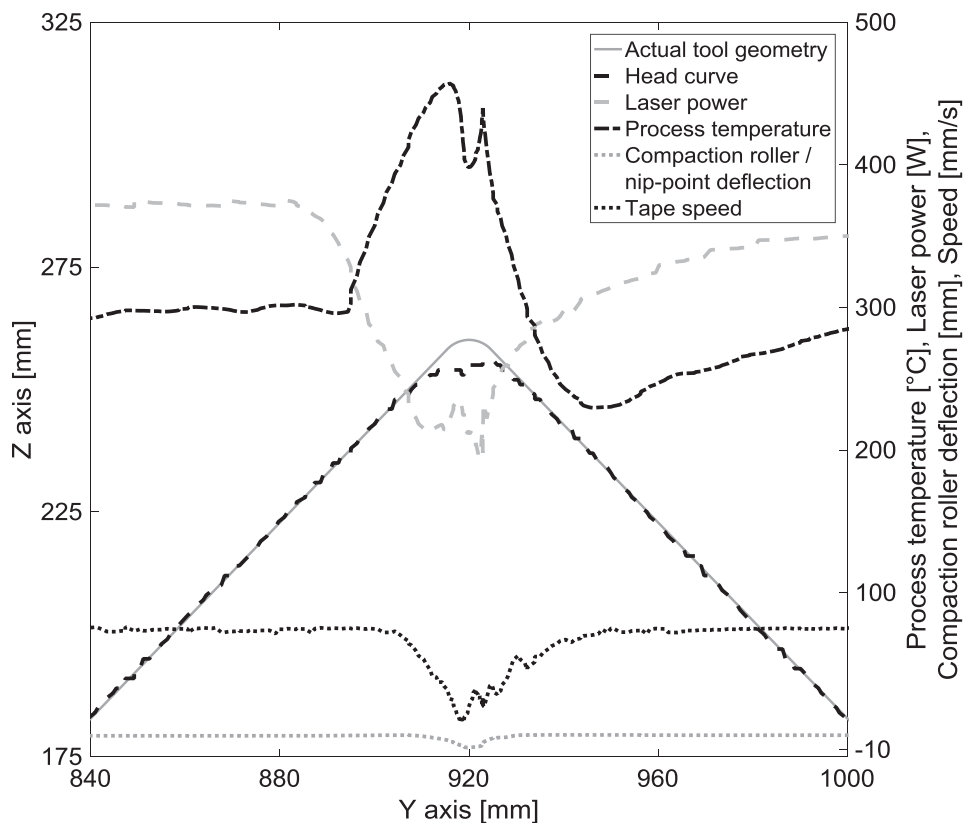
Fig. 5-7:   **Log file data of a track from 90° specimen with closed loop controlled lay-up**

Around 35 mm before the nip-point reaches the tip of the lay-up tool, the process temperature rises from 300 °C to up to 450 °C. As the nip-point approaches the corner, part of the laser spot heating the substrate laminate is already heating the laminate around the corner and the backside of the tool. Due to the angle of the lay-up tool, the laser spot does not move with the lay-up speed at this section and the laser spot's length decreases (Fig. 5-6, picture 3 to 5). This increases the amount of absorbed

energy in this area. The resulting temperature rise is detected by the closed loop control and the laser power is reduced by 45 % (grey dashed line). The laser power reaches its minimum value, when the nip-point is at the top of the tool. Here, the process temperature reaches its maximum. Afterwards, the temperature drops, as the placement head reorients around the 90° angle. The laser power is increased again by the closed loop control. The process temperature shows two local maxima. The first one can be accounted for the substrate laminate overheating as described. The second one is due to overheating of the incoming tape. This happens all during a very short amount of time. The closed loop control for the laser optics and its actuator are too slow to react on this. As seen in Fig. 5-6, the compaction roller gets deflected towards the tape placement head. The deflection of about 7.5 mm causes a change of laser distribution between incoming tape and substrate laminate but also a change of peeling velocity from the placement head. The tape velocity drops from nominal 75 mm/s down to below 10 mm/s. This effect is intensified, as also the robot loses velocity during reorientation around the corner. Thus, the incoming tape is within the laser spot for a longer time and absorbs more energy than intended. After about 100 mm after the corner, standard 2D steady-state process conditions are reached again.

Similar to other composite production methods, the laminate thickness decreases around the corner. Compared to the flanges the laminate thickness at the corner is reduced by 18 % in average. The thickness reduction can be explained by an increase of local compaction pressure under the roller around the corner (see section 5.4.2). Additionally, high temperature at the corner promotes transverse material flow, as the matrix's viscosity is reduced. This effect can be seen on the surface texture of the test specimens. The front side of the specimens show a smooth and closed surface, while the backside reveals gaps between the individual tracks in the region right behind the corner (Fig. 5-8) due to less transverse squeeze flow of the tape.
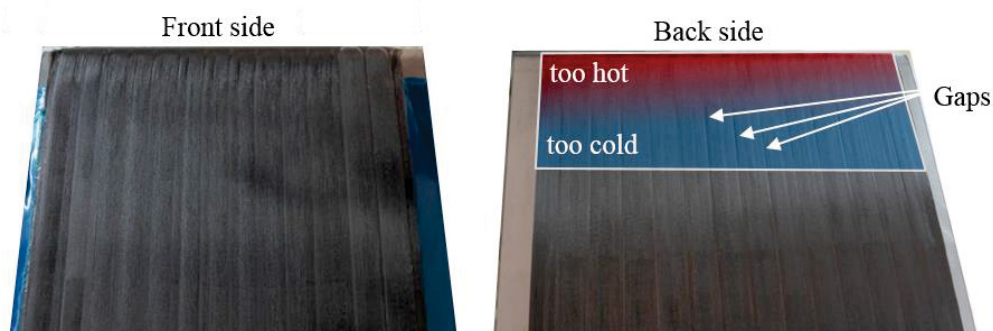
Fig. 5-8: **Front (left) and back side (right) of specimen set**
Smooth and closed surface at the front side
Gaps at the back side of the specimens between the tapes due to insufficient heating

During reorientation around the corner, the robot also deviates from the programmed path in lateral direction. At the top of the corner in Fig. 5-8, left picture, a lateral misalignment of the UD tapes to the right hand side can be observed. The robot logs

its TCP position during placement. Fig. 5-9 shows the tape velocity with respect to the TCP position in 3D space. An unintended lateral deviation of up to 5 mm for about 25 mm lay-up length can be observed at the corner of the tool, while the tape velocity is drastically reduced (blue color at the top of the corner).
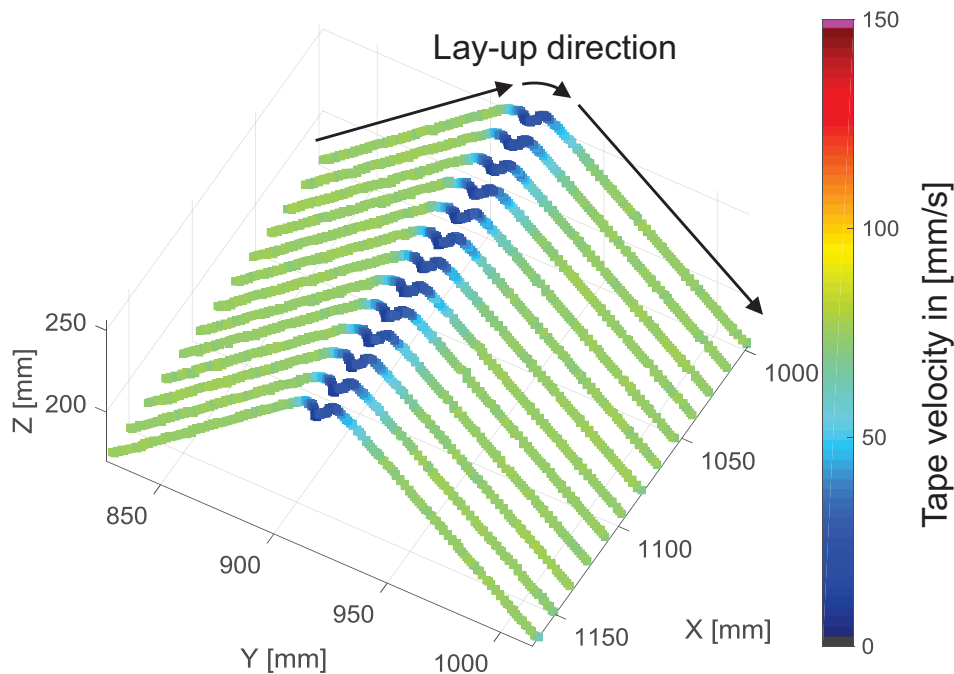
Fig. 5-9: **Lay-up speed with respect to TCP position during lay-up**
At the top of the corner the tape laying head's TCP deviates about 5 mm from the programmed path in lateral direction (x-direction), while the lay-up speed breaks down.

A track with a nominal lay-up speed of 10 mm/s is manufactured as well. While the laser power is reduced by the closed loop control to around 100 W, the overall heating behavior is the same. Due to the relative slow processing speed with respect to the closed loop control's control rate, the laser is turned off and on for short durations around the corner. A strobe like effect is observed.

Similar behavior as for the 90° tool is observed for the 105° and 120° angled tools. However, as the tape laying head does not have to reorient so strongly, the reduction of tape speed and lateral deviation of the TCP is not as distinct. Overheating due to shortening of the laser heated length on the substrate happens likewise.

5.3.2 Lay-up with constant laser power

For a better understanding of the heating characteristics around the corner, lay-up trials with constant laser power are conducted as well. In order to avoid too much overheating and thus smoke generation, a reduced constant laser power of 300 W is used. For comparison, the closed loop control used around 370 W to achieve 300 °C at the flat legs of the 90° tool (Fig. 5-7). All other process parameters are kept constant, as de-

scribed in Tab. 5-1. The closed loop control for laser optics angle was turned on after the first layer. Also, the robot programming is kept the same.

Fig. 5-10 shows the thermal camera images of the lay-up with constant laser power. The observations are the same as for lay-up with closed loop control. Overheating and deflection of the nip-point at the corner area can be seen.
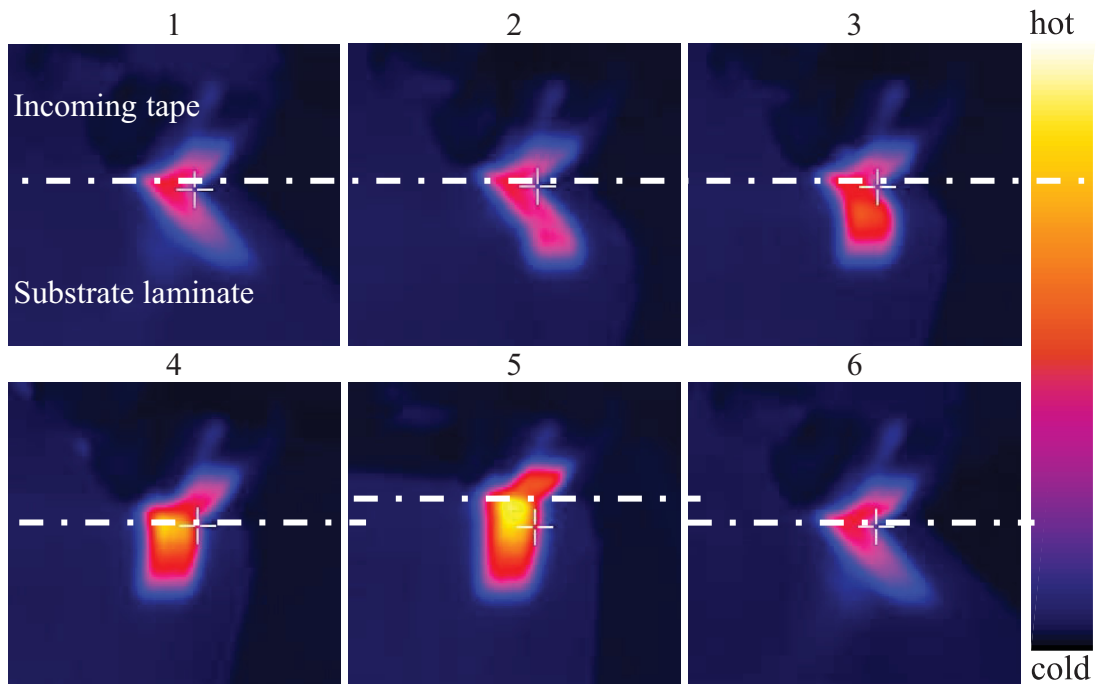
Fig. 5-10:   **Thermal camera images of the nip-point region during lay-up around the corner of a 90° specimen with constant laser power (dashed lines mark the nip-point)**

A detailed look at the log file data of the lay-up with constant laser power shows the same basic heating behavior (Fig. 5-11). However, as no closed loop control is reducing the laser power due to overheating, the maximum temperature is even higher (almost 500 °C). There are also two local maxima in the temperature curve. The first one is attributed to overheating of the substrate laminate and the second one to overheating of the incoming tape. The second one is higher as for lay-up with laser power closed loop control, although less nominal laser power is used and is overlapping with the first maxima.
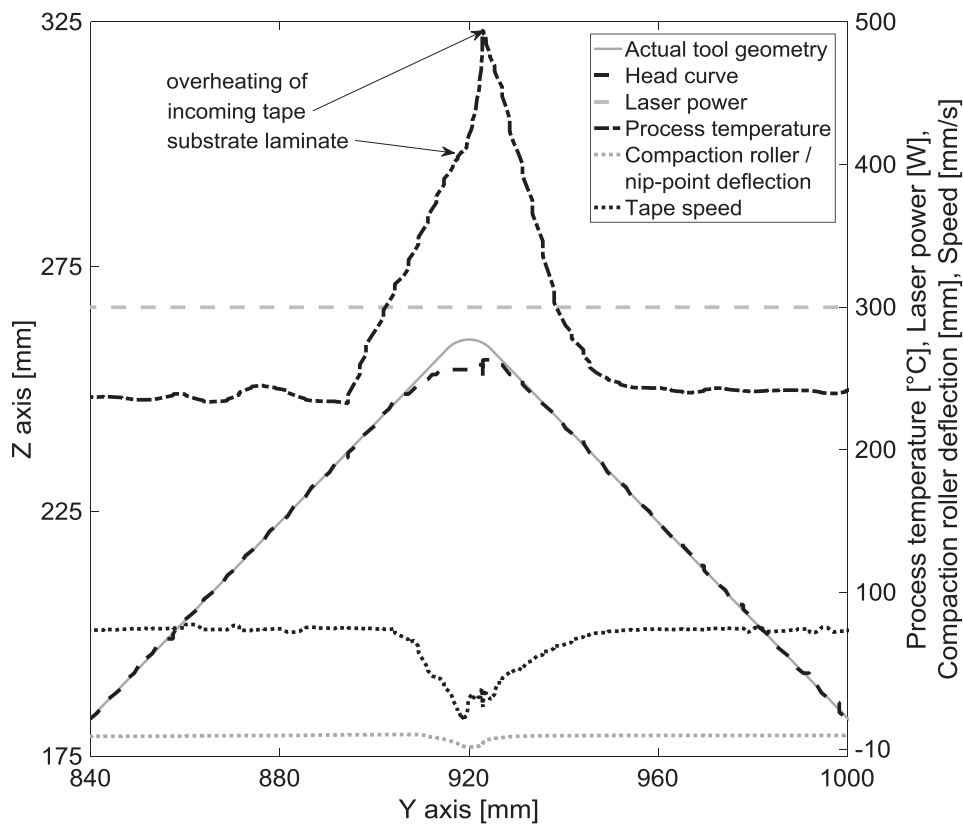
Fig. 5-11:   **Log file data of a track from 90° specimen with constant laser lay-up strategy**

In contrast to lay-up with closed loop control, there is no area, where the laminate temperature is too cold. Stable process conditions as before the corner are reached again about 40 mm after the corner.

The deflection of the compaction roller and break down of the tape speed are similar to before, as robot programming is the same.

5.4 Kinematics of 3D lay-up

In the previous section 5.3 first 3D lay-up trials with a standard 2D placement setup are described. During placement, overheating of the laminate occurs due to various reasons. In contrast to the quasi-steady-state process of flat TP-AFP lay-up, 3D lay-up around corners with a small radius is a non-stationary process. Therefore, the kinematics of the process need to be analyzed. In the following sections, the movement of the robot is investigated and optimized. Along with the robot's movement, the resulting compaction pressure distribution and the laser spot size on the composite are investigated. The cause for overheating at the corner is found in a combination of all three effects.

5.4.1   Robot movement

The robot is being programmed with the help of a virtual point called "Tool Center Point" (TCP). The TCP is laterally in the middle of the compaction roller and vertically underneath the roller's axis. As the compaction roller, with its soft silicone outer tube, gets deformed by the compaction pressure, the TCP is in the middle of the compaction zone. Towards the laser spot, the compaction zone ends with the nip-point, where the bonding of the incoming tape and substrate laminate starts (see Fig. 5-12).
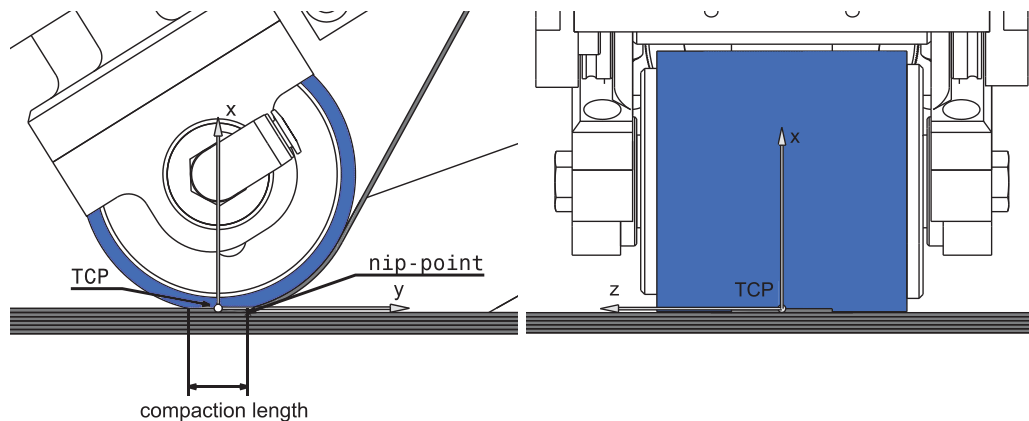
Fig. 5-12:   **Robot's Tool Center Point, nip-point and compaction zone**

By this TCP, the tape laying head is referenced in the robot's control unit. The TCP's data consist of its position (x-y-z coordinates) and its orientation in space. The lay-up tool's position and orientation is also stored within the robot's control. In the robot program a sequence of desired positions and orientations of the TCP in reference to the lay-up tool is programmed.

During 3D lay-up the TCP and thus the tape laying head keeps its orientation with respect to its current position on the lay-up tool's surface (Fig. 5-13). The angle of inclination (γ in Tab. 4-1) is kept constant.
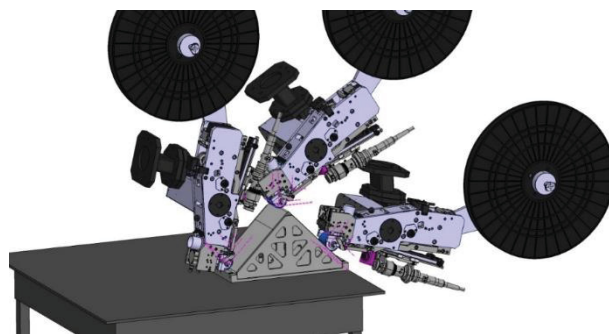
Fig. 5-13:   **Placement head orientation during 3D lay-up**

In order to investigate the heating effects caused by the 3D geometry, other process parameters like pneumatic pressure of the compaction roller's cylinder, its nominal stroke from the placement head and lay-up velocity are kept constant. The compaction

roller's stroke directly influences the tape's peel speed and the laser bias ratio of heating the incoming tape and substrate laminate (see Fig. 4-6). Especially keeping stroke and placement velocity constant is challenging, as the robot has to reorient strongly at the corner and deviates from its intended path on the tooling. This can be compensated by allowing the robot to reorient more smoothly by blending the trajectory and deviate from the programmed path. To compensate these deviations, the programmed path is shifted intentionally.

Initial programming was done according to the geometry of the lay-up tool. The exact coordinates of the three points of the rounded corner of the tool were used: Transition from straight to arc, tip of the arc and transition from arc to straight surface again (marked as dark stars in the center of Fig. 5-14). However, the robot does not follow the path correctly at the arc. Consequently, the robot's TCP is shifted during reorientation and the TCP's speed and tape peel speed are reduced. By increasing the distance between the programmed points the speed can be kept more constant. By this, the robot deviates even more from the intended path. To compensate for that, the top point needs to be shifted vertically by 13 mm for the 90° geometry. The optimized points for robot programming are shown as grey stars in Fig. 5-14. This optimization is individual for all angled geometries. With this optimized robot programming, the tape speed and TCP or nip-point position is kept within a small tolerance (grey curves).
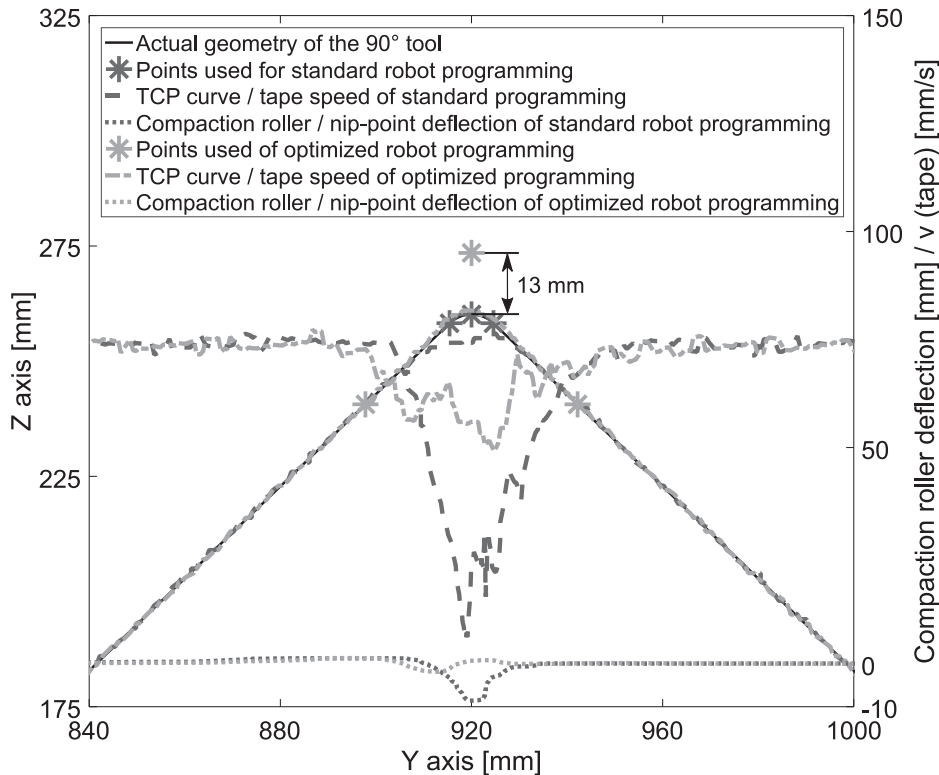
Fig. 5-14: **Placement speed and compaction cylinder stroke with respect to the lay-up geometry of a specimen with 90° leg angle**

As the compaction roller and laser optics are mounted to the moving placement head they influence the process conditions around the corner as well. This is investigated in the next sections.

Further process improvements are achieved by implementing a mechanical compensator to the tape placement head that is linking consolidation roller and laser optics. By this, the laser optics always follow the consolidation roller and compensate any unintended deflection. The alignment of the laser spot with respect to the nip-point, incoming tape and substrate laminate stays constant. The compensator can be seen in Fig. 2-16 at the bottom side of the tape placement head.

5.4.2 Consolidation pressure

Besides temperature, pressure is needed to create the bond between the incoming tape and substrate laminate. The laminates show a smaller thickness in the arc section compared to the flat legs by an average of 18 %. This can be attributed to the higher temperature and the increase of compaction pressure.

The influence of compaction pressure and its distribution has been investigated in detail in the literature, but the focus is mainly on the effects on laminate bond. Lichtinger presents a detailed analysis of the compaction pressure distribution by AFP rollers [4, 5]. However, the focus was on Thermoset-AFP with different types of rollers. According to [10, 41], high compaction pressure may increase the bond strength but the effect is not as clear as for processing temperature. Stokes-Griffin [8] and Schaefer [41] used an electronic measurement film to measure the compaction pressure distribution dynamically. Two approaches to measure the compaction behavior are described in the following:

- Static measurement of the compaction length by ink
- Dynamic measurement of the compaction pressure distribution by pressure sensitive electronic film

5.4.2.1 Static measurement by ink

A very straight forward method is chosen for the static measurements of the compaction length. The compaction pressure and the position of the roller on the tool is altered. The silicone roller, is 30 mm wide and 64 mm in diameter and consists of a 7 mm thick layer of silicone tube put on an aluminum core. The silicone has a Shore A 43 hardness.

Measurement setup

The silicone roller is covered with ink from a stamp-pad and then pressed to a sheet of paper covering the lay-up tool. The head-tool angle γ is kept at 32° (cf. Fig. 4-6). The vertical compaction force F_c is defined by the following:

$$F_c = \cos(\gamma) \cdot F_{cylinder} \sim 0.85 \cdot F_{cylinder} \qquad (5\text{-}1)$$

The compaction force is varied from 1 bar cylinder pressure to 6 bar, i.e. 130 N to 750 N respectively. Measurements are taken at the flat parts of the tool and at the arc. There is no composite tape between the roller and the paper and thus no tape tension applied. The imprints on the paper are measured with a caliper afterwards.

Results

Fig. 5-15 shows on the left the imprints of the roller on a flat sheet of paper with altered compaction force. The compaction length is measured on three positions over the width and the mean value is plotted in Fig. 5-15 as well. The right graph in Fig. 5-15 shows imprints of the compaction roller on different positions on the v-shaped tool with a compaction force of 130 N (1 bar cylinder pressure). In comparison to the compaction length on a flat surface it is reduced to 50 % length (~7 mm to 8 mm), at the rounded corner of 6.5 mm radius.
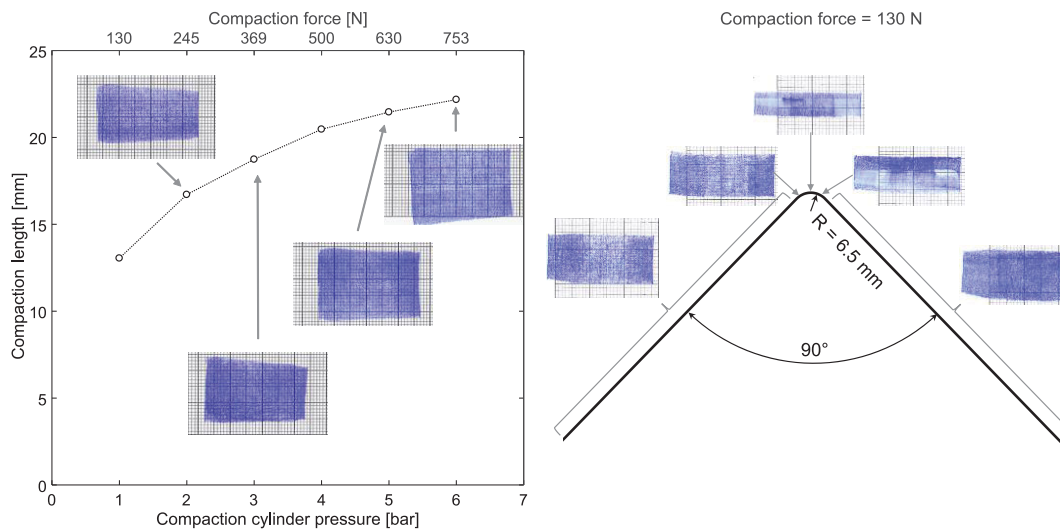
Fig. 5-15:   **Compaction roller imprints to measure the compaction length**
Medium compaction length over compaction force on a flat tool with imprints (left);
imprints of the compaction roller at altered positions of the tool with constant compaction
force of 130 N (right)

Conclusion

Static measurements of the compaction length provide a good insight on the deformation behavior of the roller. The compaction length of the used silicone roller is showing a second order polynomial increase, with increasing compaction force. For 3D lay-up, the compaction pressure distribution changes due to the surface's curvature. For the investigated geometry, the local compaction pressure is doubled at the corner while the overall compaction force is kept constant. This behavior is observed for all three tools, independent of its angle. The arc length of the tool is determining the change of local pressure.

5.4.2.2 Dynamic compaction pressure measurements

While the static measurement from section 5.4.2.1 give a good idea of the compaction length under the roller, dynamic measurements with a pressure sensitive electronic film also provide information about the pressure distribution within the compaction zone.

Measurement setup

A pressure-mapping sensor film "type 5101" from Tekscan Inc. (Boston, USA) with an "Evolution USB handle" and the corresponding software is used. The film has individual sensors every 2.5 mm in both directions to measure the local pressure. Recording frequency is set to 100 Hz and the head – tool angle γ is kept at 32°, same as for the static measurements. The compaction roller's cylinder pressure is set to 1 bar and 2 bar, resulting in a vertical compaction force of 130 N and 245 N respectively. First, measurements of the roller on a flat surface, e.g. flat table or legs of the v-shaped tools, were conducted at different speed, 50 mm/s, 75 mm/s and 100 mm/s (Fig. 5-16, left). Next, the pressure-mapping sensor was then put around the corner of all three v-shaped tools (Fig. 5-16, right). Of each set of parameters and tool, three repeating measurements were conducted. There was no composite tape and thus no tape tension used during testing.
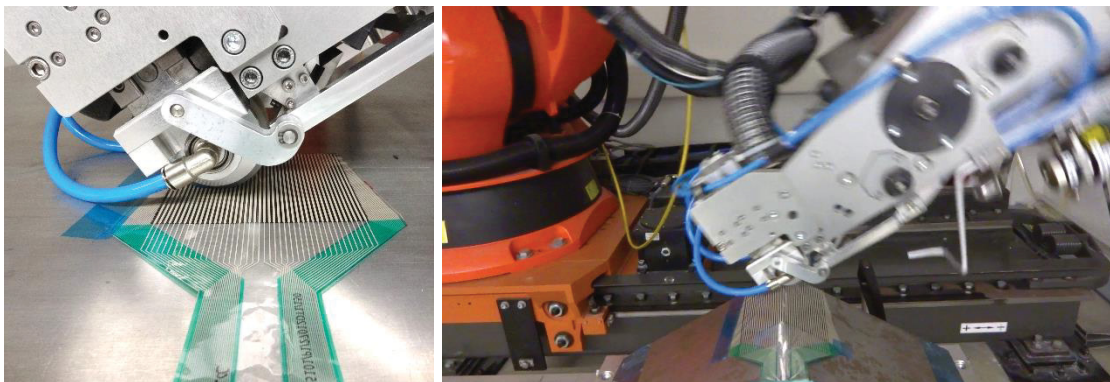
Fig. 5-16: **Dynamic pressure distribution measurements on 2D and 3D surfaces**

Results

The pressure-mapping sensor can measure the local pressure in two dimensions, in lay-up and in transverse direction (color plot within Fig. 5-17). As the pneumatic cylinder is connected to the roller in the center and the compactions roller's aluminum core is stiff, only a minor change of pressure distribution over width of the roller can be observed. The compaction pressure distribution changes in lay-up direction, the roller is moving along. Fig. 5-17 shows the medium compaction force per width for all tested cases. For a compaction force of 130 N on flat laminates, a dome like pressure distribution of more than 13 mm length can be observed. As expected, this is independent of the lay-up speed. The maximum compaction force per width is about

0.8 N/mm. Fig. 5-17 shows also the force per width for all 3D lay-up geometries. There is no difference between the 120°, 105° or 90° angled tool. The arc length of the tools' corners is always longer than the compaction length.

For a doubled compaction force, the compaction force per width also doubles. As the compaction length now is longer than the arc length for a 90° angle, the pressure distribution alters a little for the different tooling angle. In addition, more sensors of the film are activated, allowing a more precise pressure distribution measurement.
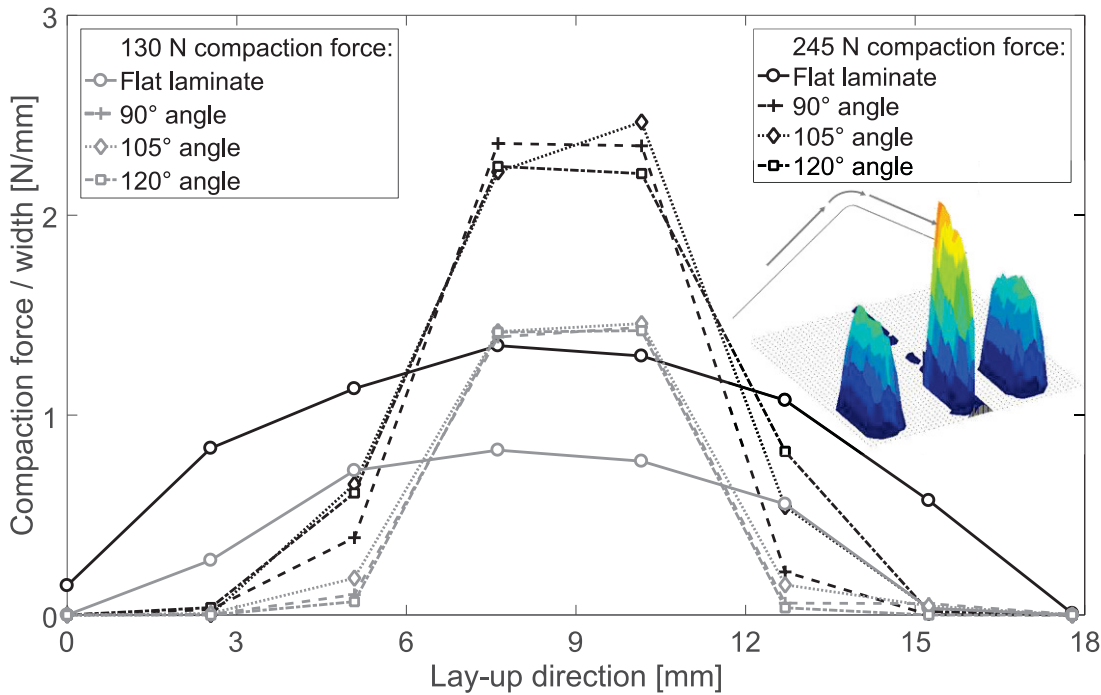
Fig. 5-17:   **2D pressure distributions and medium compaction force per width for flat and 3D lay-up**

Conclusion

With the help of the electronic pressure-mapping film, the pressure distribution can be measured dynamically. The pressure distribution under the compaction roller is measured in lateral and in movement direction. When moving around the corner with a radius of 6.5 mm, the compaction length is reduced to 50 % and the local pressure intensity is doubled. This effect is independent for the angle of the tool, when the compaction length is below the arc length of the corner. For a high compaction pressure or highly deformable compaction rollers this effect is weakened.

A higher sensor density of the electronic film would be preferable and could deliver data of higher resolution. With the used sensor film, no valid measurement of the compaction length is possible. However, the dynamic measurements confirm the ink measurements, where the compaction length can be determined. Both measurements combined are suitable to measure the change of compaction length and compaction pressure distribution around the corner area.

5.4.3   Laser heating length

During the lay-up trials described in 5.3 a change of heated length of the substrate laminate can be observed (Fig. 5-6 and Fig. 5-10). The change of the tool geometry results in a change of the laser beam projection on the tool around the corner. This is regarded as a major cause for the overheating. Geometric and kinematic boundary conditions cause this behavior, which is further investigated in this section. As the incoming tape is coming from the tape laying head, there is no change of direct laser heating caused by the 3D geometry during lay-up.

A 2D and 3D kinematic model of the tape laying head movement over the curved tool is set up in CAD. The position of the tape laying head and laser spot is altered with respect to the lay-up tool. The intersections of the laser beam with the substrate laminate and thus the heated length are calculated and measured. Fig. 5-18 shows the lay-up sequence during 3D lay-up around a convex corner with 90° and 6.5 mm corner radius. All components are drawn to scale to each other in the 2D sketches. Once the start of the laser beam on the substrate laminate reaches the corner, the heated length (highlighted in orange) is reduced. This continues until the tape laying head moves completely around the corner, i.e. the reorientation is completed.
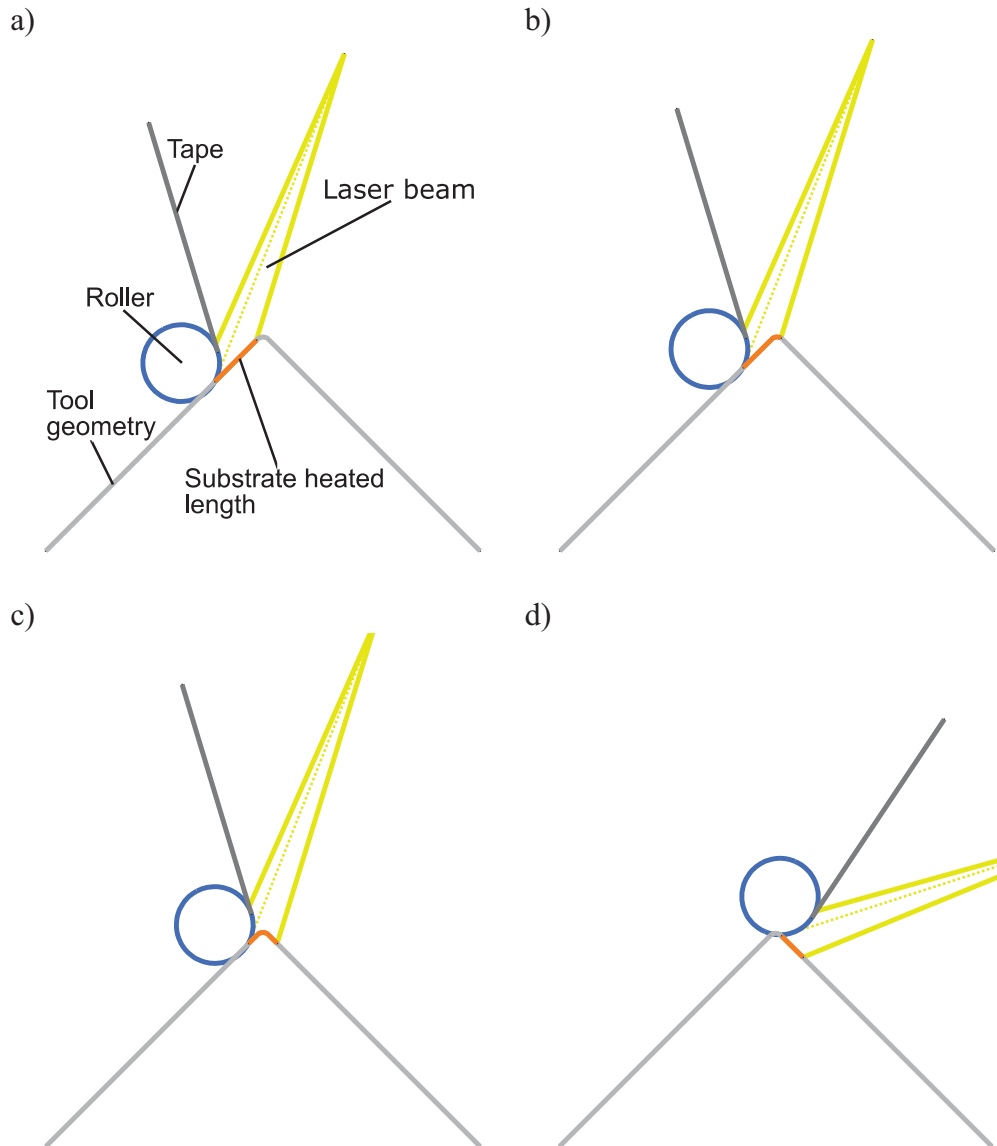
Fig. 5-18:   **Laser spot projection during 3D lay-up around a convex corner with a 90° angle**

The heated length on the substrate laminate is measured for different positions of the robot's TCP on the lay-up tool. The process parameters and laser boundary conditions from section 4.4 for CF/PA6 are used. However, the angle between laser beam and tool α is set to 24.5° (0° laser bias angle of the machine). The virtual laser beam origin with respect to the TCP is $x_1 = 278.9$ mm and $x_3 = 117.1$ mm. Four characteristic sections are identified. A linear reduction of laser heated length on the substrate laminate is measured, when the TCP approaches the arc of the tool (section II in Fig. 5-19). When the nominal laser heated length for 2D lay-up is longer than the remaining length before the corner, part of the laser beam is projected on the arc or the leg pointing downwards. An extra reduction of heated length occurs, when the TCP is on the arc of the corner and the head starts to rotate (section III). The minimum heated length at this point is 48°% of the initial heated length. When the placement head exits the

arc of the corner it is fully reoriented. At the end of this movement, the heated length increases very quickly back to its initial length (section IV).
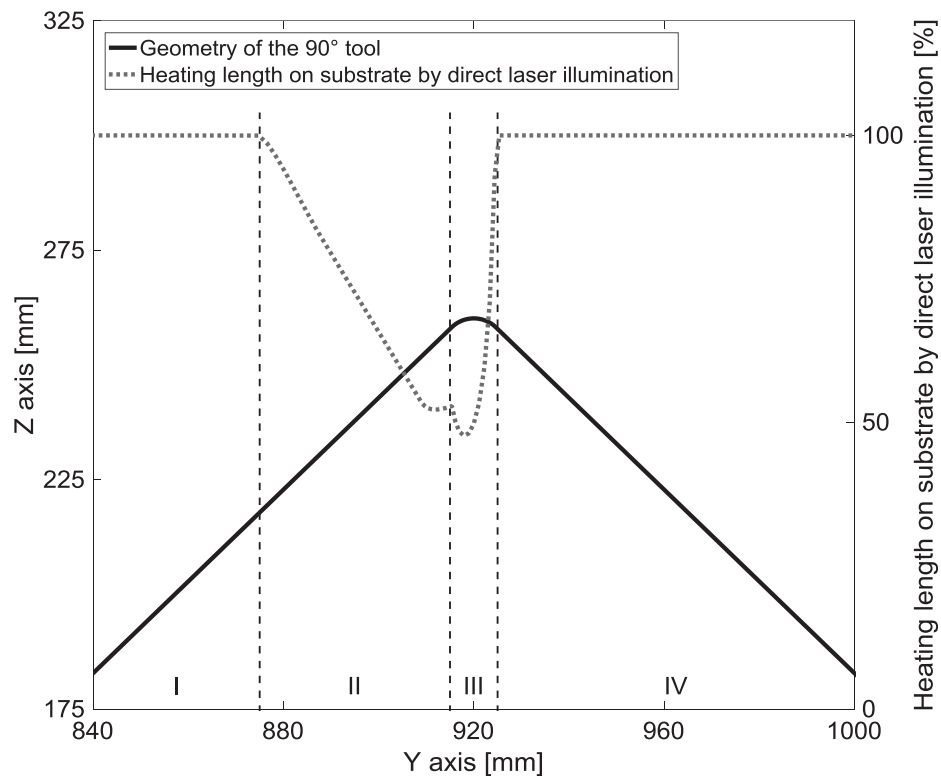
Fig. 5-19:   **Heating length by direct laser illumination on substrate laminate during 3D lay-up**

These findings are in good agreement with Weiler et al. [53]. Besides the tool geometry, also the laser spot size determines the change of heated length during 3D lay-up. However, a longer heating length results in a softer heating of the material and makes the process more stable. A better in situ consolidation can be achieved this way (see chapter 4). The kinematics of laser spot and the resulting direct laser heating length needs to be implemented in a thermal simulation for 3D lay-up. Together with the absorption behavior of the composite the exact heat input can be calculated (described in detail in section 6.3). Together with the heating time of each discretized element the calculation of the 3D laser boundary condition can be conducted.

5.5 Thermal degradation by overheating

The laminate at the corner and after it is exposed to much higher temperatures than in the straight area before and afterwards (see lay-up trials in section 5.3). This happens independently of the processing strategy, both for closed loop controlled and fixed laser power. In addition to the overheating, also insufficient heating is observed for the closed loop controlled laser power.

According to Beyler et al. degradation of PA6 starts at 342 °C under standard atmosphere and at 422 °C in nitrogen atmosphere [121]. However, no information is given about the exposure time or degradation speed. Herrera Salinas reports thermal degradation for PA6 under nitrogen atmosphere to start at 335 °C and reaches maximum at 436 °C. Under synthetic air atmosphere, the main degradation takes place between 320 °C and 475 °C [122]. Bates et al. [123] investigate the thermal degradation of PA6 at different heating rates in a Thermogravimetric analysis (TGA) setup. A higher degradation temperature is measured for higher heating rates. However, the fastest investigated heating rate with 20 °C/min is far lower than during the TP-AFP process. The heating rate was about 650 °C/s (39000 °C/min) for the lay-up trials in CF/PA6 in section 4.4.3.

Degradation of the polymer matrix in the composite leads to reduced properties of the polymer itself and weaker bond of the layers. Degradation of polymers happens due to different effects [121]:

- Random-chain scission at any point of the polymer chain
- End-chain scission
- Crosslinking between polymer chains
- Chain stripping

In order to quantify the effect of high temperatures on the laminate quality, different laminate test methods are evaluated:

- Mechanical wedge peel test:
  Wedge peel tests proved to be a valuable test method to evaluate the bonding of TP-AFP laminates. A detailed description of the wedge peel tests can be found in section 5.5.1.
- Differential Scanning Calorimetry (DSC) measurement:
  According to Eriksson et al. [124–126] and Radlmaier et al. [127] thermal degradation of Polyamides leads to a change of the melting temperature and can be measured via DSC. Section 5.5.2 describes the DSC test procedure and results.
- Dynamic Mechanical Analysis (DMA) measurement:
  An alternative method to measure the T_g via DSC is testing by DMA. Double cantilever beam specimens are tested over a temperature range exceeding the expected T_g. DMA testing of CF/PA6 specimens is described in detail in section 5.5.3.
- Thermogravimetric analysis (TGA):
  TGA is often used for measuring thermal degradation of polymers [80, 121, 123, 128]. During testing, a small specimen is exposed to increasing temperature, while its weight is monitored. Thus, degradation that is causing a loss of weight can be referenced to its temperature. According to Beyler et al. the main products of PA6 decomposition are water and CO_2, that are released from the polymer chain [121]. Just chain-scission without evaporating material can-

not be detected, as only the overall weight of the specimen is monitored. TGA tests were performed in [S18] at Fraunhofer IGCV. As the heating rate of the TGA is very slow compared to TP-AFP processing, the tape samples were test-ed comparatively. CF/PA6 specimens, exposed to a processing temperature of 280 °C and 400 °C (below and above degradation temperature of 342 °C ac-cording to Beyler et al. [121]), were tested. However, for both specimens no dissimilar loss of weight, that can be attributed to prior degradation, could be detected. The TGA curves were overlapping within their standard deviation.

- Micrographs
  Within micrograph sections the carbon fibers and the matrix as well as their distribution and void content can be observed. Micrographs of the wedge peel specimens are presented in section 5.5.4.

In the following sections the successful test methods, wedge peel test, DSC test, DMA test and micrograph measurements are described in detail.

5.5.1 Flat laminate wedge peel test

Wedge peel testing has been proven a quick and conclusive method to evaluate the bond strength between composite layers, manufactured by TP-AFP. First introduced by Hulcher et al. in 1998 [129] and 1999 [130], it has been used in literature to opti-mize the process parameters by many authors with different TP-AFP systems and different polymers in the carbon fiber tapes [10, 25, 32, 41, 62, 63, 131, 132].

Test specimens were manufactured in the temperature range of the 3D lay-up trials from section 5.3 and were tested by wedge peel test. The aim is to investigate the bond strength at all occurring process temperatures and to define a temperature thresh-old that is not supposed to be exceeded in order to avoid low bond strength. The wedge peel test is not a test for degradation, but low bond strength for specimens manufactured at high process temperatures can indicate damaged polymers that are incapable to establish a strong bond.

Principle

During wedge peel testing, a wedge is pulled through the interface of two layers (Fig. 5-20, right). The wedge's shape is designed to impel the crack front in some distance to its tip.

Specimen manufacturing and testing

Flat 2D CF/PA6 specimens are manufactured from 200 °C to 460 °C set-point temper-ature with the help of the machine's closed loop control. The temperature is kept within ±10 °C in the specimen section. A lay-up speed of 100 mm/s and consolidation pressure of 130 N is used for manufacturing. The angle between tape laying head to

tool is set to γ = 32°. For each set-point temperature at least six specimens are manufactured and tested (Fig. 5-20). The specimens consist of four layers of CF/PA6 tape. Between layer two and three, a polyimide film is inserted for crack initiation. Matrix squeeze out is observed for specimens manufactured at 380 °C set-point temperature and above (Fig. 5-20, top left).

Additionally, one test series with post consolidated samples is produced. After lay-up with 300 °C, the specimens are post consolidated under a vacuum bag in an oven at 260 °C for 20 minutes. Oven post consolidation features also slow heat up and cool down rates, which result in a more crystalline polymer structure. The specimens are dried for 72 h at 60 °C in a vacuum oven before testing.
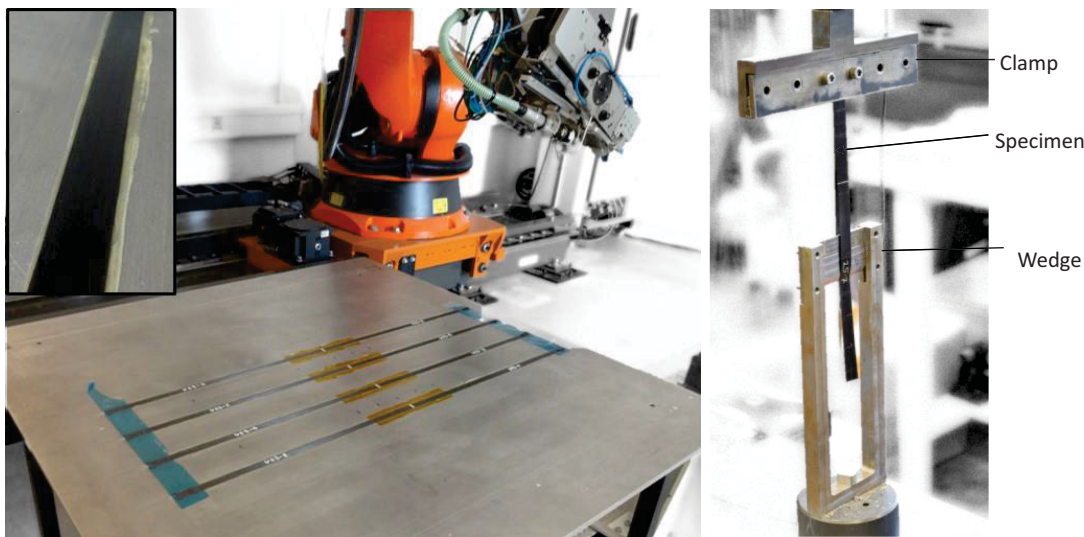
Fig. 5-20: **2D wedge peel specimen manufacturing and testing**
top left corner: matrix squeeze out for high temperature specimens
left main picture: lay-up of eight specimens with PI film in the middle for crack initiation
right: wedge peel fixture and specimen during testing

The main test setup was adopted from Schaefer [41]. A wedge with a thickness of 3.2 mm and a wedge angle of 30° is pulled through layer two and three with a speed of 1 mm/s. The force is measured by a 1 kN load cell and the crossbeam's travel is logged by the universal testing machine at a rate of 50 Hz. For each specimen the width is measured at multiple cross-sections and the mean value is used to calculate the normalized wedge peel force per width.

Results

Fig. 5-21 shows plots of specimen series manufactured at four different temperatures. The analysis section is chosen after stabilization of the peel force and ends short before the end of the specimen. For each specimen the mean value is calculated in this section.
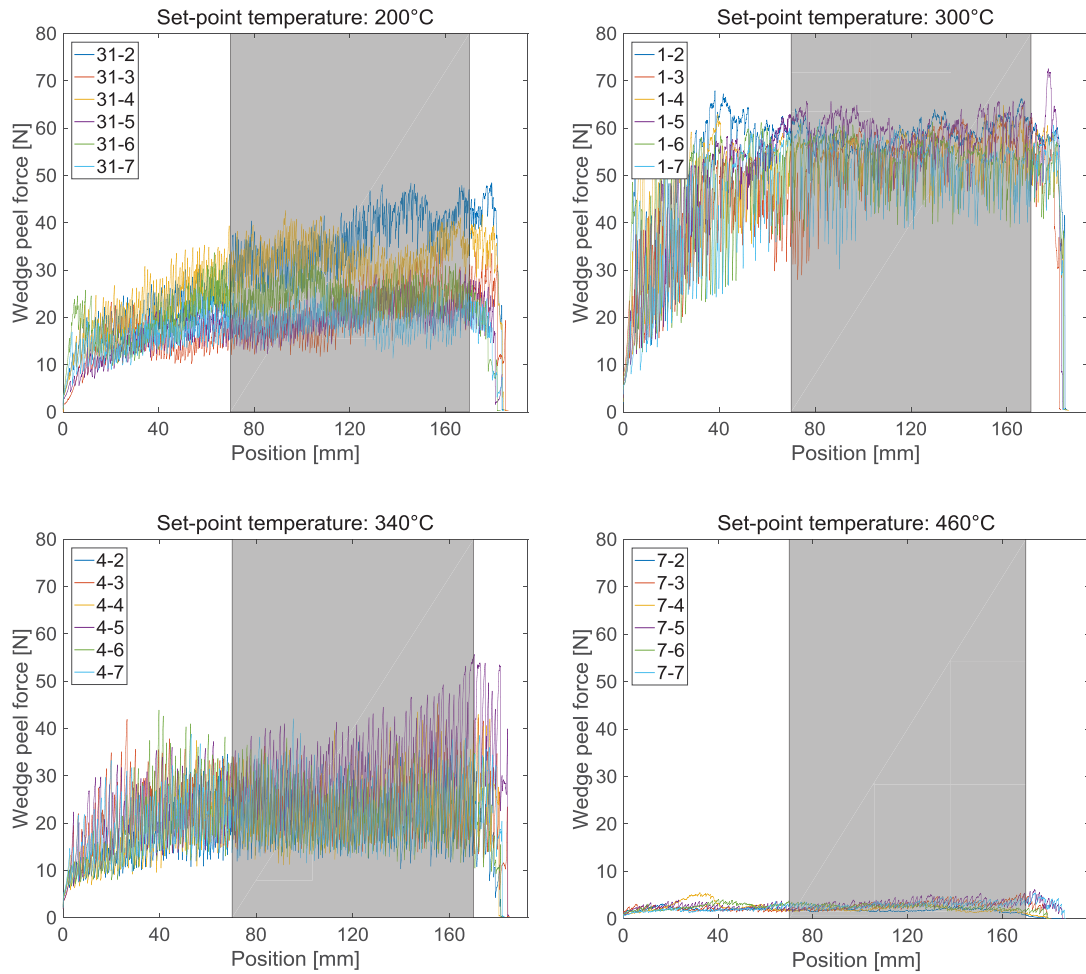
Fig. 5-21:   **Wedge peel curves of specimens manufactured at different processing temperature**
The grey area highlights the analysis area.

After normalization with the specimen's width, the mean value and standard deviation of each test series is calculated and can be seen in Fig. 5-22. The peel resistance starts at a low level and increases by more than 100 % at 260 °C set-point temperature. A high plateau is observed between 260 ° and 300 °C. For higher temperatures than 320 °C the peel resistance reduces quickly. Very poor peel resistance is measured for specimens manufactured with a set-point temperature of 360 °C and above. The post consolidated (PC) specimens show a mean peel resistance of 2.9 N/mm, which is 70 % of the highest mean value.
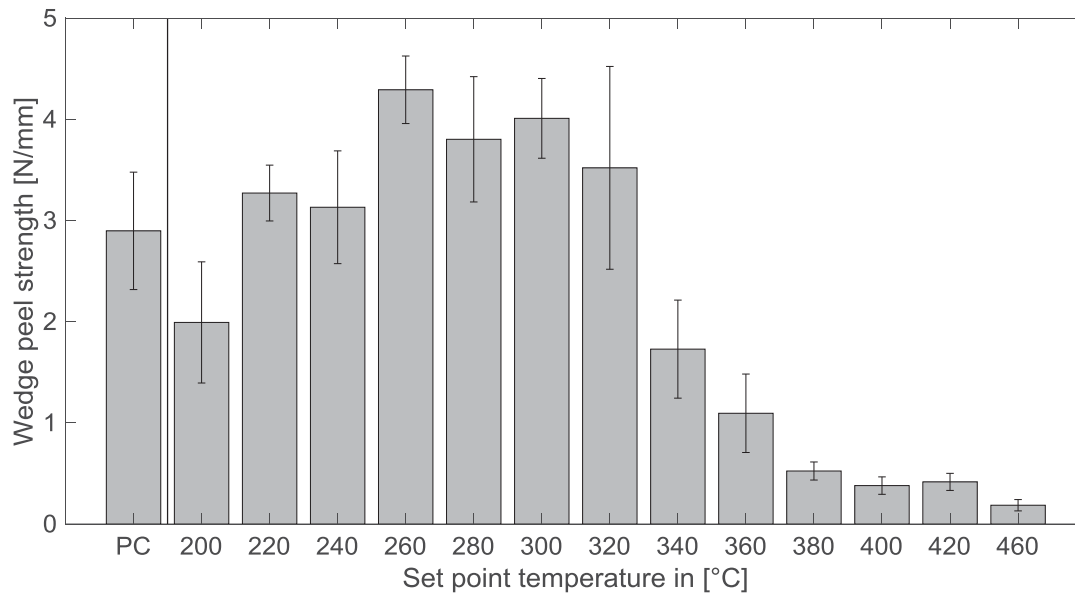
Fig. 5-22:   **Mean value and standard deviation of wedge peel strength of flat specimens manu-
              factured from 200 °C to 460 °C set-point temperature for the closed loop control**
              PC = Post consolidation

Conclusion

Wedge peel tests of specimens manufactured within the full process temperature range
of the 3D lay-up trials (section 5.3) were conducted. The peel force shows a clear
optimum at a process temperature between 260 °C and 300 °C. For lower tempera-
tures, the low peel force indicates insufficient heating and thus poor bond establish-
ment during lay-up. Higher process temperatures, especially temperatures above
340 °C, lead to poor bonding as well. This is attributed to thermal degradation of the
PA6 polymer during lay-up, as all other process parameters were kept constant for all
test series. Signs for degradation can only be detected visually by matrix squeeze out
during manufacturing. For best peel resistance the process temperature should be kept
within 260 °C and 320 °C at all regions. It can be concluded that thermal polymer
degradation occurs in the overheated areas of section 5.3's 3D specimens.

The low peel resistance of the post consolidated specimens can be explained by their
higher crystallinity due to the lower cool down rate within the oven. Similar trends are
noted in literature for autoclave post consolidated specimens [10, 41, 60]. During
manufacturing of the post consolidated specimens, special attention was given to avoid
high temperatures, to exclude polymer degradation. Due to the different polymer
structure, post consolidated specimens cannot be used as a reference to judge the bond
quality of in situ consolidated TP-AFP specimens.

5.5.2 Differential Scanning Calorimetry (DSC) test

From excess material of the wedge peel specimens, small samples are cut and tested via DSC according to DIN EN ISO 11357-1. Prior to testing, all samples are dried for 72 h at 60 °C in an evacuated oven. A heating rate of 10 °C/min to heat the samples from 0 °C to 280 °C and a dwell time of three minutes is used before they are actively cooled down to 0 °C again with the same rate. From the temperature-heat-rate diagrams the melting temperature T_m and the crystallization temperature T_c are derived (Fig. 5-23).
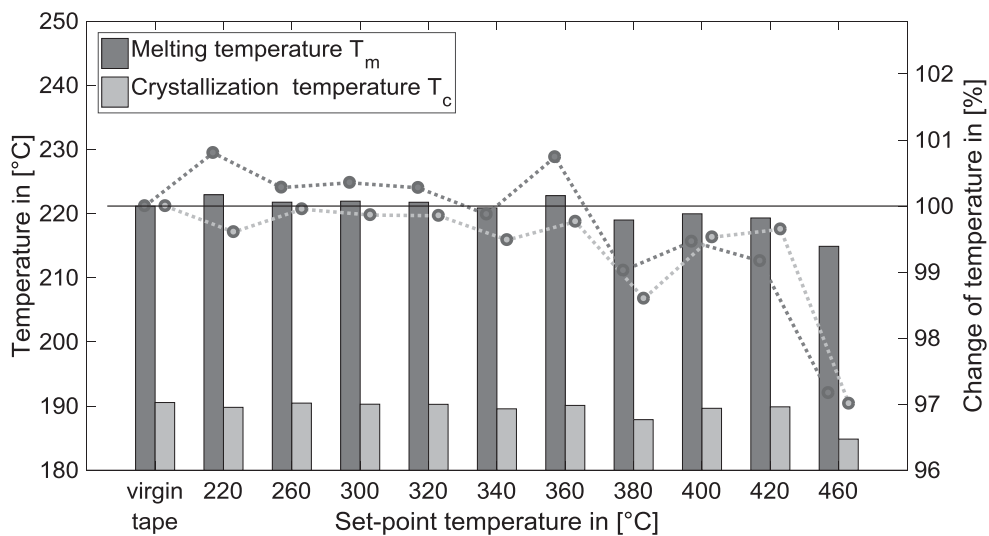
Fig. 5-23:   **Melting and crystallization temperature of CF/PA6 samples**
Bars: absolute values (left axis)
Dots and dashed lines: relative values with respect to virgin tape in °C (right axis)

Over the manufacturing temperature range, which ensures degradation for the high temperature values, a difference of the melting and crystallization temperature is observed. T_m changes by 8.0 °C and T_c by 5.7 °C. Although T_m and T_c are getting to lower values for the high temperature samples, the 360 °C sample shows the highest values among of all. Radlmaier et al. [127] report a loss of T_m of about 2.5 °C to 3 °C for temperature cycled neat PA6 in air and nitrogen atmosphere, as it would occur during normal laminate production. Eriksson et al. report a reduction of T_m between 6 °C and 10 °C for artificially aged PA66 samples [125]. The DSC measurements indicate that thermal degradation occurs for set-point temperatures above 360 °C.

Besides T_m and T_c also the glass transition temperature T_g of a polymer can be measured by DSC. A change of T_g can also point to degradation. However, the T_g of PA6 is known to be hard to measure, especially for high crystalline polymers. However, the T_g cannot be determined reliably, as the DSC curve shows hardly a peak in that temperature range.

5.5.3 Dynamic Mechanical Analysis (DMA) test

The T_g of the PA6 matrix is not detectable in the DSC measurement curves. An alternative test method is Dynamic Mechanical Analysis (DMA). Samples of 55 mm by 5 mm are cut from spare material of the four-layer wedge peel specimens and are tested according to DIN EN ISO 6721-1 in a double cantilever beam (DCB) fixture. A frequency of 1 Hz and an amplitude of 20 µm is used. The heating rate is set to 3 °C/min to heat the specimen from 0 °C to 100 °C. Before testing all specimens are dried under vacuum in an oven for 48 h at 60 °C.

The manual of the Q 800 DMA from TA Instruments (New Castle, USA) suggests a geometry factor (GF) below 35000 1/mm to achieve sufficient stiffness of the carbon composite specimens. The geometry factor is calculated by:

$$GF = \frac{1}{F} \cdot \left[\frac{L^3}{24 \cdot I} + S \cdot (1 + v) \cdot \frac{L}{2 \cdot A} \right] \tag{5-2}$$

with F = clamping factor = 0.9; L = clamping length = 35 mm; I = moment of inertia; S = shearing factor = 1.5; v = Poisson's ratio; ; A = cross-section area

However, due to the thickness reduction of the specimens for high temperatures, the specimens for 400 °C and above are out of the recommended specification.

Fig. 5-24 shows the T_g values of the specimens measured by DMA. The T_g decreases with increasing processing temperature. No valid T_g is detectable from the measurement curves of the 380 °C and 400 °C specimens. For higher temperatures a significant decrease of the T_g is measured. However, the values of the 420 °C and 460 °C specimens need to be handled with caution due to the too thin specimens. Specimens of five or six layers are recommended for future tests to fulfill the GF suggestion.
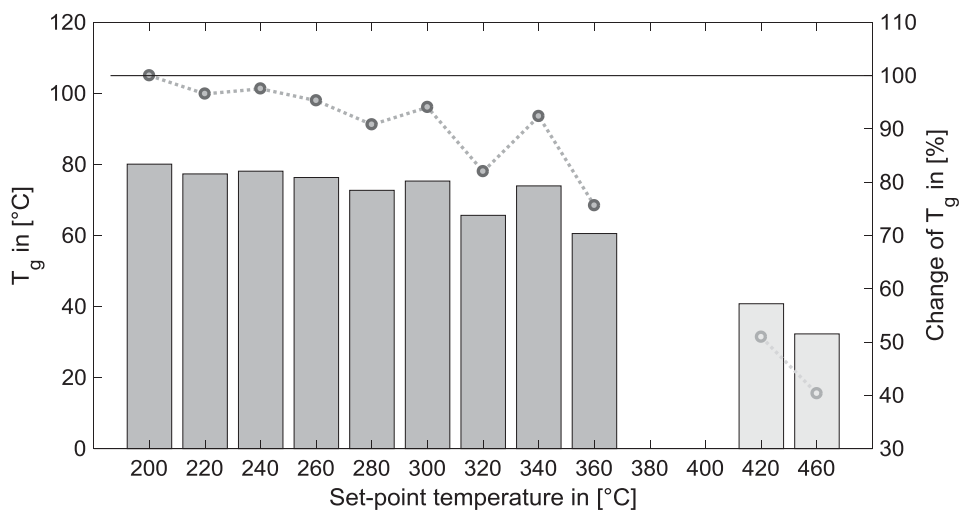
Fig. 5-24:   Glass transition temperature of CF/PA6 samples
             Bars: absolute values (left axis)
             Dots: relative values with respect to 200 °C specimen (right axis)

5.5.4 Micrographs and layer thickness

Micrographs of the four-layer wedge peel specimens were prepared in the same way as in chapter 3. Fig. 5-25 shows exemplary micrographs of specimens manufactured at different temperatures. No increase of voids with increasing process temperature can be seen. It is concluded that no polymer evaporation occurs during thermal degradation. The most obvious change in the micrograph series happens for the fiber-matrix distribution. The matrix rich interface between the layers is getting thinner with increasing processing temperature. The layers of the 460 °C specimens are hard to distinguish, as the matrix rich interface almost vanished.

260 °C   300 °C

340 °C   460 °C
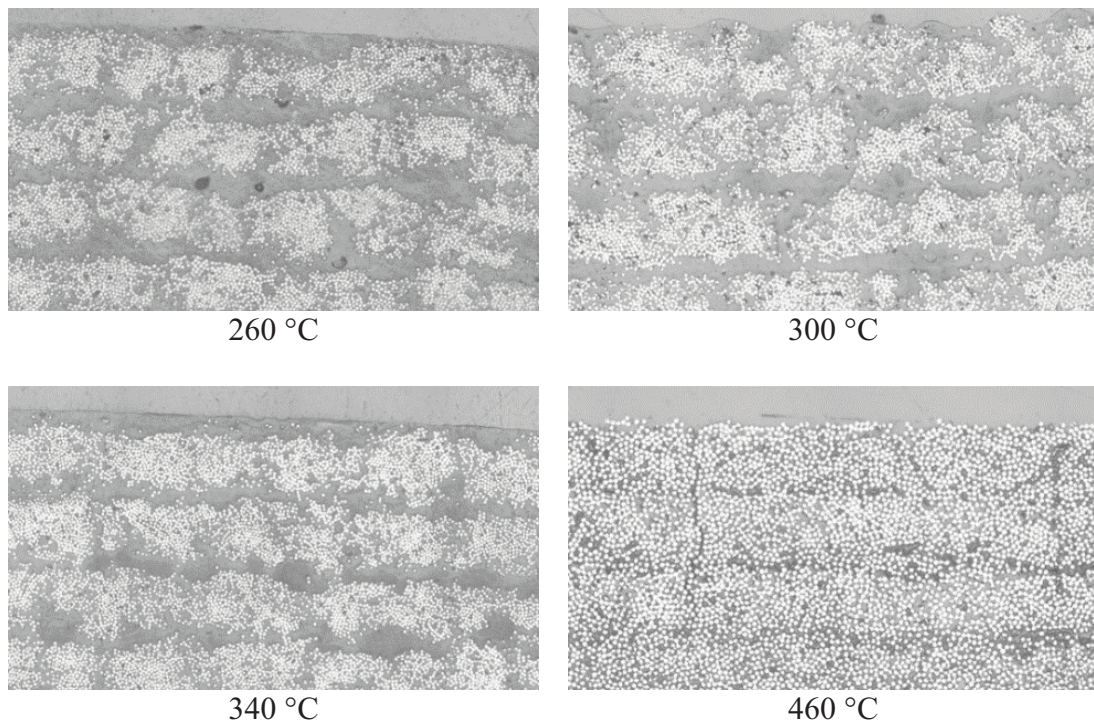
Fig. 5-25: **Micrographs of wedge peel specimens, manufactured at different set-point temperatures**

With the help of the micrographs, the thickness of the specimens can be measured. Samples manufactured with a compaction force of 130 N and increasing set-point temperature and samples with a set-point temperature of 300 °C and increasing compaction force are compared. Fig. 5-26 shows a constant layer thickness for the unprocessed tape and specimens, processed up to 340 °C. For higher set-point temperatures, the specimen and layer thickness decreases to 63 % of the tape's initial thickness. This is in good agreement with the observation of matrix squeeze out for high temperature specimens during manufacturing (see Fig. 5-20, top left). When alternating the compaction force during lay-up with the same temperature, no difference in layer thickness can be measured for 65 N and 130 N compaction force. The layer thickness is the same as for the unprocessed tape. However, when increasing the compaction force to

245 N a thickness reduction of 6.5 % can be measured. As shown in section 5.3 the local compaction pressure doubles at the round corner of the lay-up geometry, as it does, when increasing the compaction force on a flat surface from 130 N to 245 N.
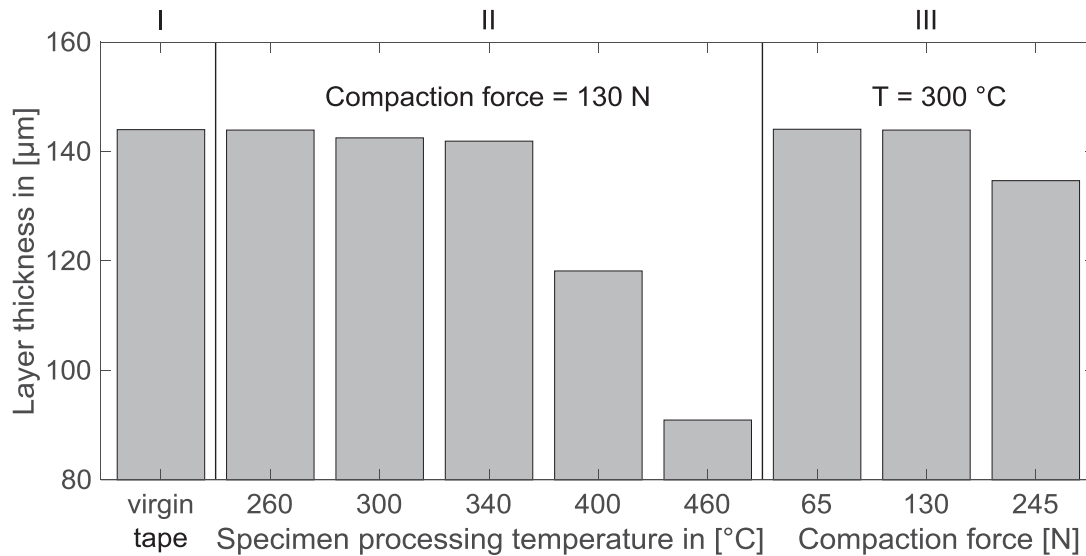
Fig. 5-26: **Layer thickness of unprocessed tape and specimens**
I. Layer thickness of unprocessed tape
II. Layer thickness of specimens that were manufactured at different set-point temperature for the closed loop control and the same compaction force.
III. Layer thickness of specimen that were manufactured with the same set-point temperature but altered compaction force.

When comparing these results with the thickness measurements from the 3D specimens from section 5.3, a combination of high temperature and increasing compaction pressure seems to be the reason for the thinner laminates around the corner. The overheating of the composite is identified as the main cause for the thinner laminates. Also, the increase of compaction pressure adds to the reduction of overall thickness in this area. The layer thickness reduction is much stronger for the four-layer wedge peel specimens than for the 18-layer specimens from section 5.3.1. While the 18-layer specimens were manufactured with 13 tracks next to each other, the four-layer specimens were manufactured as single stripes. Thus, the lateral material flow and matrix squeeze out are not obstructed by neighboring tracks.

5.6 Conclusion

In the first section of chapter 5, a literature research reveals a clear gap in research in the field of thermal behavior of the TP-AFP process for strongly curved 3D geometries. The second section defines the 3D geometry of interest in this thesis. A convex corner with a radius of 6.5 mm and leg angles of 120°, 105° and 90° is chosen for general investigations of 3D laser assisted lay-up. Lay-up trials with the well-established closed loop control for 2D lay-up and with constant laser power show a strong overheating around the corner section. The reasons are investigated in the following. The robot's trajectory has to be optimized, so the tape laying head maintains its speed and relative position to the intended path on the tool during reorientation. This can be seen as a prerequisite for the further investigations to determine the heat input by the laser. The change of heated length of the laser spot on the substrate laminate due to geometric conditions is described. The laser spot decreases down to about 50 % of its original length right before the tape laying head reaches the corner. Afterwards it increases back to its original length in a short distance or time. The change of heated length is decisive to the laser boundary condition and heat input into the laminate. Section 5.3 examines the heat input in detail. Besides heat input, also the compaction behavior of the roller due to the 3D geometry is investigated. At the rounded corner, the local compaction pressure doubles, although the overall compaction force is kept constant.

In the last section, the degradation behavior of the CF/PA6 tapes is analyzed. Different test methods are investigated. Although the mechanical wedge peel test is no direct test for degradation, a clear decrease in peel resistance for high temperature processed specimens, points to a thermal degradation. Also, the bottom threshold temperature for good consolidation is determined. The optimum process temperature for CF/PA6 is determined to be within 260 °C and 320 °C. DSC and DMA testing of the specimens confirm this behavior and temperature range.

Further examination of the specimens with micrographs show that the resin rich interface between the layers vanishes for high process temperatures. Likewise, the layer thickness is reduced. For these high process temperature specimens, matrix squeeze out was observed during manufacturing.

A local laminate thickness reduction of 18 % is measured for the 18-layer specimens in section 5.3.1. This is be mainly attributed to the overheating around the corner and increased transverse flow of the tape. The local compaction pressure increase also promotes this.

6 Development of a thermal simulation for 3D TP-AFP lay-up

Experimental 3D lay-up trials with process parameters, derived from flat lay-up, are described in the previous chapter. Local overheating leads to matrix degradation and insufficient bonding is observed. Laser spot size and compaction zone as well as the kinematics of the robot are analyzed experimentally and under geometric considerations.

In this chapter, the 3D lay-up process is further analyzed with the help of thermal simulations. A literature review reveals a clear gap in published research. Most researchers concentrate on optimizing the laminate quality of flat laminates or by tape winding. In the following, the 2D lay-up simulation for flat parts from chapter 4 is enhanced to simulate the v-shaped specimen geometry with a small corner radius. While the thermal aspects remain almost the same, special attention is given to modeling the correct laser boundary condition during 3D lay-up. Therefore, the tape laying head's and laser spot's kinematics are described in a full parametric model. The thermal simulation for 3D lay-ups is validated for CF/PA6 tape material. During 3D lay-up, the heated area, heating time and laser intensity on the composite change due to the geometric conditions of the part's geometry. The aim of the 3D lay-up simulation is to understand the heating effects of direct and reflected laser beams on both incoming tape and substrate laminate in reference to the tooling's geometry. A detailed analysis of the heat input is given for all three experimental specimen geometries. Parameter studies for corner radius and leg angle investigate the influence of the lay-up tool geometry.

The integrated laser boundary calculation of the 3D lay-up simulation allows to change process parameters like laser power and laser bias distribution during lay-up. By analyzing the predicted temperature, an optimized set of process parameters is determined (section 6.6).

6.1 Literature review

There is even less published research available on thermal simulation of the lay-up of 3D geometries, compared to experimental work on laser assisted TP-AFP of 3D structures. This is also true for the more industrialized TS-AFP process. Most process simulations are limited to flat lay-ups.

Lichtinger developed a 3D thermo-mechanical model for the TS-AFP process [4, 18]. The lay-up of a sandwich part, including the ramps of two chamfered edges is thermally investigated. High process temperatures at the chamfered edges are experimentally observed and predicted by the simulation. The robot reduces its speed during reorientation and the IR heater's alignment remains on the same spot for a short time.

Weiler et al. discuss the TP-AFP lay-up on 3D geometries [53]. They study the use of VCSELs instead of a divergent laser beam, but many aspects are transferable. The investigated geometry resembles a chamfered edge, e.g. from a honeycomb structure. The change of laser spot size is calculated analytically for different angles of attack and angles of the tapered edge. Also, a rounded edge with 90° leg angle is investigated for different corner radii. Weiler et al. predict a decreasing laser spot size and an increase in laser intensity at the beginning of the radius, followed by a decrease after the radius. With increasing corner radius, this effect gets weaker. The investigations consider only geometric observations without taking into account the absorptivity and reflectivity of the composite tapes and are only valid for a laser source with no distinctive beam divergence. No temperature predictions are calculated.

6.2 Adaptions of the thermal simulation for 3D parts

The basis for the thermal analysis of the 3D lay-up is the 2D thermal simulation from chapter 4. As the thermal problem is modeled in a Lagrangian frame, the simulation can be adapted with limited effort. The movement of the placement head and the deposition of new tape has to be adjusted to the 3D geometry, but the boundary conditions for most elements remain the same. Most critical is the calculation of the laser boundary condition with respect to the curved lay-up tool. The thermal simulation for 3D lay-up geometries was conducted within [S13], with a detailed description of the changes. The following sections describe the main changes.

Tape laying head kinematics

During flat lay-up of laminates, the tape placement head is moving along a linear path. Same is implemented in the simulation of flat lay-ups (chapter 4). All geometric aspects of the process are calculated with respect to the X_1-X_3 axis system, which represents the robot's tool center point (TCP), as depicted in Fig. 4-6. During the simulation, this axis system with all components of the tape laying head and their respective boundary conditions move along the tool in lay-up direction. Thus, lay-up direction is always congruent with the X_1 axis. In order to represent the 3D lay-up kinematics, a new R_b-ψ_b cylindrical coordinate system is introduced. It is fixed to the center point of the edge fillet of the lay-up tool (Fig. 6-1). During the course of the simulation the X_1-X_3 axis system is moving along the 3D lay-up geometry, while maintaining its orientation. The X_1 axis is always tangential and the X_3 axis is always orthogonal to

the lay-up surface. It moves relative to the R_b-ψ_b coordinate system, which describes its position on the lay-up tool at the arc section.
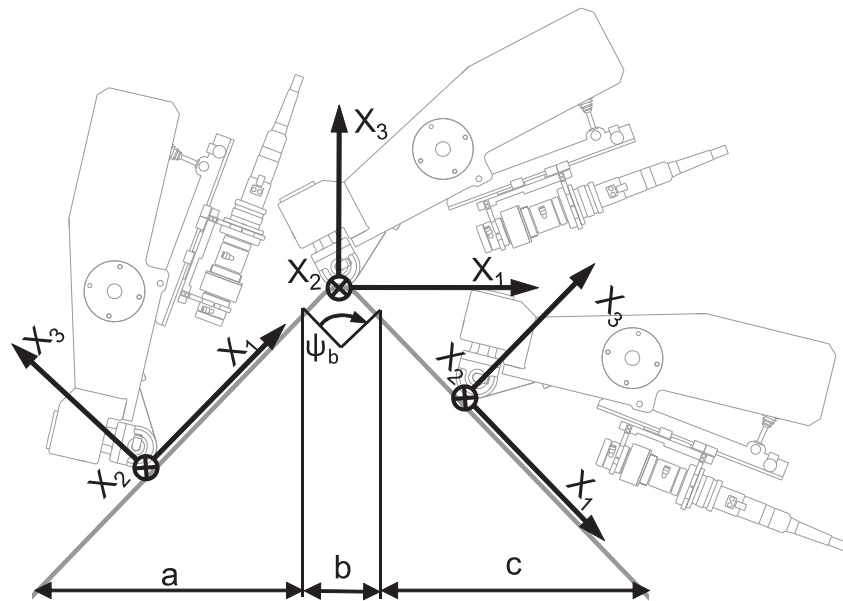
Fig. 6-1:   **Kinematics of the 3D TP-AFP process simulation**
         The X_1-X_3 TCP based axis system is moving tangentially along the lay-up geometry
         The R_b-ψ_b cylindrical coordinate system is based in the center of the edge fillet

Laser input

The most important change from flat thermal simulation to simulation of a 3D lay-up is to calculate the correct laser heated length. The boundary conditions for direct laser heating as well as for first order reflection are adapted. Only the direct laser heating boundary condition for the incoming tape is not affected by 3D lay-up, as both the incoming tape as well as the laser source are mounted to the same lay-up head and move together. The change of the direct laser heating length of the substrate laminate is already discussed in 5.4.3 by geometrical means. For implementation in the simulation code, six cases with respect to the laser spot on the substrate laminate are distinguished:

   I.   Laser spot is completely on the upward leg of the tool (section a in Fig. 6-1)
   II. Laser spot is partly on the upward leg and partly on the arc section of the tool (sections a and b in Fig. 6-1)
   III. Laser spot is completely on the arc section of the tool (section b in Fig. 6-1)
   IV. Laser spot is partly on the upward leg, partly on the arc section and partly on the downward leg of the tool (sections a, b and c in Fig. 6-1)
   V.   Laser spot is partly on the arc section and partly on the downward leg of the tool (sections b and c in Fig. 6-1)
   VI. Laser spot is completely on the downward leg of the tool (section c in Fig. 6-1)

Case I and VI can be treated as a flat lay-up simulation described in chapter 4. Case III is similar to cylindrical winding but only occurs for a large corner radius with a longer arc length than the laser spot projection. The focus for the 3D lay-up simulation is on case II, IV and V. Same as for the thermal simulation for flat lay-ups, all intersections of the laser beam and laminate are calculated via geometric equations and are transferred on the discretized model in a second step.

Fig. 6-2 shows the geometric model, which is used to calculate the laser spot limits for case IV on the substrate laminate by direct laser heating. All three sections (a, b and c) of the tool are illuminated during lay-up (compare thermal image sequence in Fig. 5-6).
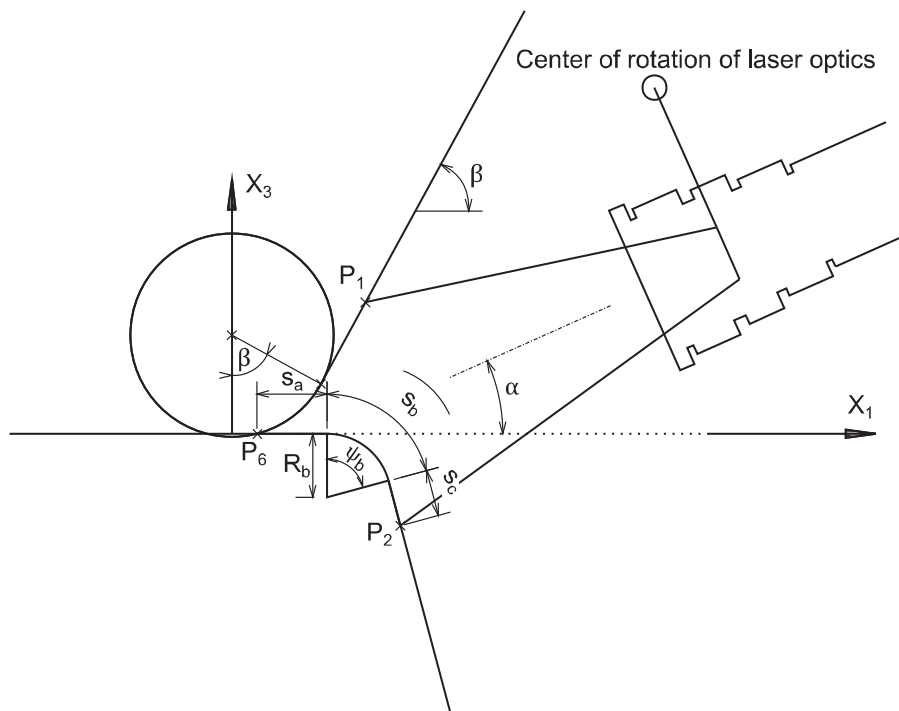
Fig. 6-2:   **Calculation of direct laser heating length on substrate laminate for case IV**
                 The TCP is still in the upwards pointing leg of the tool, while the laser beam heats all
                 three sections of the tool: upward leg, arc section and downward leg.

The heated length is calculated from the three sections:

$$s = s_a + s_b + s_c \qquad (6\text{-}1)$$

s_a = heated length on section a: distance: P_6 to end of upwards pointing leg / beginning of arc;
s_b = heated length on section b: arc length of tooling;
s_c = heated length on section c: end of arc to P_2 (Fig. 4-1).

Same as for direct laser heating on the substrate laminate the first order reflections from and onto the incoming tape are calculated with respect to the lay-up geometry. Due to the curvature of the tool, the start of the reflected laser heating on the substrate (P4 in Fig. 4-1) can be outside the tool's geometry. In this case, the heated length by

reflection is limited to the end of the lay-up tool (see laser beam sketches in appendix d). Its energy is taken into account in accordance with the reflected beam's local intensity. Also, the reflected heated length of the incoming tape can be increased significantly by the substrate laminate's geometry. However, at TUM's TP-AFP system the maximum heated length of the incoming tape is limited by tape guidance. All incoming tape, covered by the tape guidance, is not considered for the laser heating boundary condition.

Discretization and boundary conditions

The elements of the arc section are modeled as rectangular surfaces and not as circular arcs or symmetric trapezes. This simplification allows to use the same formulations for the inner composite boundary conditions. The error is assumed to be minor, as the elements are of very small thickness compared to their length dx_1 and arc length of the tool. For an element thickness $dx_3 = 0.3$ mm the difference of the element's top and bottom arc length is below 0.5 %.
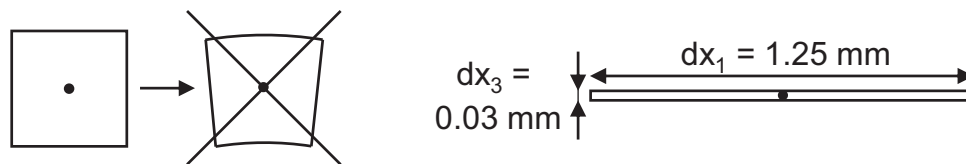
Fig. 6-3: **Element shapes for composite representation in 3D lay-up simulation**
left: geometrical correct element shape in arc section
right: rectangular element drawn to scale, used in leg and arc sections

Inner laminate boundary conditions like heat conductivity in X_1 and X_3 direction as well as interlayer thermal contact resistance are applied as described in section 4.3. Also, the boundary conditions for roller and tool are kept the same.

The boundary conditions to the ambience take into account the elevation of the tool for section a and c (Fig. 6-1). Free or forced convection is calculated for a tilted plane instead of a horizontal plane. The area of the edge fillet (section b) is simplified as horizontal for the boundary conditions. All calculation of these boundary conditions are conducted according to [88].

The 3D lay-up simulation still uses a simplified 2D finite difference representation of the process. Thus the same restrictions as for the flat lay-up simulation, as described in section 4.2, apply for the 3D lay-up simulation.

6.3 Validation of thermal simulation of 3D TP-AFP parts for CF/PA6

The adapted thermal simulation for 3D lay-up is being validated with experimental lay-up trials of CF/PA6 material on the v-shaped geometries (cf. Fig. 5-4 and Fig. 5-5).

Experimental setup

Same as for the flat lay-up simulation, the lay-up trials and simulations for validation are carried out with constant laser power and constant laser optics orientation, despite the overheating. The optimized robot path is used and the compensator is implemented to the placement head. Therefore, almost constant lay-up speed and constant laser spot orientation can be assumed. The onboard infrared thermal camera, type IRS128-I from Automation Technology (Bad Oldesloe, Germany), is used for temperature measurements. It is aimed at the nip-point area and records at 60 Hz. It is calibrated by the manufacturer up to 550 °C and uses an emissivity of 1.0. Therefore, all temperatures need to be understood as black body temperatures. Identical to the flat validation trials, sufficient layers of at least six layers of composite material are used as substrate laminate. This reduces the influence of the mold on the processing temperature and its cooling rate. This is especially necessary for 3D processing, as the compaction pressure on the laminate is higher in the corner areas, which increases heat transfer (section 5.4.2). Stable process conditions are observed after the fifth layer. Tab. 6-1 summarizes the experimental and simulation process parameters. The optics and consolidation roller parameters are kept identical and can be found in Tab. 4-1.

Tab. 6-1:   **Simulation and process parameters for 3D CF/PA6 lay-up (see Fig. 4-6)**

Name:	Description:	Value:	Unit:
$X1_L$	Virtual laser beam origin (x_1-component)	278.8	mm
$X3_L$	Virtual laser beam origin (x_3-component)	115.7	mm
α	Angle laser - lay-up tool	24.0	deg
β	Angle of incoming tape - mold	61.32	deg
γ	Angle placement head - mold	32	deg
v	Lay-up velocity	75	mm/s
P	Laser power	390	W
h_M	Height of steel mold	2	mm
t_L	Composite tape layer thickness	0.13	mm
T_0	Start temperature of tape, compaction roller, mold and ambient air	23	°C
L_a	Length of the upwards pointing leg (section a)	150	mm
R_b	Inner radius of edge fillet	6.5	mm
L_c	Length of the downwards pointing leg (section c)	150	mm

Results

A convergence study is carried out to investigate the influence of the simulation time step (dt) and element size in fiber direction (dx₁). Fig. 6-4 shows the maximum temperature in the composite predicted by the simulation during lay-up of layer six on a 120° tool for different element sizes. Lay-up speed, element size in fiber direction and time step are linked according to equation (4-14). The arc length of the edge fillet with an inner radius of 6.5 mm is 6.8 mm and 10.2 mm for the 120° and 90° tool, respectively. The small arc length limits the maximum element size. An element length smaller than 1.5 mm achieves consistent results.
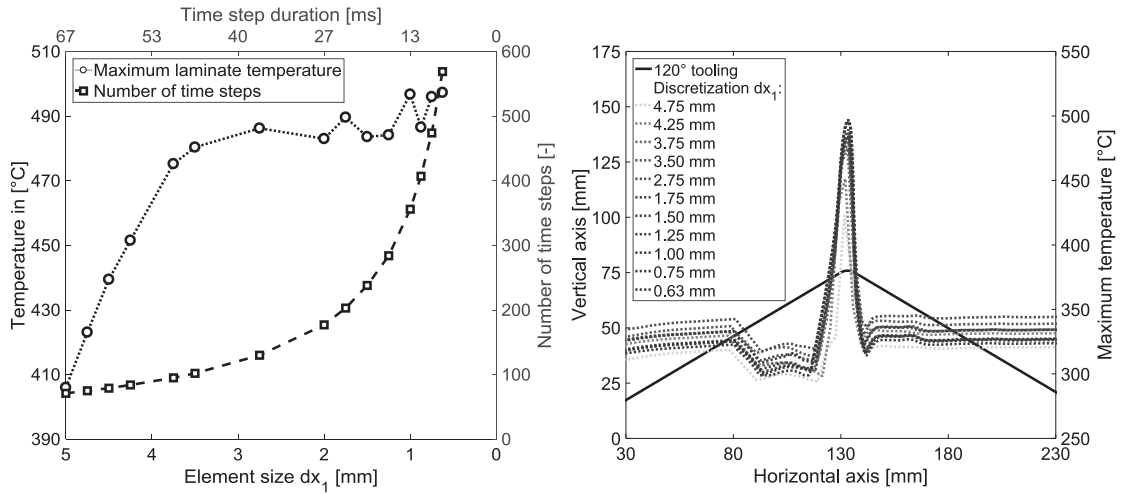
Fig. 6-4:   **Convergence study of simulated maximum temperature during lay-up of layer six on a 120° tool with respect to element size and time step duration**

Fig. 6-5 compares the simulation prediction with temperatures measured by the system's onboard IR camera during the lay-up trials. The mean value of the maximum temperatures within the IR camera spot of three lay-up trials and the maximum composite temperature by the simulation is shown with respect to the TCP's position on the tool.

As the experimental temperature is measured as a black body (bb) temperature, it is also shown corrected according to the simplifying Stefan-Boltzmann law:

$$T_{corr} = \sqrt[4]{\frac{1}{\varepsilon_{CF/PA6}} \cdot (T_{bb}^4 - T_\infty^4) + T_\infty^4} \qquad (6\text{-}2)$$

T_{corr} = corrected temperature; $\varepsilon_{CF/PA6}$ = corrected emissivity of CF/PA6;
T_{bb} = black body temperature measured by the thermal camera; T_∞ = ambient temperature

There are varying values for the emissivity of carbon fiber reinforced thermoplastic tapes published in literature. Additional uncertainty is added by the high process temperatures that might affect the emissivity. Zenker and Schwab measured an emissivity of $\varepsilon = 0.95$ for the same CF/PA6 type of material [119], while Di Francesco et

al. measured an emissivity of $\varepsilon = 0.80$ for CF/PEEK [64]. The actual temperature of the composite is higher than the measured black body temperature.

At the upwards and downwards pointing leg, the simulation over predicts the temperature. This has already been observed for flat lay-up simulation of CF/PA6 (section 4.4.3). Compared to the corrected temperature from the IR camera, the simulation over predicts the temperature by about 30 °C. When the TCP is close to the end of section a (Fig. 6-1), the temperature rises to up to more than 480 °C. The rise starts earlier and it lasts longer during the experiments than the simulation predicts. However, the overall curve of the temperature rise and its point of time during lay-up is predicted very well. Close to the end of the experimental lay-up, the placement head cuts the incoming tape. By this, the tape tension vanishes and the incoming tape is not as tight to the compaction roller as before. Consequently, the heat flow to the compaction roller is reduced and the temperature of the incoming tape rises.
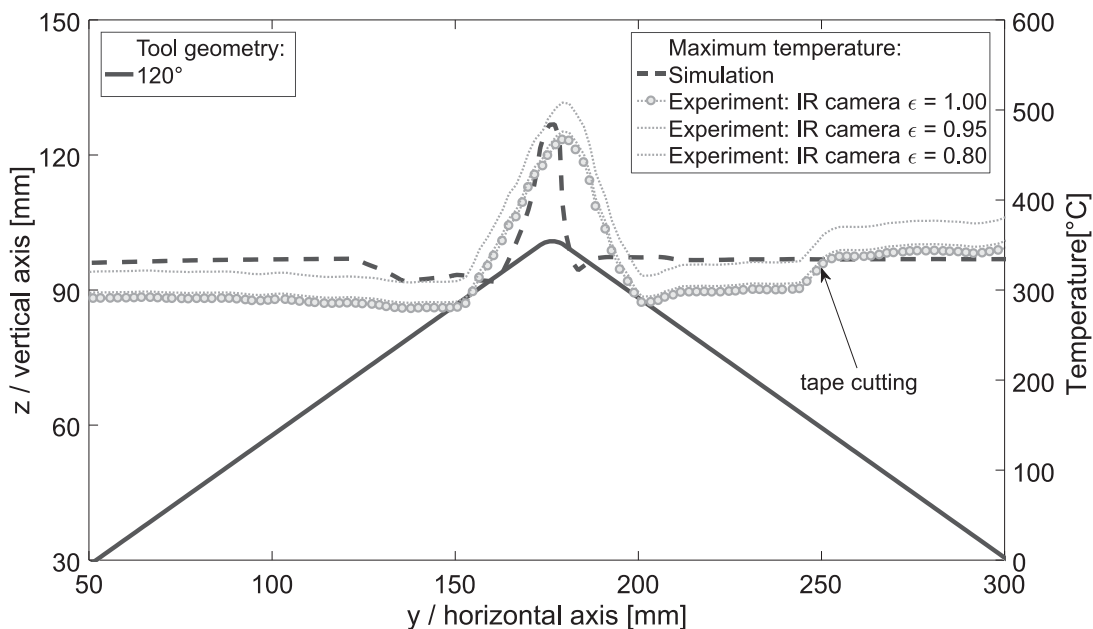
Fig. 6-5:   **Comparison of simulated and measured maximum surface temperature within the laser spot for 3D lay-up on 120° tool with constant laser power**

Simulations for the tooling geometries with 90° and 105° angle show a very similar temperature curve. A strong temperature rise is predicted in the corner region. Similar to the simulation on the 120° tooling in Fig. 6-5 the region affected by overheating is larger in the experimental lay-up trials than predicted by the simulation. The overheating starts earlier before the arc section and lasts longer, than predicted by the simulation.

Fig. 6-6 shows a series of temperature distributions for different time steps of the process. The steps a to c correspond with the TCP's position on the lay-up tool section from Fig. 6-1. While the incoming tape's temperature stays rather constant, overheating occurs behind the arc of the corner at the substrate laminate.
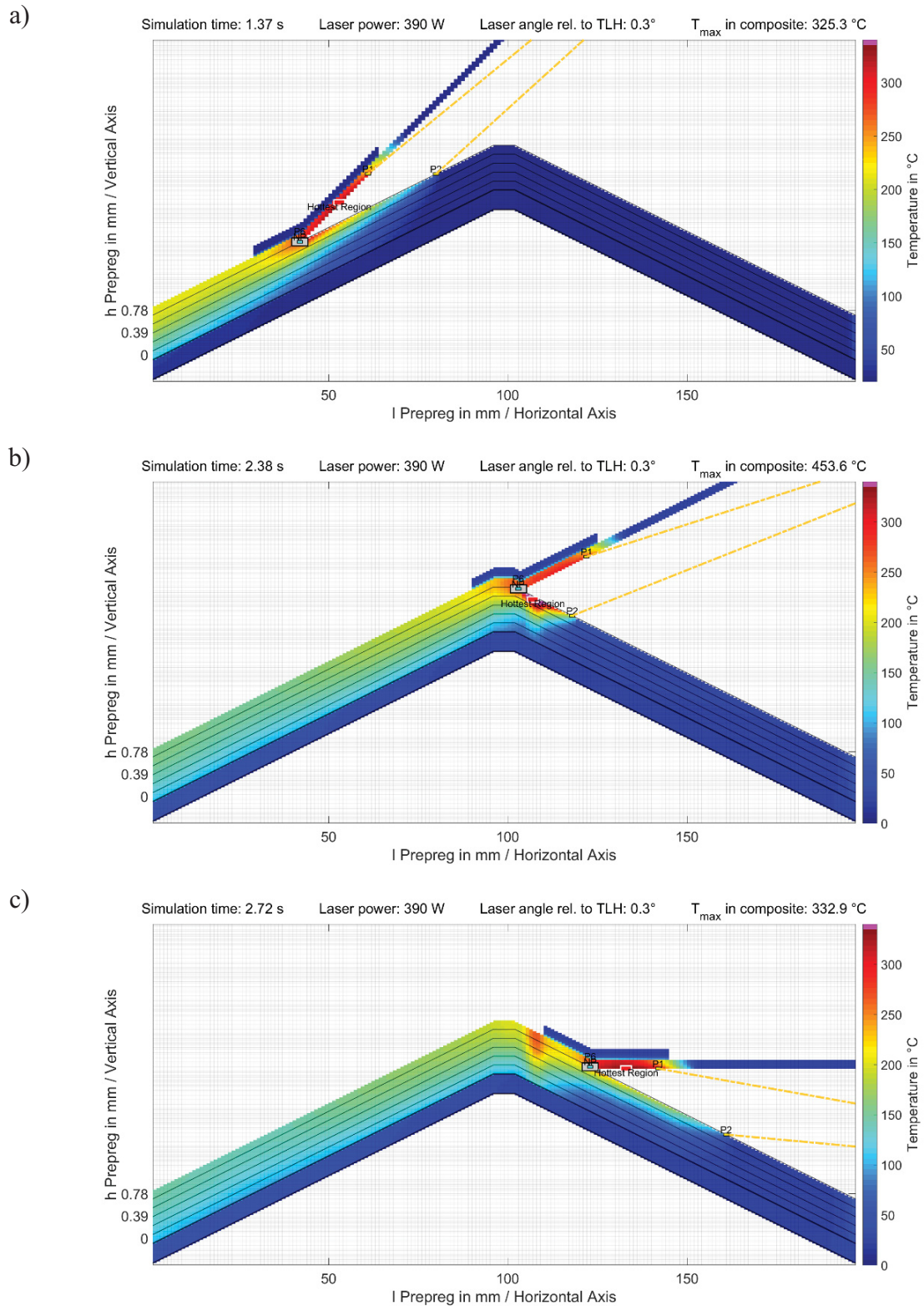
Fig. 6-6: **Series of simulated laminate temperature distribution plots for 120° angled tool**
Constant laser power of 390 W is used for the calculations
a) Tape laying head and laser spot are on upwards pointing leg
b) Tape laying head is rotating at arc section; laser spot is mainly on backside
c) Tape laying head and laser spot are on downwards pointing leg

Fig. 6-7 shows the temperature distributions within the laser spot and IR camera field of view for the simulation and experiments. The temperature bias variation during 3D lay-up can be clearly seen. Simulation and experiment show a similar temperature distribution between incoming tape and substrate laminate. However, the bars cannot directly be compared. The point of view of the IR camera on the incoming tape that is bent around the compaction roller and on the changing substrate laminate distorts the temperature distribution. This especially applies for the nip-point area.
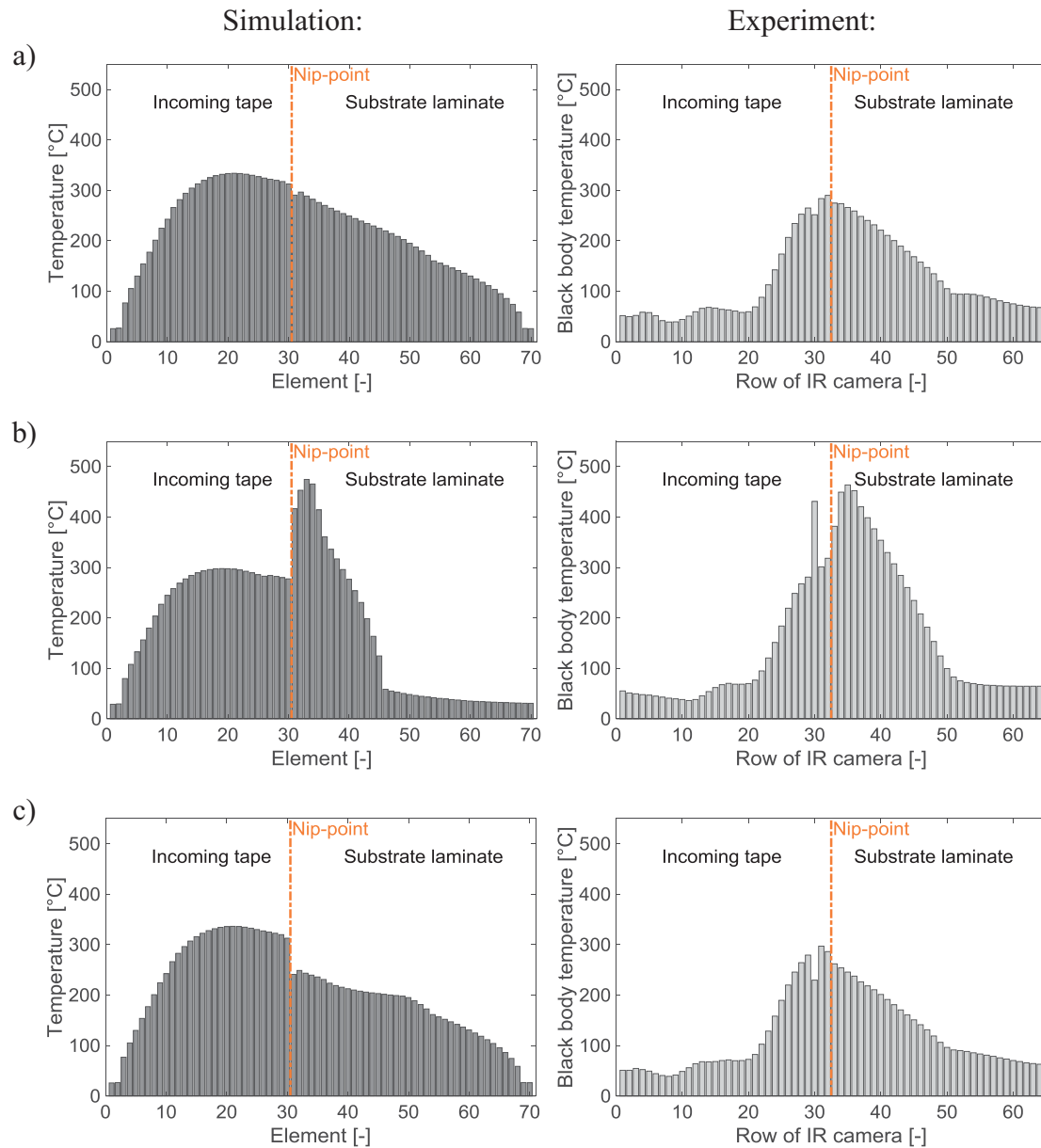
Fig. 6-7: **Series of laser spot temperature distribution plots for 120° angled tool**
Left: Simulation; right: experimental data from IR camera (black body temperature)
The pictures are from the corresponding time steps shown in Fig. 6-6.
a) Tape laying head and laser spot are on upwards pointing leg
b) Tape laying head is rotating at arc section; laser spot is mainly on backside
c) Tape laying head and laser spot are on downwards pointing leg

The surface temperature of the incoming tape is only slightly affected. The temperature drops during lay-up of the tip section of the tool, but gains its nominal temperature shortly again after the corner. Row 30 of the experimental data shows abnormal values. As only this row is affected, it is regarded as false temperature measurement and is ignored for the analysis. One reason for this can be loose filaments from the side of the slit tape that glow in the laser spot. The overheating of the substrate laminate can be clearly seen in position b for both, simulation and experiment. The heated zone of the substrate laminate decreases below 50 % of its original length, while the temperature rises strongly. After the tape laying head has left the corner section, the surface temperature of the substrate laminate needs longer time to stabilize back to its nominal temperature again.

Conclusion

The thermal simulation for flat laminates has been adjusted for 3D lay-up of a rounded corner. The most important modification is to calculate the laser boundary condition for every time step at the corner, as the laser spot changes. The laser spot projection on the composite is calculated according to the lay-up geometry. The energy input of the elements is calculated with respect to the local laser intensity and absorptivity. Together with the tape laying head kinematics, the temperature distribution within the composite is calculated. The simulation's predictions are validated by thermal camera measurements in two ways. The maximum temperature within the laser spot during lay-up shows a similar curve for simulation and experiment. The overheating of approximately 200 °C occurs at the arc section of the lay-up geometry. The other method compares the local temperature distribution of incoming tape and substrate laminate at different time steps during lay-up. For both, simulation and experiment, a strong change of the temperature distribution at the substrate laminate is observed. The heated length is reduced and the maximum temperature rises. The absolute difference of the maximum temperature between simulation and experiment is 8 °C and similar as for the flat lay-up simulation (section 4.4.3).

A calibrated IR camera records the experimental temperature data. The camera records the temperature as a black body temperature, which is underestimating the real composite temperature. A compensation during post processing is difficult as different emissivity values are given in literature for the composite. Furthermore, the emissivity is expected to change with temperature and viewing angle of the IR camera. Especially for 3D lay-ups, the composite's angle with respect to the IR camera is not constant.

6.4 Heating effects during 3D lay-up

In its first step, the adapted thermal simulation for 3D lay-up calculates the heat input boundary conditions for each simulated time step. In the following sections, the changes of the laser heated length, calculated by the simulation, are presented for the investigated 90°, 105° and 120° angled tools with a corner radius of 6.5 mm. Generally phrased, a smaller heated area means higher local power intensity and stronger surface heating of the composite. This can only be compensated by reducing laser power or heating time. From the kinematics of the tape laying head (see section 5.4), the heated time of the discretized elements is calculated. Both, heating length and heating time determine the normalized heat input into the incoming tape and substrate laminate.

6.4.1 Direct laser heating profiles

The heated length of the substrate laminate by direct laser illumination is strongly affected by the lay-up tool's geometry. This effect is discussed by geometrical analysis in section 5.4.3. Fig. 6-8 shows the direct laser heating length on the substrate laminate, calculated by the discretized simulation model, for the three investigated lay-up geometries. An element size in lay-up direction of $dx_1 = 1$ mm, the same laser bias angle of $\alpha = 24.5°$ and virtual laser origin, as in section 5.4.3 is used. Other parameters like compaction roller and laser spot size are identical to the flat lay-up simulation validation for CF/PA6 as listed in Tab. 4-1. As soon as P2 reaches the arc of the tooling, the heating length declines linearly. This effect is purely driven by the geometry of the tooling, as the intersection of the laser with the tooling (P_2) is not progressing with the tape laying head's speed anymore. Once the TCP reaches the start of the arc, a spherical drop in heating length is observed, as the head reorients. At the end of this reorientation, the heated length rises quickly back to its original length. The placement head is now on the downwards pointing leg, which can be treated as the upwards pointing leg or as flat laminate, from an optical point of view.

The simulation predicts the same heated length as investigated manually by CAD in section 5.4.3. The same four characteristic sections I to IV can be observed. The behavior is almost identical, independent of the tooling's angle. Only the different arc length of the tools is determining a different start of the laser beam hitting the arc section and a different start of rotation of the tape laying head.
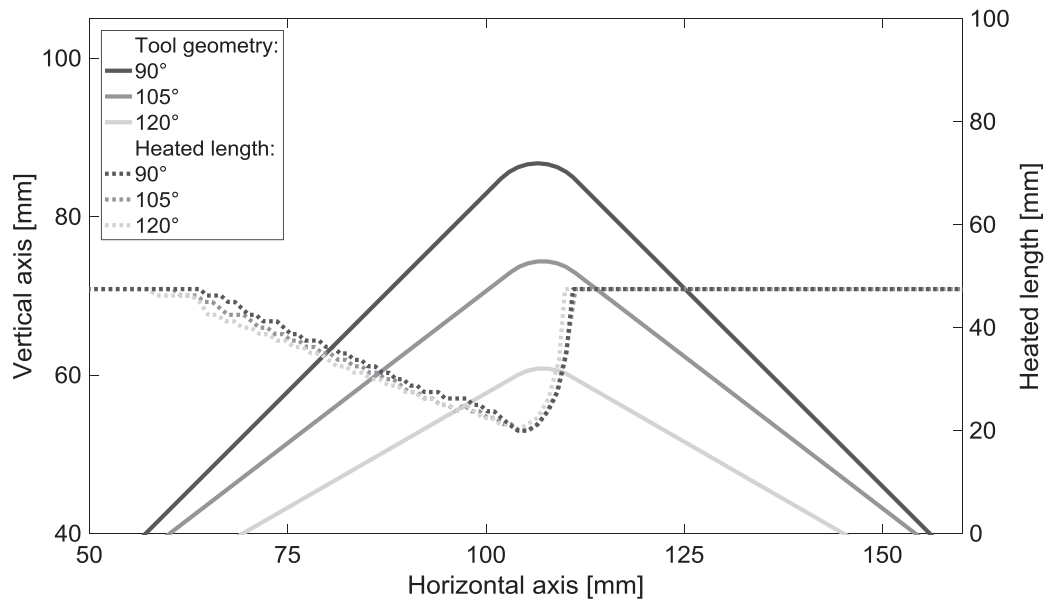
Fig. 6-8:   **Heated length by direct laser illumination on the substrate laminate**
The heating length is shown with respect to the TCP's position on the three different leg
angles of the tool: 90°, 105° and 120°. The edge fillet radius is always 6.5 mm.

The heated length of the incoming tape by direct laser illumination is not significantly
affected by the geometry of lay-up tool. Both, the incoming tape as well as the laser
beam do not change their position with respect to each other during 3D lay-up, as they
are both coming from the tape placement head. Therefore, the energy input by direct
illumination is identical to flat lay-up, as presented in section 4.3.1 and Fig. 4-13.

6.4.2   Reflected laser heating profiles

The course of the reflected heating length is not as obvious as the direct heating length.
It is a consequence of the laser beam's angle of attack for direct illumination, of the
direct heating length and of the relative angle between incoming tape and substrate
laminate. The reflected heated length has to be investigated for the substrate laminate
and for the incoming tape.

Reflection from incoming tape to substrate laminate

Fig. 6-9 shows the heating length by reflected laser radiation from the incoming tape
onto the substrate laminate with respect to the three tooling geometries. When the
lay-up head approaches the arc of the mold, the reflected laser beam from the incoming
tape is projected on the downwards pointing leg of the tool. The angle of the reflected
laser beam can become parallel or even exceed the angle of the downwards pointing
leg. Thus, the laser from the incoming tape is projected over the whole downwards
pointing leg and beyond. The intensity is rather low, when the projection destination is
long.

In case of the 90° tool, the reflected laser beam from the incoming tape is undercutting the downwards pointing leg. Thus, it cannot hit the downwards pointing part of the tool and the border of the reflected part of the laser spot (P_4 in Fig. 4-1) remains on the arc until the tape laying head starts to turn around the arc. Part of the reflected laser beam from the incoming tape is reflected into ambience. In the thermal simulation, the remaining laminate length is used as the maximum heating length. Short before the TCP reaches the beginning of the arc, the heated length by reflection vanishes completely for a short time.

Due to the angle of the 105° tool, the reflected laser beam is illuminating the whole backside of the tool long before the tape laying head reaches the arc. However, the intensity is low, as the heated length is long and the angle of attack results in low absorption.

The 120° tool is rather flat, thus the projection limit of the laser beam is still on the downwards pointing leg, but increases until the TCP reaches the beginning of the arc and the tape laying head starts to turn. During the reorientation of the placement head, the intersection of the reflected laser beam and the downwards pointing leg (P_7) is moving backwards towards the nip-point again until steady-state condition is reached again. This behavior is the same for all three geometries.

For a better understanding, the reflected laser beams from tape to substrate laminate are shown for different TCP positions on the three tools as a series of CAD sketches in Appendix d.
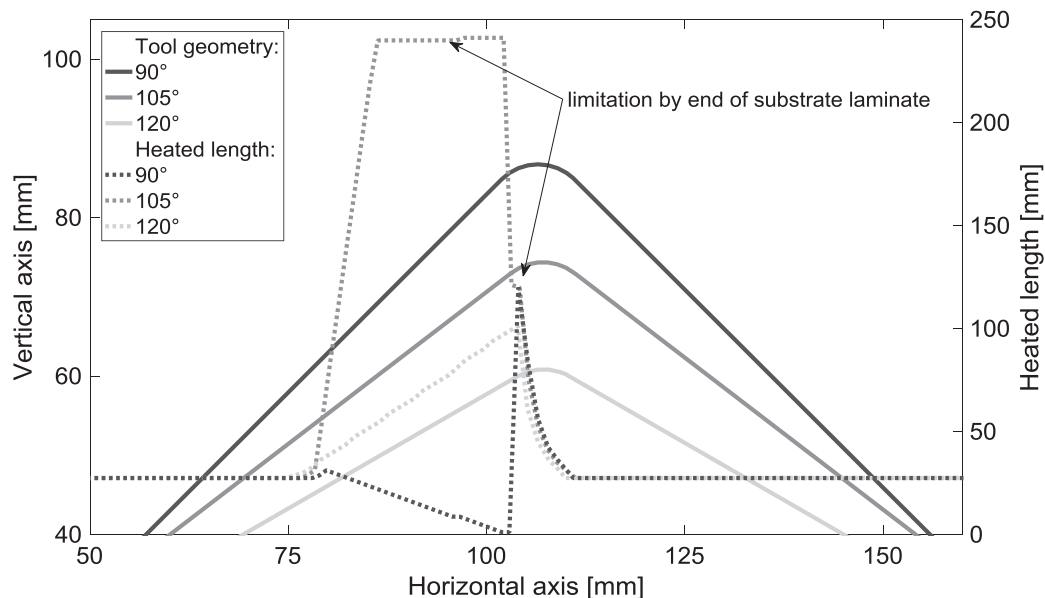
Fig. 6-9: **Heated length by reflected laser illumination from incoming tape to substrate laminate**
The heating length is shown with respect to the TCP's position on the three different leg angles of the tool: 90°, 105° and 120°. The edge fillet radius is always 6.5 mm.

Reflection from substrate laminate to incoming tape

The change of heated length by direct illumination on the substrate laminate changes the reflected length on the incoming tape (P_3 and P_7 in Fig. 4-1). Once the start of the laser spot on the substrate laminate reaches the start of the arc, its angle of attack changes. At the arc section the laser beam is reflected more upwards and even in the direction back to the laser optics. Therefore, not the whole laser beam hits the incoming tape. Furthermore, the incoming tape is blocked from irradiation in a certain distance by tape guidance. At TUM's TP-AFP machine the incoming tape can be irradiated by the laser for 49 mm between the nip-point and tape guidance. For different tool angles, the heating length by reflection is reduced differently, when the tape placement head approaches the arc.

The laser beam reflection from substrate to tape is shown for different TCP positions on the three tools as a series of CAD sketches in Appendix d.
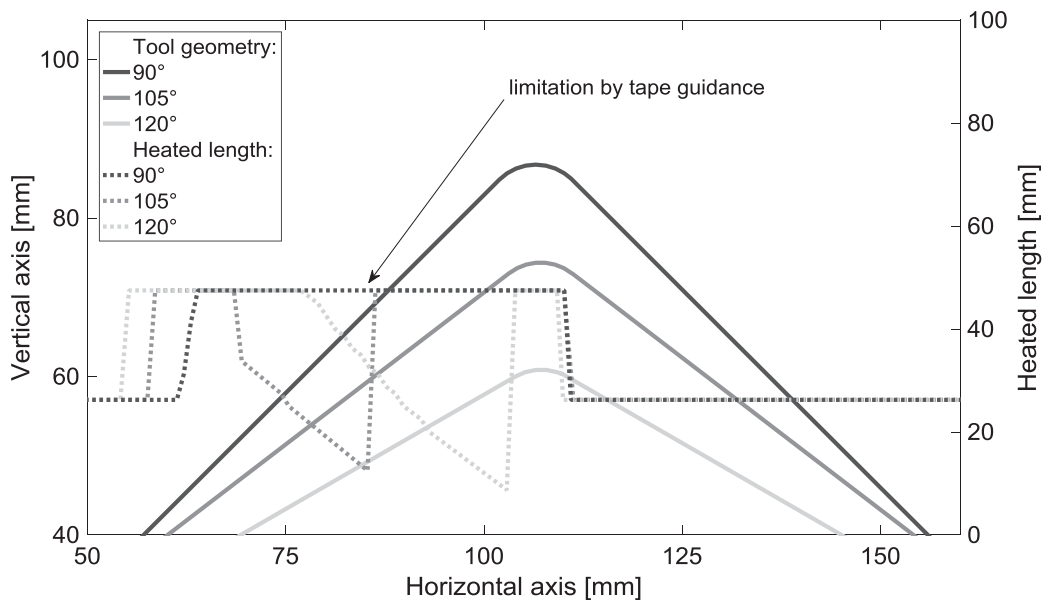
Fig. 6-10: **Heated length by reflected laser illumination from substrate laminate to incoming tape**
The heating length is shown with respect to the TCP's position on the three different leg angles of the tool: 90°, 105° and 120°. The edge fillet radius is always 6.5 mm.

6.4.3   Heating time of the composite

Despite heating length, the heating time is also influencing the composite's heating. Due to the kinematics of the robot, the laser spot movement over the substrate laminate is changing according to the tool's geometry. The kinematics of the tape laying head and laser spot are a direct response to the TCP movement with constant orientation to the lay-up surface at its current position (section 5.4.1).

As the lay-up speed is set to a constant 75 mm/s, the heating time of the elements on the substrate laminate by direct illumination is a direct result from the corresponding heating length (cf. Fig. 6-8). Fig. 6-11 shows the heating time of the substrate laminate's elements. A clear decrease of heating time below 50 % of its original heating time is observed after the arc.
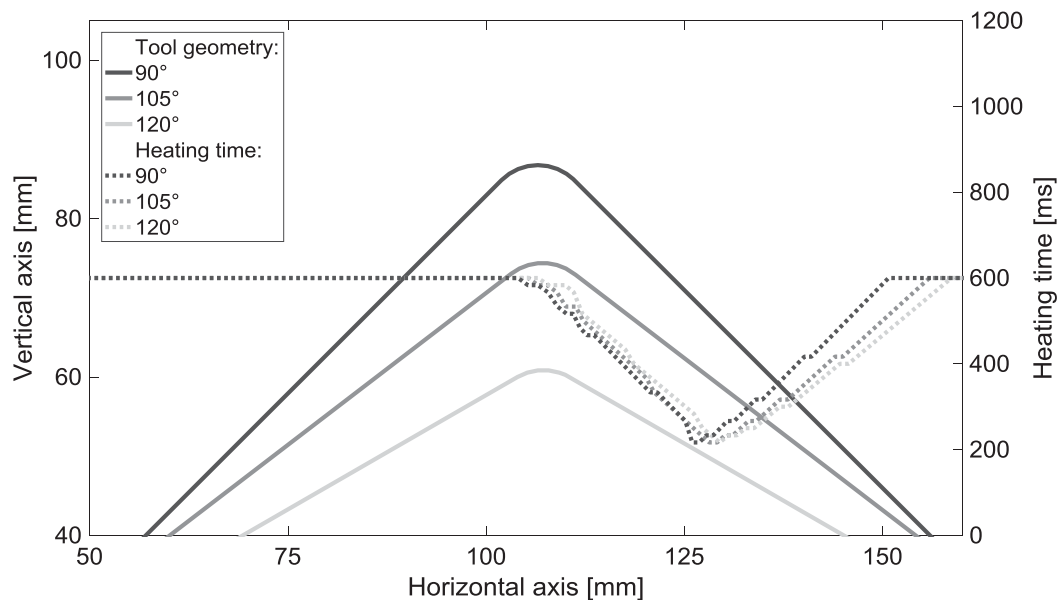
Fig. 6-11:   **Heating time by direct laser illumination on the substrate laminate**
The heating time of the elements is shown with respect to their position on the three different leg angles of the tool: 90°, 105° and 120°. The edge fillet radius is always 6.5 mm.

Fig. 6-12 shows the curve of the heating time by reflection for the substrate laminate's elements. There is no change before the tip of the tool. The backside is heated for a longer time by reflection, because the heated length by reflection increases as shown in Fig. 6-9. The curve of the 90° tool shows a different behavior. This is due to the different curve of its reflected heated length.
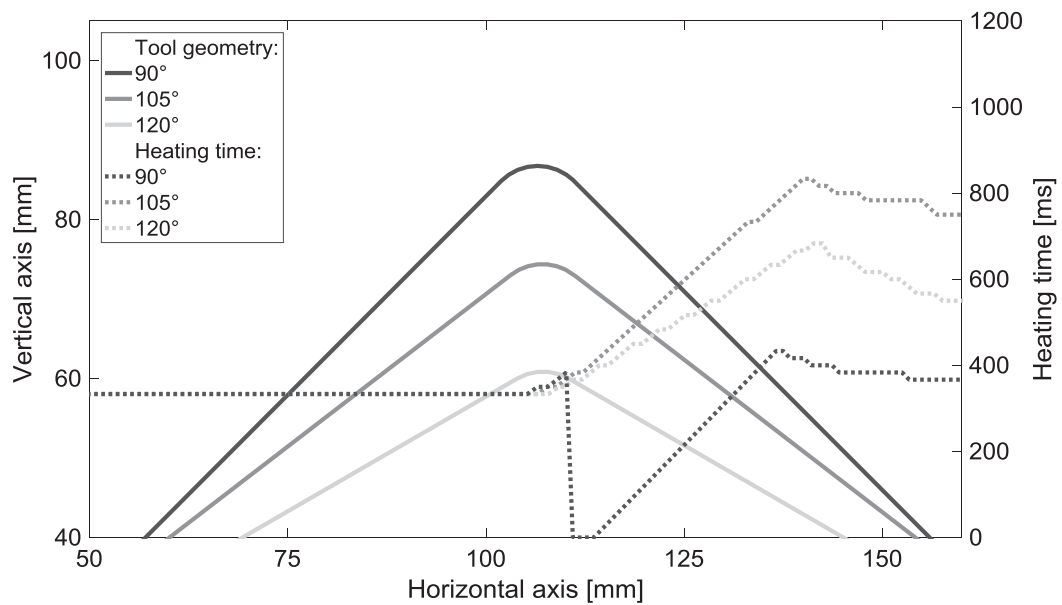
Fig. 6-12:   **Heating time by reflected laser illumination from incoming tape to substrate laminate**
The heating time of the elements is shown with respect to their position on the three different leg angles of the tool: 90°, 105° and 120°. The edge fillet radius is always 6.5 mm.

The heating time due to direct laser heating of the elements representing the incoming tape does not change during 3D lay-up. The reason is the same as for the heating length. Both, incoming tape and laser are moving with the tape laying head and do not change their relative position.

The heating time due to reflected laser heating of the elements on the bottom side of the incoming tape is affected by the tool geometry. As the heating length of the substrate laminate changes, also the reflected length from the laser spot changes. Fig. 6-13 shows the heating time by reflected laser illumination on the incoming tape for the three different tool geometries. All simulations used the same set of parameters (see section 6.4.1). The lay-up speed is set to 75 mm/s. The heating time curve is a result of the reflected laser spot length in the incoming tape. When the laser hits the arc section of the substrate laminate, its reflection is spread circular. This results in a longer heating time of the incoming tape's elements for this area. Although the heating time increases here, only low laser intensity is present here. Later the heating time drops again due to the reorientation of the head.
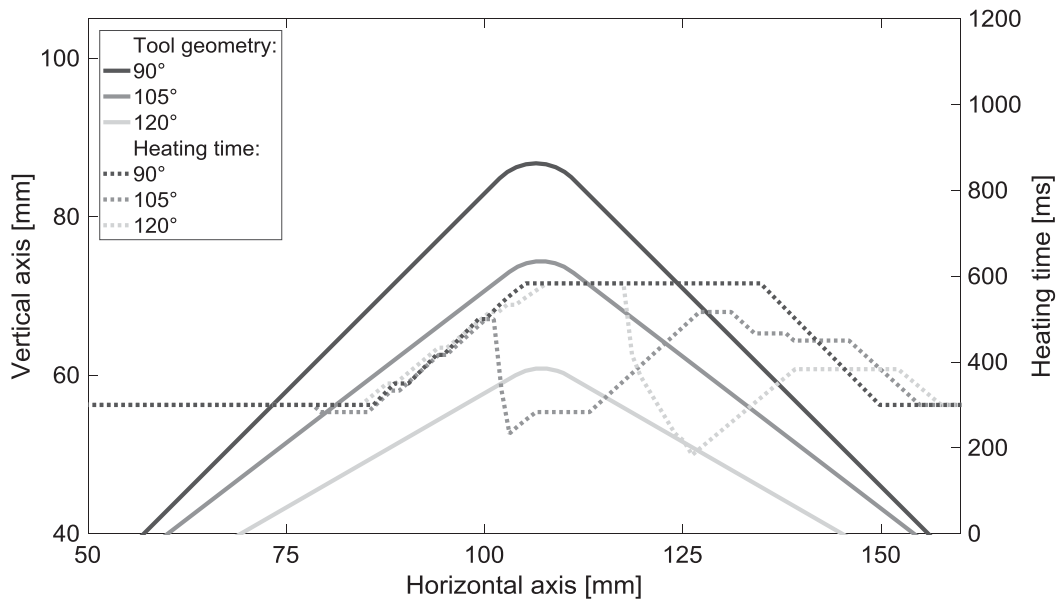
Fig. 6-13: **Heating time by reflected laser illumination from substrate laminate to incoming tape**
The heating time of the elements is shown with respect to their position on the three different leg angles of the tool: 90°, 105° and 120°. The edge fillet radius is always 6.5 mm.

6.4.4 Energy input by laser

From the heated length and the illumination time, the total energy input can be calculated. In addition to the power density of the laser spot and the heating time due to the kinematics of the robot movement, the absorptivity changes with respect to the angle of attack of the laser beam (cf. section 3.1). The energy input into an element can be described by:

$$E \sim \frac{P_{laser}}{A_{laser\ spot}} \cdot A_{element} \cdot t_{illuminated} \cdot \alpha(\theta) \qquad (6\text{-}3)$$

E = energy input into element;

P_{laser} = power of the laser beam; $A_{laser\ spot}$ = illuminated area by laser spot;

$A_{element}$ = illuminated surface of the element; $t_{illuminated}$ = laser heating time of the element;

$\alpha(\theta)$ = absorptivity, depending on the laser beam's angle of attack θ

Fig. 6-14 shows the accumulated energy input of the elements representing the top layer of the substrate laminate with respect to their position on the lay-up geometry. A normalized laser power of 1 W is used for the calculations. A steep increase of the input energy by about 100 % is calculated for the elements after the arc of the tool. A sharp drop down to 50 % of its initial value follows. The input energy rises again and reaches its initial value about 50 mm behind the arc. This behavior is observed for all three geometries, despite the different tooling angle.
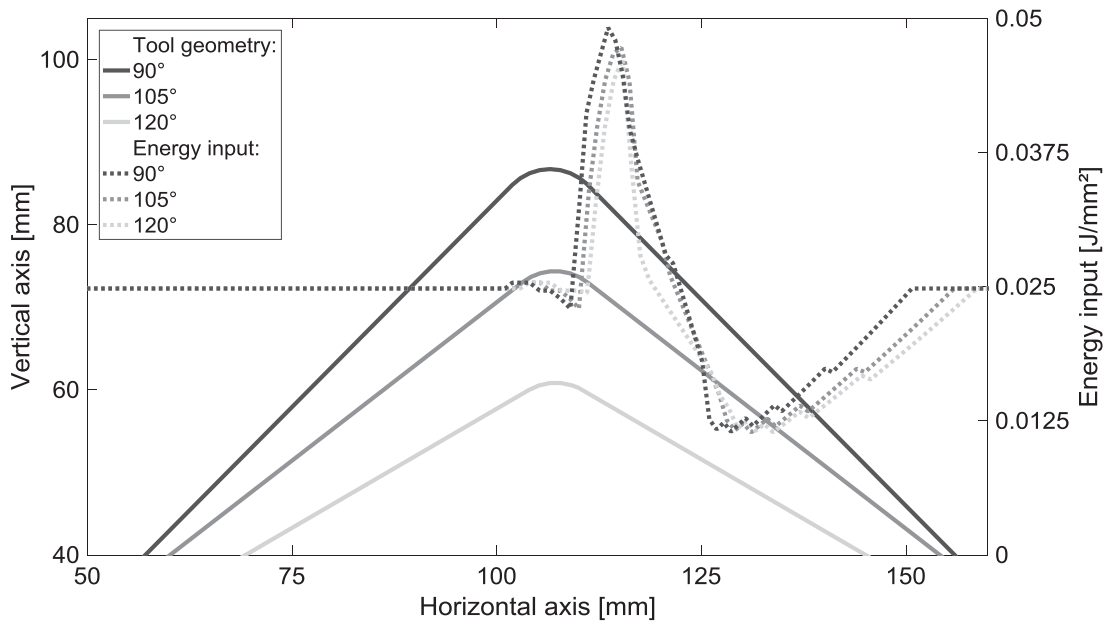
Fig. 6-14: **Energy input by direct laser illumination on the substrate laminate**
The energy input of the elements is shown with respect to their position on the three different leg angles of the tool: 90°, 105° and 120°. The edge fillet radius is always 6.5 mm. A normalized laser power of 1 W is used.

The heat input on the substrate laminate's elements by reflected illumination also changes relative to its steady-state value. However, the overall amount of energy is only about 20 % compared to direct illumination. The increase starts already for the elements representing the round arc. This increase is of about 80 % of its original value and it is almost identical for all three geometries. After the arc, the energy input decreases for the 90° tool and further increases for the 105° and 120° tool. As seen in section 6.4.2 the backside of the 90° tool undercuts the reflected laser beams from the incoming tape. Once the tape placement head leaves the arc section, the energy input slowly converges back to the initial value. The energy input for the 105° and 120° tools' backside is still little higher, as these elements are illuminated for a longer time, but only with low laser absorption. The intensity of the reflected laser is rather low, as the heated length is long and the angle of incidence of the reflected beam is high. The vast majority of these reflected beams are reflected again into the ambience instead of being absorbed.
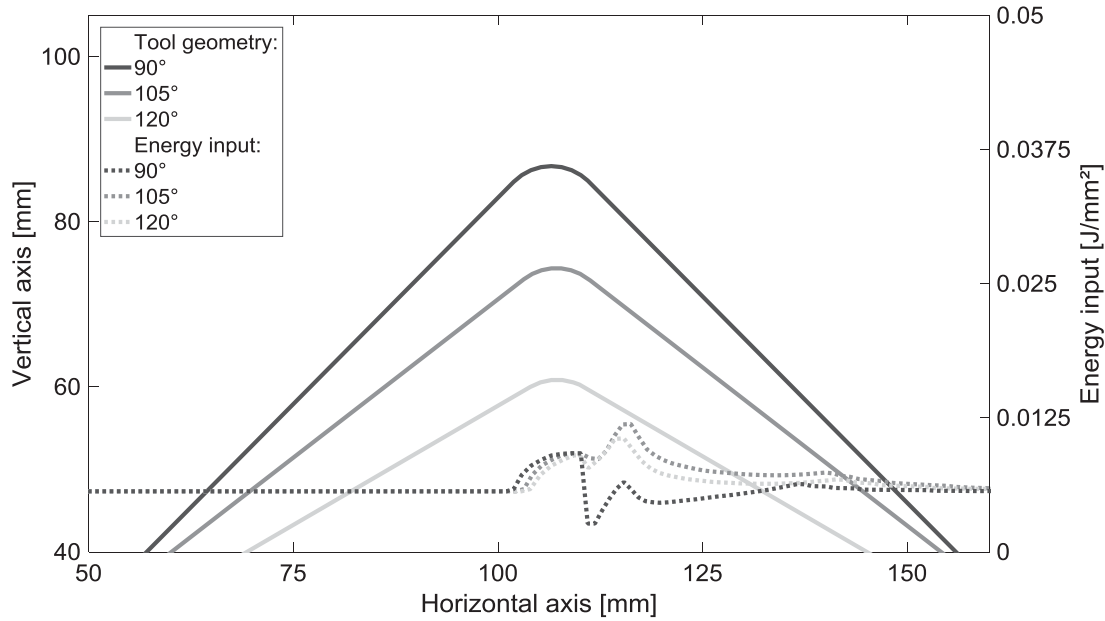
Fig. 6-15:   **Energy input by reflected laser illumination on the substrate laminate**
The energy input of the elements is shown with respect to their position on the three different leg angles of the tool: 90°, 105° and 120°. The edge fillet radius is always 6.5 mm. A normalized laser power of 1 W is used.

The energy input by direct illumination on the incoming tape does not change during 3D lay-up. The incoming tape and the laser beam do not change their position relative to each other. The results of the flat lay-up simulation remain valid for 3D lay-ups.

The energy input by reflected laser heating on the incoming tape does change however. As shown in the previous section, the heating length and the heating time do change over the 3D lay-up. Heating length and time by reflection mainly increase. However, the heating length is limited by the tape guidance of the tape laying head. This leads to a lower energy input per element. Fig. 6-16 shows an almost symmetrical decrease of the energy input on the incoming tape by reflected heating. The drop starts about 40 mm before the tip of the arc and initial heat input is reached about 30 mm after that. Relatively to the steady-state value, the drop down to about 30 % seems rather strong, but compared to the overall energy input by direct illumination, the drop is of only minor importance. The initial energy input by reflected illumination on the incoming tape is about 25 % of its total energy input. Its minimum total energy input is reduced to about 83 % during 3D lay-up.
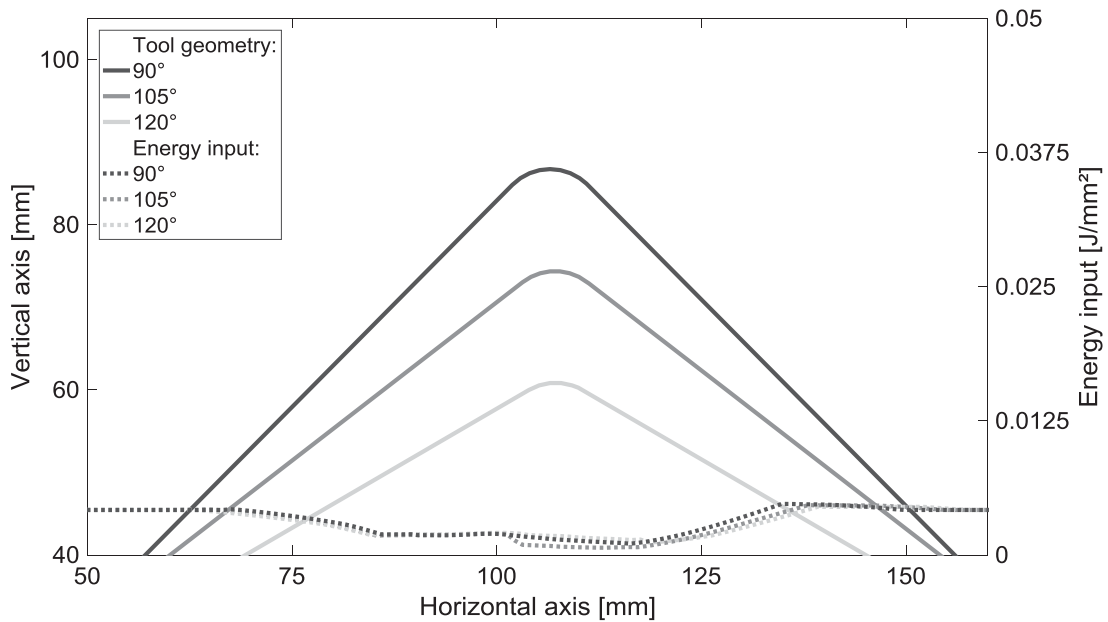
Fig. 6-16:   **Energy input by reflected laser illumination from substrate laminate to incoming tape**
The energy input of the elements is shown with respect to their position on the three different leg angles of the tool: 90°, 105° and 120°. The edge fillet radius is always 6.5 mm. A normalized laser power of 1 W is used.

6.4.5   Conclusion

A detailed analysis of the laser input boundary condition during 3D lay-up over a v-shaped tool is presented. Direct and reflected laser heating are analyzed for the incoming tape and substrate laminate. The angle of the tooling is altered to understand its influence. The local overall heat input on the composite is derived from the local intensity distribution, by analyzing the heated length and the temporal laser heating curve.

Direct heating does not change during 3D lay-up for the incoming tape. Also, heating by reflected laser illumination does not strongly affect the energy input. The energy input to the incoming tape is reduced by about 17 % around the corner of the tool. The angle of the tool has only minor effect on this.

The heating of the substrate laminate is strongly affected by the 3D geometry, as the heated length decreases at the corner. Also, the heating time changes significantly. In total, the energy input by direct laser illumination rises up to 200 % and then drops down to 50 % of its initial steady-state value right behind the corner. Due to its absolute lower value, the reflected laser energy into the substrate laminate is of lower importance.

6.5 3D TP-AFP simulation parameter study

With the help of the validated thermal simulation for 3D lay-ups (section 6.3), parameter studies are carried out. Parameters of interest are the tooling angle and the corner radius in between the two straight legs. The laser spot's projection on the substrate laminate is influenced by the tape laying head's basis angle of attack towards the tooling γ. Its influence is analyzed as well. As direct laser heating is the most dominant heating phenomena, the laser spot size is also varied.

6.5.1 Effect of tooling angle

First, the effect of the tooling angle is examined. Simulations with the same general parameters from section 6.3 are executed for the three tooling angles. The corner radius is kept constant at 6.5 mm. Fig. 6-17 shows the predicted maximum temperature in the nip-point area with respect to the nip-point position on the tooling during lay-up. Temperature rises and drops are almost synchronic for all three tooling angles. This independency is in good agreement with the considerations in section 6.4.4. The simulation calculates very similar heat input for all three tooling angles. Direct laser heating is dominating, which does not change much with the tooling angle.
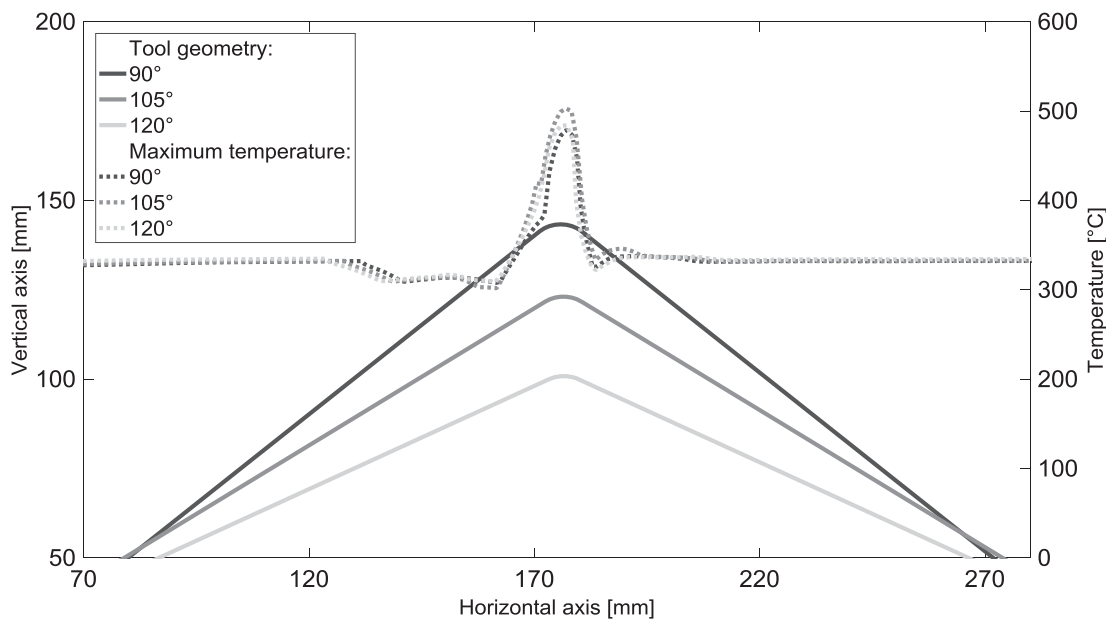
Fig. 6-17:   **Parameter study: Tooling angle 90° - 105° - 120°**
Predicted maximum temperature in the nip-point area for different tooling angles.

Fig. 7-5 in section 7.2 and Fig. A-5 and Fig. A-7 in Appendix f show the experimentally measured nip-point temperature for the three tooling angles. The maximum measured nip-point temperature varies only little for the three tooling angles but is generally at a higher level between 545 °C and 585 °C.

6.5.2   Effect of corner radius

The second characteristic parameter of the lay-up geometry is the corner radius between the two straight legs. Simulation with an increasing corner radius are performed for the 120° tooling. The initial corner radius of 6.5 mm is doubled three times up to 52 mm. For a corner radius of 26 mm and 52 mm the arc length of the tooling is longer than the laser heated length on the substrate laminate. Consequently, case III from section 6.2 describing the laser spot completely on the arc section has to be considered, too.

Fig. 6-18 shows the predicted maximum temperature in the nip-point area for different corner radii on the 120° tooling. The temperature drop at the end of the upwards pointing leg is very similar for each corner radius. This drop is attributed to the lack of reflected laser heating. With increasing corner radius, the maximum nip-point temperature decreases but the affected area increases. In general, it can be seen, that the corner radius has a big effect on the overheating while processing with constant lay-up parameters.

The minimum corner radius for the standard closed loop control to maintain constant nip-point temperature needs to be determined through experiments. The movement of the tape laying head is triggered by the distinct transitions from the straight legs to the arc in the thermal simulation (see section 6.2). The actual robot path would be smoother, as the robots blends its movement to maintain constant speed.
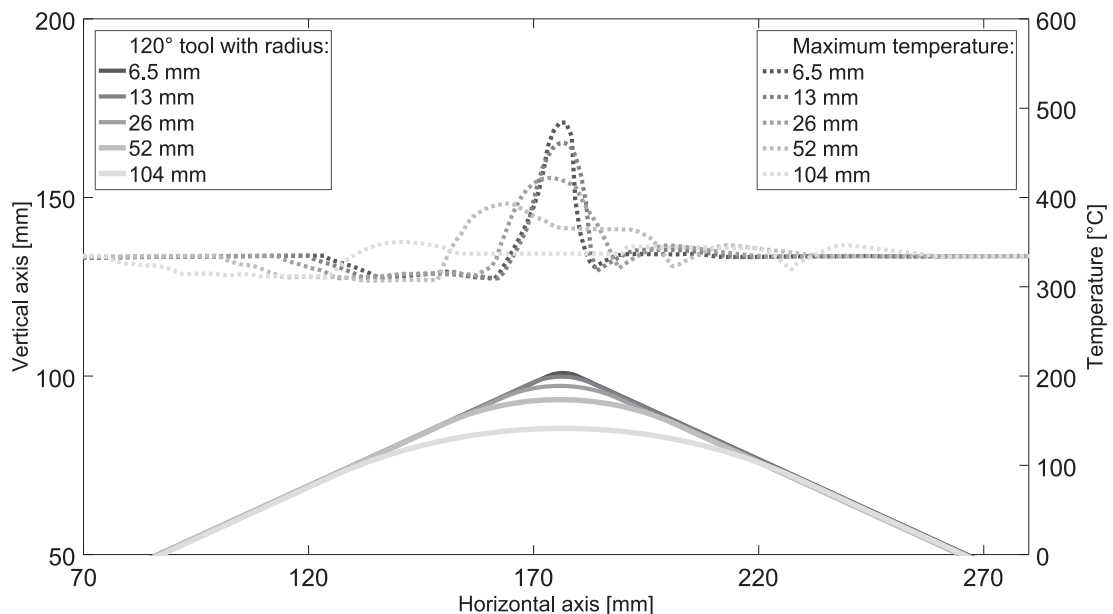
Fig. 6-18:   **Parameter study: Varied corner radius for the 120° tooling**
          Predicted maximum temperature in the nip-point area for different corner radii and a constant tooling angle of 120°.

6.5.3   Effect of tape laying head angle

The tape laying head angle relative to the tool surface is defining various parameters of the laser heating boundary condition. The tape laying head's angle is affecting the laser beams angle on the substrate laminate and the position of the virtual laser beam origin, as the laser optics is mounted onto it. This is influencing the laser energy absorption in the substrate laminate, as it is depending on the laser beam's angle of attack (section 3.1). It is also changing the laser bias ratio between incoming tape and substrate laminate that has to be adjusted by tilting the laser optics relative to the tape laying head to maintain similar surface temperatures in and before the nip-point area. Furthermore, the laser spot boundaries on the composite are influenced. A higher laser angle results in a longer shadow area before the nip-point.

Fig. 6-19 shows the predicted maximum temperature in the nip-point area for different tape laying head angles relative to the 120° tooling. The laser optics angle α is adjusted to reach similar surface temperatures as during the validation simulation from section 6.3, with a head angle of 32°. All other process parameters are kept constant. It can be seen that an increased tape laying head angle rises the maximum temperature in the steady-state before and after the arc. The temperature drop before the arc starts earlier for lower head angles, as the laser optics are moved downwards. This results in a longer laser spot on the substrate. The maximum temperature in the arc section and thus the overheating is decreasing for higher tape laying head angles. An optimum has to be found between shadow effect and overheating behavior.

Nip-point temperature data of the machine's thermal camera from experimental lay-up trials with varied tape laying head angles confirm the simulation results.
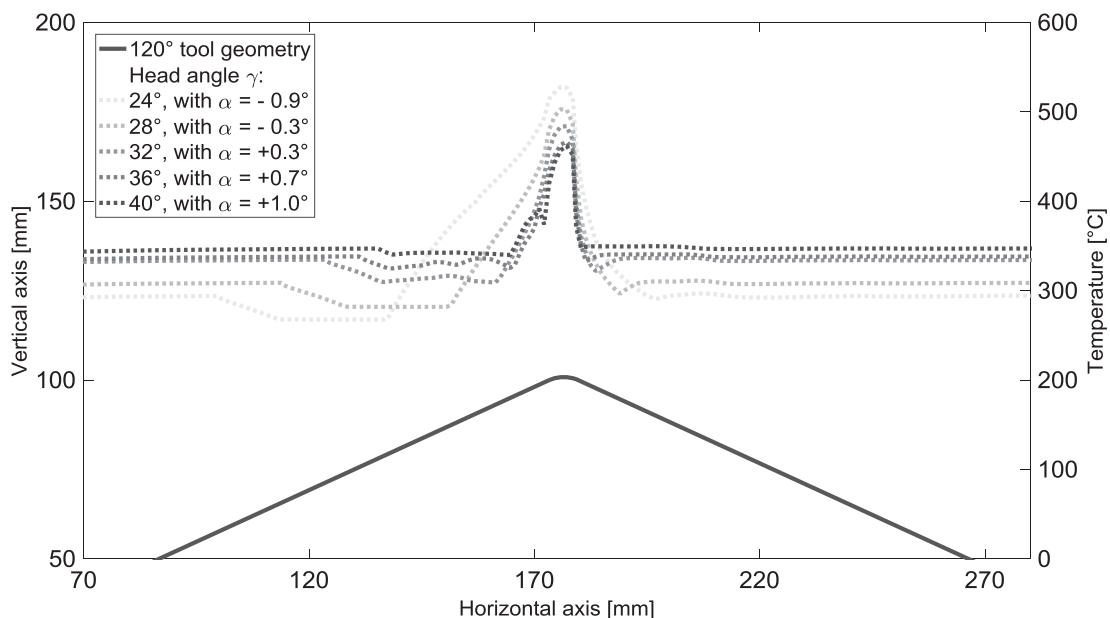
Fig. 6-19:   **Parameter study: Varied tape laying head angle**
              Predicted maximum temperature in the nip-point area for different tape laying head angles
              on the 120° tooling.

6.5.4   Effect of laser spot size

The laser spot size is determining the local power density that is heating the incoming tape and the substrate laminate. The TP-AFP machine used for the experimental trials allows adjusting the laser spot in two ways. First, the laser optics angle α can be adjusted electronically during lay-up to influence the laser spot bias between incoming tape and substrate laminate. Second, the laser optics can be moved towards or further away from the nip-point area. Due to the divergent behavior of the laser beam, this changes the laser spot width and height and thus the local power density. More distance of the laser optics from the nip-point generates a bigger laser spot with lower local intensity. The laser optics can be moved on a track and is fixed by a screw. This can only be done before the lay-up starts and cannot change during lay-up.

Fig. 6-20 shows the predicted overheating temperature in the nip-point area for different positions of the laser optics relative to the nip-point. The laser optics position is moved on its track from -70 mm to +70 mm from its standard position. The virtual laser beam origin is also indicated by dots. All simulations are conducted for lay-up on the 120° tooling with constant lay-up parameters from Tab. 6-1. Consequently, a constant laser power leads to a lower heating intensity for an increased laser spot.

Both, steady-state nip-point temperature in the straight section and maximum nip-point temperature in the arc section are higher for smaller laser spots. Both temperatures decrease with different ratios with increasing laser spot size. The overheating in the region around the arc section is decreasing with increasing laser spot size. It is assumed that the laser spot heating density is decisive for the local overheating at the arc section. A wider spread of the laser spot leads to less relative overheating.
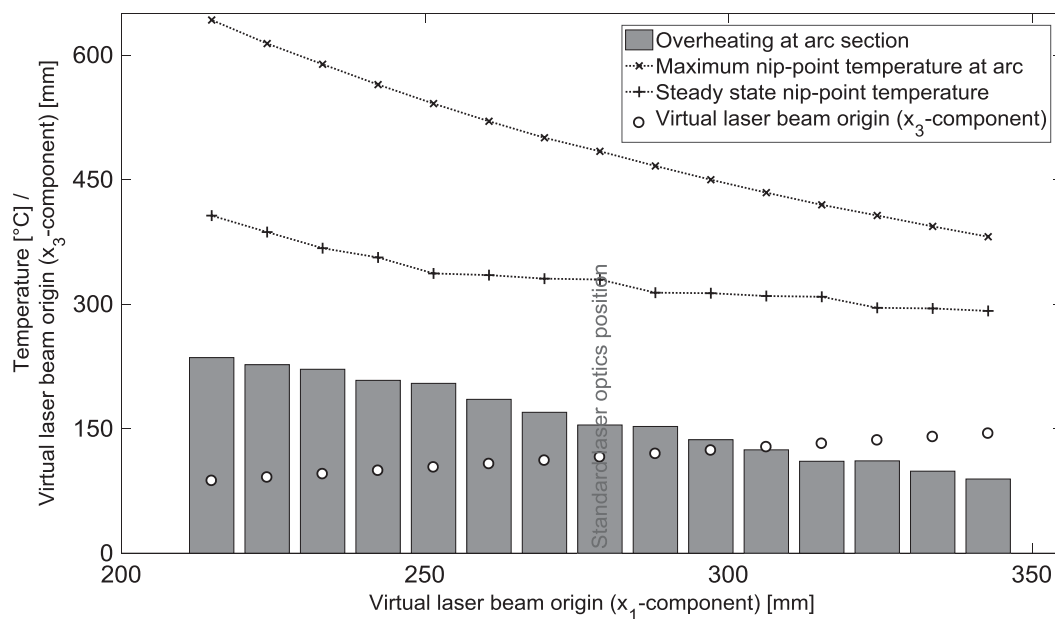
Fig. 6-20:   **Parameter study: Varied distance of the optics to the nip-point**
Predicted maximum overheating in the nip-point area at the arc section for different distances of the laser optics from the nip-point during lay-up on the 120° tooling.

6.6 Optimized process parameters for 3D lay-up

The previous sections show the importance of the laser spot distribution on the composite during 3D lay-up. Due to the movement of the tape laying head relative to the lay-up tooling, complex location-dependent heating profiles of the incoming tape and especially for the substrate laminate are generated. Direct illumination and reflection from the other side have to be considered. Based on these findings, a set of optimized process parameters is derived. The thermal simulation allows changing the process parameters that are defining the laser boundary condition during the lay-up simulation. Laser power, tape laying head angle γ and laser bias angle α can be set for each time step of the simulation. By analyzing the resulting process temperatures, a set of suitable process parameters can be defined.

The goal for excellent in situ bonding is to keep the nip-point temperature within the temperature window, defined experimentally by wedge peel tests in section 5.5. Furthermore, the temperatures of the two joining partners, incoming tape and substrate laminate, are supposed to be of equal temperature before bonding.

The process parameters laser power and laser angle α are altered iteratively to gain an almost constant nip-point temperature in all region of the 3D lay-up geometry. All other process parameters from Tab. 6-1 are used unmodified. Fig. 6-21 shows the contour of the these main process parameters and the resulting nip-point temperature during lay-up on the 120° tooling. Compared to the thermal simulation with constant laser power and constant laser angle α the effect is clearly visible.
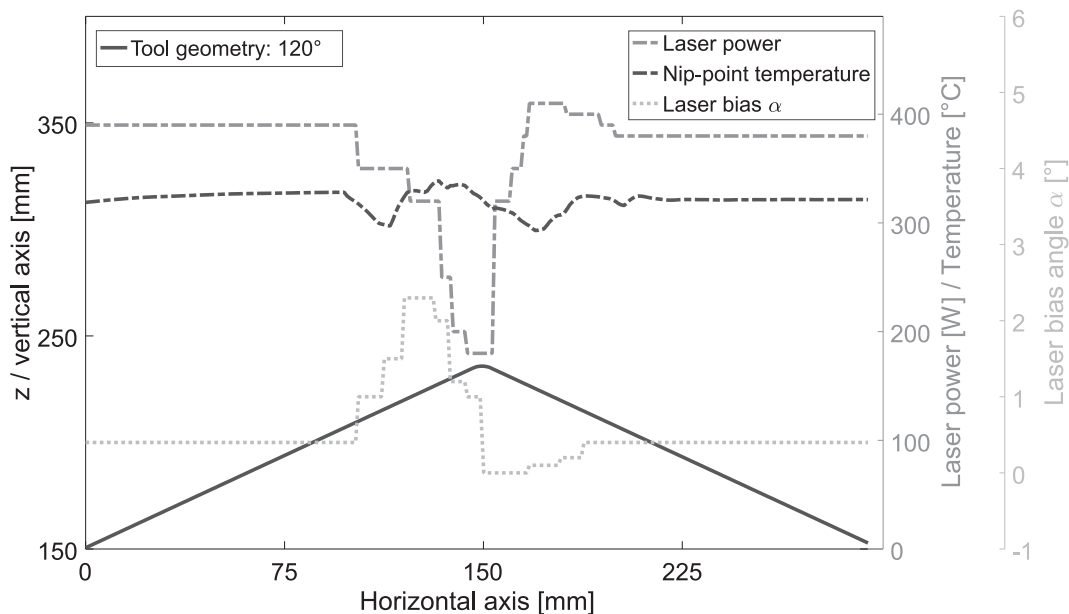
Fig. 6-21:   **Almost constant nip-point temperature is reached by optimized process parameters for laser power and laser angle α**

During lay-up, first the laser angle α is raised to move the laser spot more biased to the incoming tape. Consequently, the laser power has to be reduced in order to avoid

overheating of the incoming tape. The maximum shifted laser angle α and minimum laser power are right before the nip-point reaches the top of the lay-up geometry. As the lay-up head reorients around the arc, the process parameters can be set to their initial values again.

6.7 Conclusion

In this section, the thermal simulation for flat geometries is adapted to the v-shaped 3D geometries of interest. The lay-up geometry is split into three characteristic sections to represent the tape laying head's location during 3D lay-up. Due to the size of the laser spot, which is heating the composite in front of the nip-point, the laser boundary condition is split into characteristic cases. The calculation of the laser boundary condition for the simulation is similar for each case, but has to consider the laser spot size, angle of attack and heating time for each element. Same as for the simulation for flat lay-up geometries in chapter 3, heat input by direct laser illumination and first order reflection is considered.

The adapted thermal simulation is validated with experiments with constant laser boundary conditions. The simulation predicts the experimentally observed overheating in the corner region of the lay-up geometry correctly. Especially the subsequent overheating at the substrate laminate towards the nip-point is important to be predicted correctly. In the following sections, the laser boundary condition is examined and discussed in detail with the help of the simulation. The most dominant change on the accumulated laser energy input is observed for the substrate laminate after the corner by direct laser illumination. The energy input rises up to around 200 % for a short area and then drops down to about 50 %. This behavior is predicted for all three investigated tooling angles. Further parameter studies investigate the influence of the tooling's geometry and machine parameters that define the laser spot on the composite.

Based on these findings, an optimized set of process parameters is defined by simulations. Same as TUM's TP-AFP machine, the thermal simulation allows to adjust some process parameters according to the tape laying head's position on the lay-up tool. By changing the laser power and laser spot bias between incoming tape and substrate laminate an almost constant nip-point temperature is predicted. In the following chapter this optimized set of process parameters will be validated experimentally.

However, the iterative process to determine an optimized set of process parameters is time consuming and prone to user mistakes. In the future, an inverse thermal model could calculate the corresponding laser boundary condition for a defined surface temperature. For the steady-state processing of flat laminates, Stokes-Griffin and Compston use such an inverse model [133]. Another method could be to use time efficient surrogate models to predict the system's answer to a change of boundary condition analytically. This is demonstrated by Schaefer et al. for the lay-up simulation of flat laminates developed in chapter 3 [41, 100].

7 Improved TP-AFP 3D lay-up process[1]

In the previous chapters, the 3D lay-up on v-shaped tools is described. Chapter 5 describes experimental lay-up trials with process parameters derived from flat lay-up trials. The effects on process temperature and polymer degradation are discussed and the robot programming is optimized. Chapter 6 analyzes the 3D process via thermal simulation. The change of the laser boundary condition around the corner is investigated. Based on the results an optimized set of process parameters is derived that could enable a more constant process temperature. In the first section 7.1, two strategies for 3D lay-up are presented and implemented into TUM's TP-AFP machine. This is followed by lay-up trials, comparing the new developed strategies with standard flat process parameters. The laminates are tested mechanically by wedge peel and four-point-bending tests. This chapter is concluded by the description of the manufacture of a 3D demonstrator.

7.1 Strategies for homogeneous process temperature

Two strategies are developed and implemented into TUM's TP-AFP machine together with the machines manufacturer AFPT GmbH. The first one is aiming for a simple use, without a preliminary simulation of the process. An additional closed loop control for the substrate laminate region is implemented, so that the start of overheating can be detected and its effect reduced. The second one is meant to reproduce the set of process parameters defined by the thermal simulation. A set-point table is used to define the process beforehand.

7.1.1 Predictive Closed Loop Control (PCLC)

The aim of the "Predictive Closed Loop Control (PCLC)" strategy is an easy utilization. No process parameters need to be determined before lay-up. An additional closed loop is added, for which a separate set-point temperature is defined. As seen from the lay-up trials with constant laser power (section 5.3.2) and in the analysis of the energy input (section 6.4), the substrate laminate is exposed to the majority of temperature change during 3D lay-up. Therefore, the analysis area of this additional

closed loop control is aimed at the substrate laminate section of the IR camera image (Fig. 7-1). By the movement of the tape laying head, the laminate area in the bottom half of the IR camera is approaching the nip-point and will be bonded to the incoming tape. The composite's temperature constantly increases on its way towards the nip-point. Fig. 5-10 shows how overheating of the substrate laminate is approaching the nip-point area from the bottom of the IR camera's field of view. The PCLC can detect the start of the overheating and reduce the laser power to prevent excessive overheating that will cause polymer degradation. During the trials with CF/PA6, the set-point temperature for the PCLC is lower than the set-point temperature for the standard laser power closed loop control. Its size and position as well as its amplification on the laser power control can be adjusted to achieve optimal results.
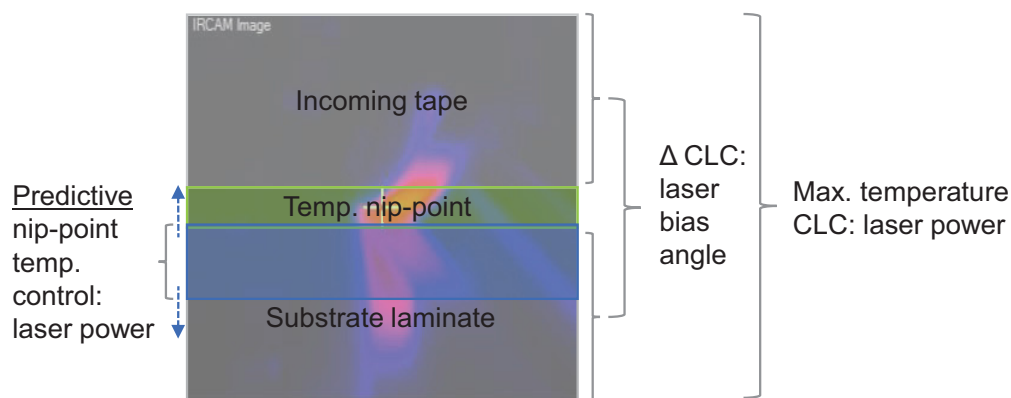
Fig. 7-1:   **Principle of the predictive closed loop control (PCLC) for the nip-point temperature**

The PCLC is interacting with the standard CLC for nip-point temperature. By balancing its parameters, both the temperature at the substrate laminate and the nip-point temperature can be kept almost constant, even for 3D lay-up. Its main purpose is to prevent overheating and insufficient heating on the substrate laminate. As a laser homogenizing optics with constant laser beam distribution is used, the PCLC also affects the temperature of the incoming tape. As discussed in section 6.4, the incoming tape's temperature is not affected as much as substrate laminate's temperature. However, when the laser power is reduced to prevent overheating of the substrate laminate, the temperature of the incoming tape obviously changes as well. This has to be considered as a major drawback.

The PCLC could also be used for other processes, that inhibit a thermal disturbance at the substrate laminate. Examples are: change of laminate thickness, change of substrate laminate material or fusion bonding of TP-AFP materials to other parts.

7.1.2 Coordinate Controlled Process Parameters (CCPP)

A module called "Coordinate Controlled Process Parameters (CCPP)" is added to the control PC of the TP-AFP machine. It allows specifying a set of process parameters through a table that are used during lay-up. It can disable the closed loop controls for laser power or laser bias angle between certain coordinates by overwriting the calculated values with values from the table. Process parameters that can be changed by this table are laser power, laser bias angle α and closed loop control parameters.

While the laser power and the closed loop control parameters can be changed almost instantaneously, an electric actuator controls the laser bias angle. Therefore, the laser bias angle changes continuously with a delay time and cannot jump to new values as fast as the electronically controlled laser power. Also, the current motor used to change the laser bias angle is not designed for large movements in a short time.

A mixed mode of operations is also possible. The closed loop control can be switched on and off by the table during lay-up of a path. The robot permanently sends its TCP coordinates to the control PC of the system. Once the TCP is within the threshold distance of a control point, the control PC sets the process parameters. This set of parameters is kept until the next control point with its set of parameters is reached. In case a parameter is set to "0" the CCPP is disabled and a value calculated by the closed loop control is used instead. Fig. 7-2 shows a lay-up path with the control points for the CCPP module. The corresponding table of set-points for the laser power and laser bias angle are listed in Appendix e. The laser power set-point curve and response curve from the laser controller are congruent, while the actual laser bias angle curve is following the set-point curve with a little delay.

The big advantage compared to PCLC is that the CCPP strategy not only adjusts the overall laser power, but also the laser bias between incoming tape and substrate laminate. However, the process parameters need to be known before processing and written into the set-point table. This can either be done iteratively by lay-up trials or be a thermal simulation, as shown in chapter 6.
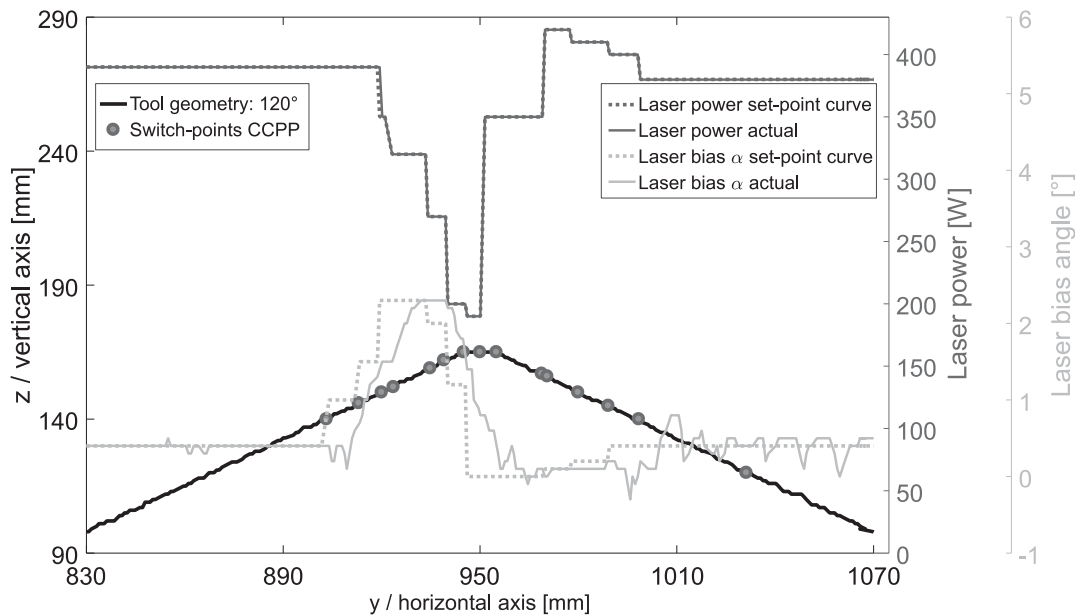
Fig. 7-2: **Coordinate controlled process parameters: Control points and corresponding set-point and actual curves for laser power and laser bias angle**

7.2 Lay-up trials and mechanical tests of 3D specimens

For both processing strategies lay-up trials on all three v-shaped tools are conducted. Both developed strategies are compared with standard CLC lay-up and lay-up with constant laser power (section 5.3). First, the lay-up parameters for all strategies are discussed. Four-layer wedge peel and 18-layer (~ 2 mm thickness) four-point-bending specimens are produced. Second, the log files are shown and the temperature curves due to the processing strategy are discussed. In the following, the test results of the wedge peel tests and four-point-bending tests are presented and the effects of the processing strategy on the mechanical strength is discussed.

7.2.1 Process parameters

Tab. 7-1 lists the general lay-up parameters that are used for all 3D lay-up strategies. Despite the compaction pressure, they are identical to the validation trials of the flat lay-up simulation from section 4.4.3 and the first 3D lay-up trials from section 5.3.

Tab. 7-1:   **General process parameters for 3D lay-up trials with CF/PA6**

Name:	Description:	Value:	Unit:
γ	Angle placement head - mold	32	deg
v	Lay-up velocity	75	mm/s
l_c	Length of compaction zone under compaction roller	13.1	mm
F_C	Compaction force of the roller	130	N
w_C	Width of compaction roller during experiment	30	mm
h_M	Thickness of unheated mold	2	mm
r_{Roller}	Radius of compaction roller	32	mm
t_{Roller}	Thickness of silicone layer of compaction roller	7	mm
T_0	Start temperature of tape, compaction roller, mold and ambient air	23	°C

Except for the specimens manufactured with standard CLC, the first layer was laid down on the tool without the laser. The tapes were fixed at start and end via double-sided adhesive tape. The individual process parameters of each process strategy are given in the following tables.

Standard 2D closed loop control

The first 3D lay-up trials are conducted with the standard closed loop control for flat laminate (see section 5.3.1). As the trials were conducted early in the project, no optimized robot-programming path was used (section 5.4.1). The thicker laminates for four-point-bending tests are produced without the compensator, while the wedge peel specimens were produced with the compensator already installed (see section 5.4.1).

Tab. 7-2:   **Process parameters for 3D lay-up with standard closed loop control**

Name:	Description:	Value:	Unit:
α	Range of angle laser - lay-up tool (by CLC)	24.3 to 25.0	deg
$X1_L$	Virtual laser beam origin (x_1-component)	~317.8 to 318.4	mm
$X3_L$	Virtual laser beam origin (x_3-component)	~132.8 to 134.2	mm
T_{set}	Temperature set-point for CLC	300	°C

Constant laser power

Specimens produced with constant laser power are used as a reference, as their thermal processing history is the easiest to understand. The laser power of the standard 2D closed loop control is chosen as a reference to achieve a nominal nip-point temperature of about 280 °C for flat lay-ups. The laser bias angle is fixed to a value that achieves

equal temperature on the incoming tape and substrate laminate in the upwards pointing leg of the tool.

No test laminates for four-point-bending are manufactured, because too much over-heating occurs on the first layers with its thin substrate laminate. In contrast to the wedge peel test samples, the four-point-bending samples are produced as a laminate with adjacent paths. The laser overshoot on both sides of the tape results in partial repeated overheating of the substrate laminate. The overheating is so strong, that in areas behind the corner the matrix is evaporated completely and dry fibers are observed.

The compensator is used to maintain the laser bias ratio between incoming tape and substrate laminate constant, despite little roller deflection around the corner. The optimized robot-programming path is used to maintain the lay-up speed almost constant.

Tab. 7-3:   **Process parameters for 3D lay-up trials with constant laser power**

Name:	Description:	Value:	Unit:
α	Range of angle laser - lay-up tool (by CLC)	23.9	deg
$X1_L$	Virtual laser beam origin (x_1-component)	~278.7	mm
$X3_L$	Virtual laser beam origin (x_3-component)	~115.5	mm
P	Laser power	390	W

Predictive closed loop control

The predictive closed loop control (PCLC) strategy requires no prior knowledge of the process parameters. Its area of interest is set to the upper third of the substrate laminate right under the nip-point region of the IR camera (Fig. 7-1). The PCLC is used complimentary to the standard CLC. Tab. 7-4 lists the process setup used for PCLC lay-up.

The compensator is used to maintain the laser bias ratio between incoming tape and substrate laminate constant, despite little roller deflection around the corner. The optimized robot-programming path is used to maintain the lay-up speed almost constant.

Tab. 7-4:   **Process parameters for 3D lay-up trials with PCLC strategy**

Name:	Description:	Value:	Unit:
α	Range of angle laser - lay-up tool (by CLC)	23.9 to 24.4	deg
$X1_L$	Virtual laser beam origin (x_1-component)	~278.4 to 279.0	mm
$X3_L$	Virtual laser beam origin (x_3-component)	~116.0 to 116.6	mm
$T_{set-PCLC}$	Temperature set-point for PCLC	260	°C
T_{set}	Temperature set-point for standard CLC	280	°C
P	Laser power (by PCLC)	~110 to 500	W

Coordinate controlled process parameters

Tab. 7-5 shows the general process parameters for CCPP strategy. The compensator is used to maintain the laser bias ratio between incoming tape and substrate laminate constant, despite little roller deflection around the corner. The optimized robot-programming path is used to maintain the lay-up speed almost constant. For the second to fourth layer a reduced laser power and a laser spot bias towards the incoming tape is used to prevent overheating due to the thin substrate laminate.

Tab. 7-5:   **Process parameters for 3D lay-up trials with CCPP strategy**

Name:	Description:	Value:	Unit:
α	Range of angle laser - lay-up tool (by table for CCPP)	25.6 to 22.3	deg
$X1_L$	Virtual laser beam origin (x_1-component)	~278.0 to 274.1	mm
$X3_L$	Virtual laser beam origin (x_3-component)	~121.9 to 117.8	mm
P	Laser power (by table for CCPP)	200 to 390	W

Fig. 7-2 shows exemplary control points and set-point curves of laser power and laser bias angle in reference to the tool geometry for the 120° tool. Tab. 7-6 lists the corresponding set of parameters for the lay-up on the 90° tooling. The set-point curves and tables for the 105° and 120° tools are listed in Appendix e.

Tab. 7-6:   **CCPP set-point table for 90° tooling lay-up**
          Lay-up in y-direction; the top of the tool is at y = 950 mm, z = 261 mm

#:	x [mm]:	y [mm]:	z [mm]:	P [W]:	α [°]:	Comment:
1	590.0	735.2	48	390	0.4	turning CCPP on
2	590.0	902.7	216	390	0.8	
3	590.0	912.9	226	390	2.5	
4	590.0	919.8	232	390	2.7	
5	590.0	923.6	236	330	3.0	Laser bias on incoming tape
6	590.0	929.1	242	230	2.5	
7	589.8	939.0	252	200	1.0	
8	589.5	944.7	259	220	0.5	
9	589.2	948.7	261	280	-0.3	~ tip of the tool
10	589.1	954.2	259	380	-0.1	
11	590.0	969.7	243	390	-0.1	
12	590.0	988.9	224	390	0.1	
13	590.0	1029.6	183	390	0.1	
14	590.0	1140.8	72	0	0	turning CCPP off

Post consolidation

Additional four-point-bending specimens are manufactured and post consolidated for reference. The initial lay-up of the specimens for post consolidation is done via PCLC, as it prevents overheating very well. Reduced set-point temperatures are used for the standard CLC and PCLC, as the aim is not to achieve best consolidation during lay-up, but via post consolidation afterwards. After lay-up the samples are preliminary trimmed and post consolidated under vacuum in an oven for about 20 minutes above 260 °C. After post consolidation, the specimens are cut to its final geometry. A higher crystallinity is expected for the post consolidated specimens.

Tab. 7-7:   **Process parameters for 3D lay-up trials with PCLC strategy for post consolidation**

Name:	Description:	Value:	Unit:
α	Range of angle laser - lay-up tool (by CLC)	23.9 to 24.4	deg
$X1_L$	Virtual laser beam origin (x_1-component)	~278.4 to 279.0	mm
$X3_L$	Virtual laser beam origin (x_3-component)	~116.0 to 116.6	mm
$T_{set-PCLC}$	Temperature set-point for PCLC	250	°C
T_{set}	Temperature set-point for standard CLC	260	°C
P	Laser power (by PCLC)	~150 to 450	W

7.2.2 Process temperatures

The temperature curves of the specimens manufactured by standard closed loop control and with constant laser power are shown and discussed in section 5.3 (see Fig. 5-7 and Fig. 5-11). Fig. 7-3 and Fig. 7-4 show the log file data of the two new strategies for 3D geometries during the lay-up on the 90° tooling. The log file data diagrams of the lay-up on the 105° and 120° tooling are listed in Appendix f. For analysis the nip-point temperature, laser power and laser bias angle curves of CCPP and PCLC lay-up strategy are of interest. Additionally the temperatures measured for the incoming tape and for the substrate laminate are plotted to examine the temperature distribution between the two joining partners.

PCLC process temperatures

The lay-up starts with a laser power around 400 W and constant nip-point temperature of around 280 °C. Before the nip-point reaches the corner, the substrate laminate's temperature is rising, as the laser spot is already at the corner. The increase of temperature is detected by the PCLC, which reduces the laser power down to around 200 W and prevents overheating in the nip-point area. The PCLC reduces the overall laser power in the whole laser spot. Thus, the temperature of the incoming tape is also affected unintentionally. Shortly after the corner, the laser power is increased by the PCLC to a level above the initial laser power, as the substrate laminate's temperature is falling. The laser power oscillates a bit in this section, but keeps the temperatures constant. The lay-up trials with PCLC show the effectiveness of the additional closed loop control. The PCLC prevents overheating at the corner and insufficient heating after the corner, by adjusting the laser power faster than the standard closed loop control does. As a drawback, the PCLC also influences the incoming tape's temperature, as the laser bias ratio is not adjusted.
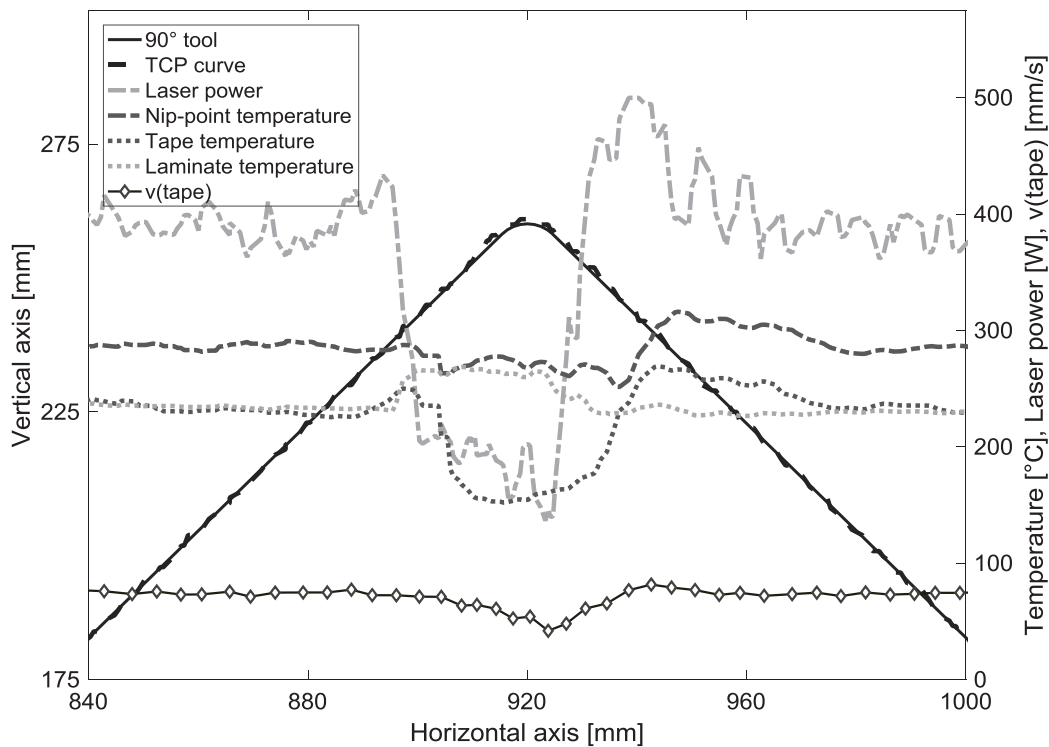
Fig. 7-3:   Log file data of a track from 90° specimen manufactured by PCLC

CCPP process temperatures

Fig. 7-4 shows the CCPP lay-up, following the set-point values from Tab. 7-6. The initial laser power is 390 W, which results in a nip-point temperature of around 280 °C. In a similar distance of the nip-point to the corner, the laser power is reduced to avoid overheating of the substrate laminate. The power reduction is not as strong, as at the same time the laser optics are moved upwards, shifting the laser bias towards the incoming tape. This reduces the laser energy input in the substrate laminate and simultaneously increases the energy input into the incoming tape. The substrate laminate's temperature remains constant until a small increase occurs right after the corner. The incoming tape's temperature rises in the area of the corner up to the nip-point's temperature level but remains within the optimum temperature window of up to 320 °C according to section 5.5. By using an adequate set-point table, the CCPP strategy also prevents overheating in all sections of the specimen. Additionally, the effect on the incoming tape is reduced by adjusting the laser bias ratio.
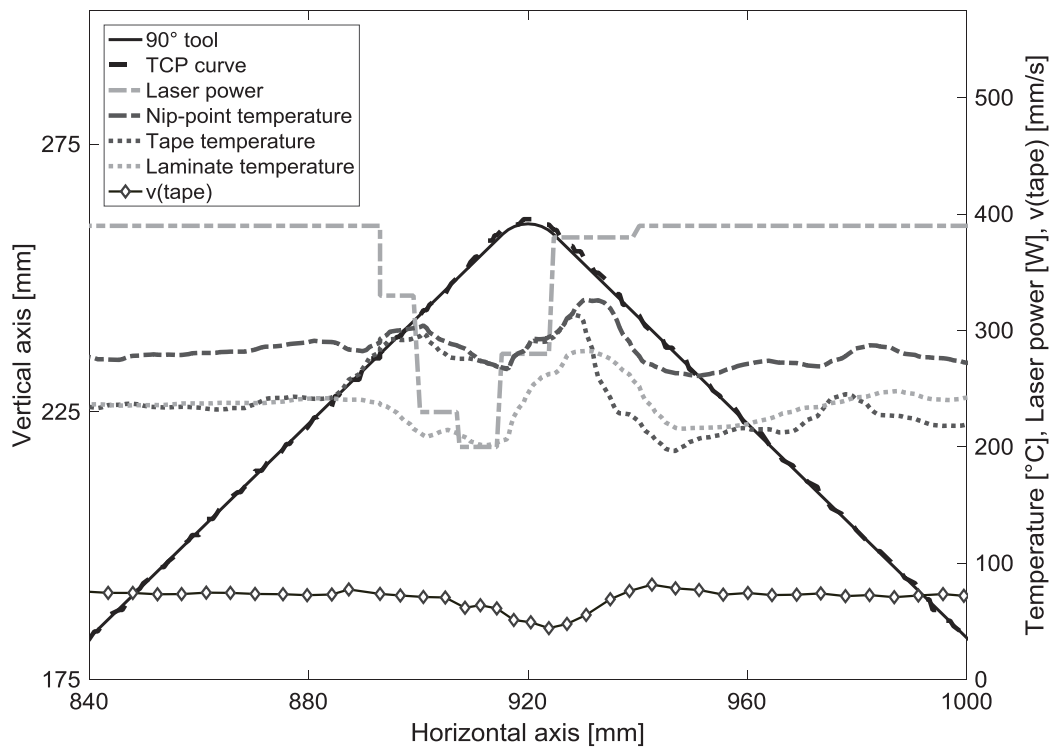
Fig. 7-4:   **Log file data of a track from 90° specimen manufactured by CCPP**

Comparison of nip-point temperature and process temperature bias

Besides the line graph representation of 3D heatmap plots are used to analyze the process behavior. Each measured data value is plotted as a color-coded dot at the current TCP position. By this method all lay-up paths of a ply can be shown at once.

Fig. 7-5 shows the nip-point temperature during lay-up of the 18th layer of the 90° four-point-bending specimens for the processing strategies. The plots show consistent behavior for all tracks of a layer, indicating stable processing. The manufacture of four-point-bending specimens with constant laser power is not possible due to massive overheating. This occurs by repeated heating during the lay-up of adjacent paths. No sound laminate can be manufactured. Instead, the heatmap of the four-layer wedge peel specimens is shown. The heatmap of the manufacture with standard 2D CLC shows the same effects as already discussed in section 5.3.1. Overheating at the tip of the tool is followed by a cool section due to the reduction of laser power by the standard CLC. The heatmap of the PCLC produced specimens shows a homogeneous nip-point temperature with only a slightly increased temperature behind the corner. The faster reduction of the laser power by the PCLC is very effective to prevent overheating of the laminate. The nip-point temperature of the specimens manufactured by the CCPP strategy also shows a homogeneous distribution, but with a little overheating behind the corner. This could be eliminated with more fine-tuning of the set-point curve. The maximum measured nip-point temperature is also given in the figure. Both

strategies, with standard closed loop control and with constant laser power, result in polymer degradation. This can be avoided by the PCLC and CCPP strategy that show only minor temperature rise at the corner section.
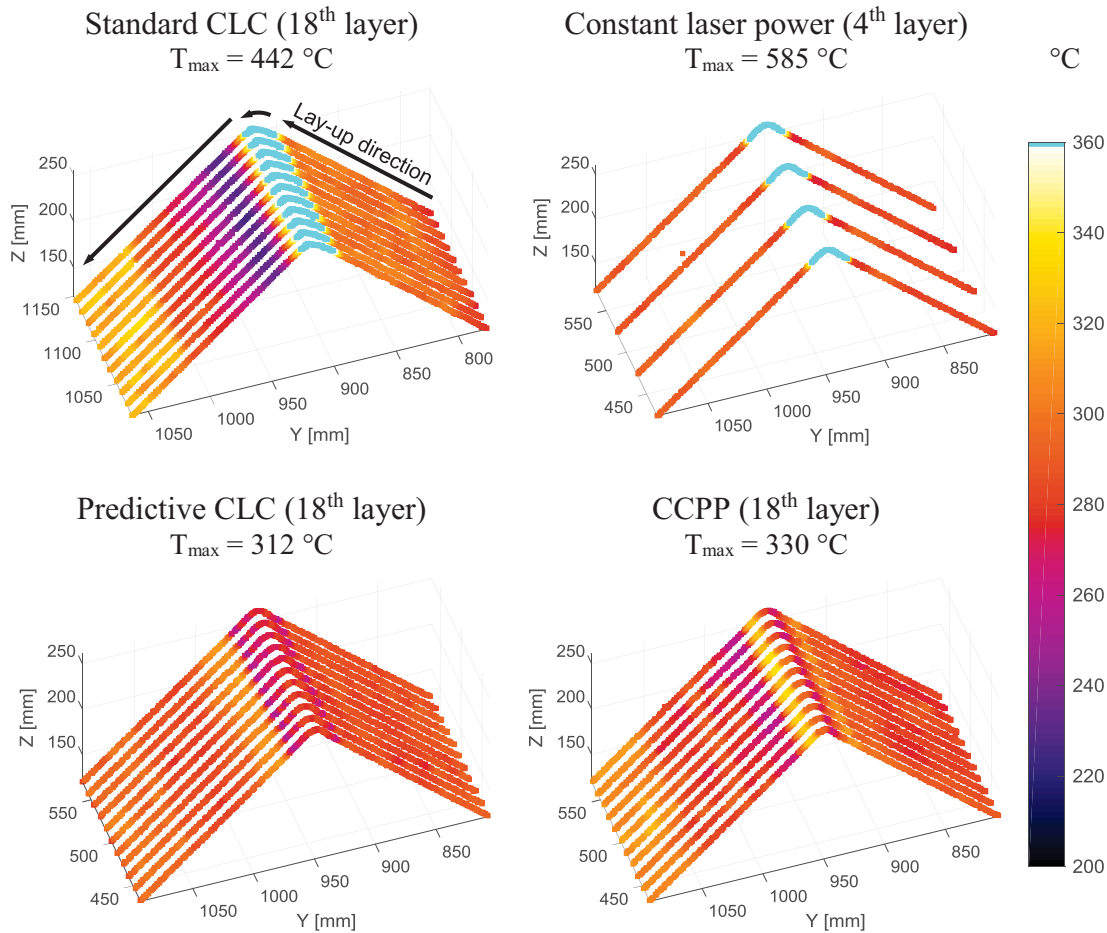
Fig. 7-5:   **Nip-point temperature 3D heatmap representation of specimens with 90° angle, manufactured by different lay-up heating strategies**
The heatmaps show the tracks of the 4th layer of the wedge peel specimens (top right), manufactured with constant laser power and the tracks of the 18th layer of the four-point-bending specimens, manufactured with the other strategies

Besides the joining temperature at the nip-point area, also the temperature difference of the joining partners, incoming tape and substrate laminate, are of interest to evaluate the processing quality. Kölzer's closed loop control for the laser bias angle aims to achieve equal temperature for both joining partners [27] (see also Fig. 2-8 and Fig. 2-17). This is the intention for the CCPP 3D lay-up strategy as well. Fig. 7-6 shows the temperature difference of the temperatures assigned to the incoming tape and the substrate laminate. The temperature around the corner occurs in a very small timeframe that the closed loop control for the laser bias cannot react fast enough.
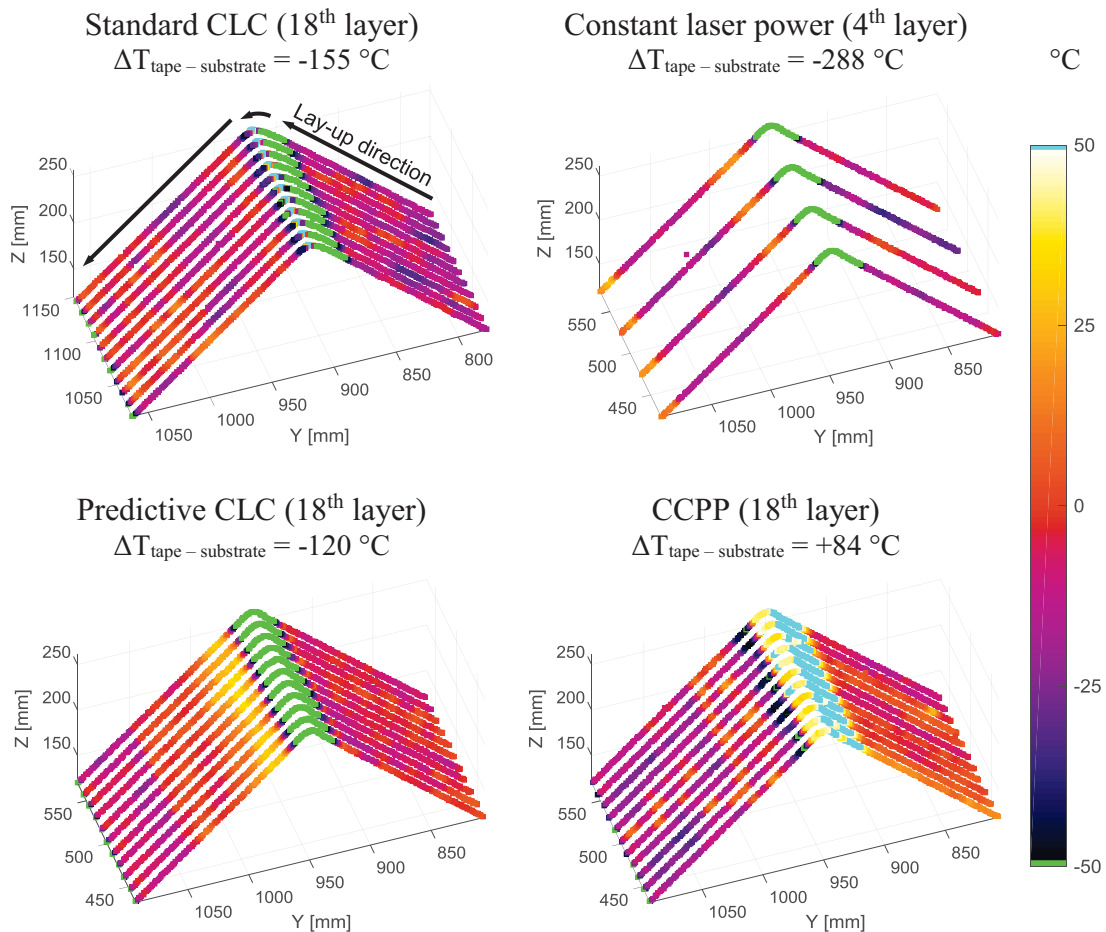
Fig. 7-6:   **Temperature difference between incoming tape and substrate laminate of four-point-bending specimens with 90° angle, manufactured by different lay-up heating strategies**
The heatmaps show the tracks of the 4th layer of the wedge peel specimens (top right), manufactured with constant laser power and the tracks of the 18th layer of the four-point-bending specimens, manufactured with the other strategies

The bright blue and green areas of the heatmap plots indicate a temperature difference than bigger 50 °C. Specimens manufactured by standard CLC, constant laser power and PCLC show a hotter substrate temperature than tape temperature. This is caused by the geometry and the maintained laser bias during lay-up. Both closed loop controls reduce only the overall laser power and not the laser bias. The biggest temperature difference is caused by processing with constant laser power. The standard CLC strategy produces the second biggest temperature difference, as soon as the tape laying head is shortly before the corner. The laser and IR camera are already partially pointed to the backside of the tool and its temperature is measured. The mean maximum temperature difference of the tracks is -155 °C. Both, tape and substrate laminate clearly exceed the degradation threshold with a maximum temperature above 400 °C. On its way to the nip-point these laminate areas are exposed to even higher temperatures.

The area facing the biggest difference for the PCLC specimens is before and after the corner with an average maximum temperature difference of -120 °C. However, the maximum tape, substrate laminate and nip-point temperatures stay around 280 °C.

The CCPP lay-up strategy adjusts both, the overall laser power and the laser bias between incoming tape and substrate laminate. The area with the biggest temperature difference is, when the tape laying head is just before the corner. Here, the incoming tape gets hotter than the substrate laminate by an average maximum temperature difference of +84 °C. In contrast to PCLC processing, this difference probably could be reduced with more fine-tuning of the set-point curves and a more accurate actuator. The maximum tape and substrate laminate temperatures stay below the degradation threshold from section 5.5.

7.2.3   Wedge peel test of 3D specimens

The wedge peel test shows good results to evaluate the bond strength and degradation due to overheating in section 5.5.1. During 3D lay-up, overheating occurs as well. Specimens produced on the 3D geometries with the four lay-up strategies are compared by wedge peel test in this chapter.

Specimen manufacturing

The wedge peel test can only be used for flat specimens. Testing around the corner is not possible. The laminate before the corner is hardly affected by the changing process conditions due to the geometry. Therefore, only the laminate after the corner is tested by wedge peel test. As discussed with the simulation results in chapter 6.4 and shown by temperature log file data in section 7.2.2, this area is mostly affected by the 3D process. First, overheating of the substrate laminate occurs, which is followed by too low process temperature, if no adjustments of the process are made.

Five to six 3D specimens are produced and tested for each tooling angle and processing strategy. The lay-up parameters from section 7.2.1 are used for each strategy, respectively. Stripes of four layers are manufactured, but not consolidated to the end. No polyimide film is used for crack initiation, but the unconsolidated ends. The specimens are cut just after the arc section to get flat specimens. Test direction is opposite to the lay-up direction (Fig. 7-7).
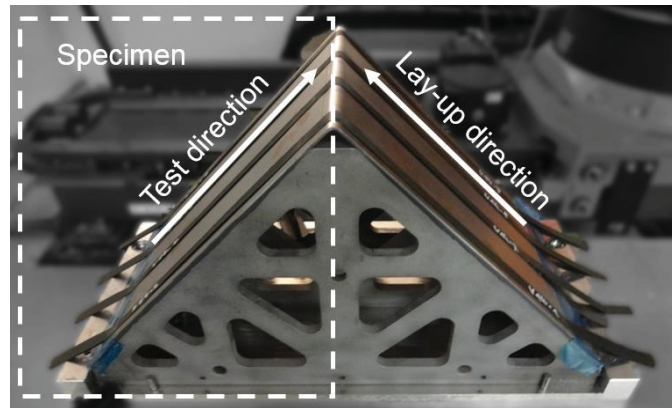
Fig. 7-7: **Specimen production and extraction for wedge peel test of 3D laminates**

The same universal testing machine, fixture and test setup as for the 2D specimens in section 5.5.1 is used for the 3D specimens.

Results

The universal testing machine records the peel force in reference to its stroke position. Fig. 7-8 shows the peel force curves for the specimens manufactured on the 90° tooling for all lay-up strategies. Both lay-up strategies, via standard closed loop control and via constant laser power, produce specimens that show characteristic wedge peel force sections.

Specimens produced with standard CLC feature two characteristic analysis sections. Section I shows a stable peel force, similar to the 2D specimens and is located at a section of the specimen, where the process is not influenced by the corner any more. Section II is located at the end of the testing length, near the corner of the tooling. This area is strongly affected by the geometry and shows much lower wedge peel force values than before. The increase at the very end of testing is attributed to the start of the corner and is excluded from analysis.

The specimens produced with constant laser power show three characteristic analysis sections of the wedge peel force curve. Section I resembles the steady-state process conditions at a distance from the corner. Section II and III show lower peel force values due to the geometry's influence on the composite heating. Section II is attributed to unbalanced heating of incoming tape and substrate laminate while section III is influenced by overheating.

Specimens produced by PCCL and CCPP show a homogeneous wedge peel force curve over the whole testing length, so only one analysis section is used.

The analysis sections end before the arc of the specimen starts and is individually calculated for each specimen, depending on the end of its test curve. All lay-up strategies produce specimens with consisted wedge peel force curves. The wedge peel force curves of the 105° and 120° specimens are shown in Appendix g. They show the same characteristic curves.
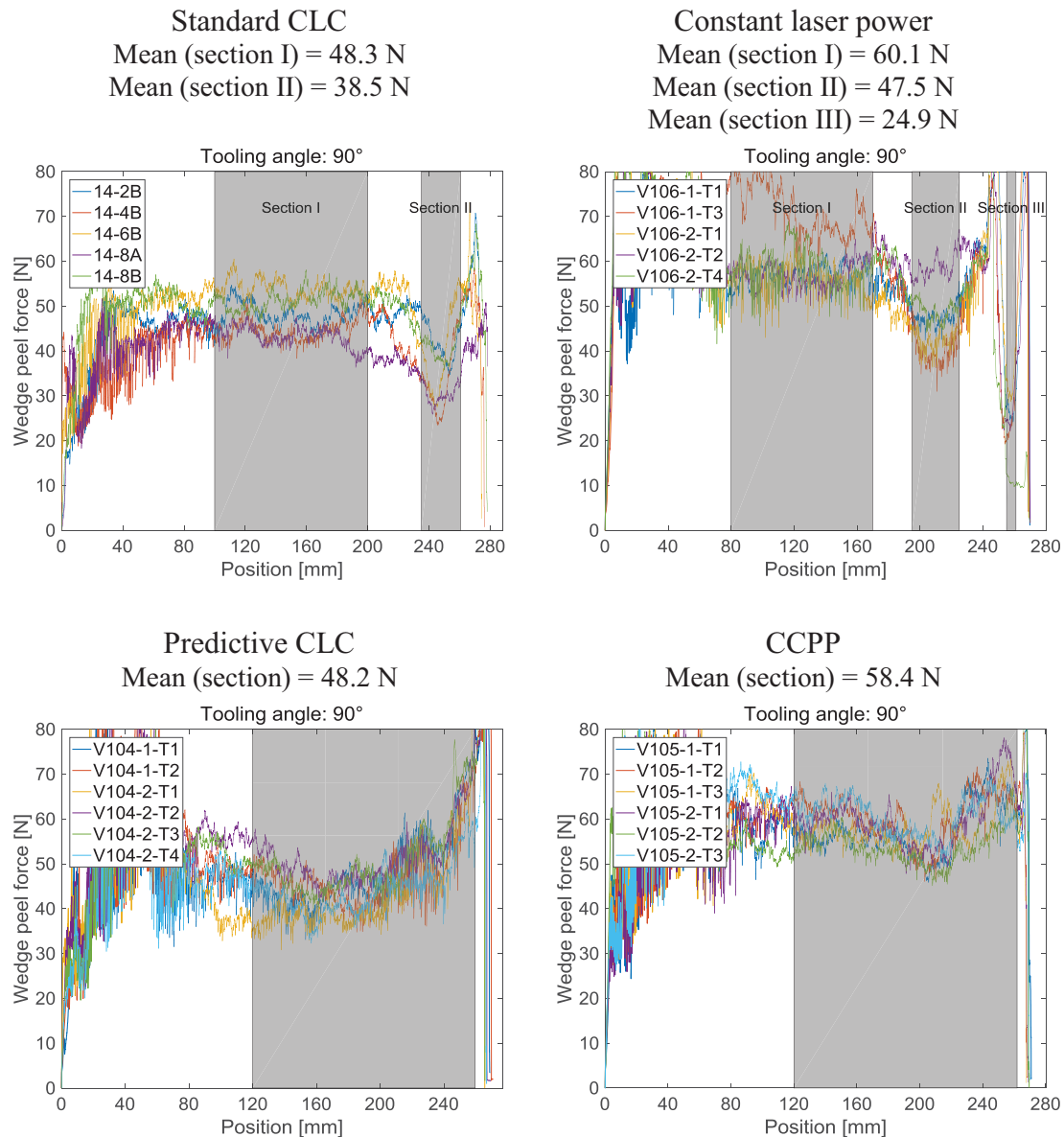
Fig. 7-8: **Wedge peel test curves of 90° specimens manufactured with different processing strategies**

The grey areas highlight the analysis sections.

Fig. 7-9 shows the mean values and the corresponding minimum and maximum values of the test series for each strategy and tooling angle. The mean values are determined over the same test length for each series and are all very close to each other. Due to the short characteristic peel force sections for the standard CLC specimens (sections II) and the specimens manufactured with constant laser power (section III), the standard deviation cannot be used to compare the lay-up strategies adequately. Nevertheless, the minimum and maximum values differ clearly and can be used for comparison. While the tooling angle seems to have only a minor effect, the processing strategy clearly has an impact. The lowest wedge peel force is measured for the standard CLC and lay-up with constant laser power. The lowest values are measured in section II of

the specimens. PCLC and CCPP produced specimen show a higher minimum wedge peel force and smaller range between minimum and maximum values.
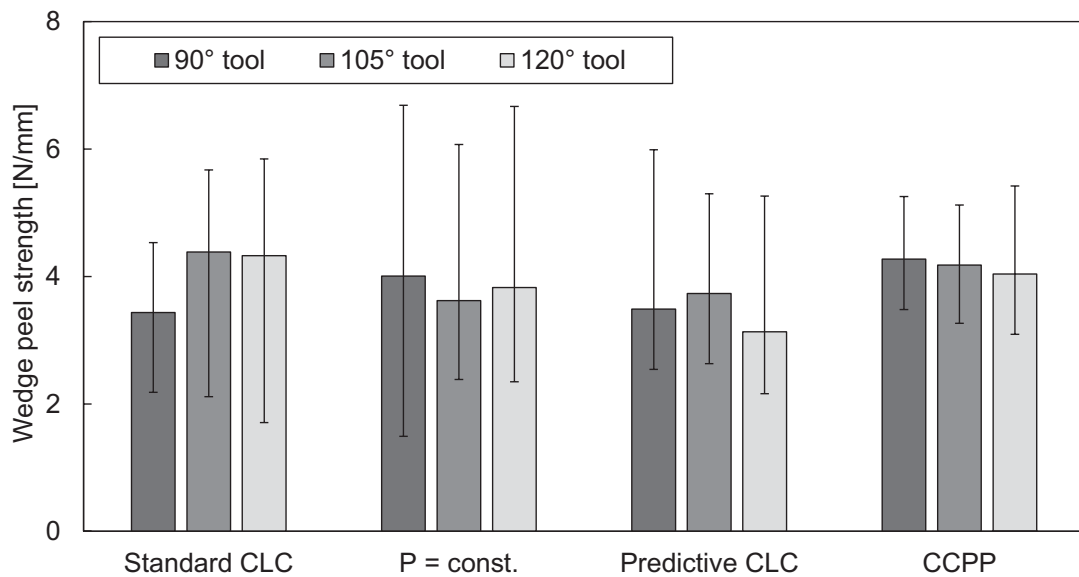
Fig. 7-9: **Mean wedge peel strength of 3D specimens, manufactured with different lay-up strategies**
The error bars indicate the minimum and maximum wedge peel strength of a series of five to six specimens.

Discussion

As the wedge peel test is continuously testing the bond strength of the specimen, the transition between different process conditions can be investigated. In case of the 3D lay-up specimen, the process conditions right after the rounded corner and the process stabilization afterwards are investigated.

Overheating occurs during the first two processing strategies, standard CLC and lay-up with constant laser power. The overheating results in distinctive sections of the wedge peel force curve. The area with overheating, right behind the rounded corner of the mold, shows a significant decrease of the wedge peel force (section II and III). The wedge peel curves stabilize until section I. Specimens manufactured by PCLC and CCPP are not exposed to overheating during manufacturing and show a homogeneous wedge peel strength curve. Only one analysis section is used for these specimens. They also show a higher minimum wedge peel strength and less scattering. Especially the CCPP specimen show high and consistent wedge peel strength for all three tooling angles. This indicates a smaller variance and better processing of the specimens by CCPP. PCLC and CCPP prevent overheating effectively but CCPP also minimizes the temperature difference between incoming tape and substrate laminate.

7.2.4   Four-Point-bending test[2]

The wedge peel test for 3D specimens from section 7.2.3 cannot test the corner section of the specimens. Only the flat area after the corner is characterized. In order to test the corner area directly, four point bending tests according ASTM D6415 [134] are used. The standard describes a mechanical test to determine the curved beam strength (CBS) and the radial tensile strength of unidirectional composite specimens, consisting of two straight legs connected by a 90° bend. First, the test principle and specimen manufacturing are described. Then, the test results are presented and discussed subsequently.

Principle

The test fixture within the universal testing machine is applying a four-point-bending load on the specimens. This results in a radial out-of-plane tension in the centered corner section of the specimen. The radial tension in the corner section causes delamination of the specimen, triggering a significant drop of the applied force (Fig. 7-10). From the force and displacement at the time of delamination, the curved beam strength is calculated according to the standard.

The standard only considers specimens with 90° between the two legs. Additionally to the 90° specimens, also 105° and 120° specimens are tested. The calculation of the radial tensile strength is adjusted corresponding to the specimen's angle. Due to the flat angle of the 105° and 120° specimens, no fixture with roller bearings can be used. Instead, a rigid fixture with the same geometry is used for all specimens. Before each specimen testing, grease is applied on the fixture to reduce friction.
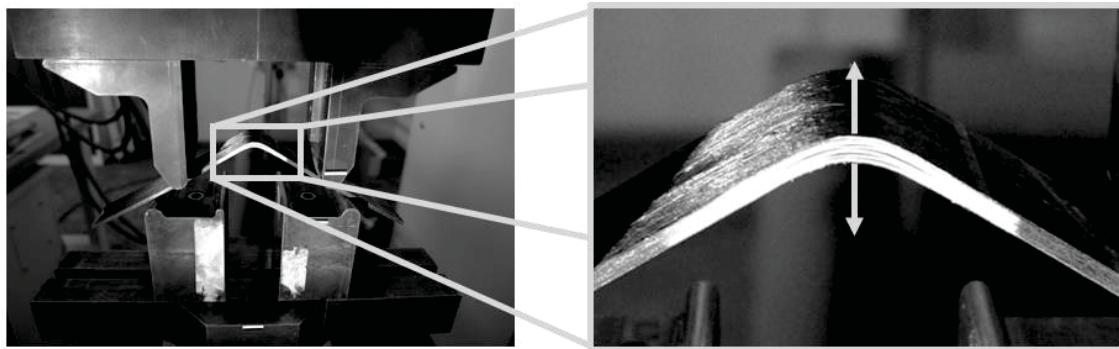
Fig. 7-10:   **Four-point-bending testing of a v-shaped specimen**
The left image shows the test fixture and specimen during testing. Load is applied symmetrically by each two bars from top and bottom.
The radial tensile stress causes delamination in the rounded corner area of the specimens.

---

[2] Parts of this chapter were published in:

Kollmannsberger, A.; Ladstätter, E.; Drechsler, K.; "Challenges for Thermoplastic-Automated Fiber Placement (TP-AFP) with in situ consolidation on 3D parts". in Proceedings of the 17th European Conference on Composite Materials, June 2016, Munich, Germany, ISBN: 978-3-00-053387-7

Specimen manufacturing and preparation

The specimens prepared for testing and their manufacturing can be seen in Fig. 5-4. The process parameters during lay-up are described in detail in section 7.2.1 and the resulting process temperatures are discussed in section 7.2.2.

It is not possible to manufacture specimens with constant laser power, as the repeated heating during lay-up of the adjacent path causes too much overheating, that locally evaporated all matrix within the substrate laminate. Instead, post consolidated specimens are manufactured. During vacuum post consolidation in the oven, wrinkles due to the bleeder and polyimide vacuum film occurred for one set of specimens. Due to the wrinkles, no valid compaction is provided at the corner section and even delamination occurred (Fig. 7-11). These specimens were tested but excluded from analysis afterwards. They failed at much lower compaction force (see Fig. 7-12, dashed lines in top right graph). Non-post consolidated but in situ processed specimens show no such error.
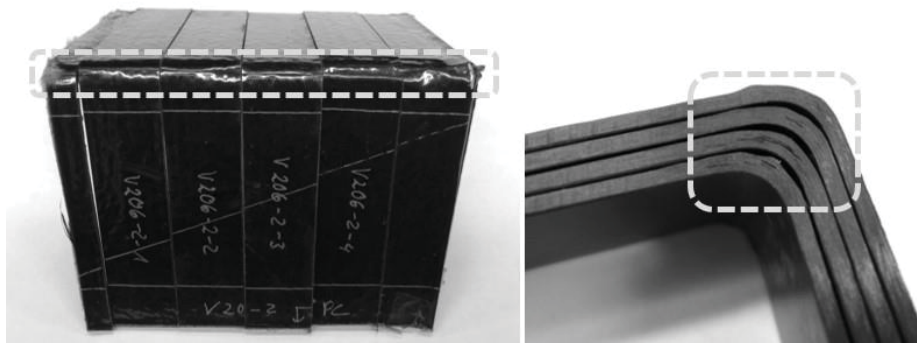
Fig. 7-11: **Four-point-bending specimen with compaction error during post consolidation**
The left image shows the wrinkle due to vacuum bagging.
The lack of consolidation pressure under the wrinkle caused delamination during post consolidation.

The inner radius of all specimens is 6.5 mm instead of 0.25 inch (6.35 mm) according to the standard. Each specimen consists of 18 layers of CF/PA6 tape. Two sets of each four specimens are manufactured for each tool and processing strategy. After lay-up the laminate was trimmed and the specimens are cut by a precision water-cooled diamond coated circular saw. Before testing, the specimens are dried in a vacuum oven for 48 h at 60 °C and the width and thickness are measured at multiple sections.

Results

Fig. 7-12 shows the force – displacement curves of the universal testing machine of 90° specimens, manufactured with different processing strategies. Within one placement strategy, the curves show similar failure behavior, indicating stable processing

and testing. Only the post consolidated specimens with wrinkles deviate from the rest of their set, as expected. All samples show similar stiffness during testing, but fail at different force levels. Specimens produced by standard CLC already fail at low force levels. PCLC and CCPP specimens reach about 50 % of the delamination force of post consolidated laminates.

The standard CLC, PCLC and CCPP produced specimens show a ductile delamination behavior, with stable or even increasing force after initial delamination. The force drops strongly for the post consolidated samples at delamination, but also reaches higher values. The force – displacement curves of the 105° and 120° specimens are listed in Appendix h.
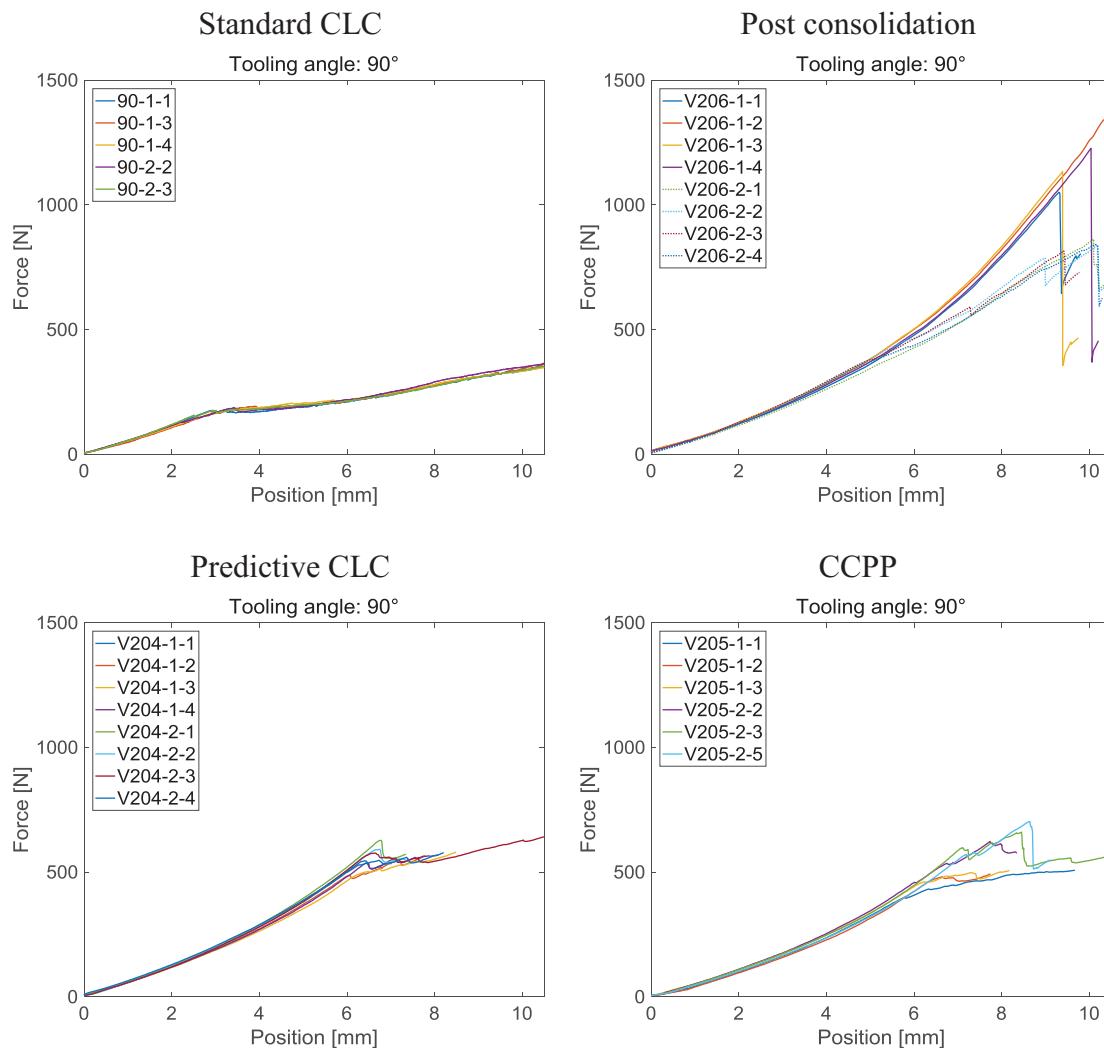
Fig. 7-12: **Four-point-bending test curves of 90° specimens manufactured with different processing strategies**

From the test curves, the radial tensile strength is calculated for each specimen. The mean value and standard deviation for each set of specimens are shown in Fig. 7-13. The standard closed loop control produces the lowest radial tensile strength for all three geometries. With increasing tool angle, the tensile strength increases a little, but

remains low. PCLC and CCPP produced specimens do not show such a clear trend but reach similar high levels for all geometries. The radial tensile strength is between 150 % and 220 % of the standard CLC produced specimens. Even higher values are determined for post consolidated specimens. Their tensile strength is between 230 % and 400 % higher than for standard CLC specimens. The higher standard deviation of the post consolidated samples is attributed to the vacuum bagging and the more brittle delamination behavior.
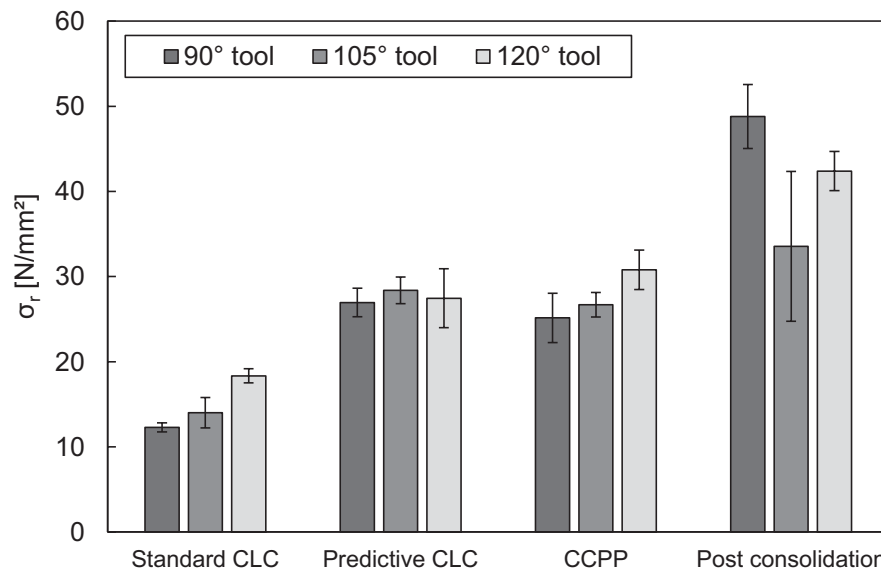
Fig. 7-13: **Mean radial tensile strength of 3D specimens, manufactured with different lay-up strategies**
The error bars indicate standard deviations.

Discussion

The four-point-bending test according to ASTM D6415 shows consistent test curves for each processing strategy. Delamination occurs in the corner area of the specimens around midplane, as intended by the standard. In contrast to wedge peel testing, the corner area of the laminate is tested directly.

The standard closed loop control produces rather low radial tensile strength, due to overheating in the corner area. Both developed 3D strategies, PCLC and CCPP produce specimens with equal high radial tensile strength, which is between 150 % and 220 % of the standard CLC. Specimens of both strategies also show a ductile behavior after delamination. In contrast to that, the force drops strongly for the post consolidated specimens. Their radial tensile strength is far higher than for any other specimen produced with in situ consolidation. Both effects can be explained by the higher crystallinity of the PA6 matrix due to the post consolidation in the oven.

Both 3D in situ strategies strongly improve the delamination strength in the four-point-bending test. As no overheating occurs, the bond between the layers can be

developed stronger in the corner area. A difference between the two strategies is not measurable by the test.

7.2.5 Conclusion

3D lay-up trials in chapter 5 show that poor bonding quality in the corner section due is to overheating, followed by insufficient heating. The simulative analysis of the 3D laser assisted TP-AFP process in chapter 6 also shows how the overheating occurs. The adaption of the laser boundary condition, both laser power and laser distribution, is identified as a possible solution for the problem.

Two strategies are presented to produce 3D laminates with consistent laminate quality by in situ consolidation. Laminates from both strategies, PCLC and CCPP, are compared to laminates produced by standard CLC and constant laser power or post consolidation. The temperature log file data during processing are analyzed. Both strategies reliably produce consistent laminates. The log files show stable processing for all tracks and layers. Both new 3D strategies are capable to prevent overheating at the corner section.

The PCLC works together with the existing standard CLC and reduces the laser power in the whole laser spot. It detects overheating of the substrate laminate, when the temperatures are still moderate and no thermal degradation occurs, yet. Thus, the bonding temperature at the nip-point area remains in the optimal process window. However, the temperature of the incoming tape is also reduced and will not be heated as much as intended. This is necessary, as no adjustment of the laser bias ratio is done. The PCLC strategy adds intelligence to the control PC of the machine and relieves the machine operator, as it adjusts the laser power online within an additional closed loop control.

The CCPP strategy allows the machine operator to control the process very precisely. In reference to the lay-up coordinates, the laser power and laser bias distribution between incoming tape and substrate laminate can be adjusted. Similar to the PCLC strategy, the nip-point temperature remains within the optimum process window. By additionally adjusting the laser bias ratio, the temperature drop of the incoming tape can be reduced. The operator has to define and store the set-point tables before lay-up of the actual laminate. They can be determined either by thermal simulation or experimentally.

Two mechanical tests evaluate the 3D processing strategies quantitatively.
The wedge peel test determines the bond strength and its transition from stable processing towards the thermal irregularities around the corner. Specimens produced by standard CLC and with constant laser power show characteristic zones that deviate from sections with nominal processing temperature. Both 3D strategies, PCLC and CCPP do not show such zones. This is attributed to the constant nip-point bonding temperature around and after the corner. The specimens show a high minimum wedge peel strength. CCPP produced specimens are superior to PCLC specimens as they

show higher minimum and mean values.

The four-point-bending test according to ASTM D6415 tests the corner section of the specimens. A clear improvement of the radial tensile strength can be seen by the two developed 3D strategies, PCLC and CCPP, compared to standard CLC lay-up. However, even higher values are achieved by post consolidation. It is assumed that the post consolidated samples feature a higher crystallinity that influences the delamination characteristics. All in situ manufactured samples show a much more ductile failure.

The lay-up trials with PCLC and CCPP strategy and their comparison to standard processing strategies, through temperature data analysis and mechanical testing, show the potential of the TP-AFP process on 3D geometries. Even though the corner radius is much smaller than the laser spot on the laminate, overheating can be successfully prevented. Furthermore, the bonding temperature remains within an acceptable tolerance, so consistent bonding strength can be developed during in situ consolidation.

7.3 Validation by demonstrator part manufacturing

In the previous sections 3D processing strategies are developed by using simple v-shaped tooling geometries. The heating principles and effects are described and strategies to reduce overheating are developed. Lay-up direction on the simple tools is always 90° with respect to the corner, as this is most challenging. As a first step to industrial use, a demonstrator with a representative geometry is manufactured. The processing strategies of the previous sections are applied and their effectiveness analyzed.

Geometry and programming

The geometry of the demonstrator represents on one side the front nose of a wing and a rectangular tube like structure or C-frame on its backside (Fig. 7-15). The front side features a 15 mm radius corner with a soft transition to a 185 mm radius. The main difficulty of this section is the small inner angle of the nose. Due to the sharp angle, even direct laser illumination may not hit the substrate laminate at all times or heat a very long length with low intensity. On the right side, the demonstrator's cross-section features two almost rectangular corners with 6.5 mm radius, similar to the v-shaped tool. However, the corners are very close to each other, so they may influence each other.

In order to achieve a smooth robot path with constant lay-up velocity, the robot programming principles from section 5.4.1 are applied. The robot is allowed to blend its trajectory but the programming points have to be shifted, so the corners are approached correctly. Fig. 7-14 shows the programming points (marker x) for the robot before it blends its path and the actual TCP curve (small dots) with respect to the actual tooling geometry.
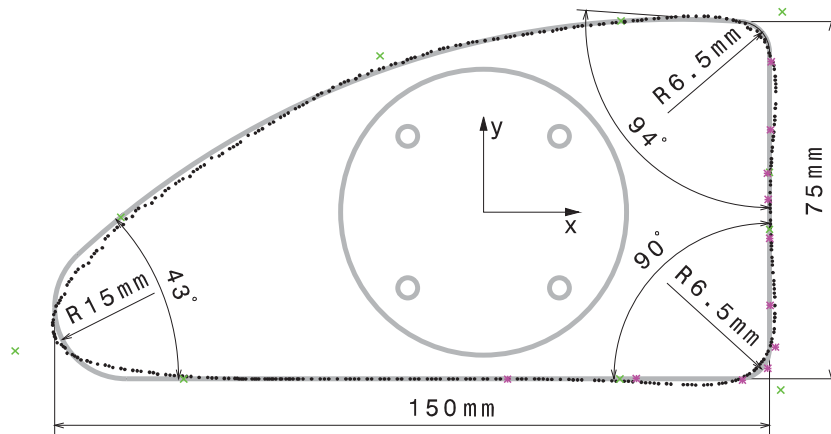
Fig. 7-14:   **Demonstrator cross-section geometry with convex corners**
                      The solid grey line represents the original cross-section of the tooling.
                      Crosses mark the programming points for the robot programming.
                      The small dots mark the TCP curve after robot program optimization.
                      The stars mark the CCPP set-points for the bottom right corner.

In contrast to the simple v-shaped tooling, a rotating tooling is used. The tooling is mounted in the winding axis of the TP-AFP system and rotates under the lay-up head. The rotating tool relieves the robot from most of it necessary motions. The robot compensates the varying distance to the center of rotation and defines the fiber orientation. Fig. 7-15 shows the lay-up on the demonstrator tooling by the TP-AFP machine using a winding axis for tool manipulation.

Fig. 7-15:   **Demonstrator manufacturing using a rotating axis**

Fig. 7-16 show the lay-up speed and the compaction roller's stroke during lay-up of a circumferential layer. Both parameters can be used as a criterion for accurate programming. Little deviations of the lay-up speed can be compensated by the laser's closed loop control, if used, and the compensator recovers the compactions roller's deviations.
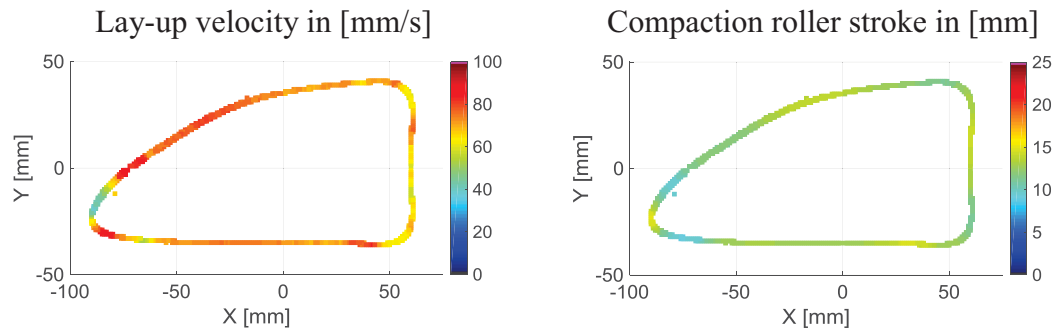
Fig. 7-16: Plot of TCP velocity (left) and compaction roller deflection (right)

Lay-up strategy

To represent a real life laminate, a quasi-isotropic lay-up is used for the demonstrator. This means, that besides circumferential layers, that approach the corners almost perpendicularly, also layers with +45° and -45° with respect to the tooling's longitudinal axis are manufactured. The 45° layers are more demanding for the compaction roller to adapt to the angular passage of the corner than for maintaining the temperature constant. The circumferential layer with +88° with respect to the corners proved to be the most challenging in terms of laminate heating and robot movement. Additionally longitudinal paths are laid up as well.

Both 3D lay-up strategies, PCLC and CCPP are tested during demonstrator manufacturing. The parameters are adapted from the lay-up trials in section 7.2. The CCPP set-points are transferred to the bottom right corner in Fig. 7-15 and are marked by stars.

Process temperatures

Fig. 7-17 shows the nip-point temperature of layer 14, with tapes in circumferential direction. For illustration three different lay-up strategies are used for this layer. The lay-up starts with constant laser power, which result is massive overheating at all corners. The middle section is laid up by standard closed loop control. Similar to the v-shaped tools, the laminate overheats for a short distance at the corner that is followed by a section with insufficient heating. In the third section the PCLC strategy achieves to maintain the nip-point temperature homogeneously at the desired value at all sections. Lay-up by CCPP shows also a very homogeneous nip-point temperature distribution.
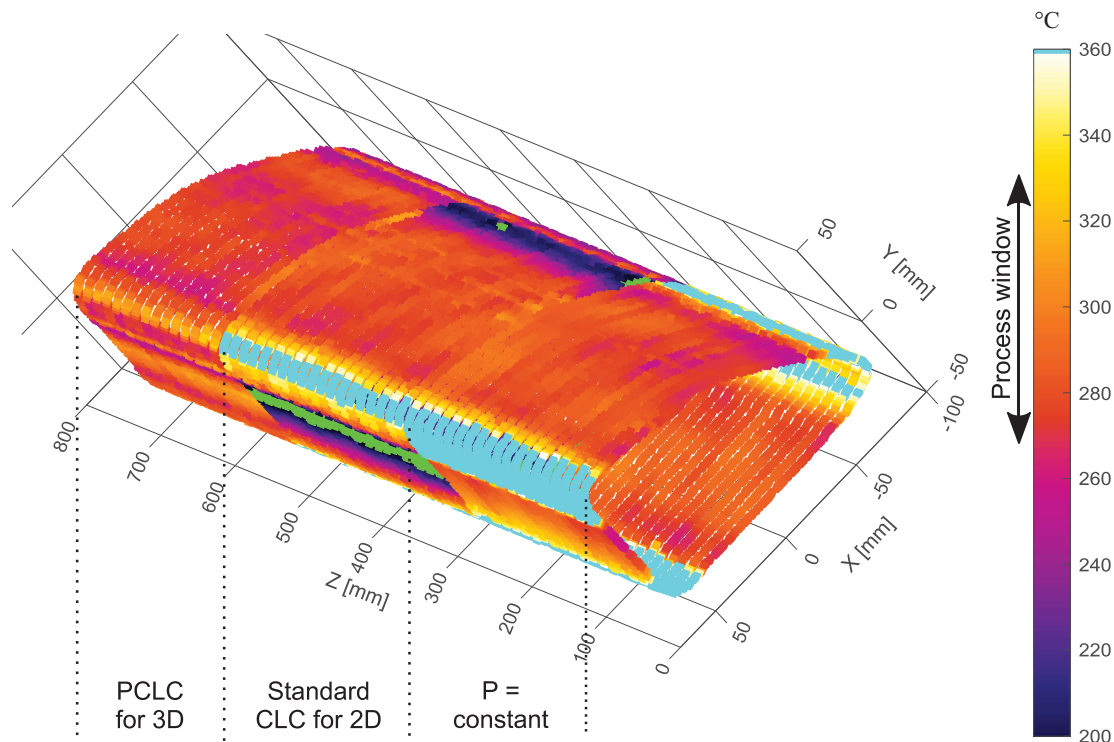
Fig. 7-17:   **Nip-point temperature during manufacturing of a circumferential layer of the demonstrator for three different processing strategies**
The 1st section shows lay-up with constant laser power.
Standard CLC is used in the 2nd section, causing overheating and insufficient heated areas.
The PCLC lay-up strategy shows homogeneous nip-point temperature in the 3rd section.

7.4 Conclusion

In chapter 5, lay-up strategies for flat lay-up are tested on 3D geometries. The standard closed loop control, as well as lay-up with constant laser power lead to overheating, causing polymer degradation and poor bond quality. Based on these result, the laser heating aspects are studied in chapter 6. Two goals are identified to achieve good bonding at all times during lay-up, despite the 3D geometry. The first goal is to maintain homogeneous temperature in the nip-point bonding area. The second aim is to also keep the temperature difference between incoming tape and substrate laminate as constant as possible.

In this chapter, two strategies for 3D TP-AFP lay-up are presented. The first processing strategy adds a predictive closed loop control (PCLC) to the machine's controller. It analyzes the surface temperature, assigned to the substrate laminate. Overheating starts in this area and can be detected before degradation starts. The PCLC reduces the laser power to avoid additional excessive heat input that will lead to overheating. By the same principle it also detects insufficient heating in the substrate laminate's area and can increase the required laser power. The second strategy (CCPP) uses set-point table that defines the process parameters for each section of the lay-up geometry. It has to be prepared by the machine operator, e.g. by simulation of

the process beforehand. Besides laser power, also the laser bias between incoming tape and substrate laminate can be adjusted. In contrast to the electronically controlled laser power, a motor, tilting the laser optics, adjusts the laser bias. This is linked with a limited adjustment speed and causes a delay.

For both lay-up strategies lay-up trials are preformed and specimens for wedge peel and four-point-bending testing are manufactured. The resulting process temperatures are analyzed and the specimens are compared to specimens produced with standard closed loop control and lay-up with constant laser power or post consolidated samples. Both new strategies, PCLC and CCPP, are capable to maintain the nip-point temperature constant during 3D lay-up. The PCLC adjust the laser power in the whole laser spot, without changing the laser bias. This successfully prevents overheating and but also reduces the heating of the incoming tape, causing a lower temperature. The CCPP strategy adjusts the laser power and laser bias according to the set-point table. By this, the temperature difference between incoming tape and substrate laminate can be minimized. The mechanical tests support the observations from the temperature analysis. Both new 3D strategies produce wedge peel specimens with homogeneous peel strength without any sectional drops. The four-point-bending strength is on the same level and highly increased by both strategies. Only the post consolidated specimens reach significantly higher values. Their brittle failure indicate a different crystallinity of the PA6 matrix that could promote the higher strength.

Finally, the applicability of both strategies is verified by the manufacture of a demonstrator. A rotating tool with two ~90° and one ~45° corner, representing the front nose of a wing and C-spar is chosen. The same processing temperatures are measured during demonstrator manufacturing, as for the test laminates.

Both strategies proved their great potential for laser assisted TP-AFP lay-up of 3D parts with fixed focus laser optics and homogeneous energy density. The tested corners are very small compared to the laser spot size and the angle between the specimen's legs was up to 90°. By optimizing the adjustment of the laser bias and further improvements of the thermal predictions, the limits of the process are still to determine.

8 Conclusion

The main objective of this work is to investigate the heating characteristics during laser assisted Thermoplastic-Automated Fiber Placement (TP-AFP) on flat and three-dimensionally curved parts. Laser heating systems are widely used for TP-AFP, as they provide the highest energy density for material heating. The highly concentrated heating inside the laser spot makes the laser spot size as well as the time of the composite material inside the heating zone decisive for processing. Additionally, the laser energy absorption depends on the laser's angle of attack. All these aspects, together with the thermal properties of the composite material, are taken into account to analyze the process for 3D lay-up.

In the following sections, the main conclusions of the investigations are summarized. Based on the steady-state process of flat laminates, the heating effects on a 3D geometry are described by experiment, simulation and mechanical testing. Finally, two strategies for 3D processing with in situ consolidation are developed and validated.

8.1 CFRTP tape material properties

In chapter 3, the optical and thermal properties of two tape materials, CF/PES and CF/PA6, are investigated. Several conclusions are drawn:

- The material data are the basis input data for the thermal simulation of the process in chapter 4 and 6. Due to the high temperature range of the process, temperature dependent material properties for heat conductance have to be used. Those are not available in literature for the CF/PES and CF/PA6 material. Temperature dependent material data sets for both types of carbon fiber tapes are investigated in this thesis.

- The angle dependent absorption behavior of both materials is described by spectrophotometer measurements. A constant high absorptivity is measured for an angle of attack below 60° and a strong decrease for higher angles. Both materials exhibit a very similar absorption behavior, also compared to CF/PEEK material from literature [8]. Besides specific heat, heat conductivities in fiber direction and in transverse direction are determined. Both tapes show a strong anisotropic nature in terms of heat conductivity due to the carbon fibers. In-fiber direction, heat conductivity is about ten times higher than in transverse direction.

- The experimental determination of temperature dependent thermal material properties is very time consuming and needs to be done for every fiber-matrix

combination and fiber volume fraction again. Thus, a comparison of experimentally determined properties and properties calculated by models from literature is presented. Specific heat and longitudinal heat conductivity can be described by a rule of mixture model with satisfying accuracy. The models only need the properties of the matrix and fiber as well as the fiber volume fraction, which are available in literature. Furthermore, it is shown that the tape's laser absorptivity can be calculated by Fresnel's equations. This reduces the experimental effort even more. Different models are compared with experimental data for the tape's transverse heat conductivity. A disagreement of up to 35 % was found for CF/PES tape material. For exact modelling it is recommended to determine the transverse heat conductivity by experiments.

- Typically, the thermal properties are determined from unprocessed single layer tape material. During processing, the material is exposed to high temperature and compaction pressure. This can change the tape's constitution, by matrix squeeze out and transverse expansion. The single layer tape's properties of CF/PES are compared to seven-layer samples produced by in situ consolidation and to samples with additional post consolidation. An increase of transverse heat conductivity is measured for the in situ processed seven-layer laminate and even higher values are determined for the post consolidated seven-layer laminates. This increase of transverse heat conductivity is explained by the decrease of layer thickness during the processing steps.

- In literature, the existence and influence of an interply thermal contact resistance is discussed. In this thesis, the interply contact resistance is determined for CF/PES by comparing the overall thermal conductivity of the seven-layer specimens produced by in situ consolidation and specimens with additional post consolidation. It is used to evaluate the quality of the in situ consolidation. A vanishingly low thermal contact resistance indicates good bonding with no voids in the interface between the layers. The measured thermal contact resistance is compared to a contact model from literature [102]. Equivalent low thermal contact values are determined by experiment and by the literature model with a full intimate contact of 100 %. It is followed that when the laser assisted TP-AFP process is performed under optimized conditions, full in situ consolidation, equivalent to an autoclave consolidation is possible. Micrographs and thermal simulations, with thermal contact resistance and with perfect thermal contact, confirm this.

- Finally, the effect of repeated heating during lay-up of additional layers on top is analyzed in more detail for both tape materials. The individual single layer thickness is determined by micrographs for specimens from one to seven layers. In addition, the overall thermal conductivity evolution is studied for these specimens. No clear trend can be derived from the measurements. This indicates constant bond quality and constant material properties, even after repeated heating during lay-up of the next layers.

8.2 Thermal process simulation for flat laminates

A two-dimensional thermal simulation is developed to describe the laser assisted TP-AFP process. In a first step, the simulation is used to analyze the lay-up of flat laminates, since the boundary conditions do not change during lay-up. As the incoming tape and substrate laminate pass through the laser spot and compaction under the roller, flat lay-up can be regarded as steady-state process. The temperature dependent material data from chapter 3 are used to describe the composite's behavior. Besides the composite tape, also the mold and compaction roller are modeled. Suitable starting and boundary conditions to ambience are implemented parametrically.

In a first step, the simulation calculates the laser input at the wedge, formed by the incoming tape and the substrate laminate. Energy input from direct laser illumination and by first order reflection from the opposite joining partner are taken into account, according to the tape's absorptivity and reflectivity. Despite the homogenizing laser optics, that produce a rather top hat like laser beam intensity, a more complex energy input is identified due to the projected shape of the laser spot in the wedge before the nip-point. About 22 % of the absorbed laser energy has been reflected before from the other joining partner. A homogeneous energy input is often used in literature. It is shown that correct modeling of the reflection behavior is necessary to achieve correct temperature predictions.

The simulation is validated for both tape materials by fine wire thermocouple measurements of test lay-ups. Experimentally measured and simulated temperature curves of the composite are in very good agreement for heating and cooling. The simulation over predicts the maximum temperature for CF/PES by 1.8 °C and for CF/PA6 by 18 °C compared to the experimental thermocouple measurements.

Simulations with modeled, measured and without interlayer thermal contact resistance show its influence. The simulations with the very low measured thermal contact resistance and with perfect thermal contact result in an almost identical temperature profile within the laminate. The thermal contact resistance model from literature results in higher temperatures in the top layers, as heat cannot penetrate into the laminate as easily. The model from literature overestimated the thermal contact resistance for laminates with good in situ quality. Better results are achieved by neglecting it or by using the much smaller measured thermal contact resistance. The simulation predicts almost congruent temperature profiles for composite properties derived from the literature models and from measurements. It is concluded, that both modeled and measured composite properties can be used for correct simulation results.

Parameter studies demonstrate the potential use of the thermal simulation. Variations of material properties as well as a change of process conditions and their complex interactions can be analyzed.

8.3 Laser heating characteristics of 3D parts

Chapter 5 starts with a literature analysis on 3D TP-AFP lay-up. Published research mostly concentrates on laminate optimization of flat lay-up. A clear gap is identified for lay-up of three-dimensional parts with convex corners featuring a small corner radius, like aerospace C-spars. V-shaped test geometries with a 6.5 mm radius and 90° to 120° angle between the leg laminates are defined for the research. Lay-up trials, with standard parameters, derived from flat lay-up identified the challenges during processing on the 3D geometry. Strong overheating of the substrate laminate around the corner leads to polymer degradation and bad bonding of the layers. This ultimately can lead to laminate failure. Suboptimal robot programming leads to unsteady lay-up velocity and to a shift of laser spot alignment with respect to the composite. Optimized robot programming and a tape laying head hardware update with a compensator linking laser optics and compaction roller solve both aspects. The compaction behavior of the conformable compaction roller is studied experimentally via a pressure sensitive film. The small corner radius of the investigated geometry leads to a strong increase of compaction pressure and a reduction of compaction length. However, in contrast to the process temperature it is identified as non critical. The direct heating length of the laser on the substrate laminate is analyzed geometrically. A reduction down below 50 % of its initial length is determined for the 90° tool. In practical terms this means, that the local laser energy input density is doubled in the area around the corner. This change of laser energy input is identified as the main reason for overheating. The resulting thermal degradation of the matrix polymer is investigated for flat specimens manufactured with the same processing temperature range as it occurs during the 3D lay-up trials. Mechanical wedge peel tests, DSC and DMA measurements show signs for polymer degradation for processing temperature above 320 °C.

The thermal simulation is adapted to analyze the lay-up of 3D geometries in chapter 6. Special attention is given to correct modelling of the tape laying head's and the laser spot's kinematics to calculate the laser boundary condition according to the geometry's curvature. The simulation is validated via IR camera measurements during lay-up trials and shows correct predictions of the overheating due to the corner of the lay-up geometry. In the following, the laser heating effects are analyzed with the help of the simulation. The heated length, heating time and energy input of direct and reflected laser irradiation on the substrate laminate and incoming tape are discussed. Little difference is determined for different tool angles for the direct laser energy input, which is the dominating laser boundary condition. Due to the geometry the reflected laser beam from the incoming tape does not always hit the substrate laminate. Instead, the laser is reflected to ambience at some lay-up positions and lost for the heating process. As a result, the reflected laser energy input changes for different tool angles. This depends on the tooling's leg angle. The thermal simulation of 3D lay-up provides the insights to understand the heating characteristics of the laser beam at the corner area. A process parameter study is presented to describe the effects of the 3D lay-up

geometry and of the laser boundary condition of the process temperature during non-steady-state 3D lay-up. The laser spot size and tape laying head angle are identified to have a major impact on the overheating around the corner. Longer laser spots result in less overheating at the arc. However, this is in contrast to the optimal process conditions for excellent bonding during 2D steady-state lay-up. Typically a larger laser spot leads to softer heating of the composite and to higher bond strength. It is concluded that 3D processing cannot be done by one set of parameters that is kept constant at all sections of the lay-up path.

A process parameter set for 3D lay-up with homogeneous processing temperature is developed. The process parameters for laser power and laser optics orientation need to be adjusted during 3D lay-up to maintain the bonding temperature within the experimentally determined limits. This set of lay-up position dependent process parameters are tested via experimental lay-up trials in chapter 7.

8.4 3D TP-AFP lay-up strategies for in situ consolidation

The processing strategies for flat laminates are proven to be insufficient for 3D lay-up. Therefore, two new strategies are developed together with the machine manufacturer. One approach complements the already existing closed loop control for laser power by an additional "Predictive Closed Loop Control (PCLC)" that can detect overheating in the substrate laminate's area before its temperature rises to critical levels. The other strategy, called "Coordinate Controlled Process Parameters (CCPP)", allows to locally influence the process parameters by a set-point table. Its biggest advantage is, that besides overall laser power, also the laser bias between the very thin incoming tape and the thicker substrate laminate can be adjusted. This way not only homogeneous temperature in the nip-point area, but also in the tape and laminate area before the nip-point can be achieved. From experience of flat laminates, this promotes good bonding. The process parameters during lay-up need to be known and put in the set-point table before lay-up. This can be done either by lay-up trials or by a thermal simulation, as developed in chapter 6.

Test laminates are manufactured with both lay-up strategies and their temperature profiles are analyzed and compared to lay-up with the standard closed loop control for flat laminates and lay-up with constant laser power. Both new strategies proved to be capable of avoiding overheating at all times during 3D lay-up. As a side effect, the PCLC strategy causes a too cold temperature of the incoming tape. By adjusting the laser bias between incoming tape and substrate laminate together with adjusting the overall laser power, a more constant temperature profile is achieved by CCPP processing.

The laminates are tested by wedge peel test and by four-point-bending test. In contrast to the laminates without processing parameters for 3D lay-up, the specimens show a

homogeneous peel force all over the area of interest after the corner. Also, the radial tensile strength, determined by four-point-bending, reaches a significant higher level, compared to specimens produced by standard closed loop control. However, they also remain lower than for post consolidated samples. Post consolidated samples feature a different molecular structure of the matrix polymer with higher crystallinity due to the lower cooling rates. This results in higher radial tensile strength, but also a more brittle behavior. In situ consolidated samples with lower crystallinity show a more ductile failure and reach higher wedge peel strengths. The optimum polymer structure has to be defined and is not part of this work.

Both strategies prove to be able to manufacture three-dimensional parts with consistent laminate quality. As a next step, a demonstrator is manufactured to show the capabilities of the TP-AFP process with a large laser spot. The demonstrator features two almost 90° corners with a small radius and an even sharper corner angle but with a larger corner radius. The demonstrator's cross-section resembles the front nose of a wing and a C-spar on its backside. Quasi-isotropic laminate is successfully laid up without overheating of the composite. Both developed strategies prove to be valuable for 3D processing, especially when aiming for in situ consolidation, and deserve a chance to be continued∎

References

[1] D. H.-J.A. Lukaszewicz, C. Ward, and K. D. Potter, "The engineering aspects of automated prepreg layup: History, present and future", *Composites Part B: Engineering*, vol. 43, no. 3, pp. 997–1009, 2012.

[2] L. Hoffjann, P. Kölzer, and C. Kok, "Andruckrolle zum Ablegen von bahnförmigem Halbzeug, Patent: DE102012108487A1", Germany.

[3] P. L. Mischler, M. C. Tingley, and K. Hoffmann, "Compaction Roller for a fiber placement machine, Patent: US 7,810,539 B2", USA 11/467,379.

[4] R. Lichtinger, *Thermo-Mechanical Coupled Simulation of the Thermoset Automated Fibre Placement Process*. München: Verlag Dr. Hut, 2016.

[5] R. Lichtinger, J. Lacalle, R. Hinterhölzl, U. Beier, and K. Drechsler, "Simulation and experimental validation of gaps and bridging in the automated fiber placement process", *Science and Engineering of Composite Materials*, vol. 22, no. 2, 2015.

[6] T.S. Angell and T. Rudberg, Eds, *Manufacture of Substructure by Automated Fiber Placement*, Okt. 2013.

[7] B.J. Jensen, M.C. Kinney, R.J. Cano, and B.W. Grimsley, Eds, *Materials for Heated Head Automated Thermoplastic Tape Placement*, Mai. 2012.

[8] C. M. Stokes-Griffin, "A Combined Optical-Thermal Model for Laser-Assisted Fibre Placement of Thermoplastic Composite Materials"

[9] R. vor dem Esche, *Herstellung langfaserverstärkter Thermoplastbauteile unter Zuhilfenahme von Hochleistungslasern als Wärmequelle*. Aachen: Shaker, 2001.

[10] F. Henne, S. Ehard, A. Kollmannsberger, B. Hoeck, M. Sause, G. Obermeier, and K. Drechsler, Eds, *Thermoplastic in situ fiber placement for future solid rocket motor casings manufacturing*, 2014.

[11] Coriolis Composites SAS, *Fiber Placement Head - Specifications.* Available: https://www.coriolis-composites.com/products/fiber-placement-process.html (April 18th 2018).

[12] K. Drechsler and T. Wettemann, "From thermoplastic composite winding to an additive manufacturing process" Paris, March 8th 2016.

[13] Fives Group, *Cincinnati Gemini.* Available: http://dk8mx37zdr9bp.cloudfront.net/metal-cutting-composites/Cincinnati%20Composites/Cincinnati%20Comp%20Photos/GEMINI/Composites%20Group-GEMINI1_4878%20LoRes%20web.jpg (March 12th 2018).

[14]   MTorres group, *torresfiber-layup_automatic_fiber%20_placement_MTorres_12.jpg.* Available: http://www.mtorres.es/sites/default/files/productos/torresfiberlayup_automatic_fiber%20_placement_MTorres_12.jpg (March 12th 2018).

[15]   Electroimpact Inc, *AFP Head on Robot.* Available: https://www.electroimpact.com/Products/Composites/images/AFP_RobotHead.jpg (March 12th 2018).

[16]   Automated Dynamics Inc, *Composite Manufacturing Equipment.* Available: http://www.automateddynamics.com/wp-content/uploads/2016/09/ADC-Composite-Manufacturing-Equipment.pdf (March 12th 2018).

[17]   CC-BY 3.0 (DLR), *GroFi-Gesamtanlage.* Available: http://www.dlr.de/zlp/de/Portaldata/17/Resources/images/zlp/GroFi2.jpg (March 12th 2018).

[18]   R. Lichtinger, P. Hörmann, D. Stelzl, and R. Hinterhölzl, "The effects of heat input on adjacent paths during Automated Fibre Placement", *Composites Part A: Applied Science and Manufacturing*, vol. 68, pp. 387–397, 2015.

[19]   P. Hörmann, D. Stelzl, R. Lichtinger, S. van Nieuwenhove, G. Mazón Carro, and K. Drechsler, "On the numerical prediction of radiative heat transfer for thermoset automated fiber placement", *Composites Part A: Applied Science and Manufacturing*, vol. 67, pp. 282–288, 2014.

[20]   R. Calawa and J. Nancarrow, Eds, *Medium Wave Infrared Heater for High-Speed Fiber Placement*: SAE International 400 Commonwealth Drive, Warrendale, PA, United States, 2007.

[21]   C. M. Stokes-Griffin and P. Compston, "The effect of processing temperature and placement rate on the short beam strength of carbon fibre–PEEK manufactured using a laser tape placement process", *Composites Part A: Applied Science and Manufacturing*, vol. 78, pp. 274–283, 2015.

[22]   M. Di Francesco, L. Veldenz, G. Dell'Anno, and K. Potter, "Heater power control for multi-material, variable speed Automated Fibre Placement", *Composites Part A: Applied Science and Manufacturing*, vol. 101, pp. 408–421, 2017.

[23]   A. Yousefpour and M. N. Ghasemi Nejhad, "Experimental and Computational Study of APC-2/AS4 Thermoplastic Composite C-Rings", *Journal of Thermoplastic Composite Materials*, vol. 14, no. 2, pp. 129–145, http://journals.sagepub.com/doi/abs/10.1106/1RQV-317Q-36K0-1E6P, 2016.

[24]   D. L. James and W. Z. Black, "Thermal Analysis of Continuous Filament-Wound Composites", *Journal of Thermoplastic Composite Materials*, vol. 9, no. 1, pp. 54–75, 2016.

[25]   R. Schledjewski, Ed, *Mechanical performance of in-situ consolidated thermo-plastic fiber reinforced tape materials*, 2004.

[26]   C. Ehlers, *Beitrag zur Qualitatssicherung bei der Verarbeitung kontinuierlich faserverstarkter Thermoplaste*. Dusseldorf: VDI Verlag, 1998.

[27]   P. Kölzer, *Temperaturerfassungssystem und Prozessregelung des laserunter-stützten Wickelns und Tapelegens von endlos faserverstärkten thermoplasti-schen Verbundkunststoffen*. Aachen: Shaker, 2008.

[28]   Z. Qureshi, T. Swait, R. Scaife, and H. M. El-Dessouky, "In situ consolidation of thermoplastic prepreg tape using automated tape placement technology: Po-tential and possibilities", *Composites Part B: Engineering*, vol. 66, pp. 255–267, 2014.

[29]   R. Funck and M. Neitzel, "Improved thermoplastic tape winding using laser or direct-flame heating", *Composites Manufacturing*, vol. 6, no. 3-4, pp. 189–192, 1995.

[30]   M. Neitzel, P. Mitschang, and U. Breuer, *Handbuch Verbundwerkstoffe*: CARL HANSER VERLAG GMBH &, 2014.

[31]   D. Hauber and R. Marcario, "Additive manufacturing of high-performance composite structures", *JEC Magazine #119*, vol. 2018, no. 119, pp. 29–31, 2018.

[32]   R. Schledjewski and A. Miaris, Eds, *Thermoplastic Tape Placement by Means of Diode Laser Heating*: Society for the Advancement of Material and Process Engineering, 2009.

[33]   J. Stimpfl, *CO2-laserunterstütztes Tapelege-/ Wickelverfahren zur Verarbei-tung von ungefärbten, endlos glasfaserverstärkten Thermoplast-Tapes,* 1st ed. Aachen: Apprimus Verlag, 2014.

[34]   F. Bachmann, "Hochleistungs-Diodenlaser für die Materialbearbeitung: Dio-denlaser mit bis zu 6 kW Leistung eignen sich zum Schweißen und Härten", *Physikalische Blätter*, vol. 57, no. 3, pp. 63–67, http://onlinelibrary.wiley.com/doi/10.1002/phbl.20010570314/epdf, 2001.

[35]   Laserline GmbH, *Laserline LDF Die Referenzklasse für Diodenlaser*. Available: https://www.laserline.de/fileadmin/Dokumente/Broschueren_DE/Laserline_L DF_Die_Referenzklasse_fuer_Diodenlaser.pdf (March 21th 2018).

[36]   A. Kollmannsberger, R. Lichtinger, F. Hohenester, C. Ebel, and K. Drechsler, "Numerical analysis of the temperature profile during the laser-assisted auto-mated fiber placement of CFRP tapes with thermoplastic matrix", *Journal of Thermoplastic Composite Materials*, vol. 2, 2017.

[37]   T. Orth, C. Weimer, M. Krahl, and N. Modler, "A review of radiative heating in automated layup and its modelling", *Journal of Plastics Technology*, no. 02, 2017.

[38]   R. Funck, *Entwicklung innovativer Fertigungstechniken zur Verarbeitung kontinuierlich faserverstärkter Thermoplaste im Wickelverfahren*. Düsseldorf: VDI-Verl, 1996.

[39]   Research Inc, *Model 5194 User's Manual: A106687-001 Rev. 1.* Available: http://www.pcscontrols.com/sites/default/files/LineIR%20Model5194%20User%20Manual.pdf (March 20th, 2018).

[40]   P. A. Zaffiro, "Control of radiant heating system for thermoplastic composite tape", USA 739,782, January 5th, 1993

[41]   P. Schaefer, *Consolidation of carbon fiber reinforced Polyamide 6 tapes using laser-assisted tape placement*. München: Verlag Dr. Hut.

[42]   C. Werdermann, K. Friedrich, M. Cirino, and R. Byron Pipes, "Design and Fabrication of an On-Line Consolidation Facility for Thermoplastic Composites", *Journal of Thermoplastic Composite Materials*, vol. 2, no. 4, pp. 293–306, 2016.

[43]   C. M. Stokes-Griffin and P. Compston, "A combined optical-thermal model for near-infrared laser heating of thermoplastic composites in an automated tape placement process", *Composites Part A: Applied Science and Manufacturing*, vol. 75, pp. 104–115, 2015.

[44]   A. Barasinski, A. Leygue, E. Soccard, and P. Arnaud, Eds, *An Improvement in Thermal Modelling of Automated Tape Placement Process*: AIP, 2011.

[45]   J. W. van Ingen, "Thermoplastic orthogrid fuselage shell", *Sampe Journal*, vol. 2016, no. 52(5), pp. 7–15, https://www.researchgate.net/publication/307926694_Thermoplastic_Orthogrid_Fuselage_Shell, 2016.

[46]   A. Offringa and J. Oosterhof, "Continuous Ultrasonic Tacking and Real-Time Verification; Breakthrough in Effective Tape Laying and Fiber Placement", *Sampe Journal*, vol. 2018, no. Volume 54, No 01, pp. 18–25, 2018.

[47]   D. Williams, "A new light on composites heating", *JEC Magazine #111*, vol. 2017, no. 111, pp. 46–48, 2017.

[48]   Heraeus Noblelight Limited, *Intelligent heat for Automated Fibre Placement: humm3 Technology.* Available: https://www.heraeus.com/media/media/hng/doc_hng/products_and_solutions_1/arc_and_flash_lamps_1/humm3.pdf (March 20th 2018).

[49]   T. Weiler, M. Emonts, P. Striet, S. Gronenborn, and H. Janssen, Eds, *Optical modelling of VCSEL-assisted thermoplastic tape placement: 17th European Conference on Composite Materials, Munich, Germany, 26 - 30th June 2016*, 2016.

[50]   C. Kukla, T. Peters, H. Janssen, and C. Brecher, "Joining of Thermoplastic Tapes with Metal Alloys Utilizing Novel Laser Sources and Enhanced Process Control in a Tape Placement Process", *Procedia CIRP*, vol. 66, pp. 85–90, 2017.

[51]   H. Moench, R. Conrads, S. Gronenborn, X. Gu, M. Miller, P. Pekarski, J. Pollmann-Retsch, A. Pruijmboom, and U. Weichmann, "Integrated high power VCSEL systems" in *High-Power Diode Laser Technology and Applications XIV*, 10.1117/12.2210909.

[52]   A. Pruijmboom, R. Apetz, R. Conrads, C. Deppe, G. Derra, S. Gronenborn, J. Sophie Kolb, H. Moench, F. Ogiewa, P. Pekarski, J. Pollmann-Retsch, U. Weichmann, X. Gu, and M. Miller, "Vertical-cavity surface emitting laser-diodes arrays expanding the range of high-power laser systems and applications", *Journal of Laser Applications*, vol. 28, no. 3, p. 32005, 2016.

[53]   T. Weiler, M. Emonts, and H. Janssen, Eds, *On the Use of Flexible Intensity Distributions for Thermoplastic Tape Placement by Means of Vertical-Cavity Surface-Emitting Laser (VCSEL)*. Bremen, Germany: WFB Wirtschaftsförderung Bremen GmbH, 2016.

[54]   DLR-ZLP, *ZLP Zentrum für Leichtbau - Flyer.* Available: http://www.dlr.de/zlp/Portaldata/17/Resources/dokumente/publikationen/infob roschueren/2015/ZLP_flyer_deutsch_low.pdf (March 12th 2018).

[55]   S. Ehard, A. Mader, E. Ladstätter, and K. Drechsler, Eds, *Thermoplastic automated fiber placement for manufacturing of metal-composite hybrid parts*, 2016.

[56]   J. Mondo, S. Wijskamp, and R. Lenferink, Eds, *Overview of thermoplastic composite ATL and AFP technologies*, 2012.

[57]   M.B. Gruber, I.Z. Lockwood, T.L. Dolan, S.B. Funck, J.J. Tierney, P. Simacek, J.W. Gillespie, Jr, S.G. Advani, B.J. Jensen, R.J. Cano, and B.W. Grimsley, Eds, *Thermoplastic in situ placement requires better impregnated tapes and tows*, 2012.

[58]   M.A. Lamontia, M.B. Gruber, J. Tierney, J.W. Gillespie, B.J. Jensen, and R.J. Cano, Eds, *Modeling the Accudyne Thermoplastic In Situ ATP Process*, 2009.

[59]   M.A. Lamontia, M.B. Gruber, J. Tierney, J.W. Gillespie, B.J. Jensen, and R.J. Cano, Eds, *In Situ Thermoplastic ATP Needs Flat Tapes and Tows with Few Voids*, 2009.

[60]   A. Comer, Dipa Ray, P. Hammond, D. Jones, J. Lyons, M. McCarthy, W. Obande, and R. O ' Higgins, Eds, *WEDGE PEEL INTERLAMINAR TOUGH-NESS OF CARBON- FIBRE/PEEK THERMOPLASTIC LAMINATES MANU-FACTURED BY LASER-ASSISTED AUTOMATED-TAPE-PLACEMENT (LATP)*, 2014.

[61]   V. Radlmaier, G. Obermeier, S. Ehard, A. Kollmannsberger, H. Koerber, and E. Ladstätter, Eds, *Interlaminar Fracture Toughness of Carbon Fiber Rein-forced Thermoplastic In-situ Joints*, 2015.

[62]   C. Brecher, A. Kermer-Meyer, M. Steyer, M. Dubratz, and M. Emonts, "La-ser-assisted thermoplastic tape laying", *JEC Magazine #56,* http://www.jeccomposites.com/knowledge/international-composites-news/laser-assisted-thermoplastic-tape-laying, Apr. 2010.

[63]   A. J. Comer, D. Ray, W. O. Obande, D. Jones, J. Lyons, I. Rosca, R. M. O' Higgins, and M. A. McCarthy, "Mechanical characterisation of carbon fibre–PEEK manufactured by laser-assisted automated-tape-placement and auto-clave", *Composites Part A: Applied Science and Manufacturing*, vol. 69, pp. 10–20, 2015.

[64]   M. Di Francesco, M.A. Valverde, C. Ward, P.F. Giddings, G. Dell'Anno, and K. Potter, Eds, *Influence of layup speed on the quality of thermoplastic pre-forms manufactured by laser-assisted Automated Fiber Placement: 17th Eu-ropean Conference on Composite Materials, Munich, Germany, 26 - 30th June 2016*, 2016.

[65]   Automated Dynamics Inc, *Laser Heating System Introduced at University Of Sheffield.* Available: http://www.automateddynamics.com/2016/company-news/automated-dynamics-brings-laser-heating-system-to-university-of-sheffield (March 12th 2018).

[66]   A. Bush, *Laser Heating System Introduced at LIFT.* Available: http://www.automateddynamics.com/2015/company-news/automated-dynamics-brings-laser-heating-system-to-lift (March 12th 2018).

[67]   M. LeGault, "Building a better tail boom", *High Performance Composites*, vol. 2013, no. Vol. 21, No. 3, pp. 62–67, http://short.compositesworld.com/158cG3pz, 2013.

[68]   G. Gardiner, *Thermoplastic composite demonstrators — EU roadmap for future airframes.* Available: https://www.compositesworld.com/articles/thermoplastic-composite-demonstrators-eu-roadmap-for-future-airframes- (March 12th 2018).

[69]   A. Kermer-Meyer, *Formhaltige und komplexe Laminatstrukturen in Thermo-plast-Tapelegeverfahren,* 1st ed. Aachen: Apprimus-Verl, 2015.

[70] G. Beresheim, *Thermoplast-Tapelegen: Ganzheitliche Prozessanalyse und -entwicklung.* Kaiserslautern: IVW, 2002.

[71] T. Zenker, C. Schuerger, and K. Drechsler, Eds, *Experimental analysis of gaps and overlaps caused by intra-ply sectorization in the Thermoplastic Automated Fiber Placement process: 17th European Conference on Composite Materials, Munich, Germany, 26 - 30th June 2016*, 2016.

[72] R. Pitchumani, J. W. Gillespie, and M. A. Lamontia, "Design and Optimization of a Thermoplastic Tow-Placement Process with In-Situ Consolidation", *Journal of Composite Materials*, vol. 31, no. 3, pp. 244–275, 1997.

[73] R. Pitchumani, S. Ranganathan, R. C. Don, J. W. Gillespie, and M. A. Lamontia, "Analysis of transport phenomena governing interfacial bonding and void dynamics during thermoplastic tow-placement", *International Journal of Heat and Mass Transfer*, vol. 39, no. 9, pp. 1883–1897, 1996.

[74] W.J.B. Grouve, "Weld strength of laser-assisted tape-placed thermoplastic composites"

[75] Laserline GmbH, *OTS Optics, Power on the spot: Modular tools for materials processing.* Available: https://www.laserline.de/fileadmin/Dokumente/Broschueren_EN/Laserline_OTS_Optics.pdf (March 9th 2018).

[76] Celanese Corporation, *Standard product values Celstran® CFR-TP PA6 CF60-01* (March 29th 2018).

[77] J.F. Ready, Ed, *LIA handbook of laser materials processing.* Berlin, Orlando: Springer; Magnolia publ.; Laser Institute of america, 2001.

[78] C. M. Stokes-Griffin, S. Ehard, A. Kollmannsberger, P. Compston, and K. Drechsler, "A laser tape placement process for selective reinforcement of steel with CF/PA6 composites: Effects of surface preparation and laser angle", *Materials & Design*, vol. 116, pp. 545–553, 2017.

[79] Sumitomo Chemical, "Technical Note: Sumikaexcel PES Polyethersulfone: High heat resistance amorphous polymer", Sep. 2010.

[80] H. Saechtling and E. Baur, *Saechtling Kunststoff-Taschenbuch Ausg. 31,* 31st ed. München: Hanser, 2013.

[81] G. W. Ehrenstein, G. Riedel, and P. Trawiel, *Praxis der Thermischen Analyse von Kunststoffen,* 2nd ed. München: Carl Hanser Verlag, 2003.

[82] H. Schürmann, *Konstruieren Mit Faser-Kunststoff-Verbunden,* 2nd ed. Berlin: Springer-Verlag Berlin and Heidelberg GmbH & Co. KG, 2008.

[83] S. Standl, "Thermische Eigenschaften von duroplastischen und thermoplastischen Kohlenstofffaserhalbzeugen" Semesterarbeit / Forschungspraktikum,

Chair of Carbon Composites, Technische Universtiät München, München, August 15th 2014.

[84]   Hexcel Corporation, *HexTow® AS4 Carbon Fiber Product Data Sheet.* Available: http://www.hexcel.com/user_area/content_media/raw/AS4_HexTow_DataShe et.pdf (March 23th 2018).

[85]   A. A. Johnston, "An integrated model of the development of process-induced deformation in autoclave processing of composite structures", 1997.

[86]   M. Varma-Nair, Y. Jin, and B. Wunderlich, "Heat capacities of aliphatic and aromatic polysulphones", *Polymer*, vol. 33, no. 24, pp. 5272–5281, 1992.

[87]   J. E. Mark, *Physical properties of polymers handbook,* 2nd ed. New York: Springer, 2007.

[88]   *VDI-Wärmeatlas,* 10th ed. Berlin, Heidelberg, New York: Springer, 2006.

[89]   W. N. dos Santos, J. A. de Sousa, and R. Gregorio, "Thermal conductivity behaviour of polymers around glass transition and crystalline melting temperatures", *Polymer Testing*, vol. 32, no. 5, pp. 987–994, 2013.

[90]   G. W. C. Kaye and T. H. Laby, *Tables of physical and chemical constants,* 16th ed. Beijing: Shi jie tu shu chu ban gong si, 1999.

[91]   *Kunststoffe – Bestimmung der Wärmeleitfähigkeit und der Temperaturleitfähigkeit*, DIN EN ISO 22007-1 to 6, 2012.

[92]   H.-B. Shim, M.-K. Seo, and S.-J. Park, "Thermal conductivity and mechanical properties of various cross-section types carbon fiber-reinforced composites", *Journal of Materials Science*, vol. 37, no. 9, pp. 1881–1885, 2002.

[93]   A. Saleem, L. Frormann, and A. Iqbal, "High performance thermoplastic composites: Study on the mechanical, thermal, and electrical resistivity properties of carbon fiber-reinforced polyetheretherketone and polyethersulphone", *Polym. Compos,* vol. 28, no. 6, pp. 785–796, 2007.

[94]   W. J. Parker, R. J. Jenkins, C. P. Butler, and G. L. Abbott, "Flash Method of Determining Thermal Diffusivity, Heat Capacity, and Thermal Conductivity", *Journal of Applied Physics*, vol. 32, no. 9, pp. 1679–1684, 1961.

[95]   D. W. van Krevelen and K. t. Nijenhuis, *Properties of polymers: Their correlation with chemical structure; their numerical estimation and prediction from additive group contributions,* 4th ed. Amsterdam: Elsevier, 2009, r2012.

[96]   M. Ehleben, *Herstellung von endlosfaserverstärkten Rohren mit thermoplastischer Matrix im Schleuderverfahren*. Aachen: Shaker, 2002.

[97]   G. S. Springer and S. W. Tsai, "Thermal Conductivities of Unidirectional Materials", *Journal of Composite Materials*, vol. 1, no. 2, pp. 166–173, 1967.

[98]   T. E. Twardowski, S. E. Lin, and P. H. Geil, "Curing in Thick Composite Laminates: Experiment and Simulation", *Journal of Composite Materials*, vol. 27, no. 3, pp. 216–250, 1993.

[99]   R. Rolfes, "Transverse thermal conductivity of CFRP laminates: A numerical and experimental validation of approximation formulae", *Composites Science and Technology*, vol. 54, no. 1, pp. 45–54, 1995.

[100]   P. M. Schaefer, D. Gierszewski, A. Kollmannsberger, S. Zaremba, and K. Drechsler, "Analysis and improved process response prediction of laser- assisted automated tape placement with PA-6/carbon tapes using Design of Experiments and numerical simulations", *Composites Part A: Applied Science and Manufacturing*, vol. 96, pp. 137–146, 2017.

[101]   A. Barasinski, A. Leygue, E. Soccard, and A. Poitou, "Identification of non uniform thermal contact resistance in automated tape placement process", *Int J Mater Form*, vol. 7, no. 4, pp. 479–486, 2014.

[102]   A. Levy, J. Tierney, D. Heider, J.W. Gillespie, Jr, P. Lefebure, and D. Lang, Eds, *Modeling of Inter-Layer Thermal Contact Resistance During Thermoplastic Tape Placement*, 2012.

[103]   A. Levy, D. Heider, J. Tierney, and J. W. Gillespie, "Inter-layer thermal contact resistance evolution with the degree of intimate contact in the processing of thermoplastic composite laminates", *Journal of Composite Materials*, vol. 48, no. 4, pp. 491–503, 2014.

[104]   F. O. Sonmez and H. T. Hahn, "Analysis of the On-Line Consolidation Process in Thermoplastic Composite Tape Placement", *Journal of Thermoplastic Composite Materials*, vol. 10, no. 6, pp. 543–572, 1997.

[105]   S. C. Mantell and G. S. Springer, "Manufacturing Process Models for Thermoplastic Composites", *Journal of Composite Materials*, vol. 26, no. 16, pp. 2348–2377, 1992.

[106]   F. O. Sonmez and M. Akbulut, "Process optimization of tape placement for thermoplastic composites", *Composites Part A: Applied Science and Manufacturing*, vol. 38, no. 9, pp. 2013–2023, 2007.

[107]   F. O. Sonmez and H. T. Hahn, "Modeling of Heat Transfer and Crystallization in Thermoplastic Composite Tape Placement Process", *Journal of Thermoplastic Composite Materials*, vol. 10, no. 3, pp. 198–240, 1997.

[108]   F. Lemarchand, P. Beauchêne, B. Laine, and F. Chinesta, "A Multi-scale Method to Predict Residual Stress Appearance in the Process of on-line Consolidation of Thermoplastic Composites", *Int. J. Forming Processes*, vol. 10, no. 4, pp. 471–498, 2007.

[109]   H. Sarrazin and G. S. Springer, "Thermochemical and Mechanical Aspects of Composite Tape Laying", *Journal of Composite Materials*, vol. 29, no. 14, pp. 1908–1943, 1995.

[110]   J. Tierney and J. W. Gillespie, "Modeling of Heat Transfer and Void Dynamics for the Thermoplastic Composite Tow-Placement Process", *Journal of Composite Materials*, vol. 37, no. 19, pp. 1745–1768, 2003.

[111]   V. Agarwal, S. I. Guceri, R. L. Mccullough, and J. M. Schultz, "Thermal Characterization of the Laser-Assisted Consolidation Process", *Journal of Thermoplastic Composite Materials*, vol. 5, no. 2, pp. 115–135, 1992.

[112]   S. M. Grove, "Thermal modelling of tape laying with continuous carbon fibre-reinforced thermoplastic", *Composites*, vol. 19, no. 5, pp. 367–375, 1988.

[113]   C. M. Stokes-Griffin, P. Compston, T. I. Matuszyk, and M. J. Cardew-Hall, "Thermal modelling of the laser-assisted thermoplastic tape placement process", *Journal of Thermoplastic Composite Materials*, vol. 28, no. 10, pp. 1445–1462, 2015.

[114]   A. Levy, J. Tierney, D. Heider, P. Lefebure, and D. Lang, Eds, *Simulation And Optimization Of The Thermoplastic Automated Tape Placement (ATP) Process*, 2012.

[115]   Y.D. Kergomard, B. Satheesh, L. Dufort, and R. Schledjewski, Eds, *AUTOMATED TAPE LAYING (ATL) PROCESS SIMULATION THROUGH 3D THERMO-MECHANICAL MODEL: ECCM17 - 17th European Conference on Composite*, 2016.

[116]   Y. M.P. Toso, P. Ermanni, and D. Poulikakos, "Thermal Phenomena in Fiber-reinforced Thermoplastic Tape Winding Process: Computational Simulations and Experimental Validations", *Journal of Composite Materials*, vol. 38, no. 2, pp. 107–135, 2016.

[117]   Laserline GmbH, "Wirkungsgrad des Lasers und der Homogenisierungsoptik", E-mail, January 28th, 2015.

[118]   T. Weiler, M. Emonts, L. Wollenburg, and H. Janssen, "Transient thermal analysis of laser-assisted thermoplastic tape placement at high process speeds by use of analytical solutions", *Jnl of Thermoplastic Composite Materials*, vol. 31, no. 3, pp. 311–338, 2017.

[119]   T. Zenker and M. Schwab, Eds, *Analysis of fiber steering effects in thermoplastic automated fiber placement*, 2018.

[120]   G. Dell'Anno, I. K. Partridge, D. D.R. Cartié, A. Hamlyn, E. Chehura, S. W. James, and R. P. Tatam, "Automated Manufacture of 3D reinforced aerospace composite structures", *International Journal of Structural Integrity*, vol. 2012, no. Vol. 03 Iss. 01, pp. 22–40,

https://dspace.lib.cranfield.ac.uk/bitstream/handle/1826/7255/Automated_man ufacture_of_3D_reinforced_composite_structures-2012.pdf?sequence=1&isAllowed=y, 2012.

[121]   C. L. Beyler and M. M. Hirschler, "Chapter 7: Thermal Decomposition of Polymers" in *SFPE Handbook of Fire Protection Engineering*, P. J. DiNenno, Ed, Quincy, Massachusetts, 2002, pp. 110–130.

[122]   M. Herrera Salinas, "Untersuchung flüchtiger Verbindungen bei der thermischen Zersetzung von stickstoffhaltigen Polymerwerkstoffen" Dissertation, Fakultät Wissenschaftszentrum Weihenstephan, Technische Universtiät München, Munich, 2001.

[123]   P. J. Bates, T. B. Okoro, and M. Chen, "Thermal degradation of PC and PA6 during laser transmission welding", *Weld World*, vol. 59, no. 3, pp. 381–390, 2015.

[124]   P.-A. Eriksson, A.-C. Albertsson, K. Eriksson, and J.-A.E. Månson, "Thermal oxidative stability of heat-stabilised Polyamide 66 by Differential Scanning Calorimetry", *Journal of Thermal Analysis and Calorimetry*, vol. 53, no. 1, pp. 19–26, 1998.

[125]   P.-A. Eriksson, P. Boydell, K. Eriksson, J.-A. E. Mnson, and A.-C. Albertsson, "Effect of thermal-oxidative aging on mechanical, chemical, and thermal properties of recycled polyamide 66", *J. Appl. Polym. Sci,* vol. 65, no. 8, pp. 1619–1630, 1997.

[126]   P.-A. Eriksson, P. Boydell, J.-A. E. Mnson, and A.-C. Albertsson, "Durability study of recycled glass-fiber-reinforced polyamide 66 in a service-related environment", *J. Appl. Polym. Sci,* vol. 65, no. 8, pp. 1631–1641, 1997.

[127]   V. Radlmaier, C. Heckel, M. Winnacker, A. Erber, and H. Koerber, "Effects of thermal cycling on polyamides during processing", *Thermochimica Acta*, vol. 648, pp. 44–51, 2017.

[128]   M. Herrera, G. Matuschek, and A. Kettrup, "Main products and kinetics of the thermal degradation of polyamides", *Chemosphere*, vol. 42, no. 5-7, pp. 601–607, 2001.

[129]   B.A. Hulcher, J.M. Marchello, and J.A. Hinkley, Eds, *Correlation between double cantilever beam and wedge peel tests for automated tow placement*: Society for the Advancement of Material and Process Engineering (SAMPE), 1998.

[130]   B.A. Hulcher, J.M. Marchello, and J.A. Hinkley, "Wedge Peel Testing for Automated Fiber Placement", *Journal of advanced material*, vol. 1999, no. 31(3), pp. 37–43, 1999.

[131] D. Maurer and P. Mitschang, Eds, *Laser-powered thermoplastic tape place-ment process - simulation and optimization*, 2014.

[132] F. Rodriguez-Lence, I. Martin-Hernando, and K. Fernandez, Eds, *In-situ con-solidation of Polyamide(PA) composites by Automated Fiber Placement tech-nology*, 2016.

[133] C. M. Stokes-Griffin and P. Compston, "An inverse model for optimisation of laser heat flux distributions in an automated laser tape placement process for carbon-fibre/PEEK", *Composites Part A: Applied Science and Manufacturing*, vol. 88, pp. 190–197, 2016.

[134] *Test Method for Measuring the Curved Beam Strength of a Fiber-Reinforced Polymer-Matrix Composite.*

[135] Wacker Chemie AG, "Fest- und Flüssigsilikonkautschuk: Der Leitfaden für die Praxis.", 2013.

[136] Wacker Chemie AG, "RTV Siliconkautschuke: Kleben, Abdichten, Vergies-sen und Beschichten", 2013.

[137] GLEICH Aluminiumwerk GmbH & Co. KG, "EN AW 5083 Technisches Datenblatt", Feb. 2015.

A Appendix

a Carbon fiber tape material data

Tab. A-1: Measured absorptivity of CF/PES and CF/PA6 tapes from Fig. 3-3

Angle of incidence θ °	Absorptivity of CF/PES (SD) %	Absorptivity of CF/PA6 [78] %
5	90.75 (0.62)	
10	90.30 (0.55)	90.21
15	90.08 (0.53)	
20	90.00 (0.54)	89.78
25	89.89 (0.55)	
30	89.77 (0.55)	89.81
35	89.67 (0.55)	89.85
40	89.78 (0.55)	90.32
45	89.66 (0.53)	90.28
50	89.23 (0.57)	90.32
55	88.20 (0.59)	89.47
60	85.83 (0.91)	88.24
65	82.61 (1.05)	84.72
70	78.01 (1.45)	80.62
75	71.72 (1.79)	73.96
80	62.31 (2.92)	64.64
85	48.01 (4.70)	48.37

Tab. A-2: **Specific heat data values of CF/PES and CF/PA6 tapes from Fig. 3-4**

Tempera-ture:	AS4 car-bon fiber: [84, 85]	PES: [86]	CF/PES - model:	CF/PES – measure-ment (SD): [83]	PA6: [90]	CF/PA6 – model:
°C	J/(kg K)	J/(kg K)	J/(kg K)	J/(kg K)	J/(kg K)	J/(kg K)
0	1130.4	918.2	1048.7		1311.2	1204.4
20				793 (53.5)		
25	1130.4	981.7	1073.2		1508.7	1285.3
50	1130.4	1049.4	1099.2	882 (49.6)	1706.2	1366.1
75	1130.4	1124.7	1128.2		1903.7	1446.9
100	1130.4	1203.1	1158.4	1020 (46.2)	2100.5	1527.5
125	1130.4	1281.2	1188.5		2181.7	1560.8
150	1130.4	1356.1	1217.3	1149 (44.0)	2263.0	1594.0
175	1130.4	1425.4	1244.0		2344.2	1627.3
200	1160.0	1487.0	1285.9		2425.5	1678.0
224				1393 (45.4)		
225	1211.3	1625.6	1370.8		2506.7	1741.5
250	1262.5	1686.9	1425.9		2588.0	1805.1
275	1313.8	1707.2	1465.2		2669.2	1868.6
300	1365.0	1715.1	1499.8	1585 (44.6)	2750.0	1931.9
325	1416.3	1723.1	1534.4		2750.0	1962.2
350	1467.5	1730.9	1568.9		2750.0	1992.5
375	1518.8	1738.8	1603.5		2750.0	2022.7
400	1570.0	1746.6	1638.0	1728 (35.8)	2750.0	2053.0

Tab. A-3: **In-fiber direction heat conductivity of CF/PES and CF/PA6 tapes from Fig. 3-7**

Temperature:	AS4 carbon fiber: [85]	PES: [95]	CF/PES - model:	CF/PES – measurement (SD):	PA6: [96]	CF/PA6 – model:
°C	W/(m K)	W/(m K)	W/(m K)	W/(m K)	W/(m K)	W/(m K)
0	7.69	0.18	4.31		0.32	3.86
25	8.08	0.18	4.53	4.39 (0.22)	0.32	4.05
50	8.47	0.18	4.74	4.94 (0.18)	0.32	4.23
75	8.86	0.19	4.96		0.32	4.42
100	9.25	0.19	5.17	5.45 (0.15)	0.31	4.60
125	9.64	0.19	5.39		0.29	4.78
150	10.03	0.20	5.60	5.99 (0.12)	0.27	4.96
175	10.42	0.20	5.82		0.24	5.13
200	10.81	0.20	6.04	6.56 (0.21)	0.22	5.30
225	11.20	0.20	6.25		0.22	5.49
250	11.59	0.20	6.46	6.73 (0.15)	0.22	5.68
275	11.98	0.20	6.68		0.22	5.86
300	12.37	0.20	6.89	7.36 (0.30)	0.22	6.05
325	12.76	0.19	7.11		0.22	6.24
350	13.15	0.19	7.32	7.50 (0.17)	0.22	6.42
375	13.54	0.19	7.53		0.22	6.61
400	13.93	0.19	7.75	7.49 (0.34)	0.22	6.80

Tab. A-4: **Transverse fiber direction heat conductivity data values of CF/PES and CF/PA6 tapes from Fig. 3-8**

Tempera-ture:	AS4 car-bon fiber: [85]	PES: [95]	CF/PES - model:	CF/PES – measure-ment (SD):	PA6: [96]	CF/PA6 – model:
°C	W/(m K)	W/(m K)	W/(m K)	W/(m K)	W/(m K)	W/(m K)
25	2.53	0.18	0.48	0.32 (0.06)	0.32	0.66
50	2.65	0.18	0.50	0.34 (0.06)	0.32	0.67
100	2.91	0.19	0.52	0.38 (0.06)	0.31	0.65
150	3.16	0.20	0.54	0.40 (0.07)	0.27	0.60
200	3.41	0.20	0.55	0.42 (0.07)	0.22	0.50
250	3.67	0.20	0.56	0.42 (0.07)	0.22	0.50
300	3.92	0.20	0.56	0.48 (0.08)	0.22	0.50
350	4.17	0.19	0.55	0.50 (0.08)	0.22	0.50
400	4.43	0.19	0.54	0.52 (0.08)	0.22	0.51
450				0.55 (0.08)		

Tab. A-5: **Comparison of transverse fiber direction heat conductivity of one-layer CF/PES tapes and seven-layer CF/PES laminates with and without post consolidation from Fig. 3-10 (left)**

Tempera-ture:	One-layer CF/PES (SD):	Seven-layer CF/PES in situ (SD):	Seven-layer CF/PES post consolidated (SD):
°C	W/(m K)	W/(m K)	W/(m K)
25	0.32 (0.06)	0.41 (0.03)	0.43 (0.03)
50	0.34 (0.06)	0.41 (0.02)	0.46 (0.01)
100	0.38 (0.06)	0.45 (0.04)	0.53 (0.03)
150	0.40 (0.07)	0.48 (0.03)	0.57 (0.03)
200	0.42 (0.07)	0.50 (0.02)	0.60 (0.05)
225			0.60 (0.05)
235			0.58 (0.03)
250	0.42 (0.07)	0.48 (0.01)	0.59 (0.03)
300	0.48 (0.08)		
350	0.50 (0.08)		
400	0.52 (0.08)		
450	0.55 (0.08)		

Tab. A-6: **CF/PES thermal contact resistance, calculated according to Levy et al. [103] and from measurements, from Fig. 3-10 (right)**

Tempera-ture:	Levy et al. $D_{ic} = 0.75$	Levy et al. $D_{ic} = 0.95$	R_c from meas-urements:
°C	m² K/W	m² K/W	m² K/W
25	3.44E-04	1.76E-04	2.73E-05
50	3.34E-04	1.66E-04	4.60E-05
100	3.20E-04	1.52E-04	5.18E-05
150	3.14E-04	1.47E-04	5.56E-05
200	3.08E-04	1.40E-04	5.33E-05
250	3.09E-04	1.42E-04	6.64E-05

b Laser beam divergence

The following equations describe the linear approximations of the laser beam divergence with respect to the distance from the optics front (Fig. 4-3).

Optics 1: used for 25.4 mm wide CF/PES tape
Nominal laser spot size in 250 mm focal distance is 57 mm x 57 mm.

$$height = width = 13.8333 + 0.16833 * distance \; [mm] \qquad \text{(b-1)}$$

Optics 2: used for 12 mm wide CF/PA6 tape
Nominal laser spot size in 250 mm focal distance is 40 mm x 20 mm.

$$height = 7.2944 + 0.11918 * distance \; [mm] \qquad \text{(b-2)}$$

$$width = 4.8294 + 0.04888 * distance \; [mm] \qquad \text{(b-3)}$$

c Compaction roller and lay-up tool material properties

Tab. A-7:   **Thermal properties of silicone compaction roller and tool materials**

Roller: Silicone Elastosil RT 625 [135, 136]		
Temperature	**Heat conductivity λ**	**Specific heat c$_p$**
K	W/m·K	J/kg·K
293.15	0.2	1250

Tool: Aluminum EN AW-5083 [88, 137]		
Temperature	**Heat conductivity λ**	**Specific heat c$_p$**
K	W/m·K	J/kg·K
273.15	113	900
373.15	126	1047
473.15	137	
673.15		1143

| Tool: Mild steel S235 [88]		
Temperature	**Heat conductivity λ**	**Specific heat c$_p$**
K	W/m·K	J/kg·K
293.15	57	430
373.15	57	500
473.15	54	540
573.15	50	580
673.15	45	620
773.15	42	690
873.15	37	780

d Laser beam sketches during 3D placement

Tab. A-8:   **Laser beam sketches for different tooling angles**
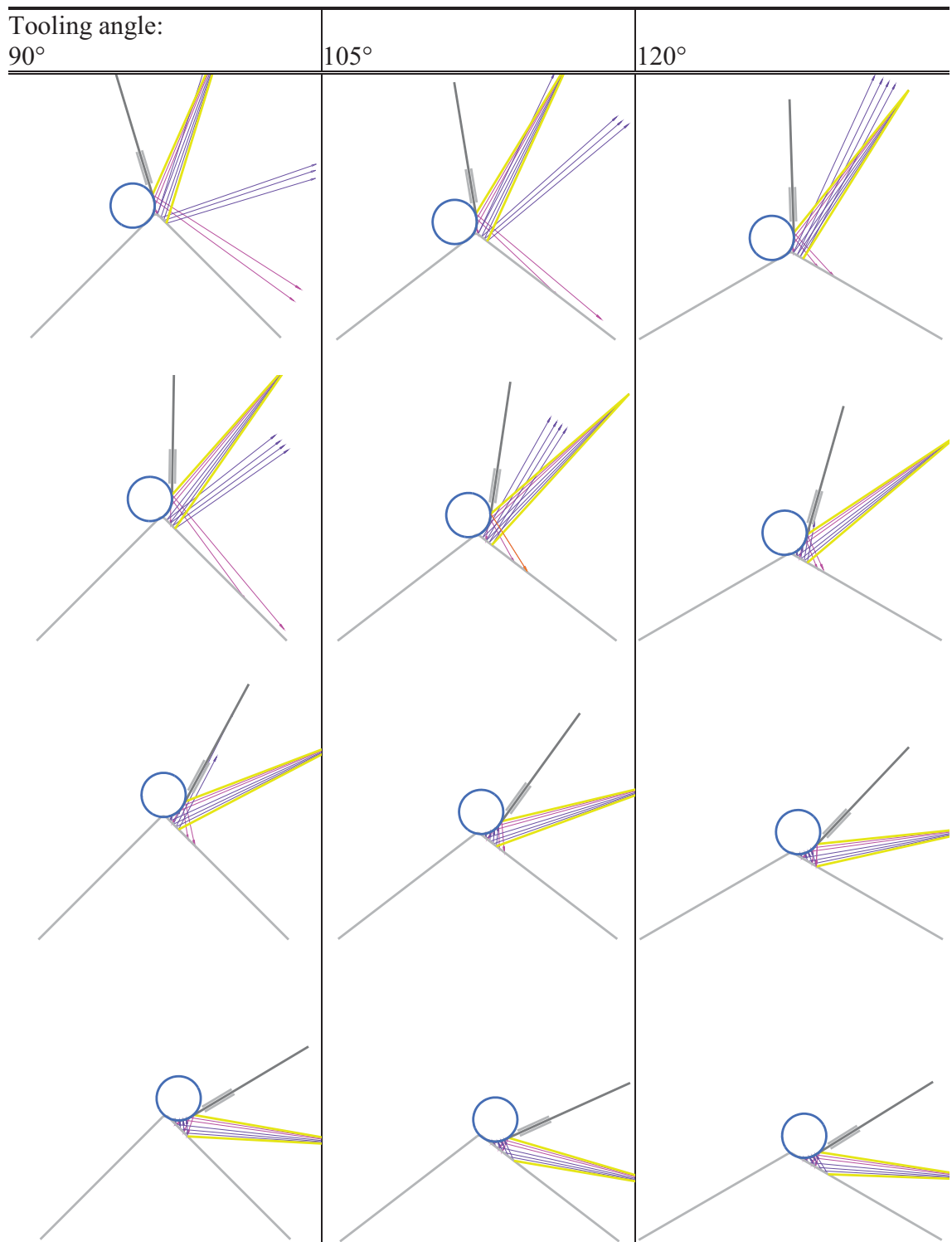
Sketches of direct and reflected illumination for different time steps during3D lay-up;

laser beam, compaction and tooling are drawn to scale with each other;

pink: laser beams first hitting incoming tape; violet: laser beams first hitting substrate laminate

Tooling angle: 90°	105°	120°

Tooling angle: 90°	105°	120°
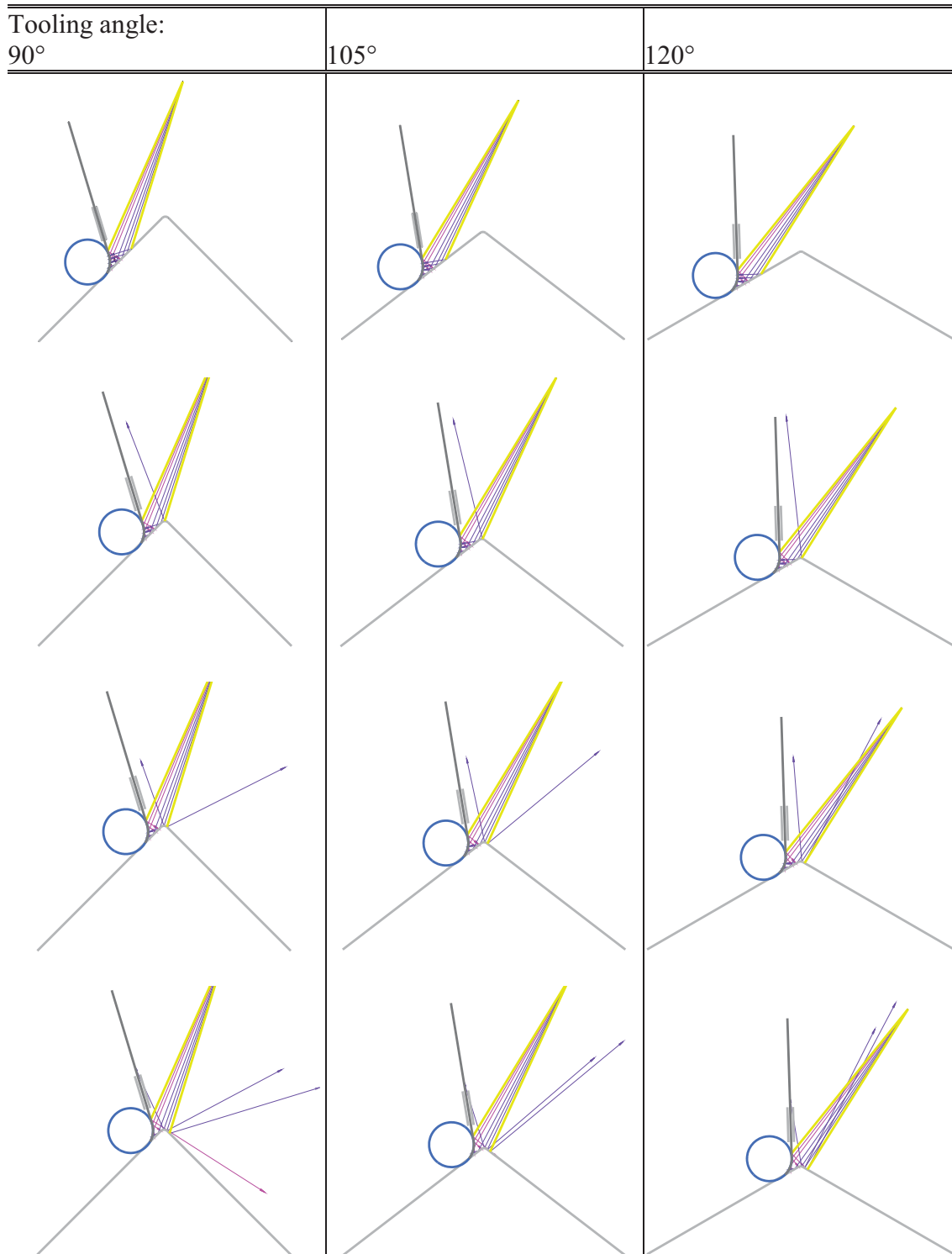
e Set-point tables for CCPP strategy

Tab. A-9: **CCPP set-point table for 90° tooling lay-up**
Lay-up in y-direction; the top of the tool is at y = 950 mm, z = 261 mm

#:	x [mm]:	y [mm]:	z [mm]:	P [W]:	α [°]:	Comment:
1	590.0	735.2	48	390	0.4	turning CCPP on
2	590.0	902.7	216	390	0.8	
3	590.0	912.9	226	390	2.5	
4	590.0	919.8	232	390	2.7	
5	590.0	923.6	236	330	3.0	Laser bias on incoming tape
6	590.0	929.1	242	230	2.5	
7	589.8	939.0	252	200	1.0	
8	589.5	944.7	259	220	0.5	
9	589.2	948.7	261	280	-0.3	~ tip of the tool
10	589.1	954.2	259	380	-0.1	
11	590.0	969.7	243	390	-0.1	
12	590.0	988.9	224	390	0.1	
13	590.0	1029.6	183	390	0.1	
14	590.0	1140.8	72	0	0	turning CCPP off

Tab. A-10: **CCPP set-point table for 105° tooling lay-up**
Lay-up in y-direction; the top of the tool is at y = 950 mm, z = 210 mm

#:	x [mm]:	y [mm]:	z [mm]:	P [W]:	α [°]:	Comment:
1	524.7	735.2	45	390	0.4	turning CCPP on
2	524.7	902.9	174	390	1.0	
3	524.7	912.9	182	390	2.2	
4	524.7	919.9	187	390	2.5	
5	524.7	922.6	189	300	2.6	Laser bias on incoming tape
6	524.7	928.6	194	230	2.4	
7	524.5	937.6	202	200	1.0	
8	524.2	943.0	207	200	0.2	
9	523.9	945.7	209	250	-0.3	
10	523.8	950.0	210	350	-0.2	~ tip of the tool
11	524.7	966.2	199	410	0.2	
12	524.7	969.4	196	440	0.4	
13	524.7	977.4	190	430	0.2	
14	524.7	987.7	181	400	0.2	
15	524.7	998.4	173	390	0.2	
16	524.7	1140.1	64	0	0	turning CCPP off

Tab. A-11: CCPP set-point table for 120° tooling lay-up
     Lay-up in y-direction; the top of the tool is at y = 950 mm, z = 165 mm

#:	x [mm]:	y [mm]:	z [mm]:	P [W]:	α [°]:	Comment:
1	535.4	732.0	42	390	0.40	turning CCPP on
2	535.4	903.2	140	390	1.00	
3	535.4	913.0	146	390	1.50	
4	535.4	920.0	150	390	2.30	Laser bias on incoming tape
5	535.4	923.6	152	350	2.30	
6	535.4	934.8	159	270	2.00	
7	535.4	939.0	162	200	1.20	
8	535.4	945.0	165	190	1.00	
9	535.4	950.0	165	190	0.00	~ tip of the tool
10	535.4	955.0	165	350	0.00	
11	535.4	968.8	157	390	0.10	
12	535.4	970.5	156	410	0.10	
13	535.4	979.9	150	410	0.20	
14	535.4	989.1	145	400	0.40	
15	535.4	998.4	140	380	0.40	
16	535.4	1031.2	120	380	0.40	
17	535.4	1141.3	57	0	0.00	turning CCPP off

f Log file data of CCPP and PCLC lay-up on the 105° and 120° tool

Exemplary log file data curves of the manufacturing of 105° and 120° specimens are shown. The general discussion and the curves of the 90° specimens is given in section 7.2.2.
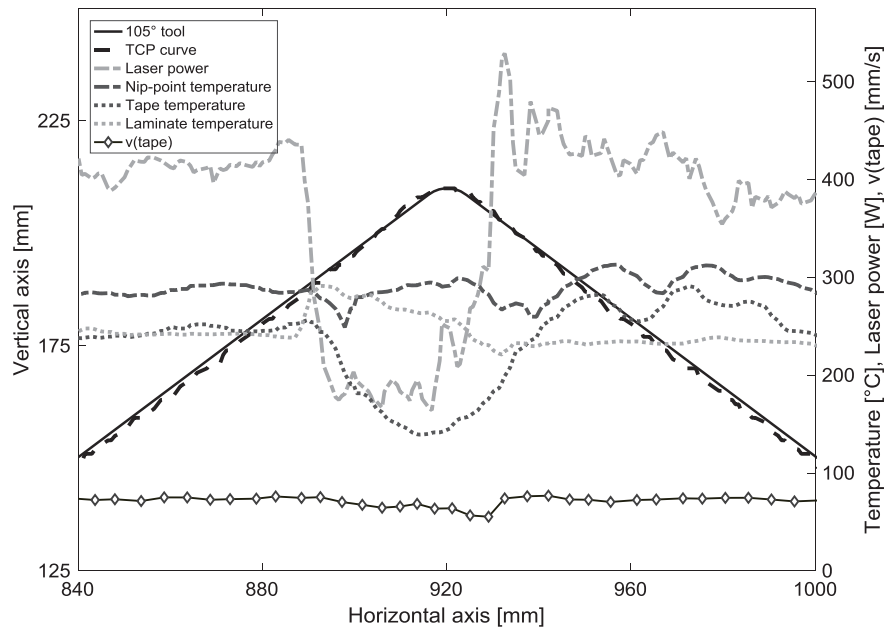

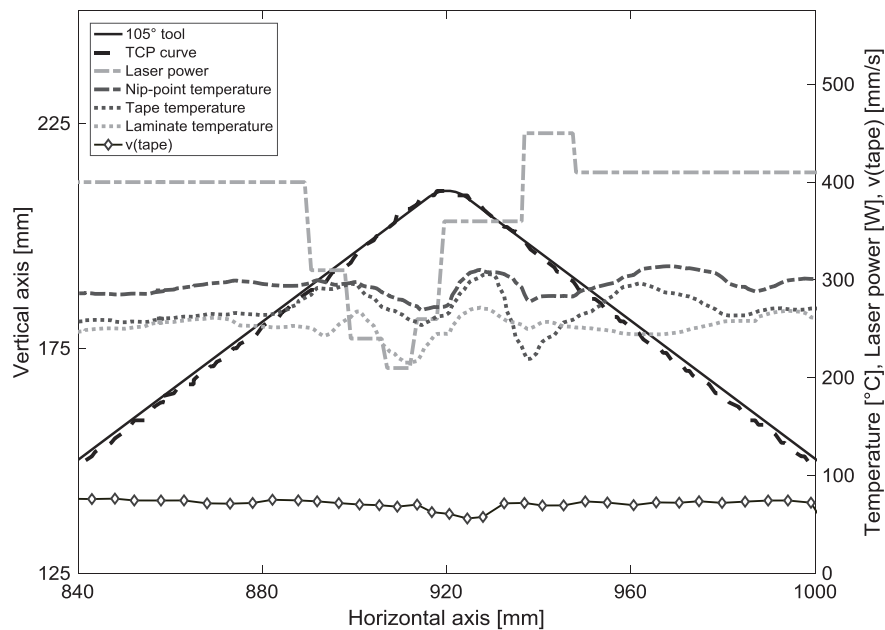**Fig. A-1:**   **Log file data of a track from 105° specimen manufactured by PCLC**

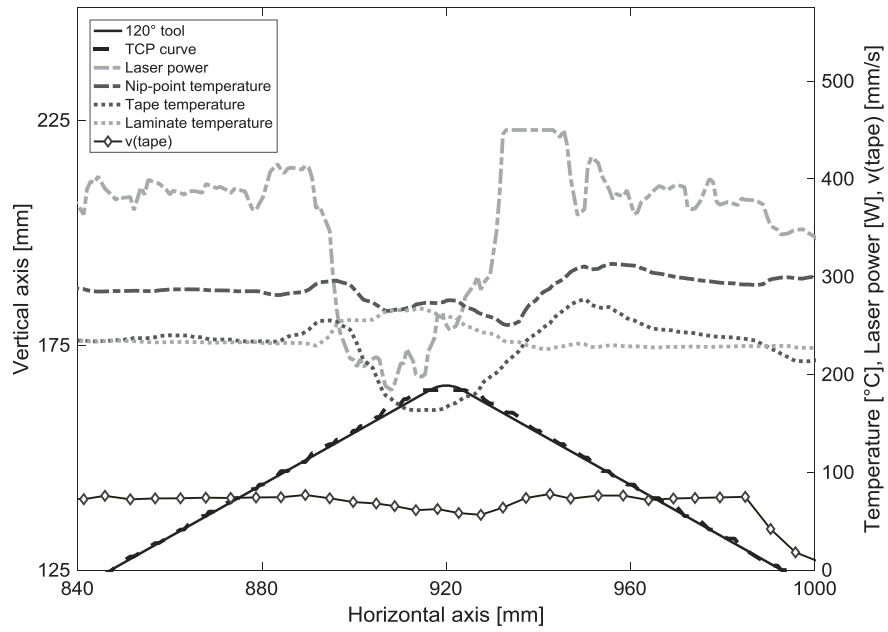**Fig. A-2:**   **Log file data of a track from 105° specimen manufactured by CCPP**

Fig. A-3: Log file data of a track from 120° specimen manufactured by PCLC
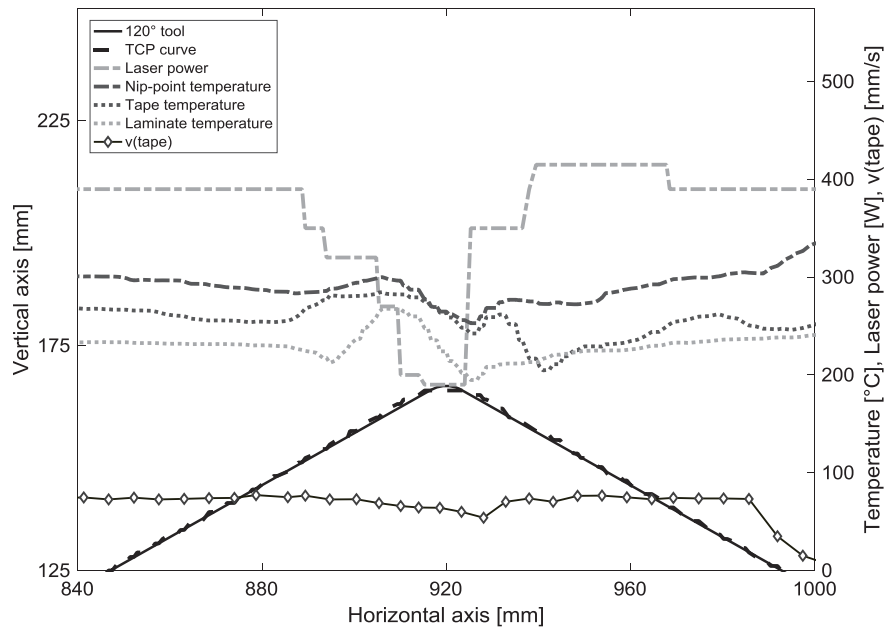

Fig. A-4: Log file data of a track from 120° specimen manufactured by CCPP

Exemplary temperature heatmaps of the manufacturing of 105° and 120° specimens are shown. The general discussion and the curves of the 90° specimens is given in section 7.2.2.
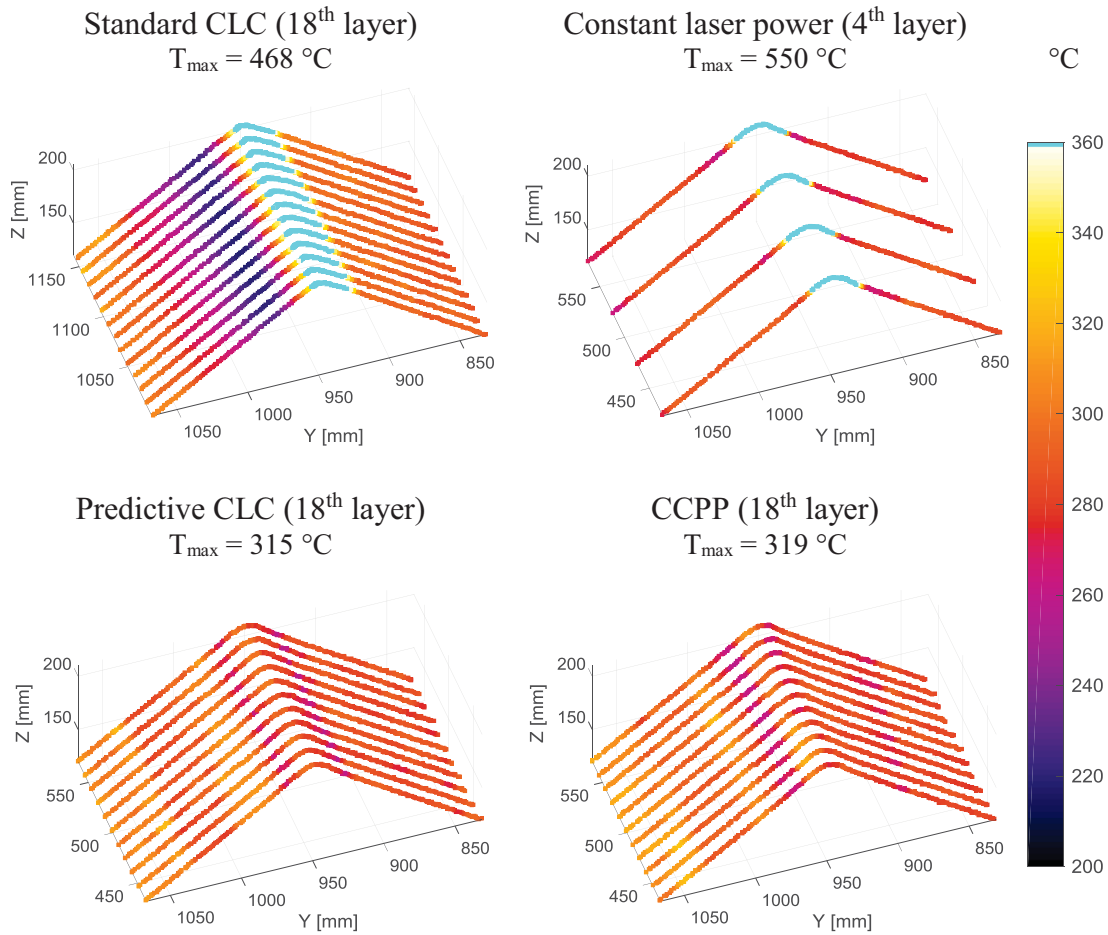

Fig. A-5: **Nip-point temperature 3D heatmap representation of specimens with 105° angle, manufactured by different lay-up heating strategies**
The heatmaps show the tracks of the 4th layer of the wedge peel specimens (top right), manufactured with constant laser power and the tracks of the 18th layer of the four-point-bending specimens, manufactured with the other strategies
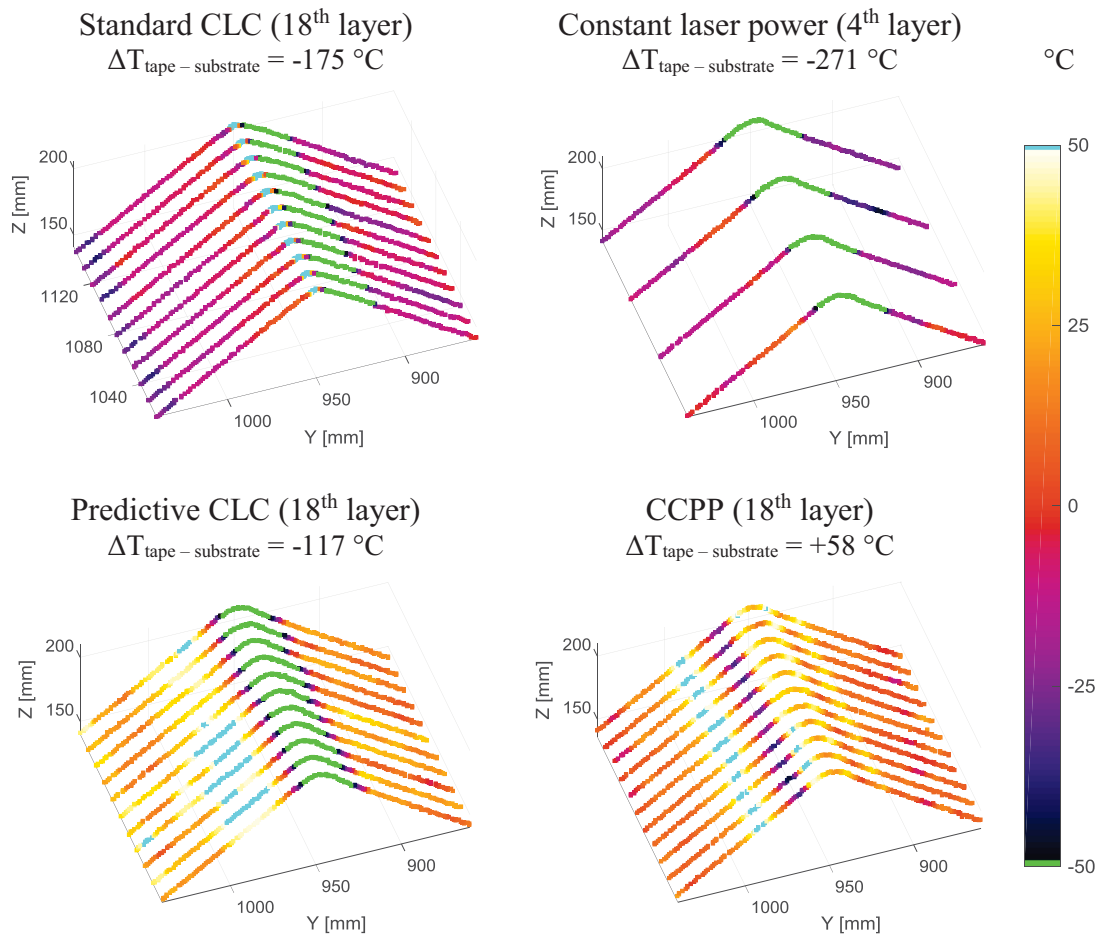
Fig. A-6:   Temperature difference between incoming tape and substrate laminate of four-point-bending specimens with 105° angle, manufactured by different lay-up heating strategies

The heatmaps show the tracks of the 4th layer of the wedge peel specimens (top right), manufactured with constant laser power and the tracks of the 18th layer of the four-point-bending specimens, manufactured with the other strategies

Fig. A-7:   **Nip-point temperature 3D heatmap representation of specimens with 120° angle, manufactured by different lay-up heating strategies**
The heatmaps show the tracks of the 4th layer of the wedge peel specimens (top right), manufactured with constant laser power and the tracks of the 18th layer of the four-point-bending specimens, manufactured with the other strategies
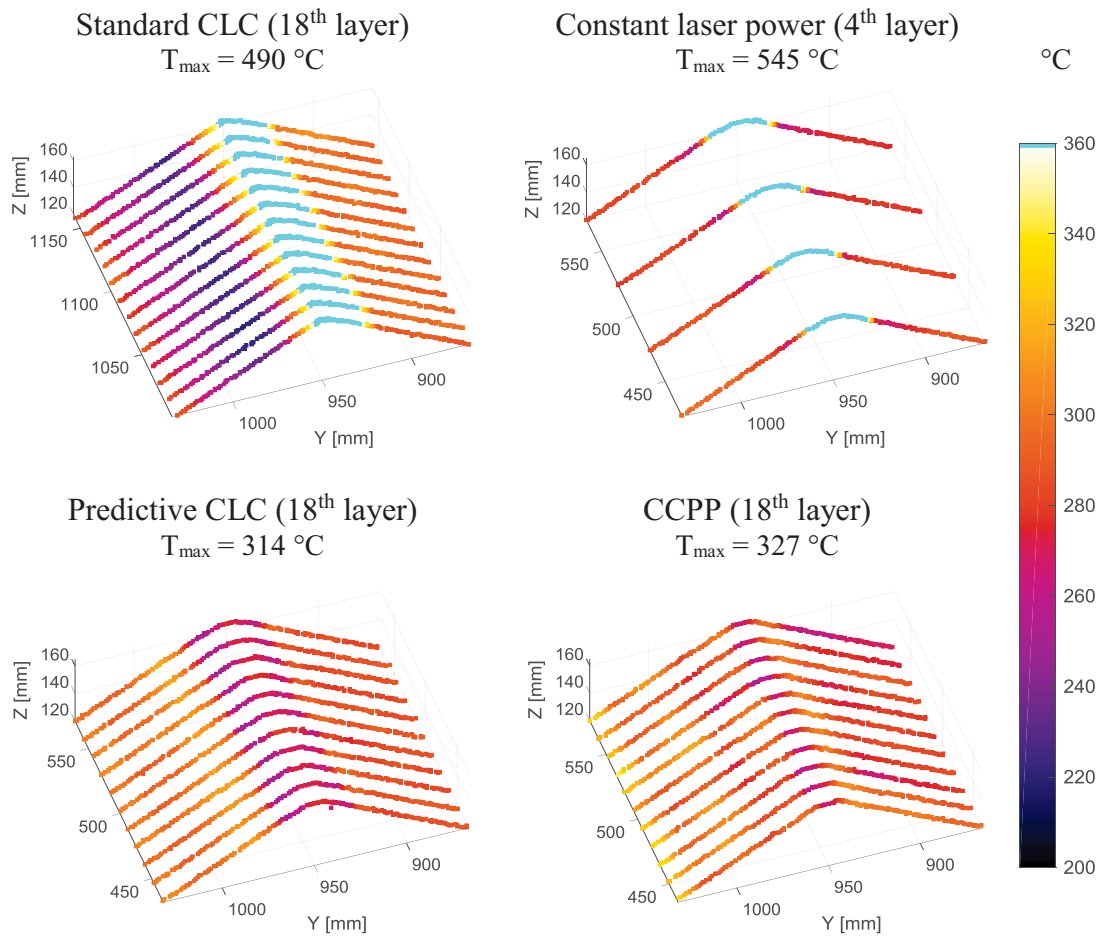
Fig. A-8: **Temperature difference between incoming tape and substrate laminate of four-point-bending specimens with 120° angle, manufactured by different lay-up heating strategies**

The heatmaps show the tracks of the 4th layer of the wedge peel specimens (top right), manufactured with constant laser power and the tracks of the 18th layer of the four-point-bending specimens, manufactured with the other strategies
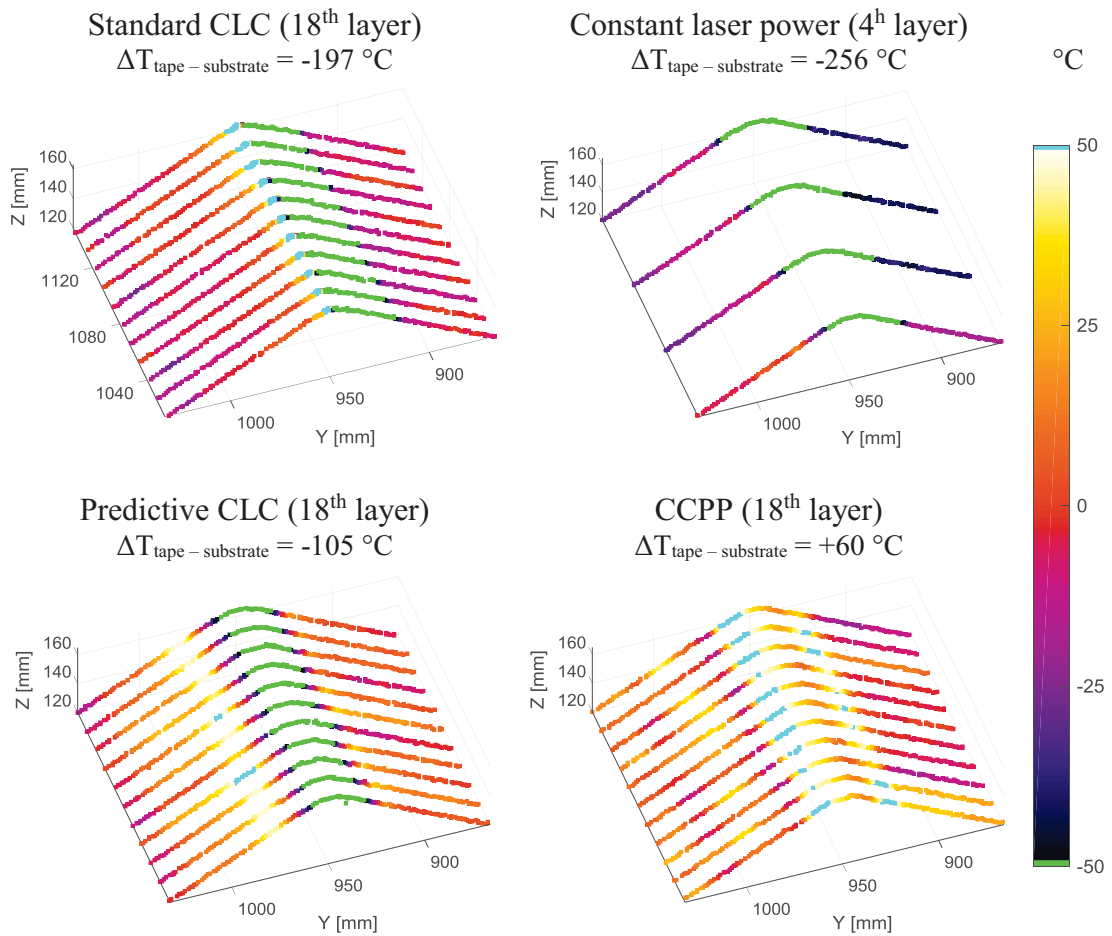
g Wedge peel test curves of the 105° and 120° specimens

The wedge peel test curves of the specimens laid up on the 105° and 120° tools are shown. The general discussion and the curves of the 90° specimens are given in section 7.2.3.

Standard CLC
Mean (section I) = 65.5 N
Mean (section II) = 36.3 N

Constant laser power
Mean (section I) = 50.4 N
Mean (section II) = 42.4 N
Mean (section III) = 48.2 N

Predictive CLC
Mean (section) = 52.5 N
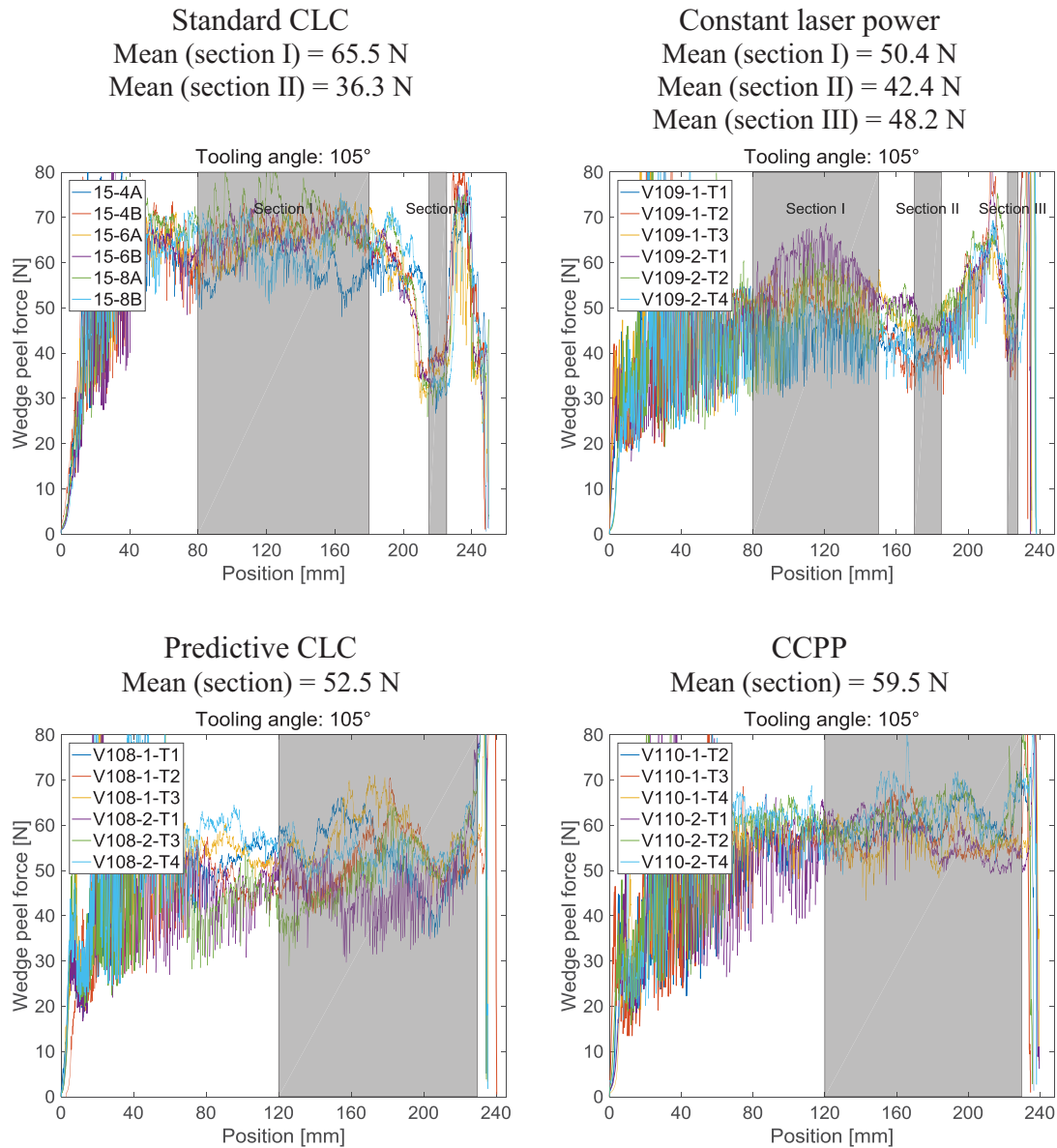
CCPP
Mean (section) = 59.5 N

Fig. A-9: **Wedge peel curves of 105° specimens manufactured with different processing strategies**
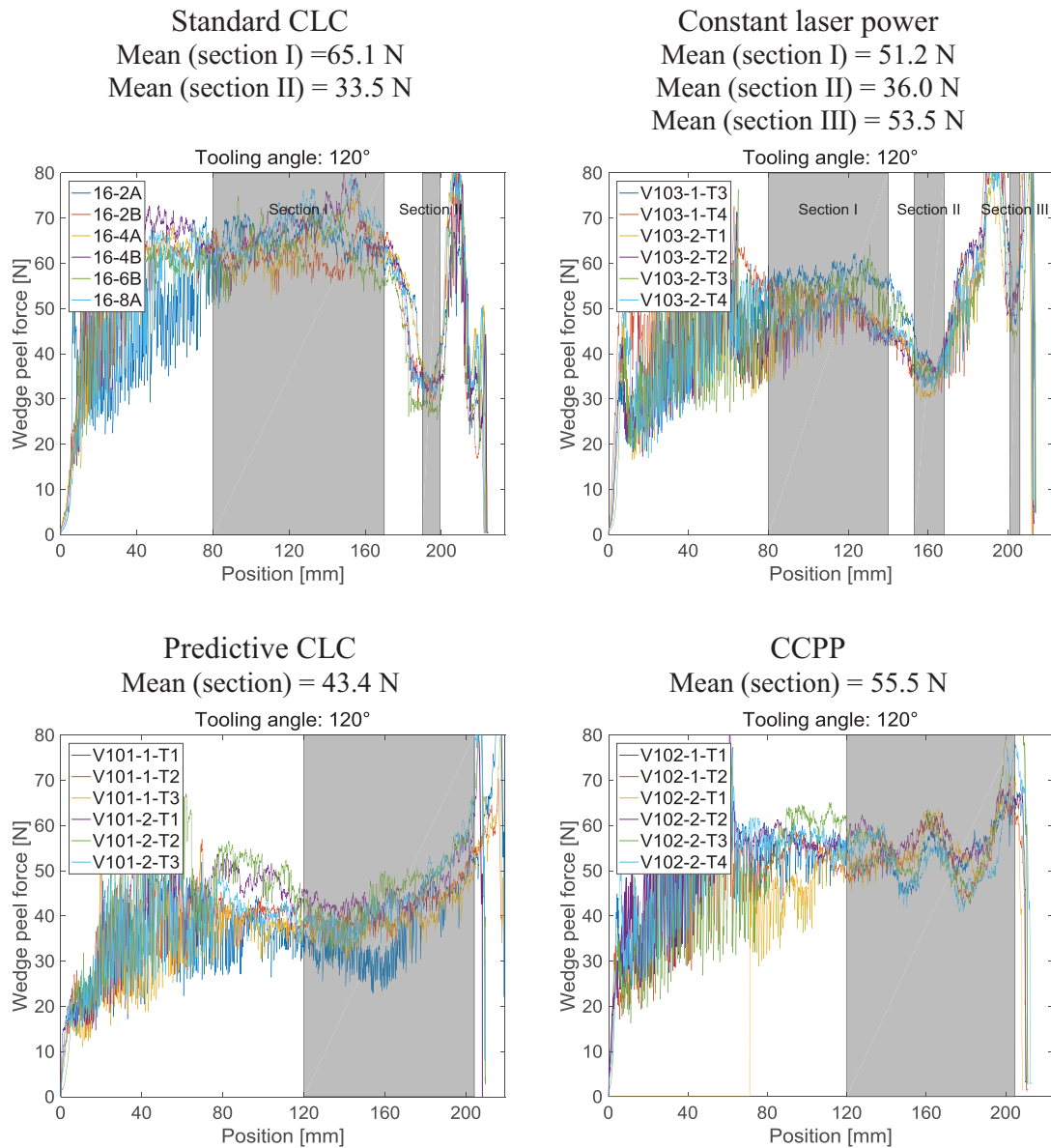The grey areas highlight the analysis sections.

Fig. A-10:   Wedge peel curves of 120° specimens manufactured with different processing strategies

The grey areas highlight the analysis sections.

h Four-point-bending test curves of the 105° and 120° specimens
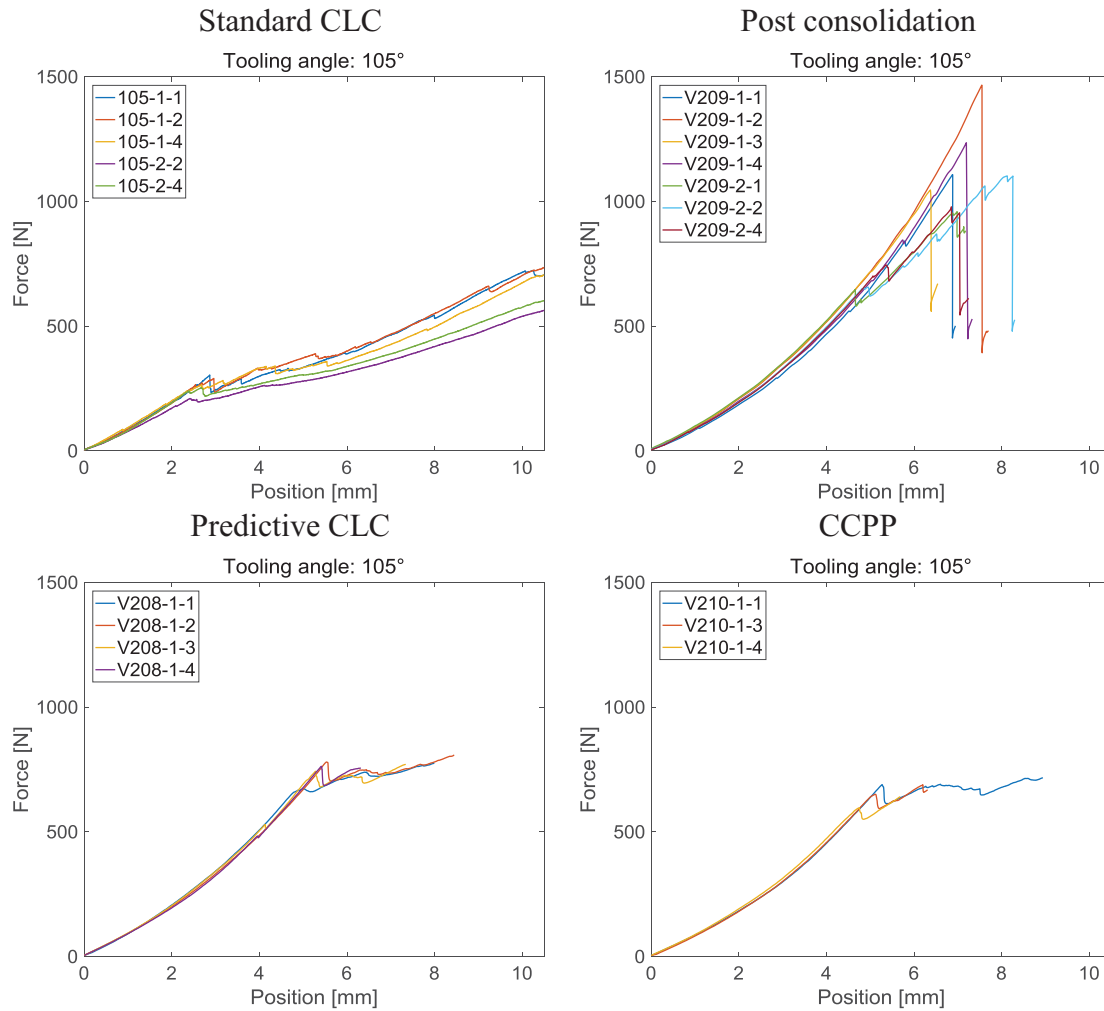

Fig. A-11: Four-point-bending test curves of 105° specimens manufactured with different processing strategies
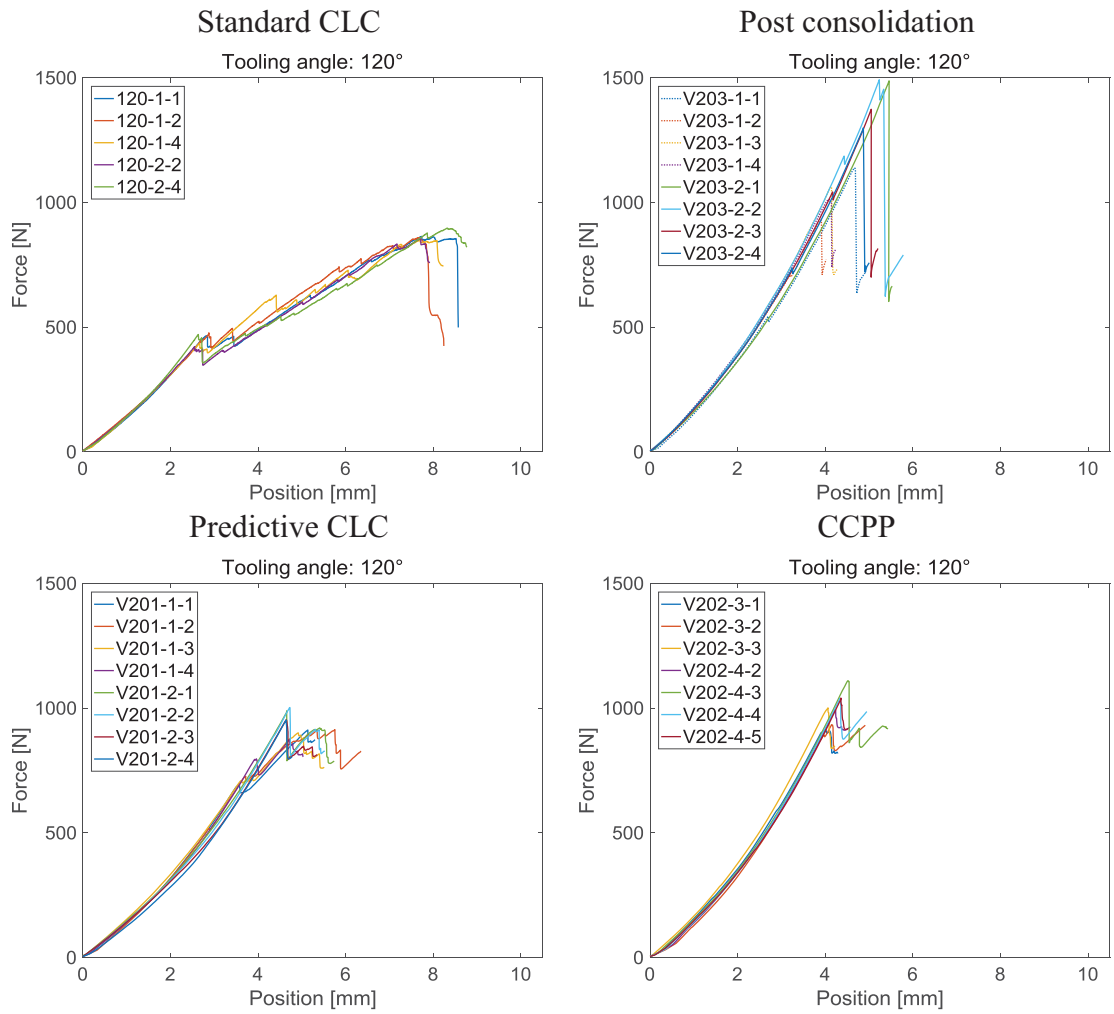
Fig. A-12: **Four-point-bending test curves of 120° specimens manufactured with different processing strategies**

B Publications

Journal articles

[J1] Stokes-Griffin, C.M.; Ehard, S.; Kollmannsberger, A.; Compston, P.; Drechsler, K.; "A laser tape placement process for selective reinforcement of steel with CF/PA6 composites: Effects of surface preparation and laser angle", *Materials & Design* vol. 116, 2017, 545-553, http://dx.doi.org/10.1016/j.matdes.2016.12.013

[J2] Schaefer, P.M.; Gierszewski, D.; Kollmannsberger, A.; Zaremba, S.; Drechsler, K.; "Analysis and improved process response prediction of laser-assisted automated tape placement with PA-6/carbon tapes using Design of Experiments and numerical simulations", *Composites Part A: Applied Science and Manufacturing*, vol. 96, 2017, 137-146, http://doi.org/10.1016/j.compositesa.2017.02.008

[J3] Kollmannsberger, A.; Lichtinger, R.; Hohenester, F.; Ebel, C.; Drechsler, K.; "Numerical analysis of the temperature profile during the laser assisted automated fiber placement of CFRP-tapes with thermoplastic matrix", *Journal of Thermoplastic Composite Materials*, 2017, http://doi.org/10.1177/0892705717738304

[J4] Stokes-Griffin, C.M.; Kollmannsberger, A.; Ehard, S.; Compston, P.; Drechsler, K.; "Manufacture of steel–CF/PA6 hybrids in a laser tape placement process: Effect of first-ply placement rate on thermal history and lap shear strength", *Composites Part A: Applied Science and Manufacturing*, vol.111, 2018, 42-53, https://doi.org/10.1016/j.compositesa.2018.05.007

Conferences

[C1]   Henne, F.; Ehard, S.; Kollmannsberger, A.; Höck, B.; Sause, M.; Drechsler, K.; "Thermoplastic in situ fiber placement for future solid rocket motor casing manufacturing", *SAMPE Europe SETEC 14,* September 2014, Tampere (Finland), ISBN: 978-90-821727-1-3.

[C2]   Radlmaier, V.; Obermeier, G.; Ehard, S.; Kollmannsberger, A.; Körber, H.; Ladstätter, E.; "Interlaminar Fracture Toughness of Carbon Fiber Reinforced Thermoplastic In-situ Joints", *Polymer Processing Society Conference (PPS)*, 2015, Graz (Austria).

[C3]   Stokes-Griffin, C.; Ehard, S.; Kollmannsberger, A.; Compston, P.; Drechsler, K.; "Selective reinforcement of steel with CF/PA6 composites in a laser tape placement process: Effect of surface preparation and laser angle on interfacial bond strength", *Proceedings of the 17th European Conference on Composite Materials*, June 2016, Munich (Germany), ISBN: 978-3-00-053387-7.

[C4]   Kollmannsberger, A.; Ladstätter, E.; Drechsler, K.; "Challenges for Thermoplastic-Automated Fiber Placement (TP-AFP) with in situ consolidation on 3D parts", *Proceedings of the 17th European Conference on Composite Materials*, June 2016, Munich (Germany), ISBN: 978-3-00-053387-7.

[C5]   Stokes-Griffin, C.M.; Kollmannsberger, A.; Compston, P.; "Investigation of the effects of heating bias and placement head angle on the short beam strength of CF/PEEK laminates manufactured in a laser tape placement process", *9TH Australasian Congress on Applied Mechanics ACAM9*, November 2017.

[C6]   Engelhardt, R.; Oelhafen, J., Ehard, S., Kollmannsberger, A.; Drechsler, K.; "Manufacturing of a Thermoplastic CFRP Rocket Module with Integrated Fiber Optical Temperature Sensors", *29th SICOMP Conference on Manufacturing and Design*, May 2018, Luleå (Sweden).

[C7]   Stokes-Griffin, C.M.; Kollmannsberger, A.; Compston, P.; Drechsler, K.; "Steel-CF/PA6 hybrids manufactured by a laser tape placement process: Effect of first-ply placement rate on lap shear strength for garnet blasted substrates", *18th International Conference on Sheet Metal SHEMET 2019*, April 2019, Leuven (Belgium).

Poster

[P1]   Engelhardt, R.; Oelhafen, J.; Ehard, S.; Kollmannsberger, A.; Drechsler, K.; CFRP Rocket Module with Integrated Fiber Optical Temperature Sensors, *SSEA Conference*, April 2018, Budapest (Hungary).

C Supervised student theses

During the employment at the Chair of Carbon Composites, the following student theses were supervised:

[S01]   F. Yüksel, „Ermittlung des Gewichtspotentials von CFK gegenüber Aluminium für Crashanwendungen anhand einer substituierten Hutprofilgeometrie", Semesterarbeit, Lehrstuhl für Carbon Composites, TUM, 2012.

[S02]   T. Schulz, „Verbindungselement- und Fügenahtgeometrien beim Vibrationsfügen von Thermoplasten mit Duromeren", Semesterarbeit, Lehrstuhl für Carbon Composites, TUM, 2013.

[S03]   S. Gebhard, „Konzeption, Konstruktion und Validierung des A-Säulen seitigen Strukturknotens im Türinnenblech aus CFK", Semesterarbeit, Lehrstuhl für Carbon Composites, TUM, 2013.

[S04]   F. Hohenester, „Numerische Analyse der Temperaturverteilung des lasergestützten Automated Fiber Placement Prozesses von CFK-Tapes mit thermoplastischer Matrix in Matlab", Semesterarbeit, Lehrstuhl für Carbon Composites, TUM, 2014.

[S05]   J. Devecka, „Konstruktion einer Kohlenstofffaserverbund-Karosserie eines Fahrzeuges für einen Effizienzwettbewerb in CatiaV5", Semesterarbeit, Lehrstuhl für Carbon Composites, TUM, 2014.

[S06]   H. Wu, „Analyse der Prozessparameter des lasergestützten Automated Fiber Placement (AFP) Prozesses von CFK-Tapes mit thermoplastischer Matrix in Versuch und Simulation", Semesterarbeit, Lehrstuhl für Carbon Composites, TUM, 2015.

[S07]   J. Reich, „Simulative und experimentelle Steifigkeitsuntersuchung geflochtener Hohlbauteile", Semesterarbeit, Lehrstuhl für Carbon Composites, TUM, 2015.

[S08]   A. Carrels, „Investigation of the material properties for simulating the temperature distribution of laser assisted Automated Fibre Placement of carbon tapes with thermoplastic matrix in Matlab", Semesterarbeit, Lehrstuhl für Carbon Composites, TUM, 2015.

[S09]   H. Wu, „Analyse der Prozessparameter des lasergestützten Automated Fiber Placement (AFP) Prozesses von CFK-Tapes mit thermoplastischer Matrix in Versuch und Simulation", Masterarbeit, Lehrstuhl für Carbon Composites, TUM, 2015.

[S10]   S. Aschauer, „Entwicklung einer automatisierten Auswertemethode von Anlagenlogdaten des TP-AFP Prozesses", Semesterarbeit, Lehrstuhl für Carbon Composites, TUM, 2016.

[S11] H. Fruja, „Bestimmung der Wärmeleitungseigenschaften von im TP-AFP Prozess hergestellten CFK-Laminaten", Semesterarbeit, Lehrstuhl für Carbon Composites, TUM, 2016.

[S12] A. Dittmar, „Entwicklung einer Vorrichtung zur Kompensation von Schwankungen der Position des Laserbrennflecks im TP-AFP Prozess", Semesterarbeit, Lehrstuhl für Carbon Composites, TUM, 2016.

[S13] P. Weis, „Temperatursimulation des instationären Automated Fiber Placement Verfahrens auf gekrümmten Oberflächen in Matlab", Semesterarbeit, Lehrstuhl für Carbon Composites, TUM, 2016.

[S14] M. Bösl, „REXUS - Werkzeugdesign für die Herstellung eines REXUS-Raketenmodules", Semesterarbeit, Lehrstuhl für Carbon Composites, TUM, 2016.

[S15] H. Latiri, „Development of a visualisation method for an automated evaluation of the process parameters of the TP-AFP Process", Bachelor's thesis, Lehrstuhl für Carbon Composites, TUM, 2016.

[S16] F. Wagner, „Umwandlung und Export von 3D-Bahndaten aus Catia in ein Kuka Roboterprogramm für den Thermoplast Automated Fiber Placement Prozess", Bachelor's thesis, Lehrstuhl für Carbon Composites, TUM, 2016.

[S17] F. Steinemann, „Untersuchung der thermischen Zersetzung des Laminats aufgrund zu hoher Prozess-temperaturen im TP-AFP Verfahren", Semesterarbeit, Lehrstuhl für Carbon Composites, TUM, 2017.

[S18] M. Schwab, „Experimentelle Parameterstudie: Ablage von dreidimensionalen CFK-Preforms im thermoplastischen Automated Fiber Placement Prozess", Master's thesis, Lehrstuhl für Carbon Composites, TUM, 2017.

[S19] H. Waller-Ehrat, „Untersuchung der Prozesstemperaturen im laserunterstützten Thermoplast-AFP Verfahren anhand thermografischer Aufnahmen", Semesterarbeit, Lehrstuhl für Carbon Composites, TUM, 2017.

Parts of the following theses contributed to the underlying doctoral thesis:
[S04], [S06], [S08], [S09], [S10], [S11], [S12], [S13], [S15], [S16], [S17], [S18], [S19]